Regulation of osteoclastogenesis by purinergic signalling

Ankita Agrawal

Thesis submitted in accordance with the requirements of The University of Sheffield for the degree of Doctor of Philosophy.

Department of Human Metabolism
Faculty of Medicine, Dentistry & Health

July 2013

Acknowledgements

I owe a debt of gratitude to my supervisor Dr. Alison Gartland for giving me an opportunity to do this project and help me understand research in the way she has. Her patient guidance at different stages of the project, invaluable advice during experiments, constant encouragement to present my work in meetings and plenty of support when things got tough (no dearth of these instances), has made my PhD experience one that I wouldn't trade for anything in the world (cliché, I know but totally apt!). Thank you!!! Your energy both inside and outside the laboratory has been inspirational!

I would also like to thank Dr. Niklas Rye Jørgensen for welcoming me to his group and making those morning trips to collect blood samples! Susanne and Zanne for tolerating my constant pestering during my stay in Denmark and even afterwards- to get the bones delivered!! Thank you ATPBone consortium- for being so great with opportunities.

I am grateful to Mellanby Centre For Bone Research for being a resourceful place; Bone Analysis Lab and Flow Lab for dealing with my samples so efficiently.

Members of The Gartland Bone Group- Karan, Robin, Eric, Iain and ex- Ning, Becky, Swati you have been great colleagues and even more amazing friends- It's been an absolute pleasure! Hannah, Gareth, Marco, Sindhu, Adi for providing a much needed break from all the stresses during my stay in Sheffield.

Back home, I am grateful to Saurabh- for his un-ending faith and support. And last, but in no way the least- I am obliged to my family, for believing in me and standing by my decisions. Ma- your motivation and advice kept me going and Papa- without your support, none of this would be possible. I hope I have made you proud.

Summary

There is now conclusive evidence that extra cellular nucleotides act as signalling molecules and mediate diverse biological effects via corresponding cell surface purinoceptors. These can be released to the bone microenvironment as a consequence of either lytic or controlled release. These nucleotides, activate their corresponding purinoceptors to mediate bone resorption and bone formation- key regulators of bone homeostasis. In this study, firstly, the absence of P2X7R was examined in osteoclast formation and function using an *in vitro* osteoclastogenesis assay. Osteoclasts differentiated either from precursors with a targeted deletion in P2X7R or using an antagonist showed reduced resorption *in vitro*, a finding, in line with existing evidence in the literature.

Tantalising evidence suggests interplay of oestrogen and P2X7R in determining cell fate. Changes in bone homeostasis are evident in post menopausal osteoporosis, which is associated with loss of oestrogen, due to an increased activity and reduced apoptosis of osteoclasts. This study provides evidence that a combined absence of oestrogen and P2X7R results in an exacerbated bone resorption. Firstly, P2X7R blockade could not rescue the bone phenotype associated with oestrogen loss as was expected based on the current literature. Using an *in vitro* mode of osteoclast function, it was evident that absence of both oestrogen and P2X7R resulted in excessive bone resorption. These findings explain, for the first time, the mechanism underlying an increased bone loss in postmenopausal women associated with a loss of P2X7R function.

Functional changes in P2X7R due to SNPs altered the activity in cells of osteoclastic lineage with potentially biological consequences. These findings address the involvement of P2X7R in controlling the fate and activity of osteoclasts and future work associating P2X7R function in other oestrogen-responsive bone cells- osteoblasts and bone lining cells, would provide valuable mechanistic insights to diseases with impaired bone remodelling.

Table of Contents

List of Figures

List of Tables

List of Abbreviations

˚ C	Degree Celsius
µg	Microgram
µl	Microliter
µM	Micromolar
ATP	Adenosine triphosphate
BM	Bone marrow
BMC	Bone mineral content
BMD	Bone mineral density
BMU	Basic multicellular units
BSA	Bovine serum albumin
BV	Bone volume
BzATP	2,3 (4-benzoyl) benzoyl ATP
Ca^{2+}	Calcium
CAMKII	Calmodulin protein kinase II
cAMP	Cyclic adenosine monophosphate
cDNA	Complementary DNA
cm	Centimeter
CT	Cycle threshold
CTX	C-telopeptide collagen
DA	Degree of anisotropy
Da	Dalton
DAB	3,3'-diaminobenzidine
DMSO	Dimethyl sulfoxide
DNA	Deoxy-ribonucleic acid
DOPS	Danish Osteoporosis Prevention Study
DPX	DePeX mounting medium
DXA	Dual energy X-ray absorptiometry
E	Oestrogen
EL	Extracellular loop
ER	Oestrogen receptor
FBS	Fetal bovine serum
FN	Femoral neck
GAPDH	Glyceraldehyde-3-phosphate dehydrogenase
GOF	Gain of function
HBSS	Hank's balanced salt solution
293HEK	Human embryonic kidney 293 cells
IFN- γ	Interferon-γ
IL	Interleukin
IP_3	Inositol trisphosphate
KO	Knockout
lacZ	β-galactosidase
LOF	Loss of function
LPS	Lipopolysaccharides
LS	Lumbar spine
M	Molar
Ma.V	Marrow volume
mAB	Monoclonal antibody
M-CSF	Macrophage-colony stimulating factor
mg	Milligram

ml	Millilitre
mm	Millimeter
mM	Millimolar
mRNA	Messenger RNA
NANC	Non-adrenergic and non-cholinergic
NaOH	Sodium hydroxide
NF-κB	Nuclear factor kappa-light-chain-enhancer of activated B cells
ng	Nanogram
NGS	Normal goat serum
osteoblast	Ob
osteoclast	Oc
OVX	Ovariectomy
P2R	P2 receptor
PBMCs	Peripheral blood mononuclear cells
PBS	Phosphate-buffered saline
PCR	Polymerase chain reaction
pg	Picogram
PKC	Protein Kinase C
PLC-β	Phospholipase C-β
pm	Perimeter
PTH	Parathyroid hormone
qRT-PCR	Quantitative real-time PCR
r.Oc	Resorbing osteoclast
RA	Rhematoid arthritis
RANKL	Receptor activator for nuclear factor κ B ligand
RIN	RNA integrity number
RNA	Ribonucleic acid
ROI	Region of interest
R-PE	R-phycoerythrin
RT	Room temperature
SEM	Standard error of mean
SMI	Structure model index
SNP	Single nucleotide polymorphism
Tb.N	Trabecular number
Tb.Pf	Trabecular bone pattern factor
Tb.Sp	Trabecular separation
Tb.Th	Trabecular thickness
TH	Total hip
TM	Transmembrane domains
TNF	Tumour necrosis factor-alpha
TRAP	Tartrate resistant acid phosphatase
TV	Tissue volume
WT	Wild type

Chapter 1. Introduction

1.1. Purinoceptors

In the last 40 years, the role of Adenosine triphosphate (ATP) solely as a ‘molecular unit of energy’, to its recognition as an extracellular messenger, has met with an exponential interest. ATP has a well established universal role as an intracellular energy source in all living cells however, in recent years, ATP in extracellular space has been demonstrated to mediate diverse biological effects thereby, helping it gain a foothold as a signalling molecule. To date, ATP signalling has been implicated in both short-term (acute) events such as neurotransmission, exocrine and endocrine secretion, chemotaxis, inflammation, mechanosensory transduction and ranges to long-term (trophic) signalling involving cellular growth, proliferation, differentiation and death, angiogenesis, atherosclerosis, regeneration and wound healing, pain, cancer and ageing (Abbracchio and Burnstock, 1998; Burnstock, 2009; Burnstock and Verkhratsky, 2010). All of these biological effects are mediated via cell surface receptors called purinoceptors.

1.1.1. Historical overview

In 1929, Drury and Szent-Györgyi first recognised the potent and reversible action of adenine compounds on mammalian cardiac rhythm and blood vessels (Drury and Szent-Gyorgyi, 1929). These observations and early studies focussed on the cardiovascular system, led to the recognition of adenosine and ATP as potential vasodilators (Berne, 1963; Holton, 1959). Although a role of purine nucleotides and nucleosides in physiological regulation was emerging, it wasn't for another decade that Professor Geoffrey Burnstock's article hypothesising ATP as a neurotransmitter was published (Burnstock, 1972). This landmark event was supported by evidence that ATP was the principal transmitter substance released by inhibitory nerves supplying the gastro-intestinal muscle (Burnstock et al., 1970). These nerves were tentatively termed 'purinergic' since they were involved in non-adrenergic and non-cholinergic (NANC) neurotransmission. With the help of experimental evidence, the purinergic theory was further strengthened and identified that ATP was released as a co-transmitter during nerve transmission (Burnstock, 1976; Sneddon and Burnstock, 1984; Su et al., 1971). At that time, a basis of classification of purinergic receptors by Prof. Burnstock placed them into two types, P1-purinoceptors and P2-purinoceptors preferentially activated by ligands adenosine and ATP respectively (Burnstock, 1978). Till today, extensive investigations in the purinergic field have helped support and extend the P1/P2 classification. Subdivisions were based on receptor pharmacological profiles and tissue distribution but current classification is based on their distinct molecular structures and is well-established and adopted by the IUPHAR Committee on Receptor Nomenclature and Drug Classification (Fredholm et al., 1994).

1.1.2. Adenosine/P1 receptors

The P1 receptor family comprises of A_1, A_{2A}, A_{2B} and A_3 receptors, all of which couple to G protein (Ralevic and Burnstock, 1998). As reviewed by Ralevic and Burnstock, receptors from each of these subtypes have been cloned from a variety of mammalian species and are widely distributed in biological tissues. Each of the receptor shows variable potency towards

adenosine and its derivatives and has both non-selective and selective antagonists (Table 1-1). There is strong evidence that adenosine has a functional role in many disease as genetic deletions in receptors have been associated with several physiological consequences (Table 1-2).

However, as the main focus of this project is on P2 receptors, the other subtype of purinoceptors, these will be discussed below in more detail.

Table 1-1 Distribution and characteristics of P1 receptors.
Table showing the distribution of P1 receptors in mammalian tissues and their corresponding transduction mechanisms. Known receptor agonists and antagonists are also listed. [Modified from (Burnstock, 2012) with permission from]

Receptor	Main distribution	Transduction mechanisms	Agonists	Antagonists
A_1	Brain, spinal cord, testis, heart and autonomic nerve terminals	$G_i/G_o\downarrow$cAMP	CCPA > R-PIA = S-ENBA; CVT-510; GR79236 2′-MeCCPA, SDZ WAG 994	DPCPX, N-0840, MRS1754, WRC-0571, PSB36, SLV320, CGS 16943
A_{2A}	Brain, heart, lungs and spleen	$G_S\uparrow$cAMP	HENECA > CGS 21680 = CVT-3146; ATL-146e	KF17837, SCH58261, ZM241385, KW 6002
A_{2B}	Large intestine and bladder	$G_S\uparrow$cAMP	Bay60-6583	PSB603, MRE-2029-F20, MRS1754, PSB0788 MRS1706, PSB1115, alloxazine
A_3	Lung, liver, brain, testis and heart	G_i/G_o, G_q/G_{11}, ↓cAMP, PLC-β activation	IB-MECA > MRS5151 > MRS5168 > 2-Cl-IB-MECA; DBXRM; VT160; HEMADO	MRS1220, L-268605, MRS1191, MRS1523 (rat), VUF8504, VUF5574, MRS1334 (human), PSB10

Table 1-2 Functional consequences of genetic deletion in P1 receptors.
Table showing the known functional physiological consequences of P1 receptor deletion. [Modified with permission from (Burnstock and Verkhratsky, 2010)].

Receptor	Phenotype
A_1	i. Behavioural phenotype: increased aggression and anxiety; decreased motor activity ii. Neural phenotype: neuroprotection in newborns; hyperalgesia; no inhibition of synaptic transmission; decreased long-term potentiation; reduced hypoxia-associated decrease in neural activity and recovery after hypoxia iii. Kidney phenotype: absent tubuloglomerular feedback iv. Metabolic phenotype: increased insulin and glucagon secretion
A_{2A}	i. Behavioural phenotype: increased aggression and anxiety; decreased exploratory activity; attenuated psychostimulant responses; decreased alcohol sensitivity and withdrawal; decreased amphetamine- and cocaine-induced locomotor response ii. Neural phenotype: neuroprotection in adults; hypoalgesia iii. Cardiovascular phenotype: increased blood pressure, heart rate and rennin activity iv. Haemostatic phenotype: increased platelet aggregation; increased brain damage after focal ischaemia v. Immunological phenotype: increased inflammatory response vi. Sensory phenotype: decreased pain threshold
A_{2B}	i. Immunological phenotype: increased histamine release but decreased IL-13 release from mast cells
A_3	i. Behavioural phenotype: increased despair and motor activity ii. Neural phenotype: reduced neuroprotection; hyperalgesia iii. Immunological phenotype: attenuated lipopolysaccharide-induced TNFα production and adenosine-induced histamine release from mast cells; decreased neutrophil infiltration of damaged myocardium; decreased local inflammatory response iv. Cardiovascular phenotype: decreased infarct size following ischaemic–reperfusion injury; loss of adenosine-induced cutaneous vasopermeability; i.v. adenosine produces and greater drop in blood pressure; increased tolerance to ischaemia; lower intraocular pressure

1.1.3. P2 receptors

Burnstock and Kennedy first divided the P2 receptor (P2R) family into 2 subclasses namely, P2Y and P2X which was based on their agonist potency and antagonist activity and tissue distribution (Burnstock and Kennedy, 1985). Other P2Rs were identified in biological tissues, P2U, P2T, P2Z based on their pharmacological profiles and subtypes called P2S, P2T, P2D, P3 and P4 were also proposed. Cloning of the receptors was a turning point in the field and the evidence that extracellular ATP signals by two distinct transduction mechanisms prompted a revision of this classification. Since 1994, the P2Rs are divided on the basis of their transduction mechanisms and membrane topology according to whether they are G-protein coupled (P2Y receptors, P2YR) or ligand-gated ion channels (P2X receptors, P2XR) (Abbracchio and Burnstock, 1994; Fredholm et al., 1994). To date, eight P2YRs and seven P2XRs have been cloned, pharmacologically characterized and validated in humans (Ralevic and Burnstock, 1998).

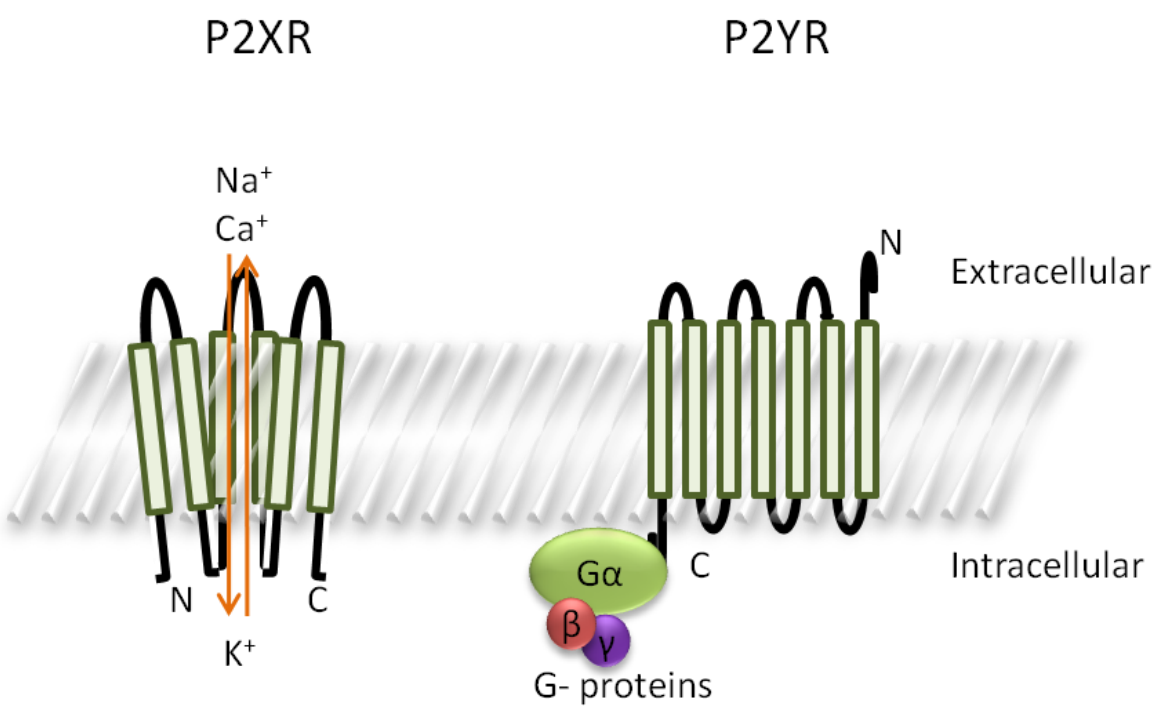

Figure 1-1 Membrane topology of P2 receptors

The P2X protein is a trimeric structure composed of units each with two membrane-spanning domains, extracellular loop and intracellular N and C termini (left). In contrast, the P2YRs have seven transmembrane domains linked by alternating extracellular and intracellular loops, which couple to G-proteins in the cell cytoplasm.

1.1.3.1. P2Y receptors

P2YRs (1-15) have been defined but $P2Y_1$, $P2Y_2$, $P2Y_4$, $P2Y_6$, $P2Y_{11}$; $P2Y_{12}$, $P2Y_{13}$ and $P2Y_{14}$ are the 8 mammalian P2YRs identified by the IUPHAR committee. The jump in the sequence is caused due to functional non-mammalian homologues, chick p2y3 (a suggested unconfirmed homolog of mammalian $P2Y_6$), turkey tp2y and Xenopus p2y8 (suggested homologues of $P2Y_4$) or erroneous identification of sequence homologues p2y7 (leukotriene B4 receptor), p2y9 (receptor for lysophosphatidic acid) and p2y5, p2y10 (orphan receptors) as nucleotide receptors. $P2Y_{15}$ was introduced but soon dropped due to its activity to α-ketoglutarate, a non-nucleotide (Abbracchio et al., 2005). Other P2YRs are P2D, P3 and P4 but their existence remains controversial due to a lack of their structure and signal transduction mechanisms and has been omitted (Ralevic and Burnstock, 1998).

All members have a common 7 trans-membrane domain tertiary structure with an extracellular N-terminus and an intracellular C-terminus (Figure 1-1). Positively charged amino acid residues located in trans-membrane domains 3, 5, 6 and 7 are conserved between the G-protein coupled receptors (Jacobson et al., 2012). Site-directed mutagenesis for human $P2Y_1R$ has shown that the interactions between the positive residues and the negatively charged phosphate groups of nucleotide ligands are critical determinants of the ligand binding pocket as their replacement reduced the receptor potency (Jiang et al., 1997). Substitution of amino acids in extracellular loops (EL2 and EL3), alters two disulphide bridges and are also identified to be critical for receptor function (Hoffmann et al., 1999).

The main signal transduction pathway in all 8 P2YRs involves second-messenger systems and based on their structural evolution and similarity of protein sequence; there are two clusters of P2YRs encompassing (a) $P2Y_{1,2,4,6,11}$ and (b) $P2Y_{12,13,14}$ subtypes. A low level sequence similarity has been reported between the clusters (up to 28%) while sequence similarity between the members is up to 48% (Abbracchio et al., 2006). Subtypes in group a, couple through $G_{\alpha q/11}$ to activate phospholipase C-β (PLC-β), whereas subtypes in group b, couple via $G_{\alpha i}$ to inhibit adenylate cyclase

(Table 1-3). Although grouped in cluster a, $P2Y_{11}$ is functionally different as it can activate both PLC-β and adenylate cyclase (coupling with $G_{\alpha s}$). G-protein coupling has been described to interact with ion channels in neurons but is relatively unexplored in other cells.

Coupling of P2YRs with functionally distinct G proteins leads to activation of inositol trisphosphate (IP_3), second messenger for calcium (Ca^{2+}) release from intracellular stores or adenylate cyclase, causing rise in cyclic adenosine monophosphate (cAMP). Ca^{2+} mobilization or cAMP rise stimulates a variety of downstream signal pathways according to the receptor and cell type.

Whether or not the different P2YR subtypes are capable of heteromerisation to form a functional receptor is still unclear.

1.1.3.2. P2X receptors

There are currently 7 P2XRs (1-7) all of which are ligand gated ion channels. The cDNA for P2XR subunits was first cloned in 1994 and subtypes have been shown to have two transmembrane domains (TM1 and TM2) with an intervening large extracellular loop and cytoplasmic N- and C- termini (Figure 1-1). Except the COOH terminus which shows the highest level of sequence diversity, the proteins are 40-55% identical between the seven subunits (North, 2002).

Both TM1 and TM2, the first critical for channel function and the second lining the ion pore; partaking in cation influx, are hydrophobic and less conserved than the extracellular loop. The extracellular loop has 10 cysteine residues, which contribute mainly to the formation of disulfide bridges thereby stabilizing the protein structure (North, 2002; Surprenant and North, 2009). Early works on P2X1R and P2X2R showed that the extracellular loop adjacent to TM1 and TM2 contains the ATP binding site as substitution of residues in the region reduced the agonist binding affinity (Cao et al., 2007; Jiang et al., 2000b; Roberts and Evans, 2004). The C-terminus harbours the protein kinases binding motifs which are specific to the different subunits.

Structural and stoichiometrical evidence suggests that P2XR subunits trimerise to form functional receptors (Barrera et al., 2005; Kaczmarek-Hajek et al., 2012; Mio et al., 2005; Nicke et al., 1998). The subunits are capable of forming both homomultimers or heteromultimers depending on the different subtypes. While heteromultimers of P2X2/3R are clearly established, P2X1/2R, P2X1/4R, P2X1/5R, P2X2/6R, P2X4/6R heteromultimers have also been identified (Burnstock, 2007). Except P2X6R which shows no agonist-evoked current as a homomultimer, all other P2XRs form homomultimers and could exist as a trimer or even as a hexamer of coassembled trimers

The primary agonist of all homomeric and heteromeric P2X receptors is ATP. The current view holds that ligand binding causes reduction in the disulfide bridges between the cysteine residues causing the movement of TM1 and TM2 allowing them to open the channel (Browne et al., 2010). This forms a non-selective cation channel permeable to small monovalent and divalent

cations. Elevation in intracellular calcium concentration ($[Ca^{2+}]_i$) either by direct Ca^{2+} permeation or by activation of voltage-gated Ca^{2+} channels (Koshimizu et al., 2000), triggers a range of signalling cascades resulting in both short- and long-term cellular events.

On the basis of the amplitude of the ATP-induced current in the continual presence of ATP, P2XRs are divided into rapidly desensitizing (P2X1 and P2X3) and slowly desensitizing (P2X2, P2X4, P2X5 and P2X7) (Koshimizu et al., 2000; North, 2002). Continuous agonist application causes an increase in permeability presumably caused by a progressive rotation and separation of TM1 and TM2 (Browne et al., 2010) resulting in the formation of a membrane pore.

1.1.4. Distribution and biological effects of P2 receptors

The purinergic signalling system possesses an extraordinary property- the principal mediator, ATP, can be rapidly degraded into its derivatives, ADP, AMP and adenosine, and can act on several classes of receptors on effector cells (Abbracchio et al., 2009). The distribution, pharmacological properties (agonists and antagonists) and transduction mechanisms of each of the purinoceptors are summarised in Table 1-3, adapted from (Burnstock, 2012).

Considering the extended purinoceptors family and their extensive tissue distribution specific cell-receptor interactions are implicated in different biological effects. Genetic deletion of purinoceptors manifests into physiological defects enlisted in Table 1-4, modified from (Burnstock and Verkhratsky, 2010).

Table 1-3 Distribution and characteristics of P2 receptors.
Table showing the distribution of P2 receptors in mammalian tissues and their corresponding transduction mechanisms. Known receptor agonists and antagonists are also listed. [Modified from (Burnstock, 2012) with permission from © 2012 WILEY Periodicals, Inc.]

Receptor		Main distribution	Transduction mechanisms	Agonists	Antagonists
P2Y	Y_1	Epithelial and endothelial cells, platelets, immune cells, osteoclasts and brain	G_q/G_{11}; PLC-β activation	MRS2365 > 2-MeSADP = $Ap_5(\gamma B)$ ≫ ADPβS > ATP >2-MeSATPADP	MRS2500 > MRS2279 > MRS217, PIT, A3P5P
	Y_2	Immune cells, epithelial and endothelial cells, kidney tubules and osteoblasts	G_q/G_{11} and possibly G_i/G_o; PLC-β activation	2-Thio-UTP > UTP, MRS2698 ≥ ATP, INS 365> INS 37217, UTPγS > Ap_4A > MRS 2768, Up_4-phenyl ester	AR-C126313 > Suramin> RB2, PSB-716, MRS2576
	Y_4	Endothelial cells, placenta, spleen and thymus	G_q/G_{11} and possibly G_i; PLC-β activation	2′-Azido-dUTP> UTPγS, UTP ≥ ATP ≥ Ap_4A Up_4U	ATP (human) > Reactive Blue 2 > Suramin, MRS2577, PPADS
	Y_6	Airway and intestinal epithelial cells, placenta, T cells, thymus and microglia (activated)	G_q/G_{11}; PLC-β activation	MRS2693> UDPβS, PBS0474> INS48823, Up_3U, 3-phenacyl-UDP ≫ UDP > UTP ≫ ATP, α,β-meUDP	MRS2578 > Reactive Blue 2, PPADS, MRS2567, MRS2575 (human)
	Y_{11}	Spleen, intestine and granulocytes	G_q/G_{11} and G_S; PLC-β activation	ATPγS > AR-C67085MX > BzATP ≥ ATP, NF546, NAD^+, $NAADP^+$	NF157 > Suramin > RB2, 5′-AMPS, NF340, AMP-α-5,
	Y_{12}	Platelets and glial cells	$G\alpha_i$; inhibition of adenylate cyclase	2-MeSADP ≥ ADP > ATP, ADP-β-S	AR-C69931MX> AZD6140, INS50589 > RB2 > 2-MeSAMP AR-C66096, CT50547,PSB-0413, Carba-nucleosides, MRS2395, AR-C67085
	Y_{13}	Spleen, brain, lymph nodes, bone marrow and erythrocytes	G_i/G_o	ADP = 2-MeSADP > 2-MeSATP, ATP	AR-C69931MX > AR-C67085 > MRS2211, 2-MeSAMP
	Y_{14}	Placenta, adipose tissue, stomach, intestine, discrete brain regions mast cells	G_q/G_{11}	MRS2690 > UDP > UDP glucose≥ UDP-galactose, UDP-glucosamine	-
P2X	X1	Smooth muscle, platelets, cerebellum and dorsal horn spinal neurons	Intrinsic cation channel ($Ca^{2+}$and Na^+)	BzATP > ATP = 2-MeSATP≥ α,β-meATP = L-β,γ-meATP (rapid desensitization); PAPET-ATP	NF449 > IP_5I > TNP-ATP> RO 0437626> NF279, NF023, RO1, MRS2159
	X2	Smooth muscle, CNS, retina, chromaffin cells, autonomic and sensory ganglia, pancreas	Intrinsic ion channel (particularly Ca^{2+})	ATP ≥ ATPγS ≥ 2-MeSATP > >α,β-meATP (pH + zinc sensitive); β,γ-CF_2ATP	PSB-1011 > RB2, isoPPADS > PPADS > Suramin, NF770, NF778, aminoglycoside
	X3	Sensory neurones, NTS, some sympathetic neurons	Intrinsic cation channel	2-MeSATP ≥ ATP≥ Ap_4A ≥ α,β-meATP (rapid desensitization); PAPET-ATP; BzATP	TNP-ATP, isoPPADS > A317491 > NF110 > PPADS, Ip_5I, phenol red, RO4, RN-1838, Spinorphin, AF353
	X4	CNS, testis, colon, endothelial cells and microglia	Intrinsic ion channel (especially Ca^{2+})	ATP ≫ α,β-meATP ≫ CTP, 2-eSATP; Ivermectin potentiation	5-BDBD ≫ TNP-ATP, PPADS> BBG, Paroxetine, phenolphthalein, CO donor (CORM 2)
	X5	Proliferating cells in skin, gut, bladder, thymus, spinal cord, heart and adrenal medulla	Intrinsic ion channel	ATP = 2-MeSATP = ATPγS ≫ α,β-meATP > AP_4A	BBG > PPADS, Suramin
	X6	CNS and motor neurons in spinal cord	Intrinsic ion channel	(Only functions as a heteromultimer)	-
	X7	Immune cells including dendritic cells (mast cells, macrophages), pancreas, skin and microglia	Intrinsic cation channel and a large pore with prolonged activation	BzATP > ATP ≥2-MeSATP ≫ α,β-meATP	KN62, BBG, KN04, MRS2427, O-ATP, RN-6189, AZ10606120, A740003, A-438079, A-804598, GSK-1370319, Compound 31 (GSK), AZD-9056, CE-224535

Table 1-4 Functional consequences of genetic deletion in P2 Receptors.
Table showing the known functional physiological consequences of P2 receptor deletion. [Modified with permission from (Burnstock and Verkhratsky, 2010)].

Receptor		Phenotype
P2Y	Y_1	i. Haemostatic phenotype: mildly prolonged bleeding times ii. Metabolic phenotype: increases systemic glucose levels
	Y_2	i. Epithelial phenotype: abnormal secretion ii. Bone phenotype: inhibited bone formation
	Y_4	i. Epithelial phenotype: abnormal secretion
	Y_6	i. Immunological phenotype: UDP-induced IL-6 and macrophage-inflammatory protein-2 release to lipopolysaccharide and macrophage UDP-induced inositol phosphate production are lost ii. Cardiovascular phenotype: loss of endothelium-dependent UDP vasodilation
	Y_{12}	i. Haemostatic phenotype: prolonged bleeding time, inhibition of platelet aggregation to ADP, and resistance to arterial thrombosis
P2X	X1	i. Kidney phenotype: absent tubuloglomerular feedback ii. Reproductory phenotype: male infertility due to the reduction of sperm in the ejaculate and severely impaired contractility of vas deference iii. Haemostatic phenotype: reduced thrombosis associated with injury of the walls of small arterioles
	X2	i. Neural phenotype: impaired synaptic facilitation in hippocampal interneurones ii. Sensory phenotype: impaired taste iii. Chemosensory phenotype: affected excitation of afferent nerves in carotid body by hypoxia iv. Gut phenotype: reduced peristalsis of the small intestine
	X3	i. Sensory phenotype: affected nociception, impaired temperature sensitivity, impaired taste ii. Urinary phenotype: affected voiding reflex
	X2 & X3	i. Sensory phenotype: affected nociception, impaired temperature sensitivity, severely impaired taste ii. Chemosensory phenotype: reduced ventilatory responses to a decrease in the level of inspired O_2
	X4	i. Neural phenotype: reduced hippocampal LTP ii. Sensory phenotype: reduced chronic pain (both inflammatory and neuropathic) iii. Vascular phenotype: impaired flow-sensitivity of blood vessels; decrease in NO production by endothelial cells, decreased vasodilatation, higher blood pressure
	X7	i. Immunological phenotype: impaired immune response ii. Sensory phenotype: reduced inflammatory and neuropathic chronic pain iii. Exocrine phenotype: impaired saliva production iv. Bone phenotype: abnormal bone formation and resorption

1.2. P2 Receptors and bone

In the early 1990s, Kumagai et al., reported the very first evidence of functional P2 receptors in rat osteoblast-like cells, UMR-106 (Kumagai et al., 1991). This was soon followed by another report demonstrating the effects of extracellular ATP on human osteoblasts (Schofl et al., 1992). These reports described dose-dependent effects of ATP in increasing intracellular Ca^{2+}in a manner that is consistent with the activation of purinoceptors. Since then, the role of extracellular nucleotides in regulation of bone cell physiology has emerged as a rather promising area of research.

A brief overview of bone composition and regulators of bone cells is presented below followed by current findings regarding the role of purinergic signalling. It is important to understand the normal bone physiology to understand how extracellular nucleotides might appear in the bone cell milieu and the ATP sensitivity of bone cells.

1.2.1. Normal bone structure and function

Anatomically, there are four categories of bones- long bones (i.e. femurs and humeri), short bones (i.e. carpal and tarsal bones), flat bones (i.e. skull and sternum) and irregular bones (i.e. vertebrae and sacra) (Clarke, 2008). Structurally, bone can be categorised as either cortical (compact) or trabecular (cancellous or spongy). The ratio of cortical to trabecular bone differs according to the anatomical site and the structure of the bones. There is ever-growing evidence in the literature that gender, obesity, diet supplementation, metabolic disorders, genetics, age can alter the cortical: trabecular bone ratio in adults.

A typical long bone is composed of a diaphysis (hollow shaft); which flares out on either side to form a cone shaped metaphysis (below the growth plates); and rounded epiphysis (above the growth plate) (Figure 1-2). The diaphysis is composed of thick, dense, high-strength cortical bone; the methaphyses and epiphyseal ends have a thin layer of cortical bone, containing numerous interlinked trabeculae conferring rigidity to the outer cortical shell (Clarke, 2008).

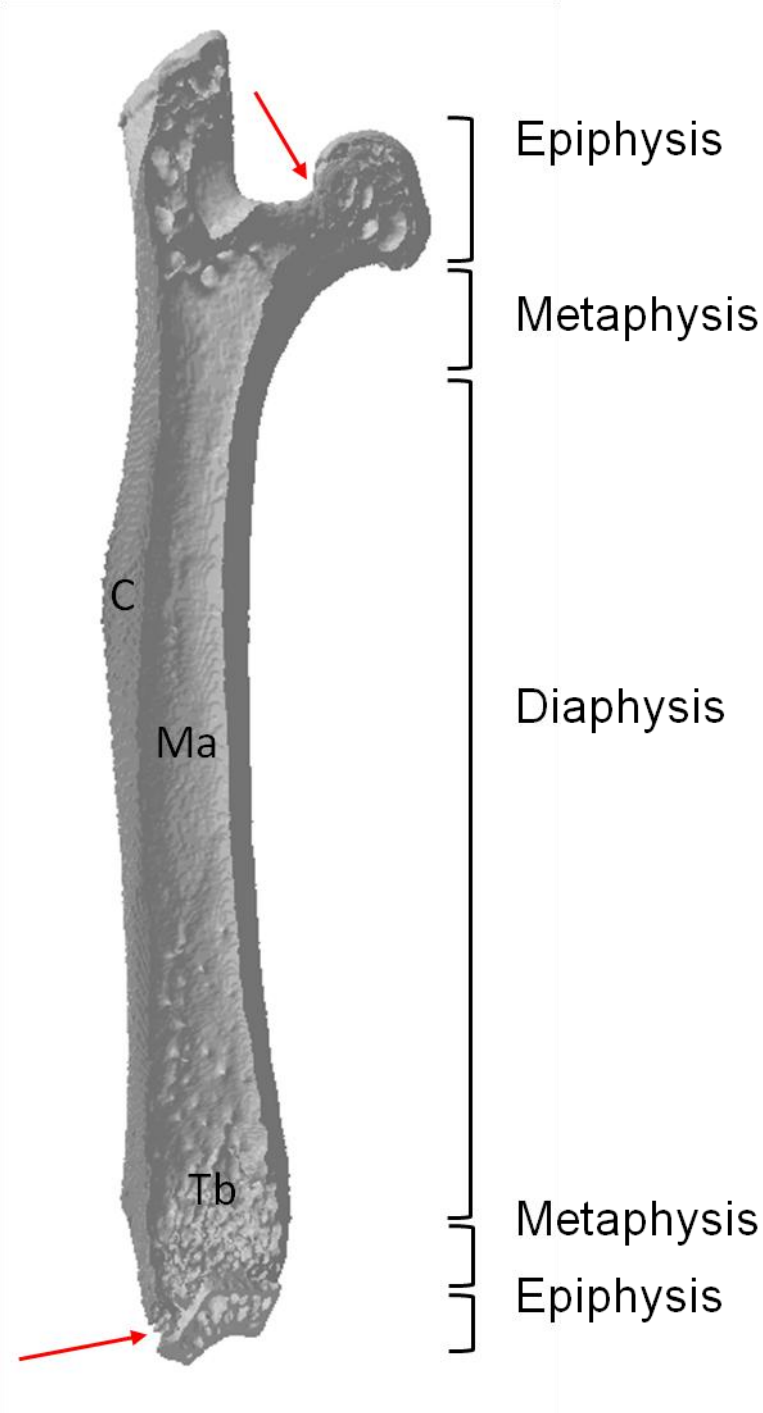

Figure 1-2 Typical structure of a long bone.

Longitudinal section (generated by µCT-3D model) showing epiphysis, metaphysis, diaphysis and growth plates (arrows) of a mouse femur. Also shown are the trabecular (Tb) and cortical (C) bone compartments and location of bone marrow (Ma).

Considering the highly specialised nature of the bone tissue, some of its functions include a) structural and mechanical support; for muscle attachment permitting movement and locomotion, b) protection; for vital organs such as brain and spinal cord, c) maintenance of mineral homeostasis, by regulating calcium and phosphate blood levels, and d) reservoir; for growth factors, cytokines and hematopoietic marrow. These functions are accomplished by continuous tissue removal and replacement, while maintaining bone strength.

1.2.2. Bone modelling and remodelling

Bone is a rather dynamic tissue undergoing longitudinal and radial growth, modelling and remodelling. Bone modelling, precedes remodelling, allowing the bones to gradually change their overall shape in response to either physiological or mechanical forces. Modelling occurs by independent actions of bone's effector cells (osteoblasts and osteoclasts) in 'formation and resorption drifts' (Frost, 2001). Modelling by drifts causes an eventual widening or lengthening of the bones allowing them to change shape in response to the mechanical and non-mechanical stresses placed on them.

While modelling causes an accumulation of the bone mass (and strength), the process plateaus in young adults and in an adult, bone modelling is less frequent than remodelling (Frost, 2001). The latter is in place to maintain bone strength and mineral homeostasis and is achieved by a highly coordinated action of both osteoblasts and osteoclasts. Bone remodelling occurs throughout life at approximately three million microscopic sites in the body, called basic multicellular units (BMUs) (Figure 1-3) (page 19). The concept of BMUs was first described in 1989 and later explained to sculpt cortical and trabecular bones (Jee, 1989; Parfitt, 1994). The characteristics of BMUs are now well established and the vital statistics of bone remodelling are described in Table 1-5 .

The overall purpose of bone remodelling is to prevent the accumulation of old bone by repairing fatigue damage and maintenance (Manolagas, 2000). For a smooth progression of BMUs on the bone surface, a continuous supply of new osteoclasts and osteoblasts from their respective progenitors is

essential. There are numerous factors that regulate the different steps of BMUs by influencing the cell development and their precise control is needed to prevent a derangement of the normal process (Harada and Rodan, 2003; Manolagas, 2000).

Table 1-5 Vital statistics of bone remodelling.
Table showing the characteristics and components involved in bone remodelling [With permission from (Manolagas, 2000)].

• Lifespan of BMU ~6–9 months
• Speed ~25 μm/day
• Bone volume replaced by a single BMU ~0.025 mm^3
• Lifespan of osteoclasts ~2 weeks
• Lifespan of osteoblasts (active) ~3 months
• Interval between successive remodelling events at the same location ~2–5 years.
• Rate of turnover of whole skeleton ~10% per year

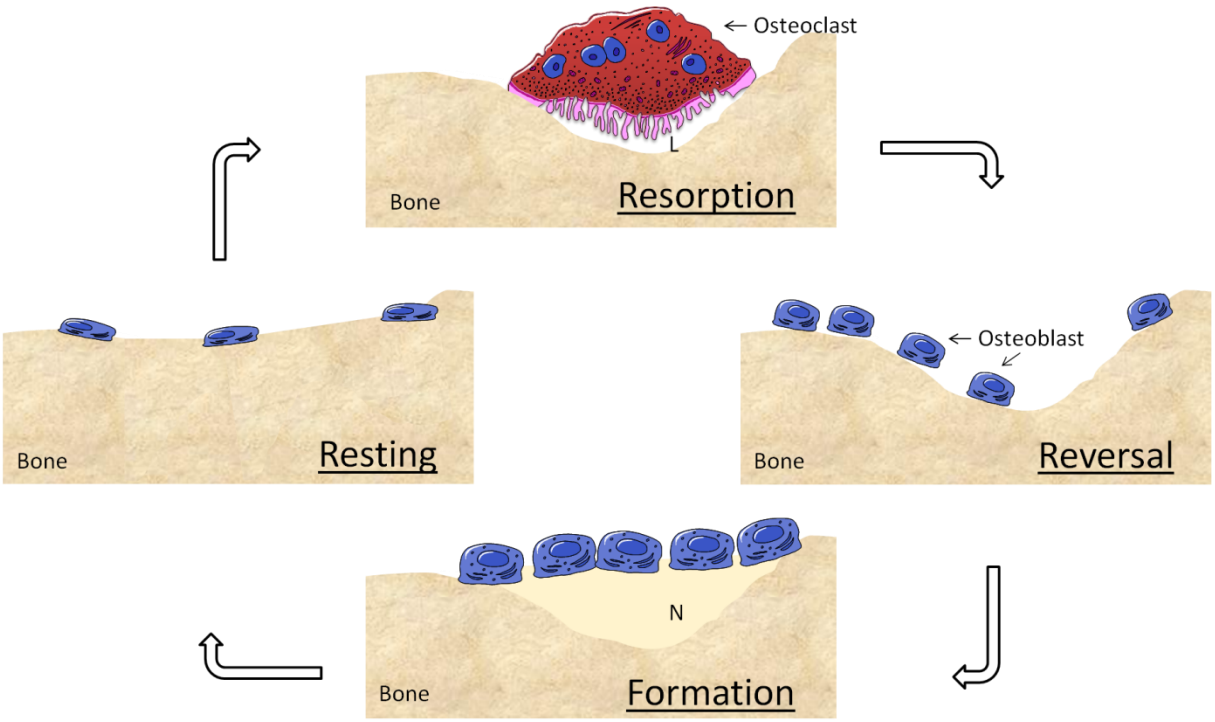

Figure 1-3 Bone remodelling by BMUs.

Cartoon showing stages of normal bone remodelling following differentiation of pre-osteoclasts under the influence of cytokines and growth factors into resorbing osteoclasts. Resorption: osteoclasts (red cell) release factors that dissolve bone mineral and matrix, creating a resorption lacuna (L). Reversal: End of resorption and beginning of arrival of bone forming osteoblasts (blue cells). Formation: Synthesis of bone matrix by osteoblasts and replacement of lacuna with new bone (N). Resting: Osteoblasts may undergo quiescence and line the surface of the newly formed bone until a new remodelling cycle begins.

1.2.3. Bone cells and function

There are four cellular elements of bone, namely: osteoblasts, osteocytes, bone lining cells, and osteoclasts. These can be classified on the basis of their origin. While the osteoblasts, osteocytes, and bone lining cells originate from mesenchymal stem cells, the osteoclasts originate from hematopoietic stem cells (Downey and Siegel, 2006).

1.2.3.1. Osteoblasts, osteocytes and bone lining cells

Osteoblasts are the primary bone forming cells and the process of bone formation occurs in two steps. In the first stage, mature osteoblasts synthesize and release organic matrix, which is mainly collagenous (85–90% of organic matrix, predominantly type I collagen) and many non-collagenous proteins, such as osteocalcin and osteonectin, (10–15% of organic matrix) with specific functions of each component in the structuring and mineralisation of the matrix (Clarke, 2008). In the second step, the organic matrix is mineralised to produce the calcified bone tissue. Mineral content is mainly hydroxyapatite [$Ca_{10}(PO_4)_6(OH)_2$] and is the major storage site of mineral salts. Bone mineral provides the mechanical rigidity whereas the organic component is responsible for imparting flexibility to the bone (Clarke, 2008; Kanis, 1996).

Eventually, mature osteoblasts could have 1 of 3 fates: cells may (1) undergo apoptosis, (2) become incorporated within the matrix and become osteocytes, or (3) become metabolically inactive and cover the surface of the bone as bone lining cells (Clarke, 2008; Downey and Siegel, 2006; Manolagas, 2000).

Osteoblasts (and the cells of bone marrow microenvironment) also secrete growth factors and cytokines that drive osteoclast development and function. These signals could work in multiple ways; there may be a direct effect of the factors on the osteoclast progenitors driving their differentiation and function; some regulate their effect in loops by mediating signalling via positive and negative feedback; others may control and amplify the production of another and act in a cascade fashion (Manolagas, 2000).

1.2.3.2. Osteoclasts

Osteoclasts, the bone-resorbing cells, are derived from their monocytic precursors by a process called osteoclastogenesis. Osteoclasts are multinuclear, can attach to the bone/mineralised matrix which induces polarization- and causes an asymmetric protein distribution and a change in shape of the now active osteoclast (Baron, 1989; Takahashi et al., 2007). The most characteristic feature of a resorbing osteoclast is its ruffled border, which is highly convoluted to provide for a larger surface area for the extensive trafficking, on the surface that is juxtaposed to the bone (Stenbeck, 2002).

The sufficient induction of osteoclastogenesis depends on two molecules: first, M-CSF (macrophage-colony stimulating factor, also CSF-1) which by engaging with its receptor c-fms on the monocyte precursors, provides signals for their survival and proliferation, and second, RANKL (Receptor Activator for Nuclear Factor κ B Ligand), which stimulates the pool of M-CSF–primed precursors to commit to an osteoclastic phenotype (Novack and Teitelbaum, 2008). *In vivo*, orchestration of several events is needed for normal osteoclast differentiation and function (Teitelbaum and Ross, 2003). Impairment of these events, either due to genetic defects or physiological changes, causes an alteration in osteoclast activity and development of an abnormal bone phenotype (Table 1-6).

Table 1-6 Regulation of osteoclast development and function

Table showing the function of regulatory factors imperative for normal osteoclast differentiation and function with their corresponding impairment defect.

	Function	Impairment defect	References
Surface receptors, molecules and cytokines			
M-CSF	Proliferation and survival of osteoclast precursors. Stimulates mature resorptive osteoclasts via c-Src activation.	Failure to generate osteoclasts, osteopetrosis	(Dai et al., 2002; Insogna et al., 1997; Yao et al., 2002; Yoshida et al., 1990)
RANKL	Commitment towards osteoclast fate; initiating transcription factors. Stimulates resorptive activity, prolongs lifespan of mature cells.	Failure to generate osteoclasts, osteopetrosis	(Burgess et al., 1999; Kong et al., 1999; Lacey et al., 1998; Yasuda et al., 1998)
OPG	Decoy receptor for RANKL	Increased osteoclast number and activity, osteoporosis	(Bucay et al., 1998; Simonet et al., 1997)
Integrin αvβ3	Osteoclast/bone recognition by actin cytoskeleton organisation, formation of sealing zone, activation of c-Src	Dysfunctional osteoclasts, osteopetrosis	(Faccio et al., 2003; McHugh et al., 2000)
H+-ATPase and chloride channel	Efficient mobilisation of bone mineral, exposed organic matrix	Failure to create resorptive microenvironment, osteopetrosis	(Frattini et al., 2000; Kornak et al., 2001; Schlesinger et al., 1997)
Cytoplasmic factors/genetic regulation			
Cathepsin-K	Enzyme, degrades collagen fibres	Lack of proteolysis, Osteopetrosis, Pycnodysostosis	(Gelb et al., 1996; Gowen et al., 1999; Saftig et al., 1998)
PU.1	Maturation of osteoclast	Lack of osteoclasts, osteopetrosis.	(Tondravi et al., 1997)
Traf6	Organization of the osteoclast cytoskeleton, controversial role in osteoclastogenesis	Dysfunctional osteoclasts or lack of osteoclasts, osteopetrosis.	(Armstrong et al., 2002; Lomaga et al., 1999; Naito et al., 1999)
NF-κB	Osteoclastogenesis	Failure to generate osteoclasts, osteopetrosis	(Franzoso et al., 1997)
c-Fos, c-Jun	Directs precursors away from macrophage pathway to an osteoclastogenic pathway.	Osteoclast deficient, osteopetrosis	(Grigoriadis et al., 1994)
c-Src and Pyk2	Activation of podosomal signalling complex with integrin αvβ3, activation of Syk	c-Src-/-, impaired osteoclast formation and function	(Boyce et al., 1992; Duong et al., 1998; Schwartzberg et al., 1997; Soriano et al., 1991)
FcRγ and DAP12	Activation of calcium signalling, co-stimulatory to RANKL mediated osteoclastogenesis	Failure to generate osteoclasts, osteopetrosis	(Koga et al., 2004)
NFATc1	Osteoclastogenesis, even in the absence of RANKL	Failure to generate osteoclasts, osteopetrosis	(Asagiri et al., 2005; Takayanagi et al., 2002; Winslow et al., 2006)

1.2.4. Osteoporosis

A strong and healthy skeleton is a result of well-balanced genesis and activity of bone cells, any deviation can result in a net gain or loss of bone. Osteoporosis is a metabolic bone disease with reduced bone mineral density (BMD) as its underlying pathogenesis. In osteoporosis, there is a net bone loss caused by excessive osteoclastic bone resorption, resulting in enhanced bone fragility and increased fracture risk (Novack and Teitelbaum, 2008). With age, both men and women lose bone (senile osteoporosis). In men, it has been studied that a slow but linear decline in bone loss occurs with an increased fracture risk (Mellstrom et al., 2008; Melton et al., 1998; Riggs et al., 1998). However, the rate of bone loss in women is accelerated due to menopause (post-menopausal osteoporosis) (Riggs et al., 1998). Almost three million people in the UK are estimated to have osteoporosis with 1,150 people dying every month as a result of hip fracture (National Osteoporosis Society, 2013) and therefore understanding the pathogenesis is a cause of concern.

In osteoporosis, a precipitous increase in bone turnover occurs but there is an imbalance in the process with bone resorption exceeding formation. The pronounced rate of bone resorption combined with lesser accumulation of bone during growth (peak bone mass) is attributed to an increased incidence of bone fractures in women by 2- to 3- fold compared to men (Orwoll and Klein, 1995). The primary driver of this process is the loss of oestrogen as oestrogen inhibits osteoclast survival and activity by its binding to receptors (ERs) (Kameda et al., 1997; Martin-Millan et al., 2010; Robinson et al., 2009). Oestrogen deficiency, therefore directly increases bone resorption by increasing osteoclast activity or mediating the production of molecules that regulate osteoclast differentiation and function.

Among the effects of oestrogen loss (Table 1-7), elevation of pro-osteoclastogenic cytokines such as Interleukins; IL-1, IL-6 and its receptor (IL-6Rα), lL-7; tumour necrosis factor (TNF-α), M-CSF and RANKL (Abbracchio et al., 2005; Azuma et al., 2000; Ishimi et al., 1990; Jilka et al., 1992; Kitazawa et al., 1994; Srivastava et al., 2001; Srivastava et al., 1999;

Srivastava et al., 1998; Weitzmann et al., 2002) have been studied. These, in addition to inhibition of anti-osteoclastic Interferon-γ (IFN-γ) and TGF-β causes increased bone resorption with deeper excavation of resorption pits (Cenci et al., 2003; Hughes et al., 1996).

Ovariectomizing (OVX) mice and rats causes oestrogen loss with similar bone turnover events in both trabecular and cortical bone compartments of these rodent bones to those observed in women following menopause (Iwaniec et al., 2006; Turner et al., 2001). Moreover, rodent bones mimic the protective effects of anabolic treatments to the responses in post-menopausal women and so are widely used as preclinical models to understand the patho-physiology of postmenopausal osteoporosis (Iwaniec et al., 2007).

Table 1-7 Regulation of osteoclast signalling associated with oestrogen loss
The effects of oestrogen loss via mediation of the molecules that regulate osteoclast differentiation and function.

Target	Regulatory mechanism	References
ERα and ERβ	loss of anti-apoptotic signals	(Manolagas et al., 2002; Nakamura et al., 2007; Piva et al., 2005)
Monocyte, IL-1 release	↑osteoclast precursor proliferation and survival, ↑resorption	(Kimble et al., 1996; Lorenzo et al., 1998; Pacifici et al., 1991)
T cell, monocyte, TNF-α release	↑osteoclast precursor proliferation and survival, ↑resorption	(Cenci et al., 2000; Kimble et al., 1996; Pacifici et al., 1991; Srivastava et al., 1999)
T-cell, IFN-γ release	↑TNF-α production, ↑resorption	(Cenci et al., 2003)
Osteoblast, IL-6 production	↑osteoclast formation	(Jilka et al., 1992; Passeri et al., 1993)
Mononuclear cell, GM-CSF production	potentially ↑osteoclast formation and resorption	(Pacifici et al., 1991)
Osteoblast, loss of TGF-β production	↑osteoclast life span and resorption	(Hughes et al., 1996)
Bone marrow, M-CSF production	↑osteoclast formation	(Srivastava et al., 1998)
Osteoclast precursors, RANKL responsiveness	↑osteoclast formation and resorption	(Robinson et al., 2009; Srivastava et al., 2001)
Bone marrow, IL-7 production	↑resorption	(Weitzmann et al., 2002)

1.2.5. P2 receptor signalling in normal and abnormal bone physiology

Bone cells of different species express a range of P2Y and P2XRs and their activation has been associated with numerous cellular functions by influencing events such as proliferation and survival, bone formation and mineralisation, ATP release, mechano-transduction, calcium signalling and transcription, cytokine regulation and overall maintenance of a structurally sound body support (Gartland, 2012; Gartland et al., 2012a; Orriss et al., 2010; Rumney et al., 2012).

In recent years, huge progress has been made towards understanding the role of P2Rs in the regulation of bone turnover. As a part of the EU Framework 7 funded project “ATPBone: Fighting osteoporosis by blocking nucleotides: purinergic signalling in bone formation and homeostasis,” the phenotypic analysis was performed to determine bone abnormalities in mice models (Jorgensen et al., 2013). Dr. N Wang investigated the effects of $P2YR_{13}$, and P2X7R deletion in female mice and also assessed their bone phenotype following OVX (Wang et al., 2012; Wang et al., 2013) (P2X7R, unpublished findings). Table 1-8 details the findings of these in all existing P2R KO (knock out) mouse models in both basal and bone challenging conditions.

Table 1-8 Bone phenotype of P2R KO mouse models.
Table describing the existing P2R KO mice with their gross bone phenotype analysed by assessing either bone mineral density (BMD) or bone mineral content (BMC). Also given are the osteogenic responses following bone challenge.

Receptor	Gross analysis (DXA/ µCT)	Challenge
$P2Y_1R$-/-	↓ BMD, ↓ BMC (Orriss et al., 2011a)	
$P2Y_2R$-/-	↑ BMC, ↑ bone volume (Orriss et al., 2011a)	
$P2Y_6R$-/-	↑ cortical bone volume, no change in trabecular bone (Orriss et al., 2011b)	
$P2Y_{13}R$-/-	↑ cortical bone, ↓ trabecular bone (Wang et al., 2012)	↓ bone turnover, protective against OVX induced bone loss (Wang et al., 2012)
		↑ osteogenic response in tibiae (Wang et al., 2013)
P2X7R KO (Distinct abnormalities different models depending on gene targeting construct and genetic background)		
Pfizer KO	↓ total and cortical BMC - effects of disuse on skeleton and oestrogen deficiency (Ke et al., 2003)	↓ mineralizing surface and ↓ bone formation in ulnar bone (Li et al., 2005)
		delayed fracture repair (Li et al., 2009)
		↓ bone formation, ↑ resorption in tooth (Viecilli et al., 2009)
Glaxo KO	unchanged BMD, ↑ cortical thickness (Gartland et al., 2003c)	
	↑ BMD (Syberg et al., 2012a)	↑ bone strength (Syberg et al., 2012a)
BALB/c KO (P2X7R-/-)	↑ BMD, ↑ BMC (Syberg et al., 2012a)	↑ bone strength (Syberg et al., 2012a)
DXA= Dual-energy X-ray absorptiometry µCT= X-ray microtomography Challenge= mechanical loading, OVX, fracture, three point bending		

1.3. P2X7 receptor

1.3.1. Structure and pharmacology

The P2X7R differs from the other P2XRs in many ways. Firstly, its activation not only leads to inward currents and ion influx, but also cell permeabilisation. A brief activation results in a rapid membrane depolarization similar to the other P2XR receptors but the most profound effect is the development of an additional permeability state in the presence of a sustained stimulus (Rassendren et al., 1997; Virginio et al., 1999a). This permeability state allows for exchange of larger cations with a molecular weight of up to 900D such as *N*-methyl-D-glucamine (NMDG) and fluorescence dyes such as the cationic propidium dye YO-PRO-1, and ethidium. (Khakh et al., 1999). P2X2 and P2X4 receptors show permeability increase with similar kinetics as P2X7R and point mutations in TM2 have been reported to affect the permeability states in P2X2R and P2X4R (Khakh et al., 1999; Virginio et al., 1999b). Using P2X7R transfected HEK cells, it was demonstrated that NMDG permeability was an intrinsic property of P2X7R activation and could be inhibited by both sodium concentrations in the extracellular medium or deletion of a segment in cytoplasmic C-terminal region of the receptor (Jiang et al., 2005). However, the authors showed that fluorescence measurements of YO-PRO-1 uptake remained unaffected and hypothesised a second distinct permeation pathway for propidium dye. It still remains unclear whether interaction with other proteins such as pannexin hemichannels is required in P2X7R associated dye uptake due to contradictory findings in the literature.

Secondly, 2,3 (4-benzoyl) benzoyl ATP (BzATP) is more potent than ATP at P2X7R whereas ATP is the most potent agonist of other P2XR subtypes. Lastly, its activation is well known to induce cellular apoptosis (Zheng et al., 1991). It was observed that activation of P2X7R induces events, including, changes in cell morphology such as membrane blebbing and upon prolonged activation leads to cell death (Di Virgilio, 1995; Ferrari et al., 1999a). It is known that its very long cytoplasmic C-terminal tail is responsible for imparting the receptor its unique properties and mediate P2X7R physiology

by its interactions with other proteins (North, 2002; Rassendren et al., 1997; Wilson et al., 2002).

1.3.2. Variations in structure

P2X7R gene is highly polymorphic and splice variants have also been identified in both mouse and human P2X7R transcripts.

In mice, the *P2rx7* gene has 13 exons spanning more than 45kb of DNA on chromosome 5 (Figure 1-4). Adriouch et al., showed a naturally occurring allelic variant in the C57BL/6 genome causing a residue change at position 451 from proline (451P) to leucine (451L) in the cytoplasmic tail of P2X7R (Adriouch et al., 2002). On transfection of cDNAs encoding these two variants into human embryonic kidney (293HEK) cell, the authors showed a reduced YO-PRO-1 uptake by 451L compared to the 451P allele. Moreover, weaker apoptosis and calcium influx in response to ATP were recorded in cells carrying the 451L allele (Adriouch et al., 2002). Because the cDNAs used for transfection in 293HEK cells differed in only one coding mutation, these experiments conclusively suggested that the natural allelic mutation (P451L) severely affected the known functions of the P2X7R.

There are 4 splice variants identified in the mouse *P2rx7* gene, all coding for a functional protein. However, recently, 3 novel variants were identified by re-analysis of existing KO mice. In 2009, Nicke et al., showed that 293HEK transfected with P2X7(k) variant showed higher BzATP sensitivity and increased dye uptake compared to the original P2X7(a) variant (Nicke et al., 2009). The P2X7(k) variant has an alternative transcription initiation site (in the newly discovered first exon- 1') which replaces the first 42 amino acid residues of the P2X7(a) and codes for intracelluar N-terminus and part of its first trans-membrane domain (Nicke et al., 2009) (Figure 1-4). The authors observed that although restricted, the P2X7(k) variant is expressed in the spleens of Glaxo KO mice and is therefore speculated that *P2rx7* gene may have escaped deletion when using the *lacZ*-insert (into exon 1 of *P2rx7* gene) method for gene KO. The Pfizer KO mice are also predicted to have escaped complete deletion of the *P2rx7* gene. Masin et al., found a C-terminal

truncated variant (ΔC) (13b) and a ΔC hybrid transcript (13c) (Figure 1-4) in the brain, salivary gland and spleens of KO mice (Masin et al., 2012). 293HEK cells showed reduced whole cell currents and reduced pore formation due to a loss of plasma membrane trafficking in homomeric P2X7Rs when transfected with 13b or 13c transcript. The authors showed that deletion of C-terminal domains in both 13b and 13c, known to be associated with receptor functionality by its interactions with other proteins, renders a reduced P2X7R function but not complete deletion in the Pfizer KO mice (Masin et al., 2012).

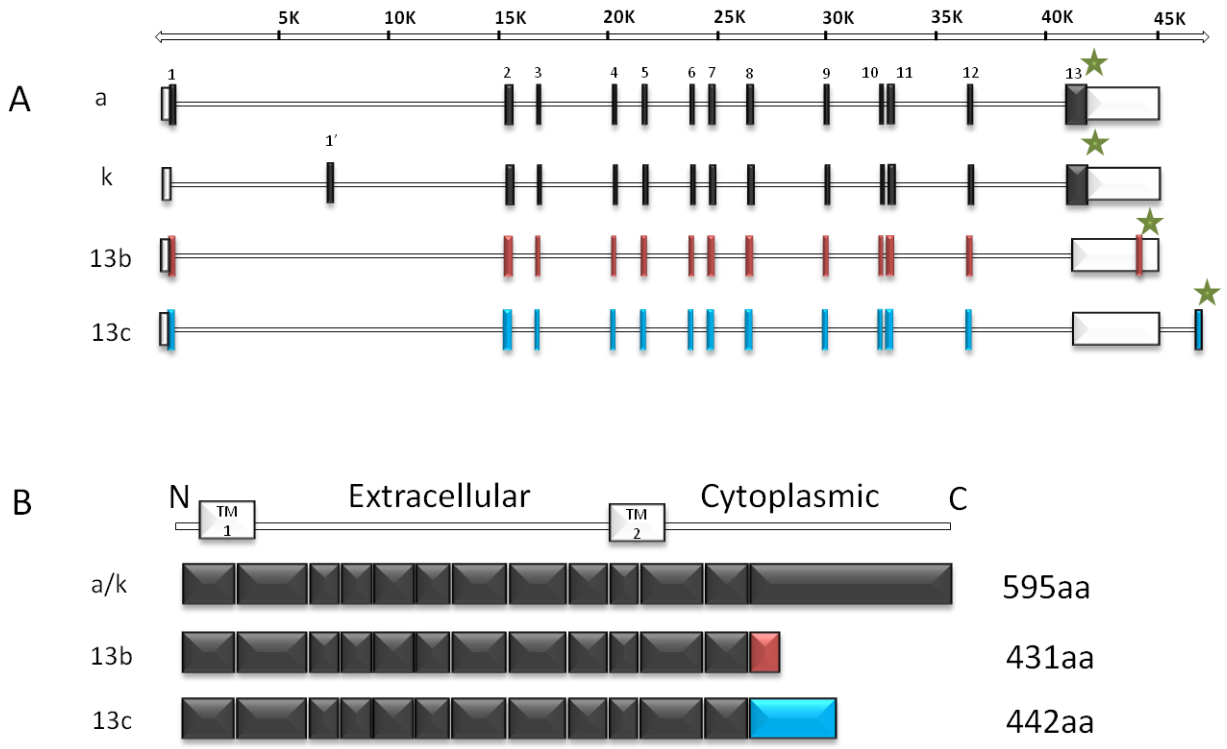

Figure 1-4 Variations in rodent *P2rx7* gene

(A) Genomic structure showing the structure and dimensions of the *P2rx7* gene indicating the position of newly identified exon 1' in P2X7(k) and 13b and 13c variants. Numbered bars represent exons and stars represent the stop codon (B) Shows the length of transcripts arising from alternate splicing of the original P2X7(a) transcript with the truncated C-terminus (coloured boxes).

In humans, *P2RX7* gene lies on the long arm of chromosome 12 (12q24.3) spanning over 53kb and consists of 13 exons. Nine naturally occurring variants resulting from alternative splicing have been identified (named P2X7A–J) (Cheewatrakoolpong et al., 2005; Feng et al., 2006). Of these, P2X7B contains a large deletion in the C-terminus, caused by retainment of an intron between exons 10 and 11, which causes insertion of a stop codon; but forms a functional plasma membrane channel (Cheewatrakoolpong et al., 2005; Feng et al., 2006). P2X7B is widely expressed in several human tissues and 293HEK expressing the variant fail to form membrane pore (Adinolfi et al., 2010; Cheewatrakoolpong et al., 2005). However, it was demonstrated to co-assemble with full-length P2X7 (P2X7A) to form a heterotrimer, which could potentiate the known P2X7R mediated responses and signalling events following activation (Adinolfi et al., 2010).

Additionally, 1510 single nucleotide polymorphisms (SNPs) in *P2RX7* gene are currently reported (NCBI database, Build 137, 19/05/2013) responsible for introducing further variation in the receptor function. Of these, at least 12 have been functionally characterised to date and are known to impart either gain or loss of function (non-synonymous) to the receptor function [International HapMap project (www.hapmap.org)] (Figure 1-5). These variations in the highly polymorphic *P2RX7* gene have been associated with various human diseases in several population based cohorts as they alter the physiological effects of P2X7R activation (Fuller et al., 2009; Sluyter and Stokes, 2011; Sperlagh et al., 2012; Wesselius et al., 2011).

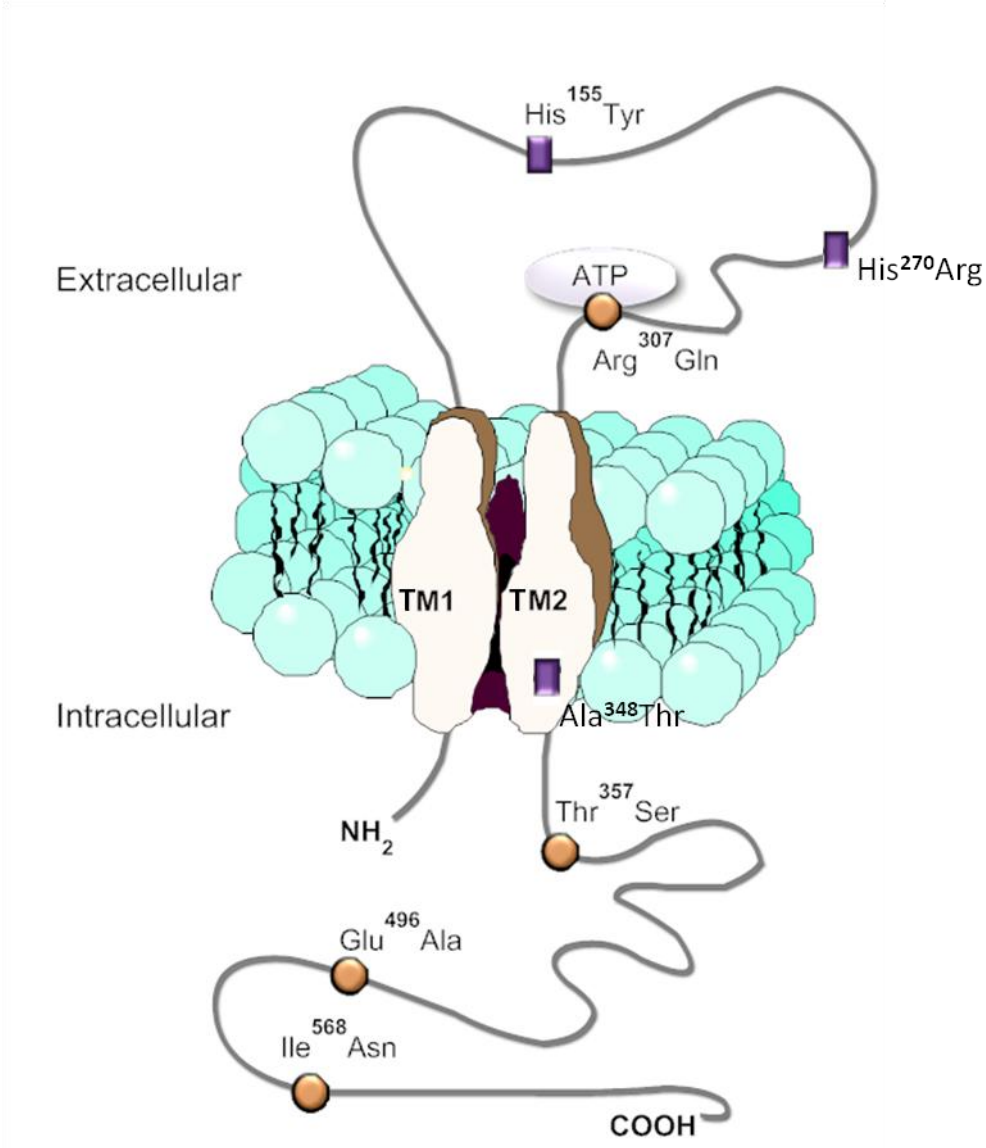

Figure 1-5 SNPs in human *P2RX7* gene.

Diagram depicting the topology of P2X7R showing intracellular N and C termini, extracellular loop and membrane spanning domains (TM1 and TM2). Non-synonymous SNPs causing loss of function (circles) and gain of function (rectangles) are shown with their corresponding residue changes. Modified with permission from (Wesselius et al., 2011).

1.3.3. Physiology of P2X7R activation

The P2X7R is expressed in almost all cell types, such as erythrocytes, lymphocytes, neutrophils, monocytes and macrophages (Gu et al., 2000; Gudipaty et al., 2001; Sluyter et al., 2001; Sluyter et al., 2004; Suh et al., 2001; Zhang et al., 2005). It has also been reported in brain and cells of the enteric system among other tissues (Bianco et al., 2006; Collo et al., 1997; Hillman et al., 2005; Koshi et al., 2005; Marin-Garcia et al., 2008; Miras-Portugal et al., 2003). Receptor expression has been extensively studied in bone cells; in osteoclasts (Gartland et al., 2003b; Hoebertz et al., 2000), osteoblasts (Gartland et al., 2001; Naemsch et al., 2001) and osteocytes (Li et al., 2005).

A range of cellular events have been identified downstream of P2X7R activation. One of its most well-characterized functions is the processing of IL-1β into its biologically active form (Ferrari et al., 1997) in response to an inflammatory stimuli by macrophages and other immune cells, a process, mediated by the assembly of an inflammasome (Ferrari et al., 2006). P2X7R knockout mice have reduced inflammatory response which is due to the failure of maturation and release of IL-1β (and release of other IL-1 family members) from monocytes (Solle et al., 2001) and their macrophages show no IL-1β release when challenged with ATP (Labasi et al., 2002). This observation is supported by *in vitro* antagonist studies where blockade of P2X7R resulted in a reduced of IL-1β production (Piccini et al., 2008; Stokes et al., 2006). In terms of disease, peripheral blood monocytes of patients with rheumatoid arthritis show elevated production of IL-1β following LPS priming and ATP exposure compared to the levels in control patients (Al-Shukaili et al., 2008). Role of IL-1β has been indicated in development of many aspects of neurodegeneration, including Alzheimer's disease (Griffin, 2006). Moreover, as previously mentioned, altered IL-1β production has been reported in P2X7R null mice which are also protected from inflammatory and neuropathic pain caused by both mechanical and thermal stimuli (Chessell et al., 2005). IL-1β production causes a positive feedback loop eventually resulting in induction of other pro-inflammatory IL-6, IL-8 and TNF-α. P2X7R

is reported to be expressed on human rheumatoid synoviocytes and therefore has a suggestive involvement in Rheumatoid Arthritis (RA) and an increase in IL-6 release from these synoviocytes following activation(Caporali et al., 2008). These cytokines also have a stimulatory effect on osteoclastogenesis and osteoclast resorption and therefore collectively, there is considerable data supporting the involvement of P2X7R mediated IL-1β release in inflammation, pain and development of bone diseases.

More recently, P2X7R activation has been reported to regulate inflammation by gene transcription of immune mediators, including VEGF, COX-2, IL-2, IL-6, IL-8, and iNOS and several transcriptional factors such as early growth response (Egr1-3) family, the nuclear factor of activated T cells (NFAT1-5), nuclear factor-κB (NF-κB) family members, the cyclic-AMP response element (CRE)-binding protein (CREB), and the AP-1 family members c-Fos, FosB, and JunB (Lenertz et al., 2011).

Given that P2X7R is expressed on various cell types, receptor activation has been shown to have an importance in immune, neurological and osteogenic regulations (Table 1-9).

In the following section, the functional significance of P2X7R and its regulation in bone homeostasis is reviewed.

Table 1-9 P2X7R expression and signalling in mammalian (rat, mouse and human) physiology			
	Expression	**Role**	**Reference**
Central Nervous System			
Neuronal transmission (brain, spinal cord and retinal neurons)	[1]mRNA, Protein, [3]Pharmacology/Biochemistry	synaptic transmission, excitotoxicity-based neuronal degeneration, neuromodulation and visual processing	(Brandle et al., 1998; Deuchars et al., 2001; Ishii et al., 2003; Monif et al., 2010; Moores et al., 2005; Puthussery and Fletcher, 2004; Sperlagh et al., 2002; Wang et al., 2004c)
Afferent signalling			
Taste bud cells	[1]mRNA, Protein, [3]Pharmacology/Biochemistry	cell regeneration.	(Hayato et al., 2007)
Pain	[1]mRNA, Protein, [3]Pharmacology/Biochemistry, [4]Genetics	inflammation-induced mechanical hyperalgesia, inflammatory and neuropathic pain	(Burnstock, 2013; Chessell et al., 2005; Chessell et al., 1997; Dell'Antonio et al., 2002; Donnelly-Roberts et al., 2008; Hughes et al., 2007; Yu et al., 2008)
Cardiovascular			
Vascular endothelium, associated risk	[1]mRNA, Protein, [3]Pharmacology/Biochemistry [4]Genetics	pathogenesis of atherosclerosis	(Gidlof et al., 2012; Piscopiello et al., 2013; Wilson et al., 2007)
Genitourinary			
Glomerular epithilium	[1]mRNA, [2]Protein, [3]Pharmacology/Biochemistry, [4]Genetics	cell apoptosis and necrosis	(Goncalves et al., 2006; Groschel-Stewart et al., 1999; Harada et al., 2000; Schulze-Lohoff et al., 1998; Solini et al., 2005)
Immunological			
Release of Interleukins, TNF-α, chemokines	[1]mRNA, Protein, [3]Pharmacology/Biochemistry, [4]Genetics	pro-inflammatory, chemotaxis, phagocytosis, mycobacterial killing	(Chessell et al., 2005; Di Virgilio, 2007; Fernando et al., 2007; Ferrari et al., 2006; Hughes et al., 2007; Saunders et al., 2003; Sharma et al., 2010; Tekin et al., 2010)
Secretion	[1]mRNA, Protein, [3]Pharmacology/Biochemistry, [4]Genetics	endocrine, exocrine secretion in autocrine, paracrine fashion	(Alzola et al., 1998; Garcia-Marcos et al., 2006; Leipziger, 2003)

P2X7R expression and signalling in mammalian (rat, mouse and human) physiology (contd.)

	Expression	Role	Reference
Bone			
Osteoporosis/ induction of bone disease/fracture risk	[1]mRNA, [2]Protein, [3]Pharmacology/Biochemistry [4]Genetics	bone formation and anti-resorptive	(Gartland et al., 2003b; Gartland et al., 2012b; Jorgensen et al., 2012; Wesselius et al., 2011; Wesselius et al., 2013)
Rheumatoid arthritis (RA)		anti-inflammatory therapeutic target	(Baroja-Mazo and Pelegrin, 2012)
Cancer	[1]mRNA, [2]Protein, [3]Pharmacology/Biochemistry [4]Genetics	proliferative, pain sensitivity, cytotoxic, cancer-induced bone disease	(Greig et al., 2003; Hansen et al., 2011; Roger and Pelegrin, 2011; Shabbir et al., 2008; White and Burnstock, 2006; White et al., 2005)

[1]mRNA= Northern-blot/RT-PCR/in situ hybridization,

[2]Protein= Immunostaining/Western-blot,

[3]Pharmacology/Biochemistry=Electrophysiology/$[Ca^{2+}]_i$measurements/miscellaneous,

[4]Genetics= Knockout model/ Single Nucleotide Polymorphism

1.3.3.1. Regulation of bone physiology

1.3.3.1.1. Phenotype of P2X7R KO mice

Mice with the *P2rx7* gene deletion are viable and fertile and do not appear to have any obvious physical or behavioural abnormalities. However, Pfizer KO mice show skeletal abnormalities associated with effects of disuse on skeleton and oestrogen deficiency (Ke et al., 2003). Mice of both genders show reduced total and cortical bone mineral content (BMC) and decreased femoral periosteal circumference. The differences are more pronounced with age and histomorphometric analyses showed reduced parameters of bone formation (mineralizing surface, bone formation rate) with an increase in parameters of bone resorption (osteoclast number, percent osteoclast surface); supportive of a phenotype with an overall reduced bone mass (Ke et al., 2003). Another murine model, Glaxo KO showed no differences in their trabecular bone volume but a thickening of cortical bones compared to the wild type controls (Gartland et al., 2003c). These conflicting findings were speculated to be due to the method of gene targeting and/or to the different genetic background of the inbred strains used to generate the KO mice.

In 2012, Syberg et al., performed an extensive analysis of the bone phenotype of 10 most common inbred strains of mice by means of dual energy X-ray absorptiometry (DXA), bone formation and resorption markers and three-point bending to determine bone strength (Syberg et al., 2012b). The authors showed that strains with the naturally occurring *P2rx7* mutation 451L, had weaker bones and lower resorption related to the reduced ATP-induced pore formation due to this allele. In comparison, strains with the P451 allele had stronger femurs and higher levels of the bone resorption marker C-telopeptide collagen (CTX) compared to the mice harbouring the 451L mutation. (Syberg et al., 2012b). As a follow up study, the group showed that the bone phenotype of P2X7R KO mice was hugely influenced by their genetic background (Syberg et al., 2012a). In the absence of P2X7R deletion, the strain containing the 451L allele showed only slight alterations in the bone parameters while the P2X7R-/- (BALB/c) mice showed more pronounced changes. The P2X7R-/- showed reduced serum CTX, higher

bone mineral density and increased bone strength compared to the WT littermates. These studies demonstrate the role of the P2X7R receptor in regulation of bone mass and highlight the importance of genetic background when looking at the functional effects of the P2X7R.

It is likely that osteoclastic formation and activity is not exclusively mediated by P2X7R signalling, as all the above mouse models maintain their ability to form functional osteoclasts either *in vivo* or *in vitro* even in the absence of *P2rx7* gene. However, the mice display abnormal bone homeostasis suggesting that P2X7R may be essential in regulating balanced bone formation and resorption activities. The imbalance could be due to impairment of cell survival or loss of osteoclast-osteoblast communication (Jorgensen et al., 2002), affecting osteogenic response (Li et al., 2005; Viecilli et al., 2009).

1.3.3.2. P2X7R and osteoclasts

1.3.3.2.1. Expression

Previous studies have shown a change in expression of P2X7R with differentiation in hematopoietic cells (Gu et al., 2000; Gudipaty et al., 2001; Hickman et al., 1994). P2X7R membrane activity was demonstrated to increase during maturation of macrophages from monocytes where the receptor expression was predominantly intracellular (Gudipaty et al., 2001; Hickman et al., 1994). Moreover, extracellular ATP induced down-regulation of receptor protein has been reported in the mouse monocyte macrophage cell line (RAW264.7) leading to inhibition of fusion to form multinucleated osteoclasts (Hiken and Steinberg, 2004). Additionally, inflammatory stimuli such as interferon-gamma (IFN-γ) and tumor necrosis factor alpha (TNF-α) could synergistically induce P2X7R mRNA and functional responses in the human THP-1 monocytic cell line (Humphreys and Dubyak, 1998). Taken together, these findings suggest that P2X7R expression is developmentally and physiologically regulated in mononuclear cells.

Expression of P2X7R is well documented in osteoclasts. Using cells of hematopoietic origin from explanted foetal metatarsal bones, Modderman et

al., described that addition of high concentrations of ATP induced dye uptake in the absence of divalent cations (Modderman et al., 1994). Since then, expression of P2X7R has been studied in rat and rabbit osteoclasts (Hoebertz et al., 2000; Naemsch et al., 2001) and in humans and confirmed by immunocytochemistry *in vitro* and *in vivo* (Gartland et al., 2003a; Jorgensen et al., 2002). P2X7R expression was shown by RT-PCR in monocytic precursors and throughout osteoclastogenesis *in vitro* suggesting that the receptor is needed in differentiation of osteoclasts (Buckley et al., 2002; Gartland et al., 2003a).

Namesch et al., showed P2X7R mediated currents using the whole-cell, patch clamp technique and agonist mediated influx of Ca^{2+} ions in rabbit osteoclasts, which was inhibited in the presence of a P2X7R antagonist (Naemsch et al., 2001). The authors observed that agonist stimulus caused currents which were slowly desensitizing and the amplitude could be reduced in the presence of divalent cations, findings typical of P2X7R activation (Naemsch et al., 2001; Surprenant et al., 1996). Agonist activated dye uptake, due to formation of a membrane pore, has also been observed in human as well as mouse osteoclasts (Gartland et al., 2003a; Hiken and Steinberg, 2004; Jorgensen et al., 2002).

1.3.3.2.2. Physiological roles of P2X7R in osteoclasts

Involvement of P2X7R has been suggested in various physiological roles in osteoclasts such as cell communication (Jorgensen et al., 2002); fusion to form multinucleated osteoclasts (Agrawal et al., 2010; Gartland et al., 2003a); and regulation of cytoskeleton (Hazama et al., 2009). Firstly, P2X7R mediated, mechanically induced propagation of calcium transients, measured by increase in $[Ca^{2+}]_i$, were demonstrated among human osteoclasts (Jorgensen et al., 2002). Induction of BzATP induced Ca^{2+} increase could be blocked by pre-treatment with P2X7R antagonist establishing the role of P2X7R mediated cell signalling.

Secondly, on human precursor cells obtained from peripheral blood, blockade of the P2X7R using a monoclonal antibody and known specific antagonists, inhibited precursor cell fusion (Agrawal et al., 2010; Gartland et al., 2003a).

The role of P2X7R in fusion of osteoclasts is consistent with the findings that macrophage cell clones expressing the receptor fused spontaneously *in vitro* whereas the ones lacking, do not (Di Virgilio et al., 1999). Localization of P2X7R to the site of cell-to-cell contact is suggestive of an imperative role of the receptor in the process of cell fusion (Falzoni et al., 2000). However, KO mice maintain their ability to form multinucleated osteoclasts *in vivo* and *in vitro* suggesting that P2X7R might not play an exclusive role in driving cell fusion.

Lastly, Hazama et al., reported that treatment of mature human osteoclasts with either BzATP or high concentrations of ATP, increased bone resorption *in vitro* (Hazama et al., 2009). Induction of resorption was accompanied by the formation of sealing-zone like structure via the reorganization of pre-existing cytoskeleton and the secretion of lytic granules at the site of osteoclast-matrix attachment (Hazama et al., 2009). Moreover, it was demonstrated that BzATP induced Ca^{2+} dependent translocation of Protein Kinase C (PKC, cytosolic proteins mediating phosphorylation of membrane proteins, in turn influencing downstream signalling activities) from murine osteoclast cytosol to membrane due to P2X7R activation (Armstrong et al., 2009). Both P2X7R mediated activation of PKC and augmentation of resorption was absent in the presence of either Brilliant Blue G, a selective P2X7R antagonist (Jiang et al., 2000a), and in osteoclasts from KO mice (Armstrong et al., 2009; Hazama et al., 2009). On the contrary, a recent study reported that extracellular ATP caused disruption of murine osteoclastic cytoskeleton and a subsequent reduction in survival and resorption (Miyazaki et al., 2012). The authors also showed that hydrolyzing ATP rescued the survival of the osteoclasts. Recently, it was demonstrated that P2X7R mediated ATP release is responsible for accumulation of adenosine, which ultimately drives cell fusion as pharmacological blockade of corresponding purinoceptors, prevented the process in human monocytes (Pellegatti et al., 2011). These studies suggest a dual role of P2X7R in regulating osteoclast survival and function. In light of this growing evidence, it is speculated that ATP release via P2X7R is needed for an autocrine/paracrine regulation of the

bone resorbing activity of mature osteoclasts, possibly via other purinergic receptors.

1.3.3.2.3. P2X7R mediated signalling in osteoclasts

NF-κB is a key transcription factor in osteoclast differentiation (Franzoso et al., 1997; Iotsova et al., 1997) and its nuclear localisation (activation) was achieved in osteoclasts from WT (wild type) mice but not from KO mice showing the involvement of P2X7R (Korcok et al., 2004). The authors also tested that the activation of NF-κB was independent of upregulated RANKL production following P2X7R stimulation as ATP has been previously demonstrated to induce RANKL production by osteoblasts (Buckley et al., 2002). P2X7R induced Ca^{2+} influx has also been shown to activate NFATc1 in microglial cells and 293HEK transfected cells (Adinolfi et al., 2009; Ferrari et al., 1999b). NFATc1 activation is the proposed master regulator of RANKL induced osteoclast differentiation and is activated by $[Ca^{2+}]_i$ (Takayanagi, 2009). It is possible that P2X7R mediated elevation of $[Ca^{2+}]_i$ via either NF-κB or NFATc1 activation regulate a variety of genes involved in osteoclast differentiation.

Intriguingly, both antagonism and activation of P2X7R inhibited resorption of human osteoclasts *in vitro*, the latter caused by initiation of apoptosis (Agrawal et al., 2010; Gartland et al., 2003a; Gartland et al., 1999). These findings reflect on the complex nature of P2X7R signalling and more studies are needed to identify the exact nature of receptor activation in osteoclastogenesis. Moreover, the exact role of P2X7R activation in osteoclast activity and activation of downstream signalling events remains to be elucidated.

At whatever stage the P2X7R is needed during osteoclast activity, it is possible that P2X7R signalling is capable of synergizing with systemic factors such as oestrogen and mediate signalling cascades in osteoclasts. Recent studies have suggested a reduced receptor function to be associated with increased susceptibility to osteoporosis and fracture risk. In different female cohorts, SNPs known to cause a functional change in P2X7R were correlated with the change in bone strength in their post menopausal years (Gartland et

al., 2012b; Jorgensen et al., 2012; Wesselius et al., 2013). The findings revealed that women with loss of P2X7R SNPs had a higher incidence of vertebral fractures and enhanced bone loss whereas women with SNPs rendering a higher function to P2X7R were at a lower risk of fracture. Menopause is marked by a gradual cessation in production of oestrogen and progesterone. Oestrogen has a well studied pro-apoptotic effect on osteoclasts but only a few findings, using cervical epithelial cells, suggest its role as an anti-apoptotic stimulus (Wang et al., 2004a; Wang et al., 2004b). These studies reported that addition of oestrogen prevented apoptosis of the cervical epithelium cells, a process mediated by P2X7R dependent rise in cytosolic Ca^{2+} (Gorodeski, 2004). These findings reveal that oestrogen is capable of interacting with P2X7R activated related signals to regulate cell survival. Interestingly, post menopausal women, with a P2X7R SNP causing loss of receptor function due to a trafficking defect (Wiley et al., 2003), are reported to be more responsive to hormone replacement therapy and prevention of their loss of bone mass (Ohlendorff et al., 2007b). It remains to be investigated whether oestrogen can potentiate P2X7R responses in osteoclasts and contribute to the development of phenotype following loss of oestrogen in post menopausal women.

1.4. Hypothesis and objectives

Given the expression of purinoceptors on osteoclasts, role of P2X7R signalling in osteoclast communication, mediation of osteoclast formation and function, and its possible modulation of oestrogen response; the hypothesis of the project is that oestrogen can exert its effects by regulating P2X7R signalling to modulate osteoclast resorption.

This hypothesis will be tested with the following objectives:

Objective 1: Determine the effect of genetic modification of P2X7R on osteoclastogenesis in mice of the BALB/c background. This will be achieved by investigating the expression of P2X7R splice variants in osteoclasts, assess osteoclastogenesis *in vitro* and numbers *in vivo*. And lastly, assess the genetic consequences of P2X7R deletion.

Objective 2: Determine the effect of P2X7R blockade during oestrogen loss induced bone phenotype. This will be achieved by testing the effects of a novel P2X7R antagonist on murine osteoclast resorption *in vitro* and assess the effects of administration of the antagonist to a mouse model of OVX induced bone loss.

Objective 3: Determine the effect of purine signalling in modulation of oestrogen response on osteoclastogenesis. This will be achieved by testing the effects of lack of oestrogen on osteoclastogenesis in the absence of P2X7R and P2YRs *in vitro*.

Objective 4: Determine the role of P2X7R non-synonymous SNPs on osteoclastogenesis. This will be achieved by assessing the expression and function of P2X7R SNPs on monocytic precursors and osteoclasts generated from post menopausal women with functional SNPs in the *P2RX7* gene.

Chapter 2. Materials and methods

2.1. Materials

Laboratory chemicals and solutions	
10% buffered formalin	Prepared in Bone Analysis Lab: Sodium dihydrogen orthophosphate dehydrate 8g Disodium hydrogen orthophosphate dehydrate 3g Concentrated formaldehyde (37-41%) 200ml Warm tap water 1800ml
2-Propanol, >99%	389710025, Thermo Fisher Scientific
Acetic Acid	20104.334, VWR International Ltd.
Adenosine 5′-triphosphate disodium salt hydrate	A7699, Sigma Aldrich
alpha-Modification of minimum essential medium (α-MEM) with Glutamax™	22571, Invitrogen, Life Technologies
BD FACSFlow™	342003, BD Biosciences
Benzoylbenzoyl ATP	B6396, Sigma Aldrich
Borax/ di-sodium tetraborate	10267, BDH Laboratories
Bovine Albumin Fraction V Solution (7.5%) (BSA)	15260, GIBCO, Life technologies
CD14 Microbeads	130-050-201, Miltenyi Biotec Ltd.
Charcoal Stripped FBS	12676, GIBCO, Life Technologies
Chloroform, minimum 99%	C2432, Sigma Aldrich
DAB Kit	SK-4100, Vector Laboratories
dATP	U120A, Promega
dCTP	U122A, Promega
DePeX mounting medium (DPX)	360294H, BDH Laboratories
dGTP	U121A, Promega
Dimethylformamide	D384108, Thermo Fisher Scientific
DMSO	D5879, Sigma Aldrich
dTTP	U123A, Promega
Ethanol	E/0065DF/17, Thermo Fisher Scientific
Ethidium Bromide	E1385, Sigma Aldrich
Fetal bovine serum (FBS)	10270, GIBCO, Life Technologies

Fluo-4/AM cell permeant	F-14217, Invitrogen, Life Technologies
FullRanger 100bp DNA Ladder	L3-0015, Geneflow Limited
Gill's Haematoxylin	1.05175, Merck
GoTaq® DNA Polymerase	M300, Promega
GoTaq® Flexi DNA Polymerase	M8301, Promega
GoTaq® Reaction Buffer (5X)	M300, Promega
Hank's Balanced Salt Solution (HBSS)	14025-050, Invitrogen, Life Technologies
HEPES buffer	BPE310-1, Fisher Bioreagents
HEPES buffer (Pore formation)	17-737E, BioWhittaker
Histopaque®-1077	10771, Sigma Aldrich
Hoechst-33342	H1399, Invitrogen, Life Technologies
Human recombinant M-CSF	Cambridge Biosciences, MA, USA
Hydrogen Peroxide Solution ≥30%	16911-250-F, Sigma Aldrich
ImProm-II X Reaction Buffer	M289A, Promega
ImProm-II™ Reverse Transcriptase	M314A, Promega
KN62, ≥95%, powder	I2142, Sigma Aldrich
Lipopolysaccharides from *Escherichia coli* (LPS)	L2630, Sigma Aldrich
Lithium Heparin vacutainer® tubes	367885, BD Biosciences
MS columns	130-042-201, Miltenyi Biotec Ltd.
Naphthol AS-BI phosphate (sodium salt)	N2250, Sigma Aldrich
Normal Goat Serum	PCN-5000, Invitrogen, Life Technologies
Nuclease free water	AM-9937, Ambion
OligodT primers	C110A, Promega
Pararosaniline	P3750, Sigma Aldrich
Penicillin-Streptomycin	15140, Invitrogen, Life Technologies
Phosphate-buffered saline (PBS)	pH 7.4, Invitrogen, Life Technologies
Phosphate-buffered saline (PBS-) without Ca^{2+} and Mg^{2+}	pH 7.4, BioWhittaker
Pluronic® F-127	P3000MP, Invitrogen, Life Technologies
Probenecid, Water Soluble	P36400, Invitrogen, Life Technologies
ProLong® Gold reagent	P36930, Invitrogen, Life Technologies
Rabbit serum	16120, Invitrogen, Life Technologies

Recombinant Human sRankL	10-1141-C, Insight Biotechnology
Recombinant Mouse M-CSF	Dr. Isabel Orriss and Dr. Tim Arnett
Recombinant Mouse RANKL	462-TEC, R&D Systems
Rhodamine-Phalloidin	R415, Invitrogen, Life technologies
Sodium acetate trihydrate	S9513, Sigma Aldrich
Sodium Hydroxide (NaOH)	28244.262, VWR International Ltd.
Sodium nitrite	S2252, Sigma Aldrich
Sodium tartrate (dihydrate)	S4797, Sigma Aldrich
Taqman 2x Universal PCR Master mix	4304449D, Applied Biosystems
TaqMan gene expression mastermix	VY4369510, Thermo Fisher Scientific
TBE buffer (10X)	A0972, Applichem
Toluidine blue	T3260, Sigma Aldrich
TRI Reagent®	T9424, Sigma Aldrich
Triton X-100	T8532, Sigma Aldrich
Trypsin Enzyme Digestion Kit.	MP-955-K25, MenaPath
UltraPure™ 0.5M EDTA, pH 8.0	15575, GIBCO, Life technologies
Universal PCR Master mix	4304449D, Applied Biosystems
YO-PRO®-1 Iodide	Y3603, Invitrogen, Life Technologies
α-MEM no phenol red	41061, Invitrogen, Life Technologies

Antibodies	
CT-R Antibody (C-19)	sc-8859, Santa Cruz Biotechnology
Mouse anti-human CD14+ (R-PE)	MHCD1404, CALTAG Laboratories
P2X7mAB	Clone L4, (Buell et al., 1998)
Isotype antibody (Goat IgG-HRP)	sc-2741, Insight Biotechnology
Isotype antibody (mouse IgG1)	MG-104, CALTAG Laboratories
Alexa Fluor® 488 Goat Anti-Mouse IgG	A11001, Invitrogen, Life Technologies
Rabbit anti-goat IgG-HRP	sc-2922, Santa Cruz Biotechnology

CPH1	Dr. Niklas Rye Jørgensen

Taqman Assays	
Cathepsin K	Hs01080388_m1, ABI
GAPDH	Hs99999905_m1, ABI
NFATc1	Hs00542678_m1, ABI
RANK	Hs00187189_m1, ABI

Primers and sequences	
Human GAPDH	Eurofins MWG Operon
GAPDH-Fv	5’-CAACGACCCCTTCATTGACC-3’
GAPDH-Rv	5’-TACTCAGCACCAGCATCACC-3’
Mouse Gapdh	Invitrogen, Life Technologies
Gapdh-Fv	5’-TTGTCAGCAATGCATCCTGC-3’
Gapdh-Rv	5’-GCTTCACCACCTTCTTGATG-3’
Mouse P2X7 splice variants	Kind gift from Prof. Dariusz C. Górecki (Nicke et al., 2009)
mX7ex1Fv-a	5'-CACATGATCGTCTTTTCCTAC-3'
mX7ex1Fv-k	5'-GCCCGTGAGCCACTTATGC-3’
mX7ex4Rv	5’-GGTCAGAAGAGCACTGTGC-3'

Laboratory Equipment	
Agilent 2100 Bioanalyser	Agilent Technologies
7900HT Real-Time PCR system	Applied Biosystems, Life technologies
BD™ Cytometric Bead Array	BD Biosciences
Bio-Rad GelDoc™ XR	Bio-Rad Laboratories
DMRB light microscope	Leica Microsystems
FACSCalibur	Becton Dickinson
Heraeus Megafuge 2.0R	DJB Labcare Limited
Inverted Light microscope	Olympus
Inverted widefield fluorescence microscope	Leica DMI 4000B
Labcut 1010 Low Speed Diamond Saw	Agar Scientific Ltd.
NanoDrop 1000 Spectrophotometer	Thermo Fisher Scientific
Neubauer haemocytometer	Weber
NOVOstar	BMG Labtech

Reflected light microscope	Olympus BX51
RNA 6000 Nano LabChip Kit	Agilent Technologies
RNA 6000 Pico LabChip Kit	Agilent Technologies
Sorvall Legend T centrifuge	Thermo Fisher Scientific
Techino Maxi table centrifuge	Thermo Fisher Scientific
Thermal cycler, Mastercycler	Eppendorf
SkyScan1172 high-resolution micro-CT scanner	Bruker microCT

Software	
Adobe®Photoshop® CS4 Extended	Version 11, Adobe systems Inc.
Cell Quest™ Pro Software	Version 3.3, BD Biosciences
Cell-D® software	Version 3.4, Olympus Soft Imaging Solutions GmbH
CT-Analyser	Version 1.8.1.2, Skyscan
CTvol: Realistic 3D-visualisation	Version 2.0.0.4, Skyscan
GraphPad Prism	Version 5.04, GraphPad Software, Inc.
IBM® SPSS® statistics	Version 20, IBM Corp.
Leica AF	Version 2.4.1 build 1111, Leica Microsystems GmbH
Leica Suite	Leica Microsystems GmbH
MARS Novostar Data Analysis	Version 2.00, BMG Labtech
Osteomeasure	Osteometrics
Quantity One software	Bio-Rad Laboratories
Seqence Detection Systems (SDS) 2.2.1	Version 2.2.1, Applied Biosystems

Plastics and disposables	
384-well PCR plate	Greiner Bio-One
6-mm cover slips	Richardson's of Leicester
96-well tissue-culture plates	Thermo Fisher Scientific
Dentine discs	Elephant ivory donated by HM Customs
Dnase, Rnase free PCR tubes, 0.5mL	Life Technologies
Eppendorfs (0.5 and 1.5mL)	The SARSTEDT Group
Filter tips (10, 20, 200 and 1000µl)	Starlab

Flow cytometer tube	ELKAY LAB PRODUCTS UK
Needle (25G x5/8")	Becton DickisonUK Ltd.
Optical adhesive covers, PCR compatible	Bio-Rad Laboratories
Parafilm	Parafilm® M
PCR tubes	Thermo Fisher Scientific
Storkbill Forceps	Richardson's of Leicester Ltd.
Strippets (5, 10 and 20ml)	Costar
Superfrost®PLUS microscope slides	VWR International
T75 flask	Thermo Fisher Scientific
Universal containers, Bijoux tubes	Starstedt

2.2. Methods

2.2.1. Cell culture

2.2.1.1. Human osteoclast generation

Peripheral blood was collected after consent from post menopausal women included in the Danish Osteoporosis Prevention Study (DOPS), under the ethical approval of the Danish Ethics Committee (up to 200mL) or from healthy donors included in the SMBRER36 study, following approval of the University of Sheffield, Research Ethics Committee (up to 100mL). CD14+ enrichment was done to isolate osteoclast precursors and procedure was optimised to obtain functional mature osteoclasts (Appendix I).

All blood samples were collected in Lithium Heparin vacutainer® tubes and diluted 1:1 (v/v) in cold PBS containing 2 mM EDTA (Buffer I). Mononuclear cells were isolated using Histopaque®-1077 and centrifuged at 400xg for 30 minutes without the brakes to isolate the 'opaque' mononuclear cell fraction. Mononuclear cells were collected from the layer and were centrifuged at 300xg in 5x vol. of Buffer I and cell number determined using haemocytometer. Cell count performed with 0.5 % (v/v) acetic acid to lyse the red blood cells. CD14 MicroBeads conjugated to monoclonal anti-human CD14 antibody were added 1:5 (v/v) in Buffer II (0.5% v/v BSA in Buffer I) per 10^7 total cells and incubated for 15 minutes at 4 °C. Cells were then washed in 2 mL Buffer II per 10^7 cells and resuspended at up to $1x10^8$ total cells in 500 µL Buffer II. The cell suspension was added to the appropriate column mounted on the magnetic separator, for positive selection of labelled cells. Unlabelled cells that passed through the column were mostly CD14-ve as assessed by flow cytometry. The column was removed from the separator and the magnetically retained cells (CD14+ fraction) were eluted and seeded at the density of $4.5 x10^4$ cells onto glass coverslips or dentine discs (day 0).

Cells were incubated in 100µl α-MEM containing 10% FCS, 100 IU/ml penicillin, 100 µg/ml streptomycin, 25 ng/ml M-CSF and 30 ng/ml RANKL.

2.2.1.2. Murine osteoclast generation

2.2.1.2.1. Animals

Colonies of P2X7R-/- were kindly obtained from Dr. Niklas Rye Jørgensen (Research Centre for Ageing and Osteoporosis, Glostrup, Denmark) which had been generated by backcrossing the Glaxo KO mice, onto the BALB/c background (Chessell et al., 2005; Syberg et al., 2012a). Briefly, KO mice were generated by targeted deletion of *P2rx7* gene by isolating partial sequences of 5' exons obtained from the genomic library of 129/Sv mice and creating a plasmid containing β-galactosidase insert (*lacZ*) as previously described (Le Mouellic et al., 1990). This plasmid was transfected in embryonic stem cells, which were selected due to their resistance to neomycin and determined positive for homologous recombination by polymerase chain reaction (PCR) prior to their injection into blastocysts. The resultant chimeric mice had disruption in the *P2rx7* gene and they were crossed with C57BL/6 females to produce heterozygotes which were then inter crossed to generate homozygous colonies. Success of gene knockout was confirmed by western blotting, PCR and by monitoring absence of YO-PRO-1 uptake following ATP stimulation of peritoneal macrophages (Chessell et al., 2005). It was only recently that KO maintained on C57Bl/6 background were backcrossed for five generations onto BALB/c background (Syberg et al., 2012a) to generate P2X7R-/- mice that are used in these experiments. The breeding colonies are now maintained in Sheffield (Sheffield, UK). Their WT controls were obtained from Charles River (Margate, UK), hereby known as P2X7R+/+.

Both $P2Y_{13}R$-/- and $P2Y_6R$-/- KO mice were supplied by Professor Jean-Marie Boeynams and Dr. Bernard Robaye (Universtité Libre de Bruxelles, Belgium) and were produced according to the method described elsewhere (Bar et al., 2008; Fabre et al., 2010). Their WT controls were obtained from Charles River (Margate, UK) and were the same strain as both $P2Y_{13}R$-/- and $P2Y_6R$-/-, hereby known as $P2Y_{13}R$+/+ and $P2Y_6R$+/+ respectively

All animals were housed in the same environmentally controlled conditions with a 12 hour light/dark cycle at 22 °C. All procedures complied with the UK Animals (Scientific Procedures) Act 1986 and were reviewed and approved by the local Research Ethics Committee of the University of Sheffield (Sheffield, UK) prior to initiating the experiments.

2.2.1.2.2. Generation of osteoclasts *in vitro*

Both KO and age matched WT female mice were sacrificed by cervical dislocation under Schedule I procedure at ages mentioned in Table 2-1. All animals were sterilized with 70% ethanol and their hind limbs or spleen were aseptically isolated.

To obtain osteoclasts from bone marrow (BM) of the mice, hind limbs were dissected and cleaned long bones were kept in PBS with 1% Penicillin/Streptomycin to avoid drying out. All connective tissue such as tendons, ligaments and muscles were removed to clean the bones as much as possible to minimize the contamination of cultures with fibroblasts and muscle filaments. Cleaned femur and tibia were washed 3 times in PBS containing 1% Penicillin/Streptomycin. The epiphysis of the bones were cut and marrow flushed out with PBS (15 mL for each mouse) using a 25-gauge needle. Marrow aspirate was centrifuged at 500xg for 3 minutes, washed once in PBS and resuspended in α-MEM, containing 10%FBS, 100 IU/ml penicillin, 100 µg/ml streptomycin, 150 ng/ml recombinant murine M-CSF (Step I medium). The cell suspension was then mixed with 0.5% acetic acid and a cell count obtained. Cells were seeded at a density of $5x10^6$ cells in T75 flask containing 15 mL step I medium. Following incubation for 24 hours at 37 °C, 5% CO_2 to allow attachment of stromal cells, non adherent cells were collected by centrifugation at 300xg for 10 minutes. Cells were washed in PBS and resuspended in Step I medium containing 30ng/ml recombinant murine RANKL (complete medium). Cells were seeded onto glass coverslips or dentine discs in 96 well plates at a density of $0.5x10^6$ per well and incubated overnight at 37 °C, 7% CO_2 to allow the attachment of osteoclast precursors. Next day, the wells were washed twice in α-MEM before replacing with 100µL complete medium.

For spleen derived osteoclasts, the spleens were removed and macerated in α-MEM to liberate the cells. The cell suspension was carefully layered onto Histopaque®-1077 and centrifuged at 400xg for 30 minutes without the brakes to isolate the mononuclear cell fraction. Cells were collected from the opaque interface layer and washed twice in α-MEM at 300xg for 20 minutes. The cell suspension was mixed with 0.5% acetic acid and a cell count obtained. Half a million cells were seeded onto glass coverslips or dentine discs and incubated for 90 minutes at 37 °C, 7% CO_2 to allow the attachment of osteoclast precursors, following which the wells were washed twice in α-MEM before replacing with complete medium.

Berthois et al., found that oestrogen-responsive cells grown in media with phenol red were significantly oestrogen stimulated, assessed by measuring cell proliferation and the levels of progesterone receptor (an oestrogen-stimulated protein) (Berthois et al., 1986). To achieve oestrogen depletory conditions *in vitro*, oestrogen free medium was used which was composed of phenol red free α-MEM, 100 Units/mL Penicillin, 100 µg/mL Streptomycin, 10% charcoal stripped FBS, 150 ng/ml M-CSF, and 30 ng/ml murine RANKL (-E). Treatment of serum with charcoal-dextran solution removes 96-98% oestradiol (ER agonist) (Eckert and Katzenellenbogen, 1982), briefly, dextran-coated charcoal is added to foetal bovine serum (1:20 v/v) for 30 minutes at 55 °C. Charcoal is then removed by centrifugation and supernatant collected and filtered before use. Commercially available charcoal stripped serum in combination with phenol-free α-MEM was used to obtain oestrogen depletion *in vitro*. Precursors obtained from either the mouse bone marrow or spleen were cultured on dentine discs at 37 °C, 7% CO_2 in normal complete medium (+E) or oestrogen depleted media (-E).

Respective media was replaced every 2–3 days until the completion of culture (Table 2-1) following which both glass coverslips and dentine discs were fixed in ice cold 10% buffered formalin.

Table 2-1 Details of murine osteoclast cultures.				
Genotype	**Age at cull**	**Substrate**	**Bone Marrow**	**Spleen**
P2X7R-/- and P2X7R+/+	12 weeks	Dentine	17 days	9 days
		Coverslips	9 days	7 days
$P2Y_6R$-/- and $P2Y_6R$+/+	5- 6 weeks	Dentine	11 days	9 days
		Coverslips	9 days	7 days
$P2Y_{13}R$-/- and $P2Y_{13}R$+/+	6- 7 weeks	Dentine	17 days	17 days
		Coverslips	9 days	9 days

* Differences in life span of osteoclasts were observed due to different genetic background of the mice and time points for $P2Y_6R$ and $P2Y_{13}R$ culture duration were previously optimised in the lab by S Gupta and N Wang respectively.

2.2.2. Immunological and Cytological Techniques

2.2.2.1. Flow cytometry

To analyse the purity of human CD14+ve enriched monocytes, at least 400,000 cells each from non-enriched PBMCs, enriched CD14+ve and CD14-ve cell fractions were collected and centrifuged at 1000xg for 5 minutes. The pellet was re-suspended in PBS (containing 1% v/v BSA to prevent non-specific binding) for 10 minutes at room temperature (RT). Cell suspension was split into two and stained with either monoclonal anti-human CD14 conjugated to R-phycoerythrin (R-PE) or isotype (mouse IgG1). Following 20 minutes incubation on ice, unbound antibodies were removed by washing twice with PBS and cells resuspended in 300 µL FACS Buffer. The fractions were analysed by Fluorescence-activated cytometry using the FACSCalibur and purity determined using Cell Quest™ Pro Software.

2.2.2.2. Dye uptake assay for pore formation

P2X7R is unique in its ability to form large membrane pores following continuous stimulation. Monocytes at day 2 and osteoclasts on glass

coverslips at day 14 were analysed for formation of membrane pores by assessing the YO-PRO-1 uptake (molecular weight 629.3).

Buffer containing 2.45µM probenecid (to prevent leakage of dye) in 0.6N NaOH and Hank's Balanced Salt Solution (HBSS) with 20mM HEPES, pH 7.4 without Ca^{2+} and Mg^{2+} was prepared (washing buffer). KN62 diluted in DMSO was used to pre-incubate cells for receptor antagonism and added to washing buffer at a concentration of 1 µM for 1 hour at 37 ° C. After the incubation, cells were washed using warm washing buffer and YO-PRO-1 was added at a final concentration of 4 µM. Using a plate reader, baseline measurements were performed for 10 seconds before stimulation for each well and measurements after stimulation with 500 µM BzATP were performed for a further 50 seconds per well. All measurements were done at 37 ° C and 5% CO_2, excitation at 485nm and emission at 520nm and auto fluorescence was obtained for a total of 60 seconds by injecting the cells with same volume of washing buffer (no stimulus). All curves were adjusted for auto-fluorescence and plotted as a fold change from baseline to obtain fold change in fluorescence and area under the curve.

2.2.2.3. Calcium influx assay

Rapid detection in changes of $[Ca^{2+}]_i$ in monocytes at day 2 and osteoclasts at day 14 were monitored by assessing the cell permeant ion sensitive fluorescent indicator Fluo-4/AM.

Fluo-4/AM binds to Ca^{2+} and absorbs light with the wavelength 485nm and emission at 520nm and was prepared in Pluronic F-127 (1:1 v/v, to help solubilisation of Fluo-4/AM). Buffer containing 2.45µM probenecid (to prevent leakage of dye) in 0.6 N NaOH and Hank's Balanced Salt Solution (HBSS) with 20 mM HEPES, pH 7.4 containing Ca^{2+} and Mg^{2+} was prepared (washing buffer). Fluo-4/AM was added to the cells at a final concentration of 2 µM with or without 1 µM KN62 (diluted in DMSO) and incubated at 37 °C in dark for 1 hour. Cells were washed using warm washing buffer and allowed to rest for 10 minutes before taking baseline readings. Using a plate reader, baseline was measured for 10 seconds before stimulation using 300 µM

BzATP and readings were taken for further 50 seconds per well. Auto-fluorescence was obtained for a total of 60 seconds by injecting cells with same volume of washing buffer (no stimulus). All measurements were done at 37 ° C and curves were adjusted for auto-fluorescence and plotted as a fold change from baseline to obtain fold change in fluorescence and area under the curve.

2.2.2.4. Soluble protein release in response to BzATP stimulation

Cell on glass coverslips were incubated with 1 µg/ml LPS at 37 ° C for 1 hour and a further incubation with 1 µM KN62 (diluted in DMSO) was performed for another 1 hour. After a total incubation of cells with LPS for 2 hours; the cells were stimulated using 300 µM BzATP for 30 minutes. Supernatant was collected and centrifuged at 300xg for 3 minutes to obtain supernatant clear of any cell debris. Control wells were treated with the same amount of complete medium (no LPS).

BD™ Cytometric Bead Array (CBA) was used to measure IL-1β, IL-6, IL-10, TNF and IL-8, in all cell supernatants. With the help of Sue Newton (Flow Cytometry Technician, Medical School, University of Sheffield), a multiplex assay was performed on all samples using a flow cytometer. The theoretical limit of detection was achieved by running individual standard curves for each cytokine, and the minimum and maximum quantifiable levels were defined for each BD™ CBA assay. Median fluorescence values are used to define the corresponding concentrations on standard curves and obtain the concentration of each cytokine. For the assays, cell culture supernatant was obtained from monocytes at day 2 or from osteoclasts grown on dentine at day 14 after treatments and snap frozen. Samples were diluted in assay diluent in order to ensure that the median fluorescence values were within the range of the standard curve (2500pg/ml - 0pg/ml). Capture beads coated with antibodies specific to the proteins were incubated with samples for 1 hour at RT. This was done in the dark to minimise the fluorescence decay of the capture beads. Photosensitive detection reagent was added to the samples and incubated for further 2 hour at RT in dark. Samples were washed to

remove unbound reagents using wash buffer after which, the supernatant was discarded. Beads bound to their corresponding protein were then resuspended in washing buffer and samples were analysed on flow cytometer.

2.2.2.5. Measurement of free calcium

Osteoclasts were grown on dentine discs and culture media was collected at day 21. Samples were sent to Pathology lab in Glostrup Hospital, (Copenhagen, Denmark) for analysis of free calcium using a calcium detection kit (Lonza).

2.2.2.6. Tartrate-Resistant Acid-Phosphatase (TRAP) staining

Cells on dentine discs and glass coverslips after 21 and 14 days in culture respectively were fixed using 10% buffered formalin and stained for TRAP. In this method, the iso-enzyme within the osteoclast reacts with the naphthol AS-BI phosphate whose product then reacts with the hexazotised pararosanaline. The end product is a red deposit in the cytoplasm of the cell (Barka, 1960).

Briefly, formalin was removed from the wells and cells were washed twice in tap water whilst attached to glass coverslips or dentine discs contained in a 96 well plate. Pre-warmed acetate-tartrate buffer (0.1 M Sodium tartrate in 0.2 M Acetate buffer, pH 5.2) was used to incubate samples at 37 °C for 5 minutes. Buffer was removed and samples were incubated for 30 minutes in 20 mg/mL Naphthol AS-BI phosphate/dimethylformamide prepared in acetate-tartrate buffer. After this, cells were incubated for 15 minutes in acetate-tartrate buffer hexazotised pararosaniline solution. Counterstaining was performed to visualise nuclei on glass coverslips and resorption pits on dentine discs using Gill's haematoxylin and wells were rinsed using tap water to remove excess stain. Both glass coverslips and dentine discs were carefully taken out from the wells and air-dried. Glass coverslips were mounted using DPX and dentine discs were stored dry.

2.2.2.7. Toluidine blue

Toluidine blue solution was prepared in distilled water by dissolving toluidine blue powder in 0.5 M sodium tetraborate (Borax in distilled water) solution to give a 0.5 % (w/v) toluidine blue solution.

Dentine discs were fixed in 10 % formalin and stained with 0.5 % toluidine blue solution for 3 minutes. Excessive stain was removed by repeated washing with 70 % ethanol and finally washed with distilled water before observing under the microscope.

2.2.2.8. Phalloidin staining

For glass coverslips: fixation was done using 10 % formalin and cells were incubated with rhodamine-conjugated phalloidin containing Hoechst solution (1 µg/ml) for 20 minutes at RT. Washing was done in PBS and coverslips were mounted in ProLong® Gold reagent. Dentine discs were fixed in 70 % ethanol and blocked using 10 % FBS before incubation with phalloidin at 4 °C for 12 hours. Washing was done in PBS and discs were air dried before observing under the microscope.

2.2.2.9. Calcitonin receptor

Following fixation, endogenous peroxidase were blocked using fresh 3 % (v/v) H_2O_2 in methanol for 10 minutes at RT. After washing in PBS, coverslips and discs were blocked using 5 % (v/v) rabbit serum made in PBS and anti-human CT-R or isotype (goat polyclonal IgG) was added at 2 µg/ml at 4 °C overnight. Following PBS washes, samples were incubated with an HRP conjugated secondary antibody (rabbit anti-goat IgG-HRP) at 0.5 µg/ml for 30 minutes at RT. DAB (3, 3'-diaminobenzidine) peroxidase solution (2.5mls H_2O, 1 drop buffer, 2 drops of DAB, 1 drop H_2O_2) was used for 5 minutes at RT (time for the development of brown substrate was determined by monitoring non-specific colour from the isotype samples). Cells were washed three times in distilled water and Gill's haematoxylin was used for nuclear counterstain on glass coverslips before mounting them in DPX. Dentine discs were air dried and observed under the microscope.

2.2.2.10. P2X7R staining

Coverslips fixed in 10 % formalin were carefully taken out of the wells and antigen retrieval was performed by trypsin digestion for 10 minutes at 37 °C. Cells were permeabilized with 0.1 % (v/v) Triton X-100 for 10 minutes and excess Triton X-100 was washed twice with PBS. Samples were blocked with 1 % (v/v) normal goat serum (NGS) for 90 minutes at RT. Mouse monoclonal anti-human P2X7 (P2X7mAB) was used at a dilution of 10µg/ml and control for non specific binding was an isotype (mouse IgG) diluted in NGS. Incubation was done for 1 hour at RT. After washing in PBS, Alexa Fluor® 488 Goat Anti-Mouse IgG (5 µg/mL) was applied for 1 hour at RT. Samples were washed to remove excess antibody and counterstained to visualize nuclei using Hoechst (1 µg/ml) for 20 minutes at RT. After a final washing, the coverslips were mounted using ProLong® Gold reagent for long-term storage. It was ensured that the coverslips were kept covered in staining solution or PBS to prevent high background.

2.2.3. Imaging and quantification

2.2.3.1. Osteoclasts

Osteoclasts on glass coverslips were defined as TRAP+ve cells containing 3 or more nuclei (Figure 2-1). Imaging was performed on a light microscope (Olympus BX51) and the number of osteoclasts were counted on the whole coverslip using the semi-automated Cell® D software. To calculate fusion index, 5 random images were taken at 10x magnification from each coverslip and all images were zoomed at 200% to better visualise the nuclei. Number of nuclei were counted and fusion index was measured as a percentage of the number of nuclei present in osteoclasts over the total number of nuclei within the field of view (Pellegatti et al., 2011). The area of TRAP+ve cells was determined by outlining each osteoclast with the help of fitted polygon function in Cell® D software.

Multiple images of whole dentine discs were taken at 5x magnification on the Olympus BX51 microscope and “stitched together” using the multiple alignment function in Cell-D® software. Osteoclasts were classed as

TRAP+ve cells (Figure 2-2) and the number of resorbing and non-resorbing osteoclasts were counted on the entire disc. Resorption lacunae were identified using reflective light microscopy and area of resorption on the entire disc was determined manually by using the wand feature in Cell-D® software.

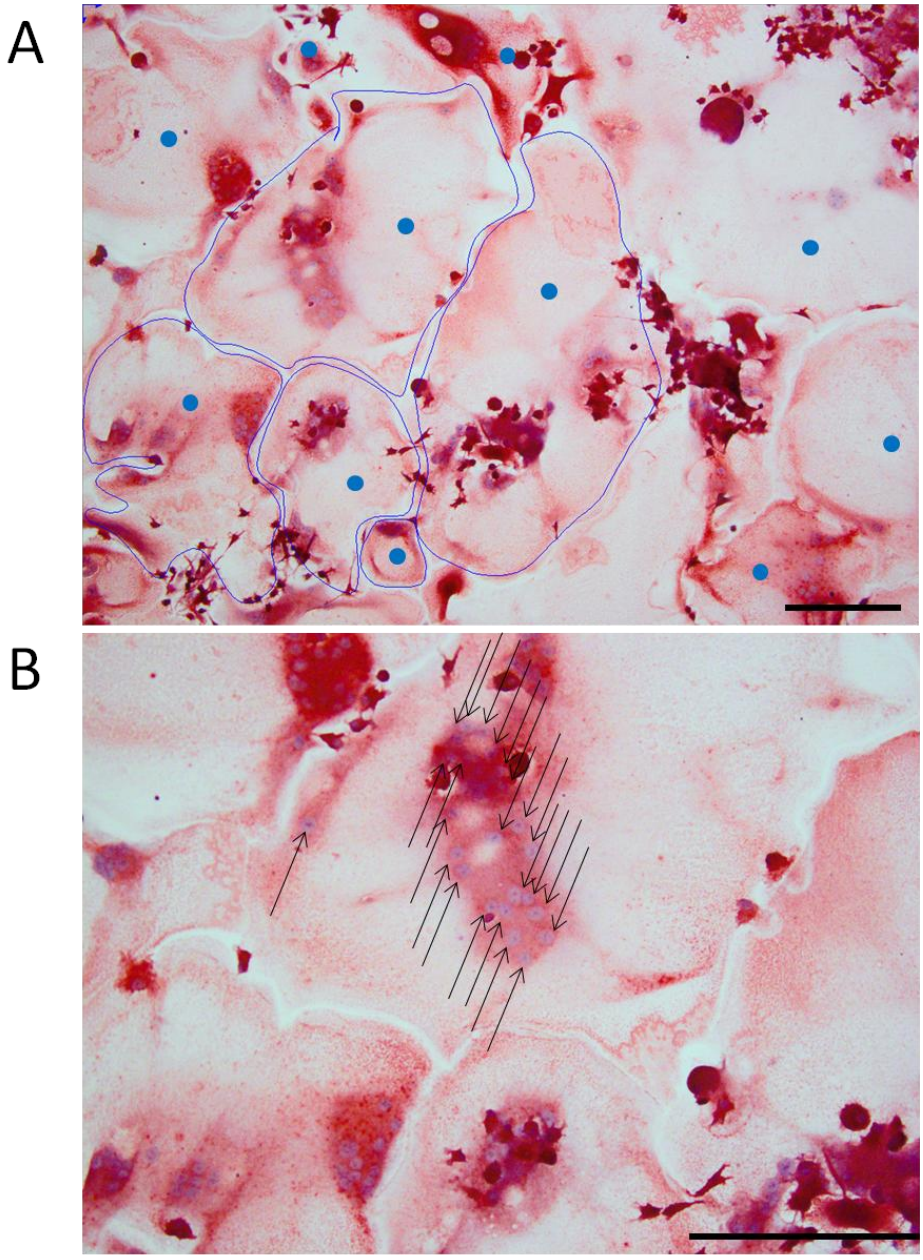

Figure 2-1 Quantification of osteoclasts on coverslip

(A) Images show mature osteoclasts classed as TRAP+ve and multinucleated (blue dots) and area of cells marked using the fitted polygon function (blue outline). (B) Higher magnification image to better visualize the nuclei (black arrows). Scale bar= 200µm.

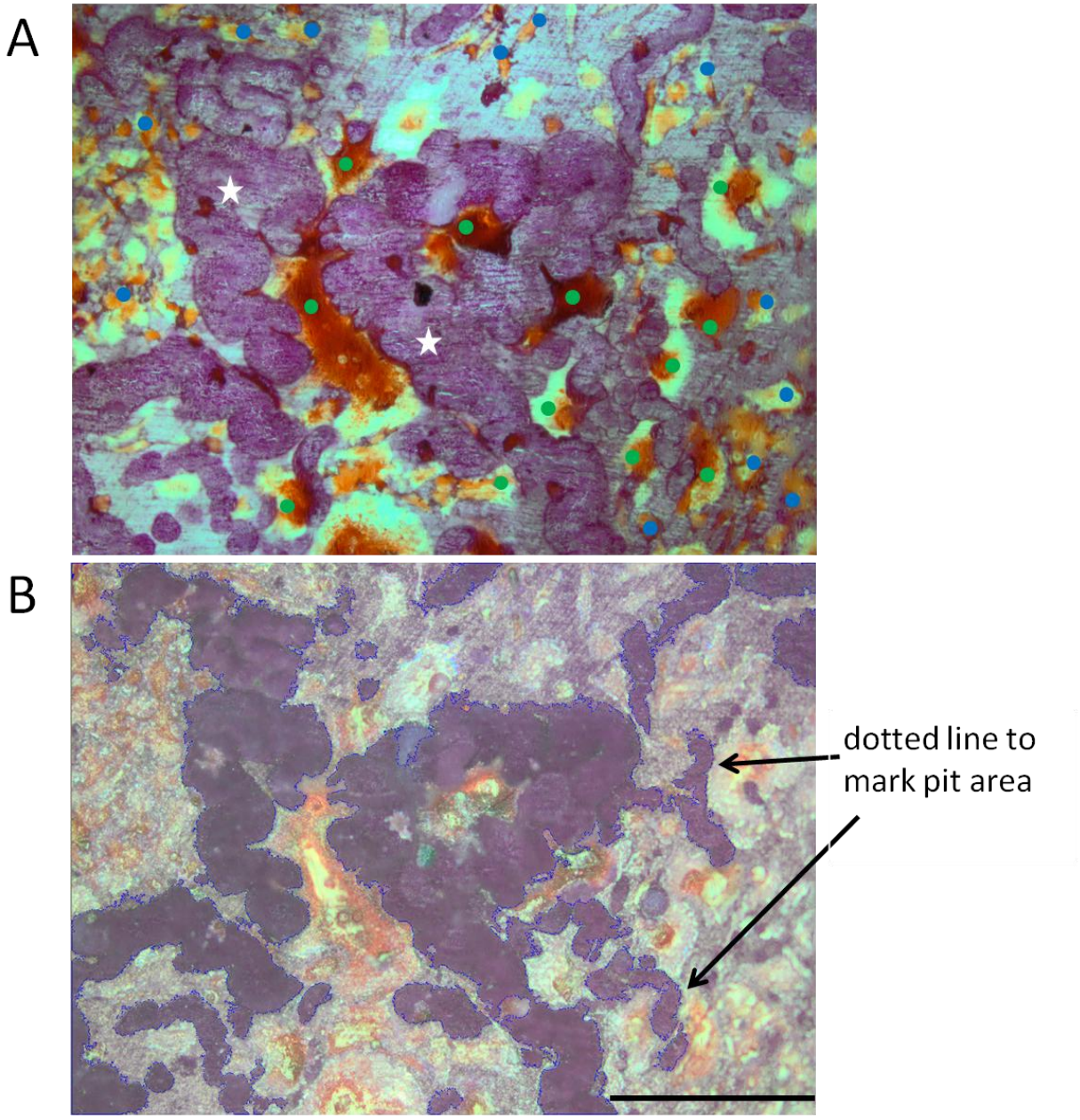

Figure 2-2 Quantification of osteoclasts on dentine disc

(A) Transmitted light image showing TRAP+ve osteoclasts classified as resorbing (green dot) in close proximity to a resorption pit (white stars). Other TRAP+ve cells were classed as non-resorbing (blue dots). (B) The corresponding reflected light image showing the area marked around the resorption pits (dotted line). Scale bar= 200µm.

2.2.3.2. P2X7R staining

To determine the expression of P2X7R on human osteoclasts, imaging was performed using the Leica DMI 4000B microscope with A4 and L5 filters for blue (nuclear stain using Hoechst) and green (Alexa Fluor® 488 conjugated to P2X7mAb) respectively.

Adobe® Photoshop® CS4 software was used on all images (including the background control) to adjust level on all raw images and uniformly eliminate the background. It was ensured that no background signal was detected by checking the settings against an isotype control.

2.2.3.3. Histomorphometry

Specimen preparation was carried out by the Bone Analysis Group, Mellanby Centre for Bone Research, The University of Sheffield. Histomorphometric analysis was performed as detailed below.

2.2.3.3.1. Sectioning of tibial bone

Briefly, left tibia of each animal was cleaned to remove connective tissue, fixed in 10 % formalin and decalcified for 4 weeks, with solution change every 7 days. Tibiae were processed through graded alcohol solutions and xylene overnight and embedded longitudinally in paraffin wax contained in a square mould. A Leica Microsystems RM2265 rotary microtome was used to cut 3 µm thick sections at 2 levels 50 µm apart. First, excess wax was trimmed from the block to expose a clear full face longitudinal sectional view of the tibia and cooled for 60 minutes on ice. Subsequently, consecutive sections were cut each 3 µm thick (L1) following which the bone was trimmed 50 µm deeper to cut more sections (L2). Strips from both levels were floated on a 45 °C water bath to flatten the marrow and endocortical bone before mounting the wrinkle-free sections on Superfrost®PLUS slides. These were dried gently without melting on a hotplate for 30 minutes and incubated at 37 °C overnight to allow attachment of sections to the glass slides. All slides were cooled to RT and stored at 4 °C before staining.

2.2.3.3.2. Osteomeasure

Slides were analysed on an upright DMRB light microscope and a semi-automated Osteomeasure system. All histomorphometric nomenclature and parameters were based on the recently revised recommendations by the ASBMR committee (Dempster et al., 2013) and were obtained using the Osteomeasure bone histomorphometry software (Osteometrics). Osteoclasts were identified as TRAP+ve (red) cells on both endocortical and trabecular bone (Figure 2-3 i). Osteoblasts were identified as 2 or more adjacent cobblestone cells on bone surfaces (Figure 2-3 ii). The number of osteoclasts per mm of bone surface (N.Oc/B.Pm), amount of bone surface occupied by osteoclasts (Oc.Pm/B.Pm), number of osteoblasts per mm of bone surface (N.Ob/B.Pm) and the coverage of osteoblast on bone surfaces (Ob.Pm/B.Pm) were determined on endocortical and trabecular surfaces. The number of adipocytes in bone marrow (N.Ad/ Ma. Ar) were also determined in the medullary area. The point where the growth plate joined the endocortical bone at a 90° angle was kept as reference and an offset was applied as shown in Figure 2-3. Endocortical bone was analysed over a total length of 3 mm on both anterior and posterior surfaces and trabecular bone over an area of 0.75 mm^2 in bone marrow was analysed.

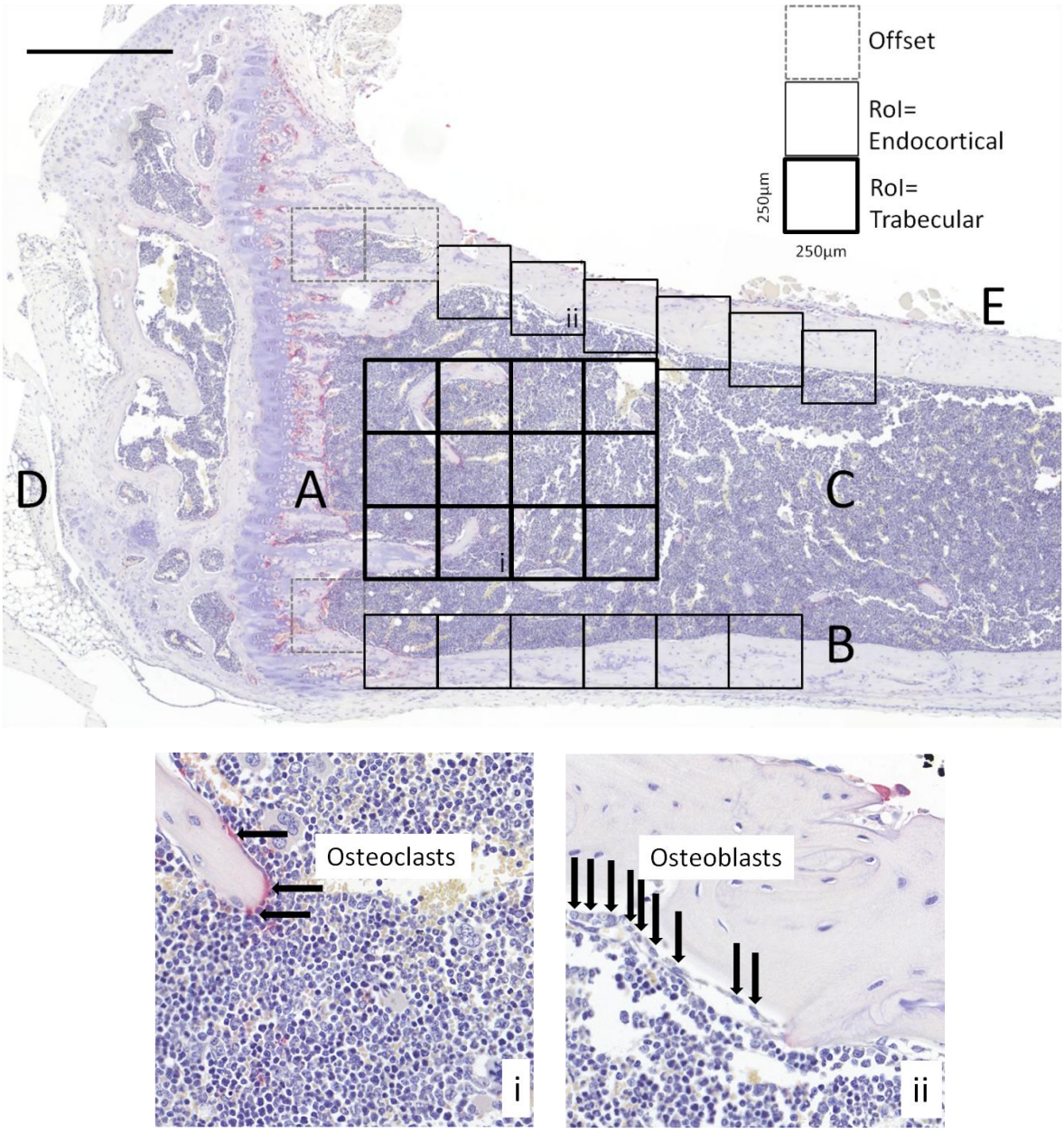

Figure 2-3 Histomorphometric analysis of bone sections

Mice tibial sections were TRAP stained and analysed on osteomeasure. Position where growth plate (A) joined endocortical bone (B) at 90° angle was kept as reference point and all measurements were performed in 250µmx 250µm fields. After applying offset, endocortical surface was analysed over a total of 3 mm length of the bone on anterior and posterior surfaces and trabecular analysis was done in 0.75 mm^2 medullary area (C). D shows the tibia-knee joint and E is periosteal bone surface. Black arrows mark the TRAP+ve osteoclasts (i) and 2 or more adjacent cobblestone cells classed as osteoblasts (ii). Scale bar= 500µm

2.2.4. Molecular Biology

2.2.4.1. Isolation of total RNA

Total RNA was extracted from all cells using TRI Reagent®, with the principle that a mono phasic solution of phenol and guanidine isothiocyanate disrupts the cells while maintaining the RNA integrity (Chomczynski, 1993). Adding chloroform results in separation of the solution with RNA contained exclusively within the aqueous phase and can be recovered by addition of isopropyl alcohol.

Precursor cells were obtained from either flushing the bone marrow or from the spleen buffy layer and lysed in 1 mL TRI Reagent® per mouse. To obtain RNA from mature osteoclasts, dentine discs were washed briefly in PBS at the completion of the culture and 30 µL of TRI Reagent® was used per disc for cell lysis. All samples were snap frozen and stored at -80 °C until needed for RNA extraction. Samples were allowed to thaw on ice and allowed to stand at RT for 5 minutes to ensure complete dissociation of nucleoprotein as per the manufacturer's instructions. Chloroform (200 µL per 1 mL of TRI Reagent®) was added and mixed vigorously by inversion for 15 seconds to obtain a biphasic mixture and incubated at RT for 5 minutes for complete dissolution of RNA. Following centrifugation at 12000xg for 5 minutes at RT, the upper aqueous phase containing RNA was carefully transferred into a clean centrifuge tube. Isopropanol (0.5 ml per 1 mL of TRI Reagent®) was added to this isolated aqueous phase and samples were mixed by inversion. Incubation was performed for 30 minutes at RT following which RNA pellet was obtained by centrifugation at 12000xg for 10 minutes at 4 °C. The pellet was washed for 5 minutes at 4 °C in ethanol (1 mL of 75 % per 1 mL of TRI Reagent®) and air dried on ice before dissolving in 20 µL ultra pure water. Aliquots were taken for RNA quantity and quality measurements and all dissolved samples were stored at -20 °C for up to a week.

2.2.4.2. Determination of RNA quantity and integrity

2.2.4.2.1. Nanodrop spectrophotometer

NanoDrop 1000 Spectrophotometer utilises absorbance of dissolved sample to assess the concentration and the purity of RNA samples. Dissolved RNA (1 µL) was added onto the lower pedestal known as the fibre optic cable (receiving fibre) and the second fibre optic cable (source fibre) was closed onto the receiving fibre, resulting in bridging the gap between the two fibre optic ends with the liquid sample contained. Using the light source, which is a xenon flash lamp, passing light is analysed by the spectrophotometer. Absorbance at 260 nm gave the value of the concentration of the nucleic acid sample and ratios 260/280 and 260/230 were used to determine the presence of proteins and co-purified contaminants respectively. Ultra pure water used to dissolve all RNA samples was also used as the blank sample both before and after the sample measurements.

2.2.4.2.2. Bioanalyser

Integrity of the samples was determined using the Agilent 2100 Bioanalyser. Agilent RNA kits were used and in principle, each chip contains reservoirs for sample, gel, intercalating dye and ladder (external standard containing fragments of known sizes and concentration) all interconnected by microchannels fabricated within the chip glass. On-chip gel electrophoresis is performed when charged RNA is driven under voltage gradient and molecules are separated by size in the presence of a sieving polymer according to their mass-to-charge ratio. Dye molecules intercalate into the RNA fragments as they migrate and are detected by laser-induced fluorescence and are translated into gel-like images (bands) and electropherograms (peaks) onto the screen.

According to the manufacturer's instructions for either RNA 6000 Nano LabChip kit or RNA 6000 Pico LabChip kit, gel matrix was spin filtered by centrifugation at 1500xg for 10 minutes at RT. Gel-dye mix was prepared by adding 1 µL dye concentrate to 65 µL of filtered gel matrix and vortexed before being spun at 13000xg for 10 minutes at RT. This gel-dye mix was

then added to the well marked for gel on the chip with the help of a priming station consisting of a plunger to push the gel into the capillaries. Loading of the gel dye mix was done in 2 steps where 9 µL is pipetted each time with a wait of 60 seconds to allow even distribution of gel and without entry of bubbles in the channels. Nano marker (5 µL) was added in all wells before addition of 1 µL of ladder or samples. The chip was then vortexed on a horizontal vortexer for 1 minute at the set speed of 2400 rpm before being analysed by the Agilent Bioanalyser. When running a pico chip, 9 µL of pico conditioning solution is added in one of the sample wells to increase the assay performance and Pico marker (5 µL) is used in all wells.

RNA integrity number (RIN) was used to determine the degradation in the RNA sample. RIN is a software algorithm that utilises the entire electrophoretic trace of a sample based on a numbering system between 1 and 10, 1 being the most degraded and 10 being the most intact sample. Figure 2-4 shows the representative electropherograms for different RIN samples and RIN in combination with the 28s/18s rRNA ratio was used to adequately determine the sample integrity. It allowed for a comparison of the samples and ensured repeatability of experiments as RIN is independent of sample concentrations and user interpretation of samples. Sampels with RIN ≥ 8 were considered good quality and used for all experiments.

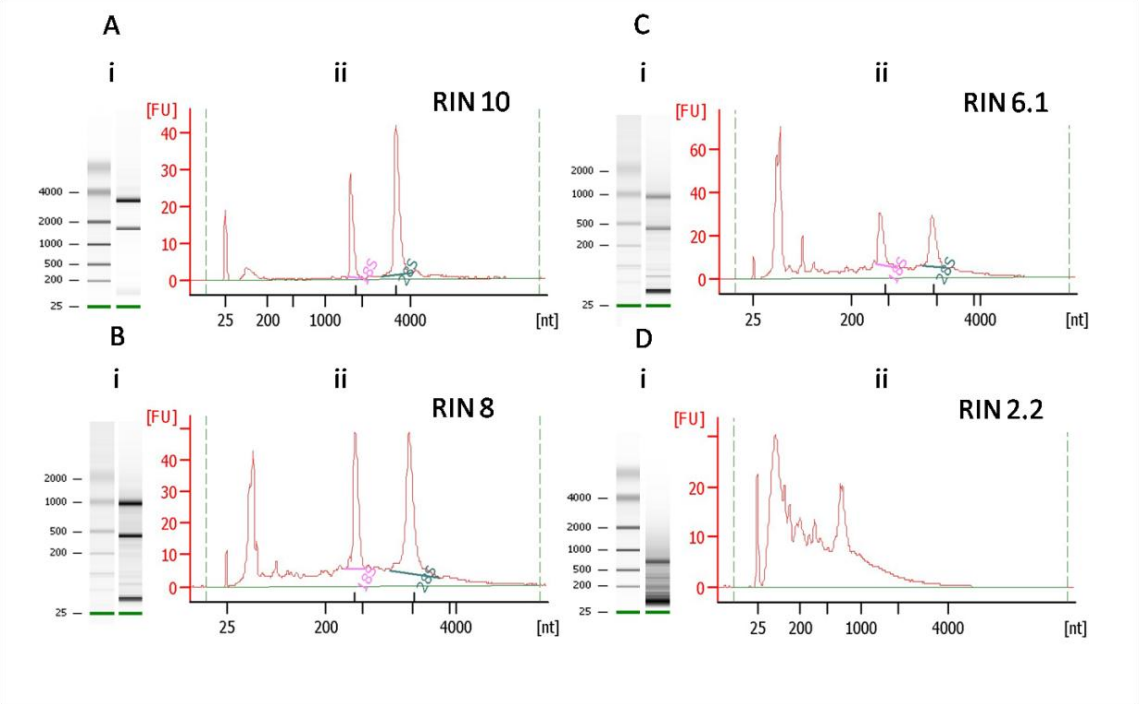

Figure 2-4 Example images showing RIN detection by bioanalyser

Total RNA samples were analysed using Agilent 2100 Bioanalyser using the RNA 6000 Nano LabChip kit or RNA 6000 Pico LabChip kit. Dye molecules intercalate with the RNA fragments and are detected by laser-induced fluorescence (y-axis) before being translated into gel-like images (i) and electropherograms (ii) according to the sizes of the bases (x-axis). A shift towards shorter fragment sizes is observed with sample degradation and corresponding electropherograms are used to calculate RIN. RIN=10 suggests no degradation in the sample (A), RIN= 8 suggests good quality sample (B), RIN=6.1 suggests some degradation (C) whilst RIN=2.2 suggests a degraded sample (D).

2.2.4.3. First strand cDNA synthesis

To synthesise cDNA, Promega ImProm-II™ reverse trancriptase and Oligo(dT) primer were used according to the manufacturer's instructions.

2.2.4.3.1. Annealing of primer to RNA template

Equivalent amounts of RNA template from all samples was added to 0.5 µg/µL Oligo(dT) primer (4:1 v/v). For no template control, water was used instead of the RNA template. The template-primer was heated at 70 °C for 5 minutes for the Oligo(dT)s to bind to the polyA tail of the mRNA, creating the first strand cDNA. Reaction was terminated by chilling at 4 °C for 5 minutes and samples were held on ice.

2.2.4.3.2. Reverse transcription

While on ice, 15 µL reverse transcription mix was prepared according to the table below and was aliquoted in each reaction tube. Negative controls were set up where reverse transcriptase was replaced by an equal amount of water (-RT) and where RNA template was replaced by an equal amount of water (no template). Reverse transcription was performed by firstly, annealing at 25 °C for 5 minutes followed by first strand synthesis of cDNA at 42 °C for 60 minutes. Reverse transcriptase was heat inactivated at 70 °C for 15 minutes. Synthesised cDNA was stored at -20 °C before confirming the success of the cDNA synthesis by endpoint PCR.

Component	Amount per reaction
Improm-II 5x Reaction Buffer	4µL
$MgCl_2$ (3mM)	2.4µL
dNTP mix (0.5mM)	1µL
ImProm-II Reverse Transcriptase	1µL
Nuclease-free water	6.6µL

2.2.4.3.3. End point PCR

Using Promega GoTaq® DNA polymerase and the primers designed to anneal to house keeping gene glyceraldehyde-3-phosphate dehydrogenase gene (GAPDH) (human, *GAPDH* gene; mouse, *Gapdh* gene), successful cDNA synthesis was confirmed by visualising the amplified products on an electrophoretic gel (Figure 2-5). No template, -RT were used in parallel with the samples to detect genomic contamination in samples. For each 10 µL reaction, the reaction mix was prepared as tabulated below and primer sequences are given in section 2.1

Component	**Amount per reaction**
5X Green GoTaq® Reaction Buffer	2µL
Forward primer (0.2µM)	0.4µL
Reverse primer (0.2µM)	0.4µL
dNTP mix (0.2mM)	0.2µL
GoTaq® DNA Polymerase (5u/µl)	0.05µL
nuclease free water.	5.95µL
cDNA template	1µL

Cycling conditions for human *GAPDH* gene, mouse *Gapdh* gene and analysis of mouse P2X7R splice variants are tabulated below. The mouse splice variants were amplified using either forward primer mX7ex1Fv-a (specific to isoform a), mX7ex1Fv-k (specific to isoform k) combined with mX7ex4Rv, common reverse primer in exon 4 for P2X7(a) and P2X7(k) respectively (Figure 2-6) (page 74). The identity of the PCR products of P2X7R splice variants was confirmed by sequencing.

	Temperature	Number of cycles	Duration
Human *GAPDH* gene			
Initial denaturation	95 C	1	1 minute
Denaturation	95 °C	20	30 second
Annealing	59 °C	20	30 second
Extension	72 °C	20	30 second
Final Extension	72 °C	1	10 minute
Mouse *Gapdh* gene			
Initial denaturation	95 °C	1	1 minute
Denaturation	95 °C	30	1 minute
Annealing	48 °C	30	1 minute
Extension	72 °C	30	1 minute
Final extension	72 °C	1	10 minute
Mouse P2X7R splice variants- P2X7(a) and P2X7(k)			
Initial denaturation	94 °C	1	1 minute
Denaturation	94 °C	35	40 second
Annealing	48 °C	35	40 second
Extension	72 °C	35	40 second
Final extension	72 °C	1	10 minute

All PCR products were examined with 1 % (w/v) agarose gel containing 50 ng/ml ethidium bromide in TBE Buffer under 200V and visualised under a Bio-Rad GelDoc ™ XR+ Gel imaging system with Quantity One software.

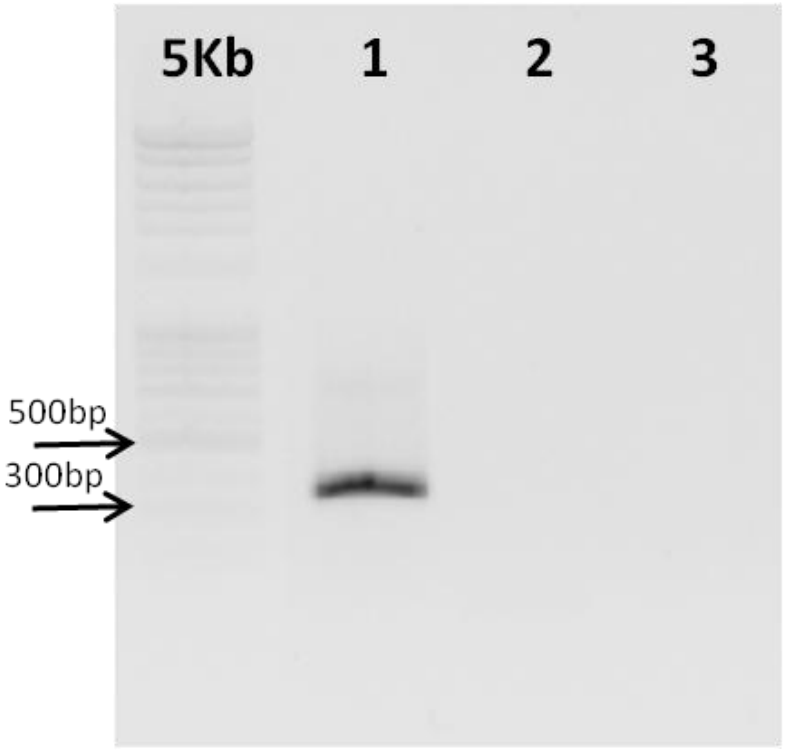

Figure 2-5 End point PCR to confirm successful cDNA synthesis

First strand cDNA synthesis using Oligo(dT) primer was performed on equivalent amounts RNA templates with no reverse transcriptase (-RT) controls. Products were visualised under UV light following electrophoresis using 1 % agarose gel in the presence of 50ng/ml ethidium bromide. A typical result showing 354bp product (*Gapdh*) (lane 1), omission of reverse transcriptase (-RT) (lane 2) and no template (water, lane 3).

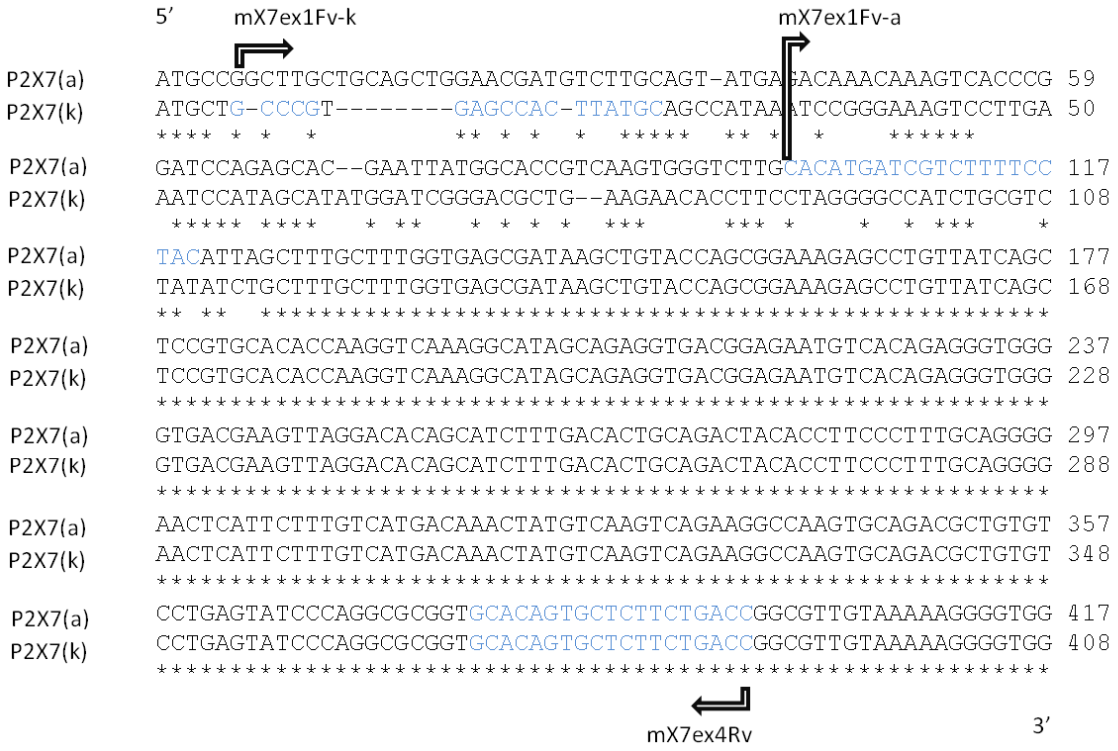

Figure 2-6 Schematic showing the location of primers for P2X7(a) and P2X7(k) variants

Primer sequences (blue) specific for P2X7(a) (mX7ex1Fv-a) and P2X7(k) (mX7ex1Fv-k) variants and a common reverse primer (mX7ex4Rv). Expected product size of mX7ex1Fv-a + mX7ex4Rv is 297bp and mX7ex1Fv-k+ mX7ex4Rv is 390bp. Stars represent conserved base pairs between the two transcripts.

2.2.4.4. TaqMan qRT-PCR

A TaqMan quantitative real-time PCR (qRT-PCR) reaction contains gene specific forward and reverse primers along with the probes labelled with a fluorescent reporter dye which was 6-carboxyfluorescein (FAM) at 5' end and a non-fluorescent quencher dye at 3' end. During the reaction, probes anneal to the complementary denatured single stranded cDNA between the sites for forward and reverse primers. The DNA polymerase cleaves the quencher dye during the extension process and the fluorescence signal from the fluorescent dye will be detected. The cycle threshold (CT) is measured which is the number of cycles at which each specific reaction crosses a selected threshold and is set to exclude the noise and usually lies in the middle of the linear region of logarithm amplification plot where the amplification was increasing exponentially. High CT values meant that more amplification cycles are needed to reach the threshold fluorescence intensity due to lower amount of template cDNA in the sample. Therefore CT is a relative measure of the concentration of the template sequences in the samples.

Species specific TaqMan® Assays were used to determine the expression of selected genes. For each gene of interest, the reaction mix contained 5 µL TaqMan gene expression mastermix, 0.5 µL Assay, 2.5 µL nuclease free water and 2 µL cDNA template. Each assay tube was mixed by vortex before loading on a 384 well PCR plate. Negative control contained 2 µL of water instead of a cDNA template. Each cDNA sample was loaded in triplicate and plate was sealed using optical adhesive covers. Plate was analysed using Applied Biosystems 7900HT Real-Time PCR system and data analysis performed on the SDS 2.2.1 software.

TaqMan® Array Custom Micro Fluidic cards (LDA) are 384 well cards, were custom designed by Dr. Ning Wang to assess the expression of 96 genes in 2 different samples simultaneously. Each reaction could be performed in duplicates and cards were designed to contain 5 housekeeping genes and 91 genes of interest. A total of 420 µL reaction mix containing equal amount of P2X7R+/+ and P2X7R-/- cDNA templates and 210 µL 2xTaqman Universal PCR Master mix was prepared and final volume was made up with nuclease-

free water. Samples were vortexed gently to ensure thorough mixing and centrifuges briefly. In each reservoir (4 per sample) 100 µL reaction mix was added and the loaded array card was centrifuged twice at 331xg for 1 minute using the Sorvall Legend T centrifuge using card specific buckets and holders. Each card was sealed using the Taqman® array micro fluidic card sealer and quantitative PCR was performed on an Applied Biosystems 7900HT Real-Time PCR system with a Taqman® micro fluidic card cycling block. The cycling conditions were 1 cycle of 50 °C for 2 minutes, 1 cycle of 94.5 °C for 10 minutes followed by 40 cycles of denaturation at 97 °C for 30 seconds and annealing/extension at 59.7 °C for 1 minute.

Using the SDS 2.2.1 software, baseline can be set to remove background fluorescence signal from the reaction mix and from the early stages of amplification. To ensure uniformity across genes and samples, constant threshold and baseline values were set at 0.2CT and 3-15 cycles respectively. Replicates within 0.5 CT of each other were analysed by ΔΔCT method as mentioned by (Livak and Schmittgen, 2001). Relative quantification of the target templates was performed by normalizing to house keeping genes that were either GAPDH (*GAPDH*) or β-actin (*Actb*) using the formula ($\Delta CT = CT_{target} - CT_{housekeeping}$). Fold changes in difference in expression of target genes was expressed as ΔΔCT ($\Delta\Delta CT = \Delta CT_{P2X7R+/+} - \Delta CT_{P2X7R-/-}$) and was calculated by taking 2 to the power of ΔΔCT ($2^{-\Delta\Delta CT}$). For LDA analysis, a heatmap showing differential expression of genes between samples was generated using 'GenePattern' web software (http://www.broadinstitute.org) from the reciprocal value of ΔCT (ΔCT^{-1}).

2.2.5. *In vivo* experiments

2.2.5.1. Animals and study design

Female mice on BALB/c strain were obtained from Charles River and all treatments and procedures were performed in Dr. Niklas Jørgensen's laboratory by Dr. Susanne Syberg, Glostrup, Denmark. Animals were housed in conditions approved by The Danish Animal Welfare Council and all animal procedures were approved in advance. After completion of the study, long bones and vertebrae were dissected and shipped to Sheffield, fixed in 10 % formalin.

Briefly, mice at 16 weeks of age were divided into 7 groups and were either ovariectomized (OVX) or sham-OVX (SHAM) operated. At 20 weeks (4 weeks after surgery), animals were assigned to the following groups (1) SHAM (baseline surgery control), (2) OVX (baseline control), (3) OVX+PTH (positive control), (4) OVX+0 (vehicle), (5) OVX+25 (25mg antagonist), (6) OVX+100 (100mg antagonist), (7) OVX+400 (400mg antagonist). Groups 1 and 2 were sacrificed at the age of 20 weeks and the rest of the OVXed animals were treated with daily injections of PTH (40 mg/kg s.c. twice daily, group 3) or oral gavage with vehicle (PEG-400, group 4) or P2X7R antagonist dissolved in PEG-400 (groups 5,6 and 7). Treatments continued for 4 weeks and mice in groups 3 to 7 were sacrificed at 24 weeks of age (Figure 2-7).

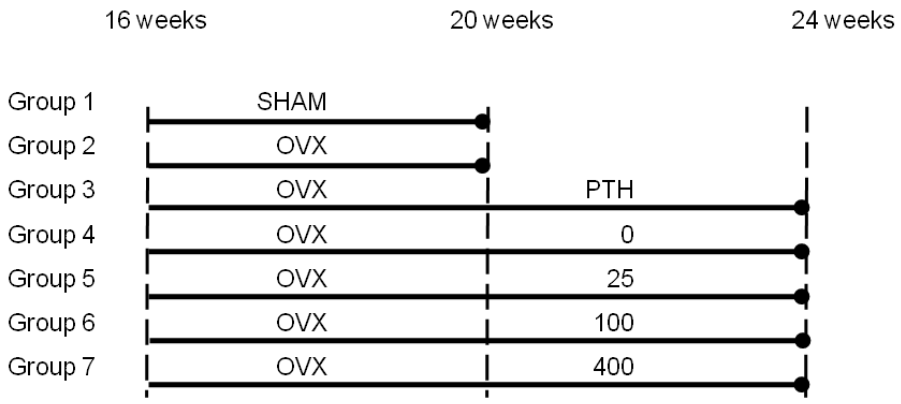

Figure 2-7 Schematic showing the treatment regime in different groups.

2.2.5.2. Micro-Computed Tomography

Vertebrae, tibia and femur were dissected free of soft tissue and scanned using Skyscan 1172 System.

High resolution scans were used to obtain trabecular bone architecture. L4 vertebra (counting down from T13, i.e. last vertebra with ribs attached) was scanned at a resolution of 4.3µm with 360° rotation with a frame being shot at every 0.7° rotation. Each scan took approximately 15 minutes. Trabecular scan areas of interest in long bones were identified as proximal tibial metaphysis and distal femoral metaphysis. Scanning was performed at a resolution of 4.3 µm at 180° degree rotation and an average of 2 frames shot at every 0.7° rotation. Each scan took approximately 12 minutes. The X-ray generator was set at approximately 50 kV voltage and 200 uA current bearing a 0.5mm filter at the x-ray source.

Whole bone scans were done at a resolution of 17µm and 360° rotation, a frame being shot at every 0.7° rotation with the source energy of 50 kV voltage and 200 uA current as before. Each scan took an average of 16minutes.

Reconstruction on all scans was performed using a greyscale range of 0-0.16 and CTAn was used to for all 2D analysis and obtain scan parameters.

To analyse the trabecular structure in L4 vertebrae, regions were selected in the central 30 % height of each vertebra for analysis (Figure 2-8). Trabecular bone was selected in the region of the centrum. In long bones, reference point was considered as the first break in growth plate bridge and consisted of regions of interest (ROIs) drawn through 0.5-1.5mm distal to tibial bridge and 0.6-1.6mm distal to femoral bridge (Figure 2-10). ROIs on both femur and tibial trabecular bone consisted of 233 slices. All trabecular ROIs were manually defined to eliminate cortical bone and the parameters measured included:

Bone volume (BV), Percent bone volume (BV/TV), Trabecular thickness (Tb.Th), Trabecular number (Tb.N), Trabecular separation (Tb.Sp),

Trabecular bone pattern factor (Tb.Pf), Structure model index (SMI) and Degree of anisotropy (DA).

As shown in Figure 2-11, whole bone ROIs in tibiae were taken as the joining of the triangular structures at the proximal end to the distal end where fibula split from the tibia. The fibula was excluded. Femora were analysed between the joining of triangular structures at the distal end until the appearance of femoral head at the proximal. Cortical ROIs were considered at the midshaft, through 1/3rd the length between the two reference regions (Figure 2-11). Parameters measured were:

Bone mineral density (BMD), Bone volume (BV), Percent bone volume (BV/TV) and Marrow volume (Ma.V).

Micro-computed tomographic analyses were performed before initiation of treatments (SHAM and OVX) and then after 4 weeks of treatment (PTH, 0, 25, 100 and 400).

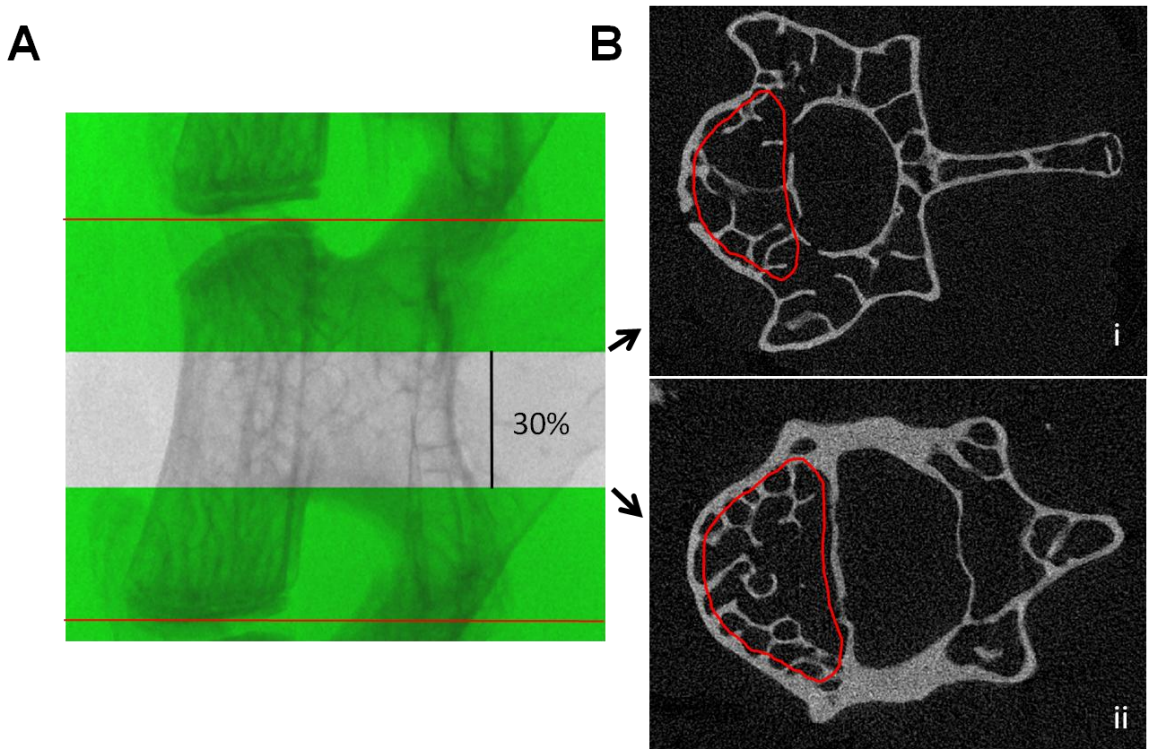

Figure 2-8 Example image of µCT ROI selection for trabecular analysis of murine L4 vertebra.

Scout view showing the reference points (red horizontal lines) (A) that were selected as region of analysis in the central 30 % height of vertebra (grey). Cross sectional views (B) showing the trabecular bone in the region of the centrum (red outline, i and ii) selected as the ROI.

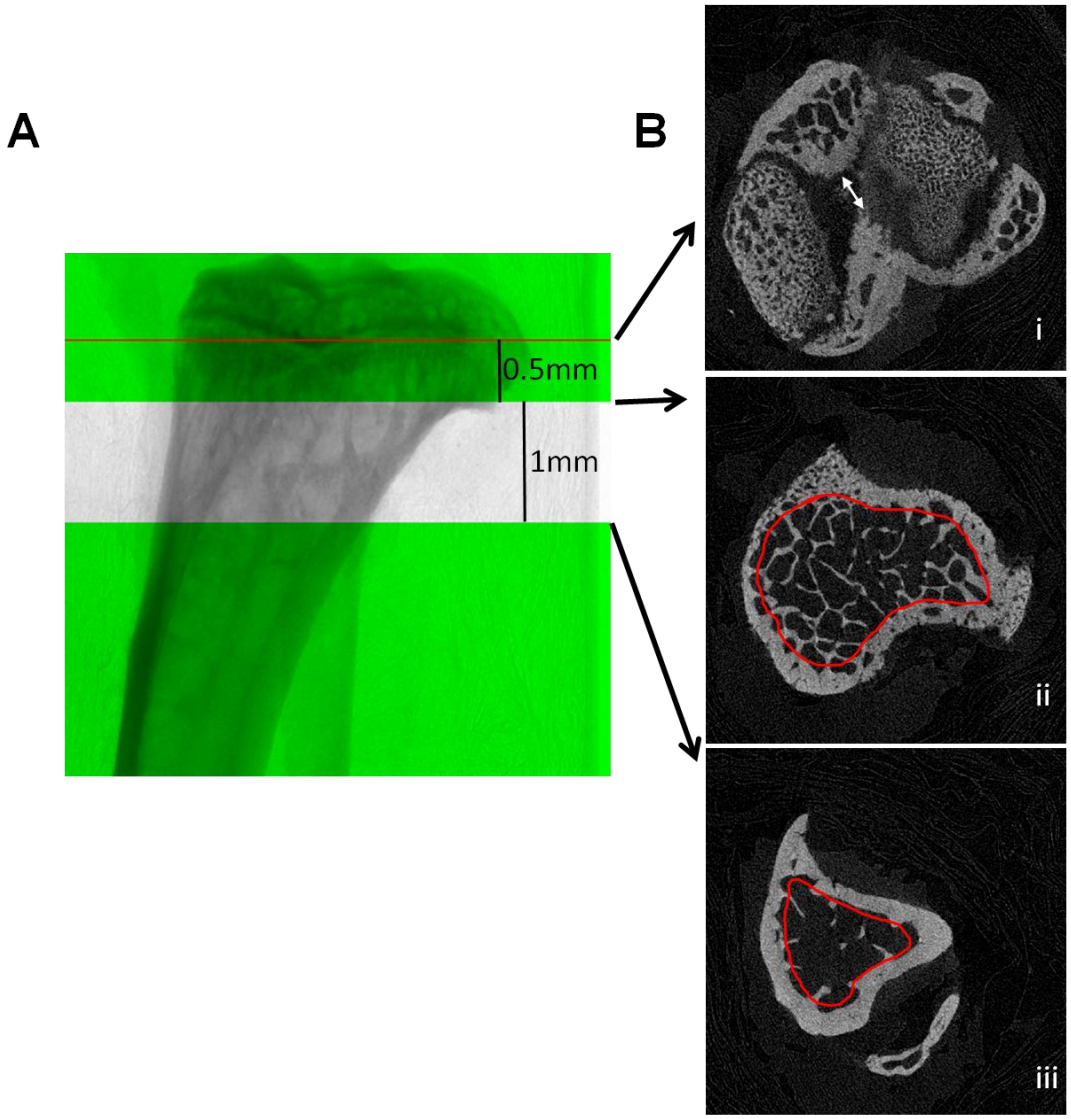

Figure 2-9 Example image of µCT ROI selection for trabecular analysis of murine tibia

Scout view showing the reference point (red horizontal line), 0.5 mm offset and the 1mm selected region of analysis (grey) (black horizontal lines) (A). Cross sectional views (B) showing the typical reference point which was considered as the first break in growth plate bridge (i, white arrow) and selected trabecular bone as the ROI (red outline, ii and iii).

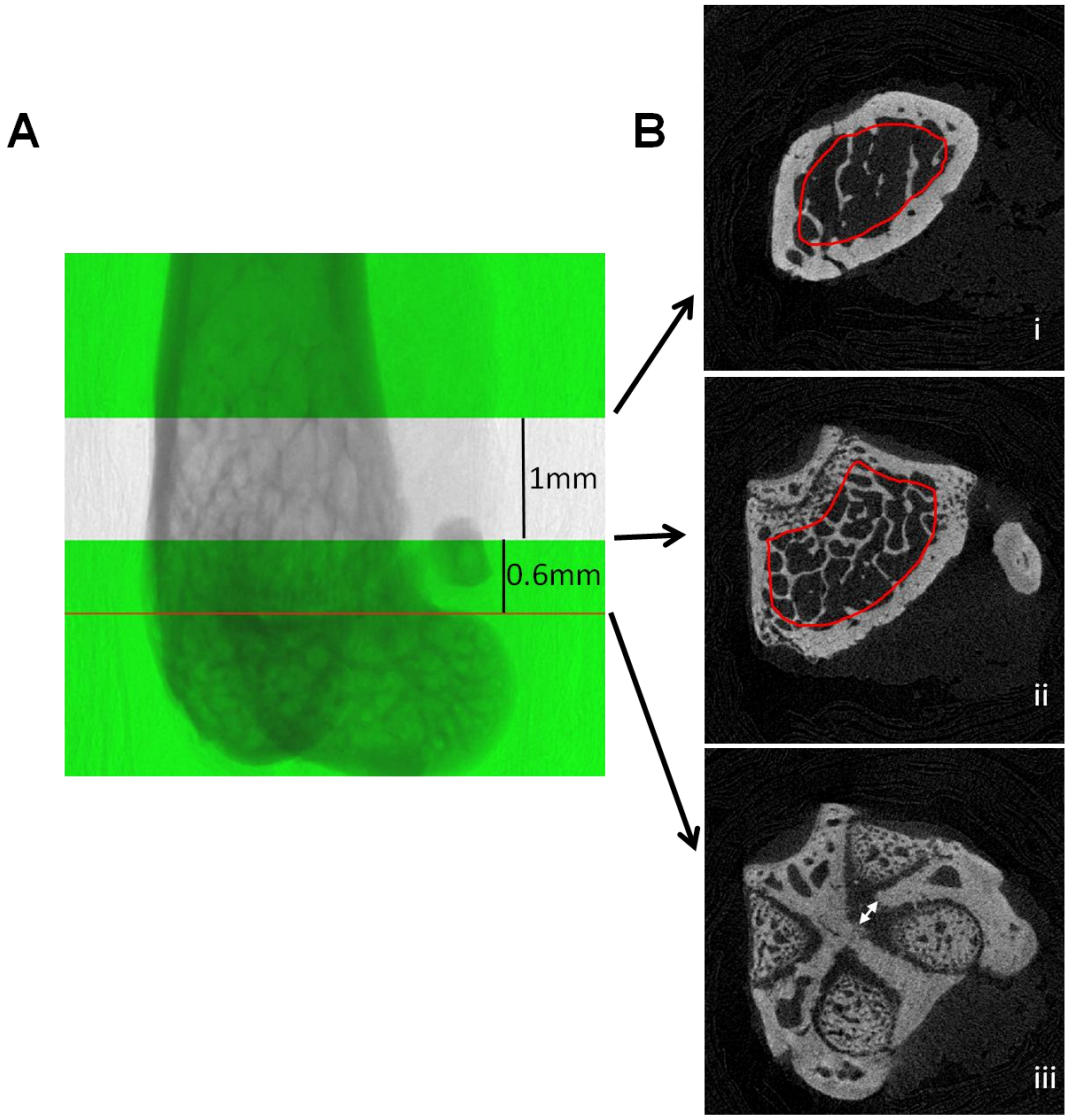

Figure 2-10 Example image of µCT ROI selection for trabecular analysis of murine femur

Scout view showing the reference point (red horizontal line), 0.6 mm offset and the 1mm selected region of analysis (grey) (black horizontal lines) (A). Cross sectional views (B) showing the typical reference point which was considered as the first break in growth plate bridge (iii, white arrow) and trabecular bone as the ROI (red outline, i and ii).

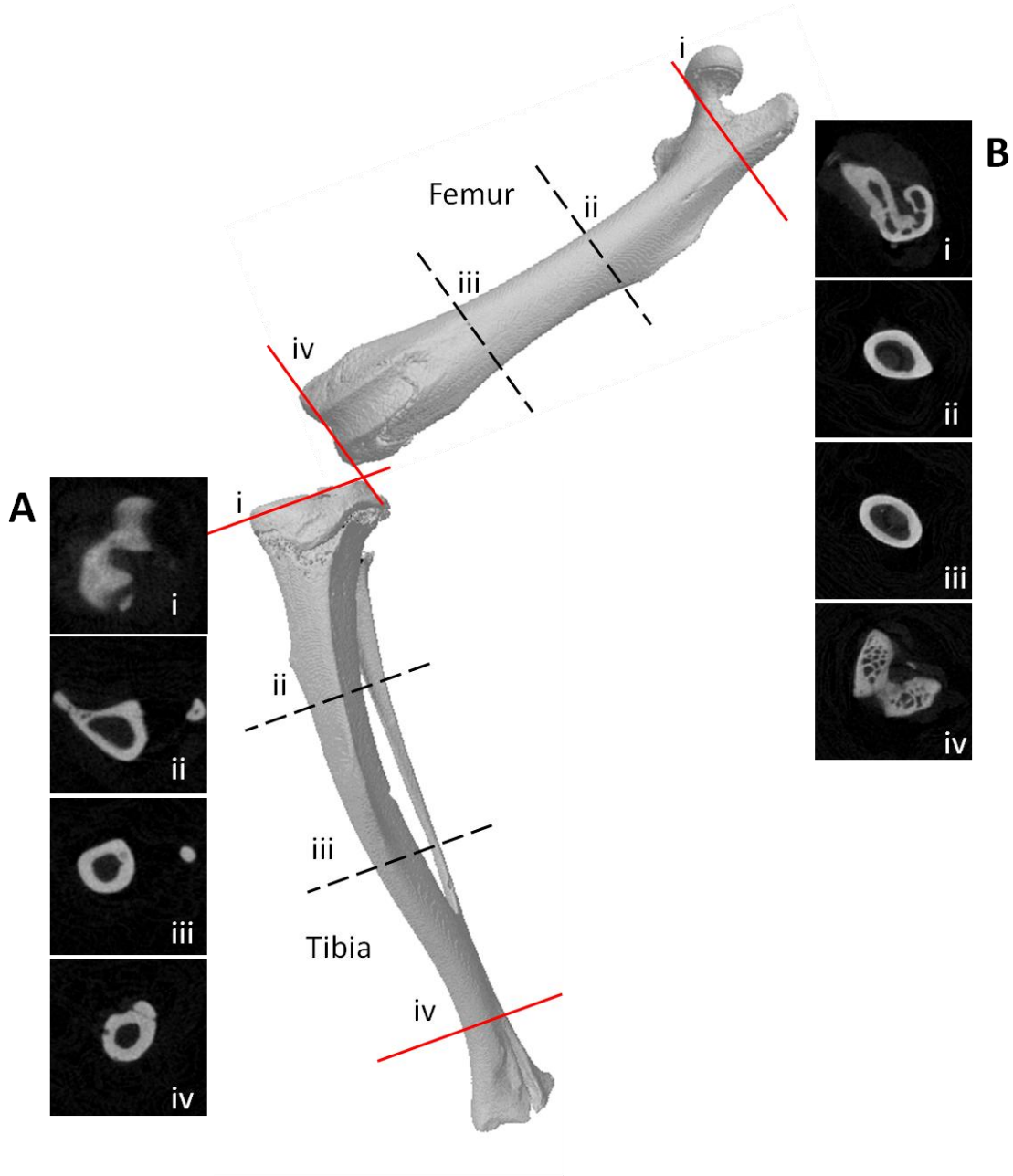

Figure 2-11 Example image showing selection of ROI for cortical and whole bone analysis of murine tibia and femur.

Images show typical reference points (horizontal lines) and the corresponding cross sections on tibia (A) and femur (B). Whole bone analysis was selected between joining of the triangular structures (red horizontal lines) (A-i and A-iv on tibia; B-i and B-iv on femur) and cortical bone analysis was selected in the central 1/3rd of the midshaft (broken lines) (A-ii and A-iii on tibia; Bi and B-iii on femur). Fibula was excluded.

2.2.6. Statistical analysis

GraphPad Prism, was used to analyse data and all graphs are expressed as mean ± standard deviation (SD). Data was tested for normality and statistical significance was determined by either parametric or non-parametric tests as appropriate using Prism 5 software. For two groups, non-parametric data was analysed by unpaired student's t-test with Mann Whitney post-test or univariate analysis of variance using IBM® SPSS® statistics. To compare the effects of treatment, 1 way ANOVA with Dunns post test for non-parametric data were used.

TaqMan® Array Custom Micro Fluidic card data analysis was expressed as fold change and values of greater than ±2 were considered significantly different as they represent doubling (>2) or halving (<-2) in the template copy numbers.

2.3. Method Optimisation- Isolation of enriched monocytes and generation mature osteoclasts from human peripheral blood

2.3.1. CD14+ve enrichment of osteoclast precursors

2.3.1.1. Assessment of purity of CD14+ve cells following enrichment

Human peripheral blood mononuclear cells (PBMC) are a heterogeneous mix of monocytes and lymphocytes. In order to obtain minimal contamination by lymphocytes, the protocol was developed to isolate an enriched population of osteoclast precursor cells (Section 2.2.1.1).

At least 200,000 cells were stained from PBMCs, eluted CD14-ve fraction and magnetically retained CD14+ fraction. Cell fractions were fixed using 10% (w/v) PFA for 10 minutes and stained with R-phycoerythrin (R-PE) conjugated antibody to either the cell surface CD14 (mouse anti-human CD14+) or an isotype control (Mouse IgG). Samples were analysed by flow cytometry and each cell was considered as an 'event'. Up to 50,000 events were recorded from each sample and dot plots of forward scatter (cell size) versus side scatter (cell granularity) (Figure 2-12). Gating was done on the Cell Quest™ Pro Software to include all monocytic populations but exclude cellular debris and clumps of cells. Corresponding histograms were obtained after gating to determine the percentage of flourescently labelled CD14+ve cells in each cell fraction (Figure 2-12) . Cells were considered labelled only if their fluorescence was brighter than the isotype control.

Using the protocol, monocultures were set up with >95% purity of CD14+ve cells monocytes. A loss of approximately 2% CD14+ve cells was seen in the eluted CD14-ve fraction.

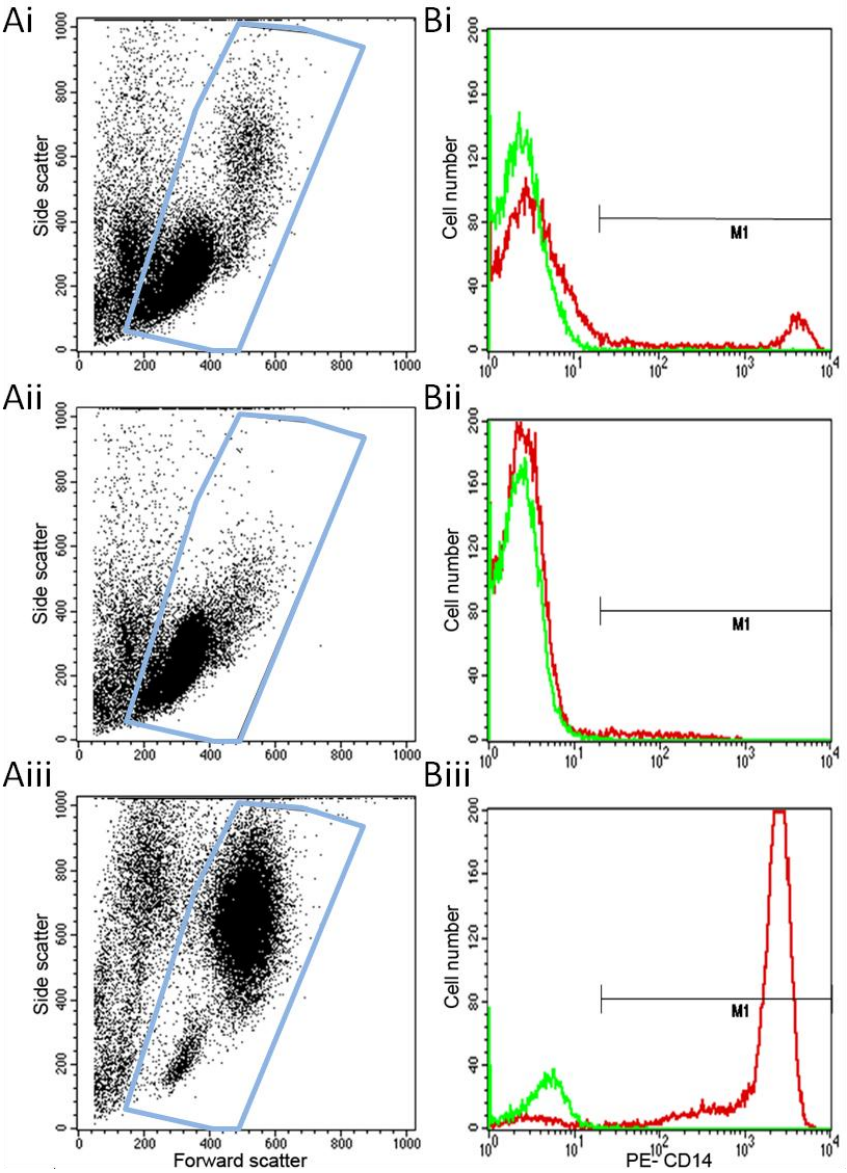

Figure 2-12 Representative flow cytometry plot following CD14+ve enrichment

Dot plots (A) showing the cell size (x axis, forward scatter) vs granularity of the cell (y axis, side scatter) were obtained from (i) post-ficoll PBMCs (ii) eluted CD14- cells and (iii) magnetically retained CD14+ cells. All cells were stained using R-PE conjugated anti-CD14 or isotype control antibody. Gating (blue rectangle) to include mononuclear cells and obtain corresponding histograms (B), showing R-PE positive (red trace) and negative (green trace) cells. M1 marks the cells that were considered positive and purity was > 95% following enrichment.

2.3.2. Characterisation of osteoclasts.

Enriched monocytes were seeded at a density of 45,000 per well in a 96 well plate in the presence of recombinant M-CSF and RANKL. Formation of multi-nucleated cells on glass coverslips was monitored from day 0 -day 21 and resorption lacunae were detected at day 21 on dentine discs, as described in (Agrawal et al., 2012). Further characterisation of osteoclasts with the help of osteoclast markers was performed and is detailed below.

2.3.2.1. TRAP staining

Osteoclasts from TRAP deficient mice have reduced resorptive ability owing to a defect in their ruffled borders and distribution of intracellular transport vesicles (Hollberg et al., 2002). The TRAP enzyme is abundantly expressed in osteoclasts and over expression is associated with increased bone turnover (Angel et al., 2000).

Enriched CD14+ve monocytes and PBMCs were fixed at day 0, day 7, day 14 and day 21 and stained to determine TRAP expression (Section 2.2.2.5). At day 0, cells were small and no TRAP expression could be detected from either CD14+ve or PBMC populations (Figure 2-13). At day 7, precursors were beginning to fuse and TRAP+ve cells were detected with varying intensity of TRAP stain between the cells. PBMC derived cells appeared to be more heterogeneous with a higher number of TRAP-ve cell clusters compared to CD14+ve population. At day 14, cell cytoplasm was larger and stained strongly for the TRAP enzyme in cells derived from the enriched CD14+ve precursors. At day 21, cells continued to fuse and cells derived from both CD14+ve precursor and PBMC populations showed a distinct osteoclast like appearance with high TRAP expression (Figure 2-13).

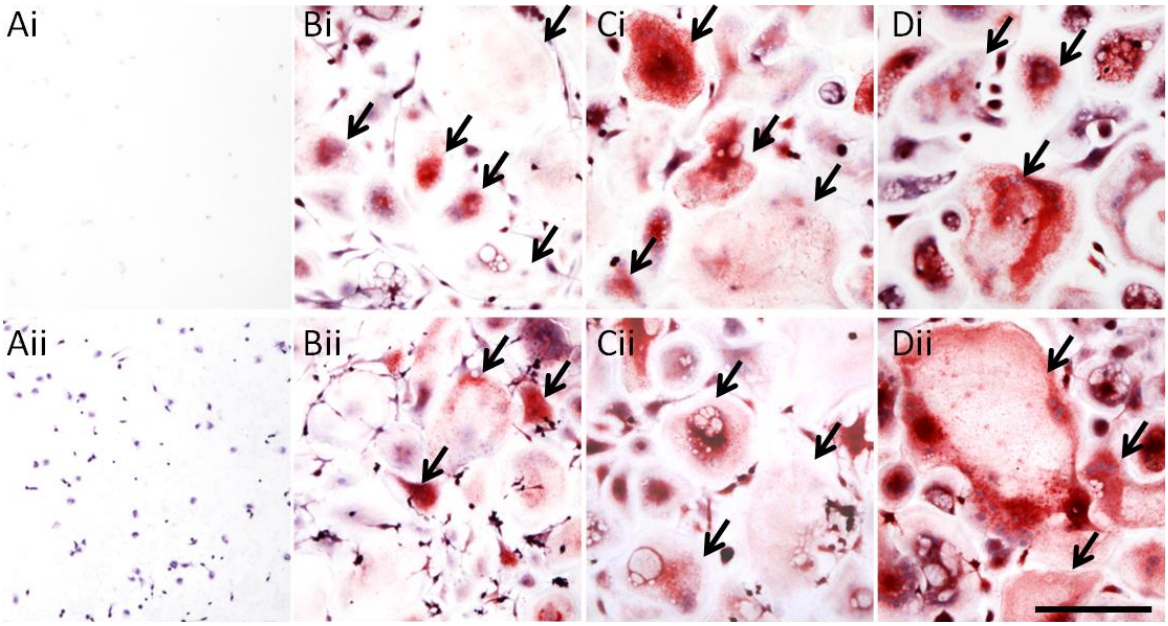

Figure 2-13 Differentiation of TRAP+ve cells on glass coverslips.

Representative images of TRAP stained osteoclasts (black arrows) formed *in vitro* from 45,000 CD14+ve precursors (i) or PBMCs (ii). Neither population showed TRAP at day 0 (A) and cells were mostly small, but cells started to fuse with TRAP expression being detected on 7 (B), day 14 (C) and day 21 (D). Scale bar= 200µm

2.3.2.2. Detection of resorption

Osteoclasts are bona fide resorbing cells and the ultimate marker of a mature and active osteoclast is its ability to resorb. Dentine discs were used as bone substrate *in vitro* and appearance of resorption lacunae was monitored after toluidine blue staining (Section 2.2.2.7).

Osteoclasts capable of creating resorption cavities were generated from both CD14+ve enriched monocytes and non-enriched PBMC cells. In general, onset of resorption occurred at day 14 and osteoclasts had a rounded morphology compared to the stromal cells which were spindle shaped. There was a higher proportion of spindle shaped cells in dentine discs seeded using unsorted PBMCs, whereas cells differentiated after microbead enrichment were more uniform and osteoclast like (Figure 2-14).

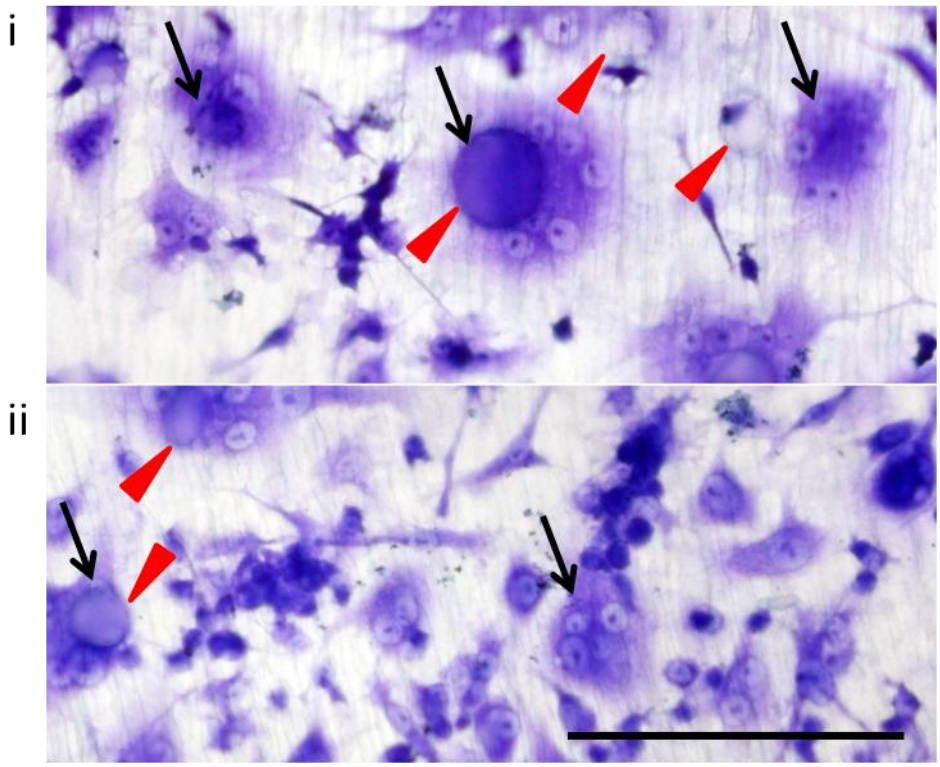

Figure 2-14 Images of toluidine blue stained dentine.

Onset of resorption *in vitro* was monitored after staining the dentine discs with toluidine blue. Resorbing osteoclasts (arrows) were obtained from both CD14+ monocytes (i) and unsorted PBMCs (ii) and resorption pits (triangles) could be detected from day 14. Scale bar= 100µm.

2.3.2.3. Actin ring formation

Osteoclasts are highly motile and in order to resorb the bone matrix, they need to form a tight attachment to the bone surface. Formation of this attachment involves the rearrangement of cytoskeleton into a dense belt-like structure, known as the actin ring (Lakkakorpi et al., 1989; Luxenburg et al., 2007). Presence of actin ring is a hallmark of a resorbing osteoclast and presence of an organised actin ring was assessed in osteoclasts differentiated from enriched CD14+ve monocytes.

Glass coverslips were stained at day 14 and dentine discs at day 21 as described in Section 2.2.2.8. On glass coverslips, initiation of belt-like structures could was detected towards the cell periphery (Figure 2-15). On dentine discs, dense rings forming a tight attachment to the dentine in close association with resorption pits were observed (Figure 2-15).

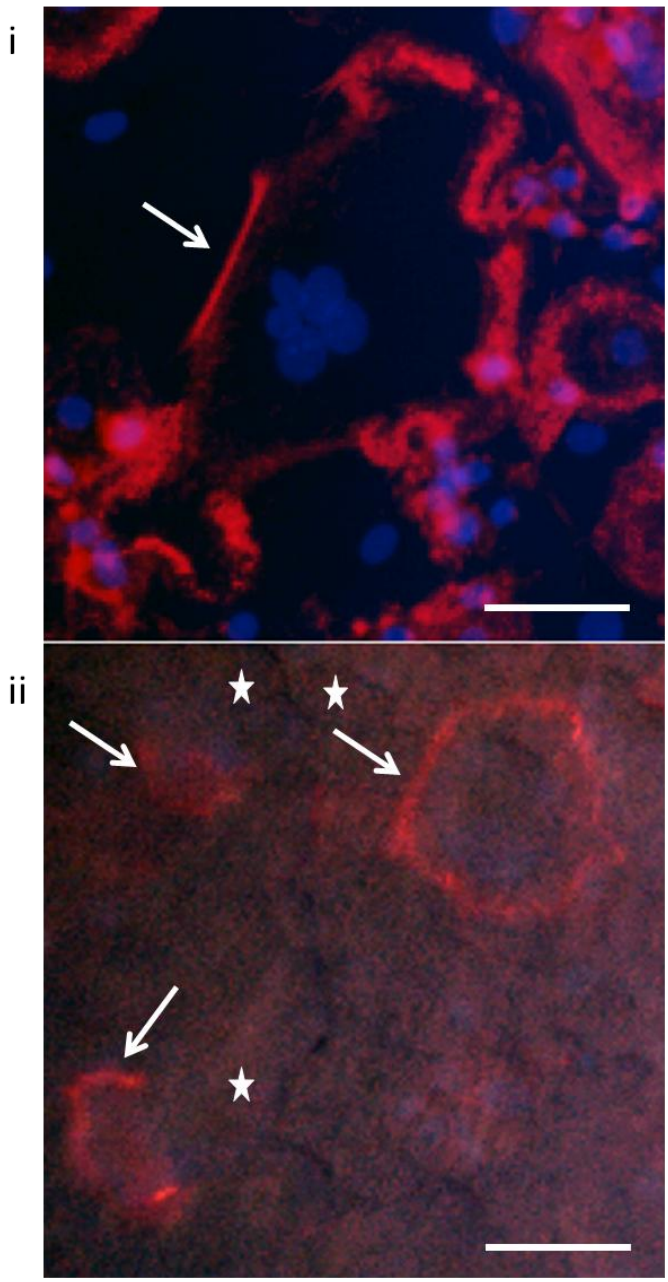

Figure 2-15 Images of actin ring formation

CD14+ve cells were stained using rhodamine phalloidin to determine the formation of actin ring (red, white arrows) on glass coverslips (i) and dentine discs (ii). Beginning of formation of belt-like structure (white arrow) was observed on glass coverslips and on dentine discs in close proximity to resorption lacunae (stars). Scale bar= 50µm

2.3.2.4. Expression of calcitonin receptor

Calcitonin (CT) hormone is a known inhibitor of osteoclastic bone resorption acting through its cell surface receptor (CT-R) present on mature osteoclasts. Calcitonin was demonstrated to block endocytosis from the ruffled border, an important event imperative during normal osteoclastic resorption (Stenbeck et al., 2012). Osteoclasts differentiated from enriched CD14+ve monocytes were stained to detect the expression of CT-R, in order to determine whether their behaviour would be identical to mature osteoclasts.

Glass coverslips were stained at day 14 and dentine discs at day 21 as described in section 2.2.2.9. CT-R expression was detected in multinucleated cells on glass coverslips and on resorbing cells on dentine discs (Figure 2-16).

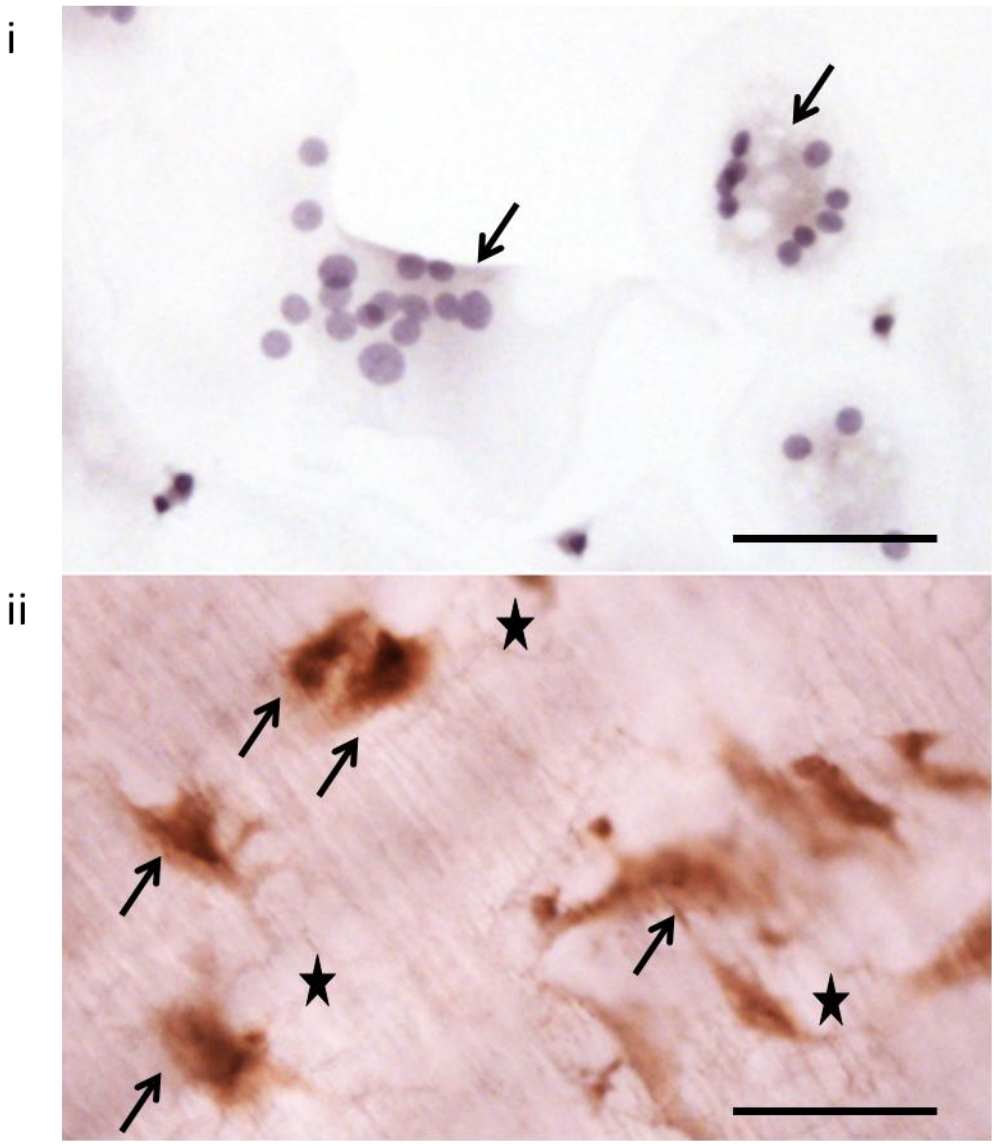

Figure 2-16 Images showing CT-R expression

CD14+ve cells were stained for anti-human CT-R and a secondary antibody (HR-P) conjugated to a peroxidase enzyme (DAB) and brown staining shows the expression of CT-R on mature osteoclasts (arrows) on glass coverslips (i) and in close proximity to resorption pits (stars) dentine discs (ii). Scale bar= 50µm

2.3.2.5. Gene expression

Expression of RANK on precursor cell surface is needed for RANKL activity and commitment of precursors to osteoclast fate whereas NFATc1 and Cathepsin-K are imperative for osteoclast differentiation and activity. TaqMan Assays were utilised to determine the expression of RANK, NFATc1 and Cathepsin-K in CD14+ve cells at different stages of osteoclastogenesis. Gene expression changes were calculated as described in section 2.2.4.4 and are shown as fold change from day 2.

Changes in expression of RANK and NFATc1 were not significant (<2 fold) in CD14+ve cells generated on glass coverslips. However, expression of cathepsin-k showed significant increases with different stages of osteoclastogenesis 764.5 fold (day 7), 2405.5 fold (day 12) and 3816.89 fold (day 14).

Significant fold changes (>2 fold) with osteoclast differentiation were observed in transcripts for RANK, Cathepsin-K and NFATc1. CD14+ve cells on dentine discs showed 10.7 fold (day7), 73.8 fold (day 12) and 30.1 fold (day 14) change in RANK transcript compared to day 2. Expression of cathepsin-K changed from 15.3 fold (day 7), 995.9 fold (day 12) and 2661.6 fold (day 14) whereas NFATc1 expression increased from 1.9 fold (day 7), 8 fold (day 12) and 6.3 fold (day 14) compared to the expression at day 2 (Figure 2-17).

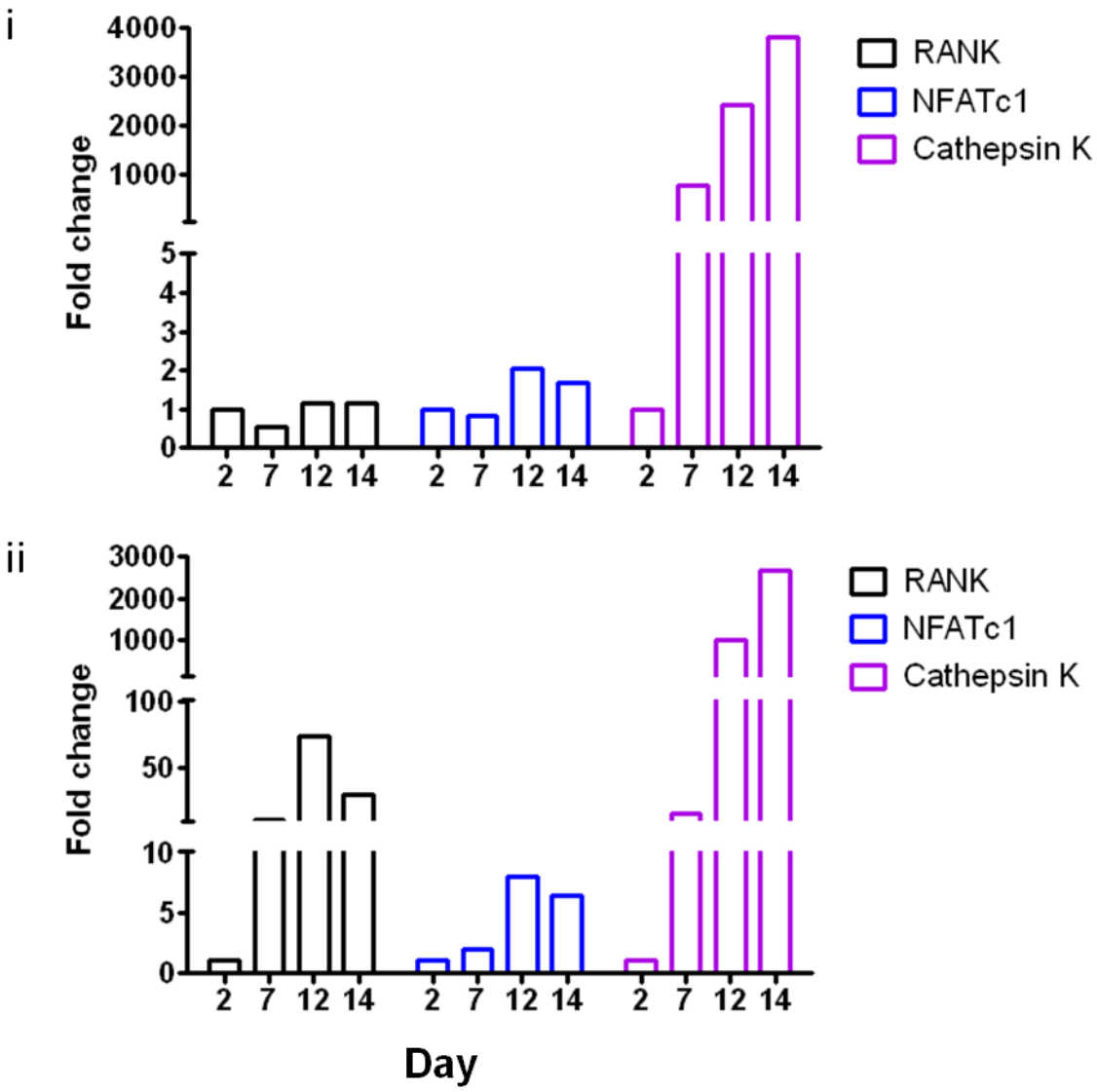

Figure 2-17 TaqMan gene assay to determine the change in expression of osteoclast specific genes.

cDNA from CD14+ve cells at different stages of osteoclastogenesis was run using TaqMan Assays and qRT-PCR was performed on cells obtained from glass coverslips (i) and dentine discs (ii) and fold change in expression of RANK, NFATc1 and Cathepsin-K was calculated as $2^{-\Delta\Delta CT}$, where $\Delta\Delta CT = \Delta CT_{day2} - \Delta CT_{dayx}$, values are mean, n=2 donors.

Chapter 3. P2X7R KO mice on BALB/c background have altered osteoclastogenesis.

3.1. Introduction

The role of P2X7R in cell fusion and multinucleation has been under scrutiny for more than a decade. Using transfected cells, it was shown that low P2X7R expressing cells are unable to form multinucleated giant cells unlike their over expressing counterparts (Falzoni et al., 2000). Additionally, blocking P2X7R using a monoclonal antibody against the receptor's external domain or receptor antagonists, inhibited multinucleated cell fusion (Agrawal et al., 2010; Di Virgilio et al., 1999; Falzoni et al., 1995; Gartland et al., 2003c).Therefore, it is speculated that P2X7R activity drives cell fusion although it may not be imperative for the migration of fusion competent precursors (Agrawal et al., 2010; Falzoni et al., 1995). Since precursor cell clumping is observed in these studies, it is possible that receptor activity might be needed at a later stage in cell fusion. Targeted deletion of P2X7R in two different mice models, did not impair fusion neither *in vivo* nor *in vitro* (Gartland et al., 2003c; Ke et al., 2003). These findings are intriguing and more studies are needed to place the role of P2X7R in the process of fusion. Osteoclasts are formed by fusion of monocytic precursors and increase in number of nuclei is associated with pathology of diseases with excessive bone resorption, such as Paget's disease (Roodman and Windle, 2005). Regulation of osteoclastic fusion therefore has consequences on its resorptive capability and a potential dysregulation in the process of bone remodelling.

The mice previously used to assess P2X7R's role in the development of bone phenotype have come under recent scrutiny and the genetic background of inbred strains and the methods of gene knockout have been determined to contribute to the contradictory findings on P2X7R signalling in various tissues including in bone. In this chapter, a novel BALB/c mouse model generated by backcrossing Glaxo KO mice (on C57BL/6 background) onto the BALB/c strain (Syberg et al., 2012a) is analysed (referred to as P2X7R-/-). The aims were 1) to investigate the effects of P2X7R deletion on bone cell numbers by static bone histomorphometry on adult tibial sections. 2) To determine the expression of P2X7R splice variants on precursors and mature osteoclasts

generated *in vitro*. 3) To determine the effects of P2X7R deletion on osteoclast formation and resorption *in vitro* by primary osteoclasts derived from BM (BM osteoclasts) or spleens (splenic osteoclasts). 4) To determine the effect of P2X7R deletion on gene expression by whole BM and mature osteoclasts derived from 2 precursor cell lineages.

3.2. Results

3.2.1. Histomorphometric analysis of P2X7R-/- BALB/c tibiae

3.2.1.1. Endocortical surface

Age matched female BALB/c P2X7R+/+ and P2X7R-/- mice at 16 weeks were used to obtain tibial bone sections at 2 levels, both of which were TRAP stained prior to histological analysis. Histomorphometrical assessment of tibia showed TRAP+ve osteoclasts and cobblestone like osteoblasts (blue) with large nucleus on the bone surface (Figure 3-1).

On the endocortical surface, the osteoclast number (N.Oc/B.Pm) in P2X7R-/- was significantly enhanced by greater than 3 fold ($p=0.015$) compared to that in P2X7R+/+ mice (0.57 versus 0.16 respectively). This was accompanied by a 4 fold significant increase ($p=0.035$) in the surface occupied by osteoclasts (Oc.Pm/B.Pm) (0.019 in P2X7R-/- versus 0.005 P2X7R+/+). Moreover, the number of osteoblasts (N.Ob/B.Pm) was halved ($p=0.009$) in P2X7R-/- (15.32 versus 29.34 in P2X7R+/+), with a non-significant reduction in their coverage on the endocortical bone (Ob.Pm/B.Pm, 0.24 versus 0.32 in P2X7R-/- and P2X7R+/+ respectively) (Figure 3-1, Table 3-1).

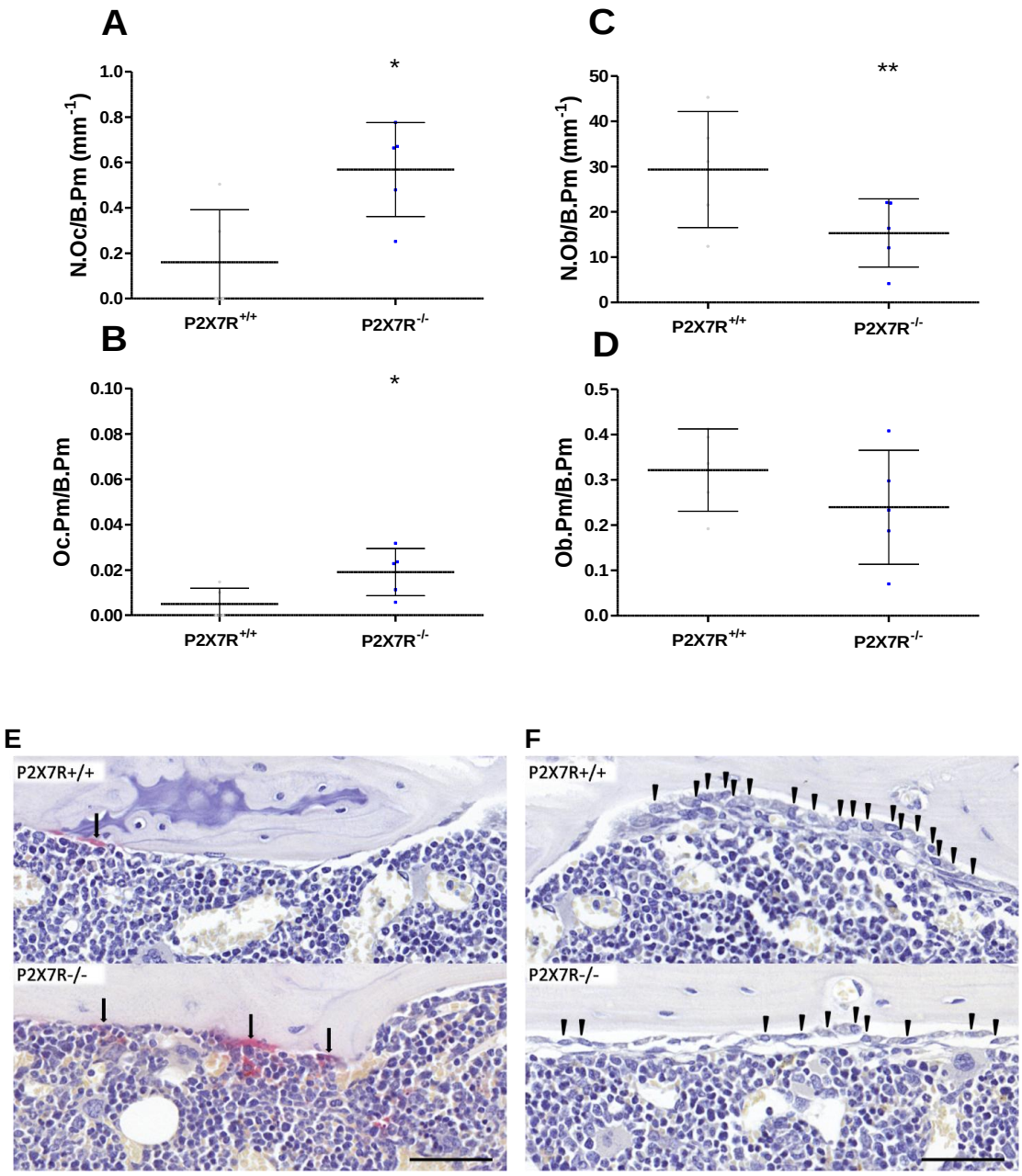

Figure 3-1 Histomorphometrical analysis of tibia at the endocortical surface.

Tibiae obtained from 16 week old P2X7R+/+ and P2X7R-/- mice were sectioned and TRAP stained to analyse a 3 mm length of endocortical surface. Number of osteoclasts per mm bone surface (N.Oc/B.Pm) (A), surface occupied by osteoclasts per mm of bone (Oc.Pm/B.Pm) (B), number of osteoblasts per mm bone surface (N.Ob/B.Pm) (C) and surface occupied by osteoblasts per mm bone (Ob.Pm/B.Pm) (D) was analysed. Representative images showing TRAP+ve osteoclasts (E) (arrows) and osteoblasts (F) (arrow heads) endocortical bone surface. Scale bar = 50 µm, all values are mean ± SD, n = 5 mice, * $p<0.05$, ** $p<0.01$ (Univariate analysis of variance).

3.2.1.2. Trabecular area

Trabecular area was defined as described in section Osteomeasure2.2.3.3.2 and 2 levels per mouse were used for histomorphometrical analysis.

Similar to endocortical observations, deletion of P2X7R resulted in a significant 2 fold increase in N.Oc/B.Pm (6.61 versus 2.93 P2X7R-/- and P2X7R+/+ respectively; p=0.001) with a 2 fold enhancement in Oc.Pm/B.Pm in trabecular bone (0.17 versus 0.08 P2X7R-/- and P2X7R+/+ respectively; p=0.003) compared to their P2X7R+/+ controls (Figure 3-2 A & B; Table 3-1).

A 2 fold reduction in N.Ob/B.Pm was observed in the trabecular bone compartment of P2X7R-/- mice, however the data failed to reach statistical significance (1.30 versus 3.05 in P2X7R+/+, p=0.098); with a significant 3 fold reduction in their coverage Ob.Pm/B.Pm (0.02 in P2X7R-/- versus 0.06 in P2X7R+/+; p=0.041) (Figure 3-2 C & D; Table 3-1) compared to P2X7R+/+ mice.

3.2.1.3. Adipocytes in bone marrow

Adipocytes were counted in the trabecular area and their number per bone marrow area (N.Ad/ Ma.A) was observed to be increased by a significant 3 fold in P2X7R-/- mice (12.83 versus 4.33 in P2X7R+/+, p=0.003) (Figure 3-2 E & F, Table 3-1).

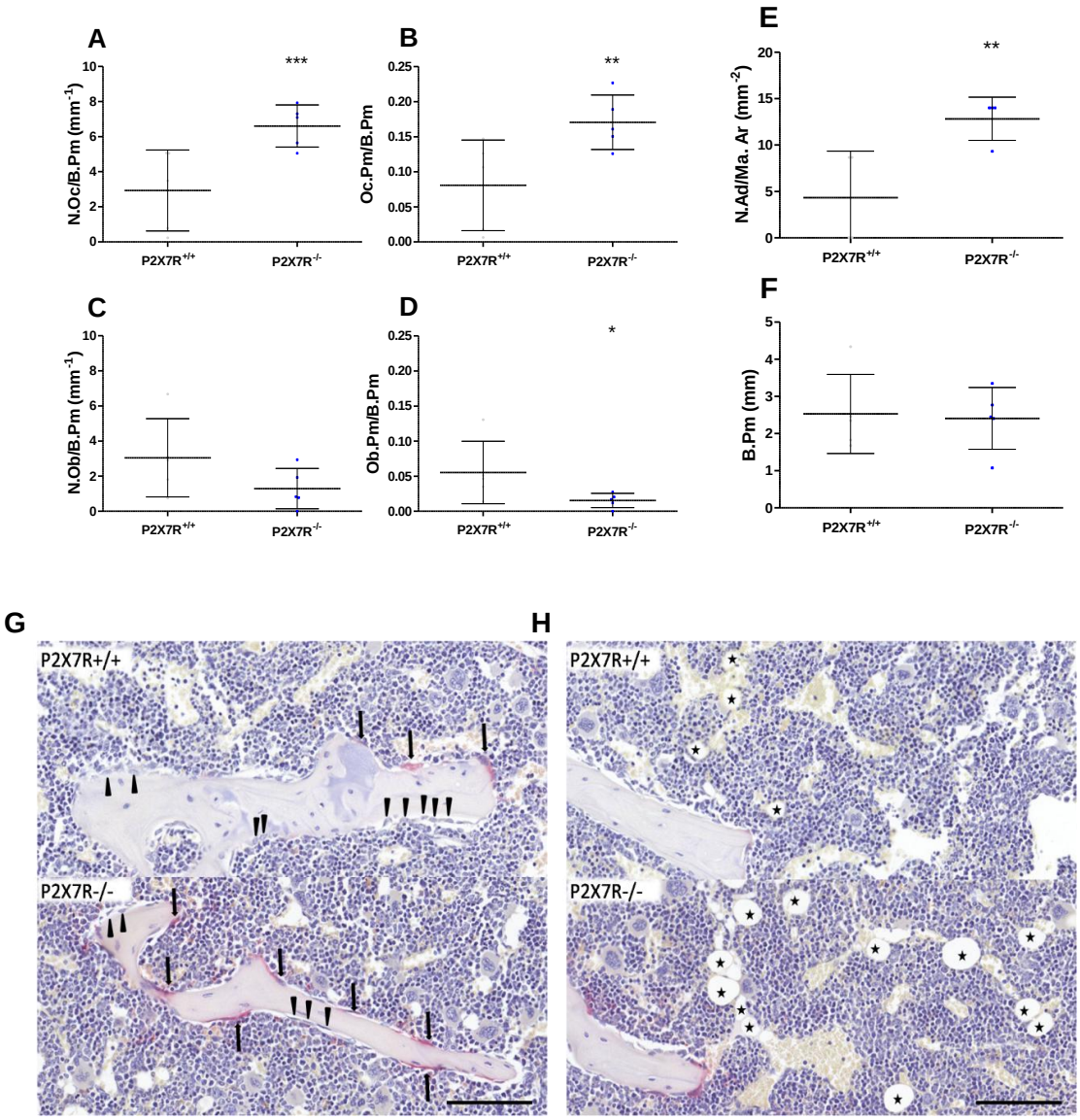

Figure 3-2 Histomorphometrical analysis of tibia in the trabecular area.

Tibiae obtained from 16 week old P2X7R+/+ and P2X7R-/- mice were sectioned and TRAP stained to analyse a 0.75 mm^2 trabecular bone area. Number of osteoclasts per mm bone surface (N.Oc/B.Pm) (A), surface occupied by osteoclasts per mm bone (Oc.Pm/B.Pm) (B), number of osteoblasts per mm bone surface (N.Ob/B.Pm) (C) and surface occupied by osteoblasts per mm bone (Ob.Pm/B.Pm) (D), number of adipocytes relative to bone marrow area (N.Ad/ Ma.Ar) (E) and trabecular bone perimeter (B.Pm) (F) was determined. Representative images TRAP+ve osteoclasts (arrows) and osteoblasts (arrow heads) on trabecular bone surface (G) and adipocytes (stars) in the bone marrow (F). Scale bar = 100 µm, all values are mean ± SD, n = 5 mice, * $p<0.05$, ** $p<0.01$, ***$p<0.001$ (Univariate analysis of variance).

Table 3-1 Histomorphometrical analysis of tibia

Summary of parameters from bone histological analysis of BALB/c P2X7R+/+ and P2X7R-/- mice.

Parameter	**P2X7R+/+ Mean ± SD**	**P2X7R-/- Mean ± SD**	**p-value**	**P2X7R+/+ Mean ± SD**	**P2X7R-/- Mean ± SD**	**p-value**
	Endocortical			Trabecular		
N.Ob/B.Pm (mm^{-1})	29.34± 12.79	15.32± 7.51	0.009 **	3.05± 2.23	1.30± 1.15	0.098
Ob.Pm/B.Pm	0.32± 0.09	0.24± 0.12	0.122	0.06± 0.04	0.02± 0.01	0.041 *
N.Oc/B.Pm (mm^{-1})	0.16± 0.23	0.57± 0.21	0.015 *	2.93± 2.31	6.61± 1.2	<0.001 ***
Oc.Pm/B.Pm	0.005± 0.007	0.019± 0.01	0.035 *	0.08± 0.07	0.17± 0.04	0.003 **
N.Ad/ Ma.Ar (mm^{-2})				4.33± 5.00	12.83± 2.33	0.003 **
B.Pm				2.53± 1.07	2.41± 0.83	0.789
p- values were calculated using Univariate analysis of Variance						

3.2.2. Analysis of splice variants of murine P2X7R in precursors and mature osteoclasts

Validation of RNA extraction and cDNA synthesis is described in section 2.2.4.3.3 and end point PCR was performed to detect P2X7(a) or P2X7(k) isoforms in precursor cells and mature osteoclasts generated from bone marrow and spleen.

The splice variants were recently described to have escaped deletion in the Glaxo P2X7R KO mice (Nicke et al., 2009), the original model that was backcrossed on BALB/c strain (Syberg et al., 2012a) to obtain the P2X7R-/- mice in this study. Presence of a highly sensitive splice variant, P2X7(k), was demonstrated in various tissues and analysis of the variant in osteoclasts was warranted. Both BM and spleen are organs of hematopoiesis in mice (Wolber et al., 2002) and although the role of BM as a reservoir for blood and bone precursors is widely established, evidence suggests that rodent spleen is also capable of deploying its resident cell population into the circulation (Swirski et al., 2009). Age matched P2X7R+/+ and P2X7R-/- female mice were culled by Schedule I and their hind limbs or spleens were collected to obtain osteoclastic precursors. Additionally, osteoclasts were differentiated *in vitro* from precursors of both lineages to determine P2X7(k) variant and also assess whether the expression could be site-specific as hinted in the literature.

Transcripts for both P2X7(a) or P2X7(k) isoforms were detected in precursors and mature osteoclasts obtained from both BM and spleens of P2X7R+/+ mice In P2X7R-/-, P2X7(a) transcript could not be detected in the cell populations from either lineage confirming the interruption in exon 1 of *P2rx7* gene in the model (Figure 3-3). Interestingly, P2X7(k) was detected in precursors from both the BM aspirate and the spleen buffy layer of P2X7R-/- (Figure 3-3 A & C) but not from either BM osteoclasts or splenic osteoclasts generated *in vitro* on dentine discs (Figure 3-3 B & D).

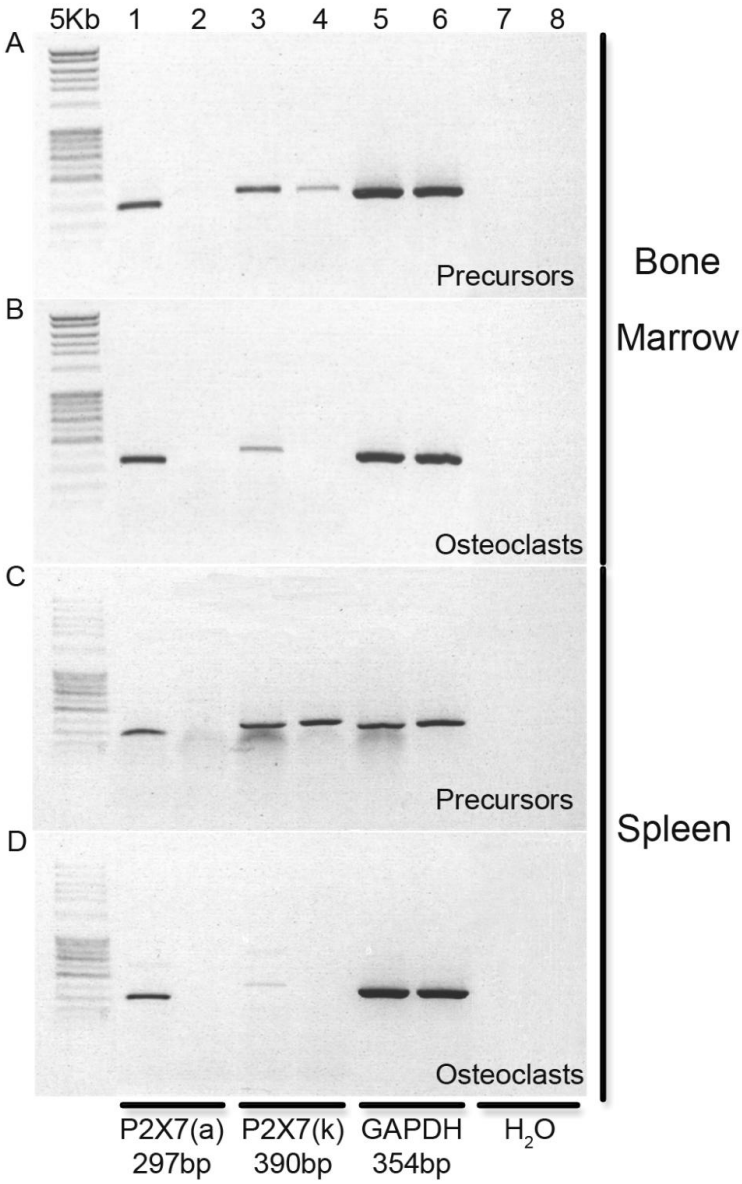

Figure 3-3 End point PCR showing splice variant expression

Equal quantities of all templates were amplified using specific forward primers for P2X7(a), P2X7(k) and common reverse primer on exon 4. Gapdh was used to compare the relative amount of amplified products between P2X7R+/+ and P2X7R-/- samples. Osteoclastic precursors (A, BM and C splenic) and mature osteoclasts differentiated *in vitro* (BM and D splenic) were used to assess the presence of 297bp P2X7(a) (Lanes 1&2) or 390bp P2X7(k) (Lanes 3&4) isoforms and 354bp Gapdh transcript (Lanes 5&6) along with water blank (Lanes 7&8). Lanes 1,3,5,7= P2X7R+/+ samples and 2,4,6,8= P2X7R-/-, images representative of 2 mice used per genotype for each cell population.

3.2.3. Osteoclastogenesis *in vitro*

Osteoclasts on glass coverslips were counted using Cell® D software and defined as multi-nucleated (containing 3 or more nuclei) TRAP positive cells (Section 2.2.3.1). Osteoclasts on dentine discs were also defined as TRAP positive cells and were classified as resorbing osteoclasts if they were located near a resorption pit (Section 2.2.3.1).

3.2.3.1. Osteoclast formation

No significant differences in total number of BM osteoclasts was obtained between P2X7R+/+ and P2X7R-/- mice on glass coverslips (216.1 in P2X7R+/+ versus 254.7 in P2X7R-/-) (Figure 3-4). Splenic osteoclasts were reduced in P2X7R-/- compared to P2X7R+/+ mice, but this did not reach statistical significance (28.43 versus 48.64 respectively; p=0.261) (Figure 3-5).

Fusion index, defined by (number of nuclei within osteoclasts/total number of nuclei counted) X 100 (Pellegatti et al., 2011) was not different in BM osteoclasts (22.92 in P2X7R+/+ versus 23.30 in P2X7R-/-) but was significantly reduced by 6 fold in P2X7R-/- splenic osteoclasts (8.86 in P2X7R+/+ versus 1.56 in P2X7R-/-; p=0.012) (Figure 3-5).

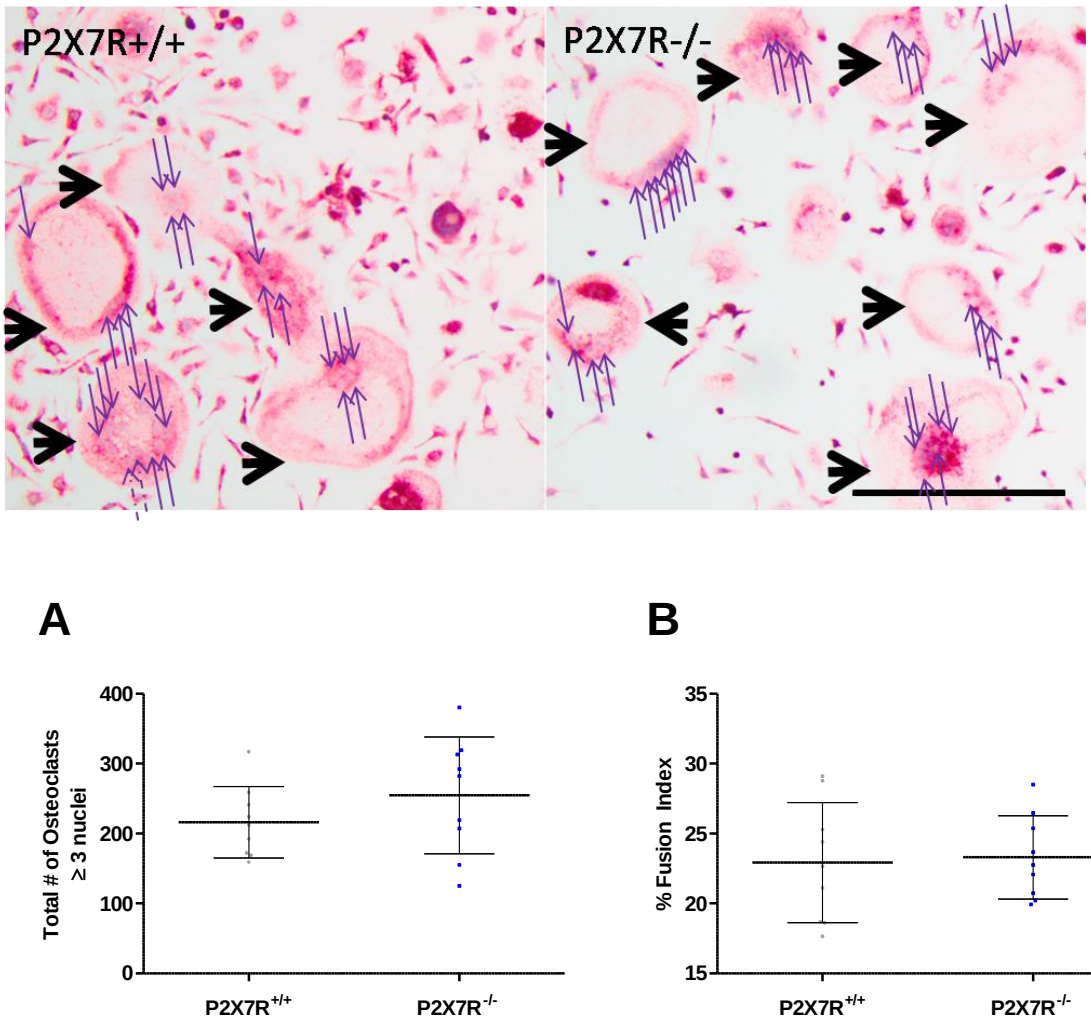

Figure 3-4 Formation of BM derived osteoclasts *in vitro*

Long bone aspirate of P2X7R+/+ and P2X7R-/- mice were collected to isolate precursor cells which were seeded onto glass coverslips in the presence of M-CSF and RANKL for 9 days and TRAP stained. Gill's haematoxylin was used to counter stain nuclei and osteoclasts were defined as TRAP positive (red, thick arrows), multi-nucleated (3 or more nuclei, thin arrows). Number of osteoclasts per coverslip (A) and fusion index (B) in BM osteoclasts from P2X7R+/+ and P2X7R-/- mice. Values are mean ± SD, n = 3 mice osteoclast cultures, 3 replicate coverslips each culture (Univariate analysis of variance). Scale bar = 200 μm

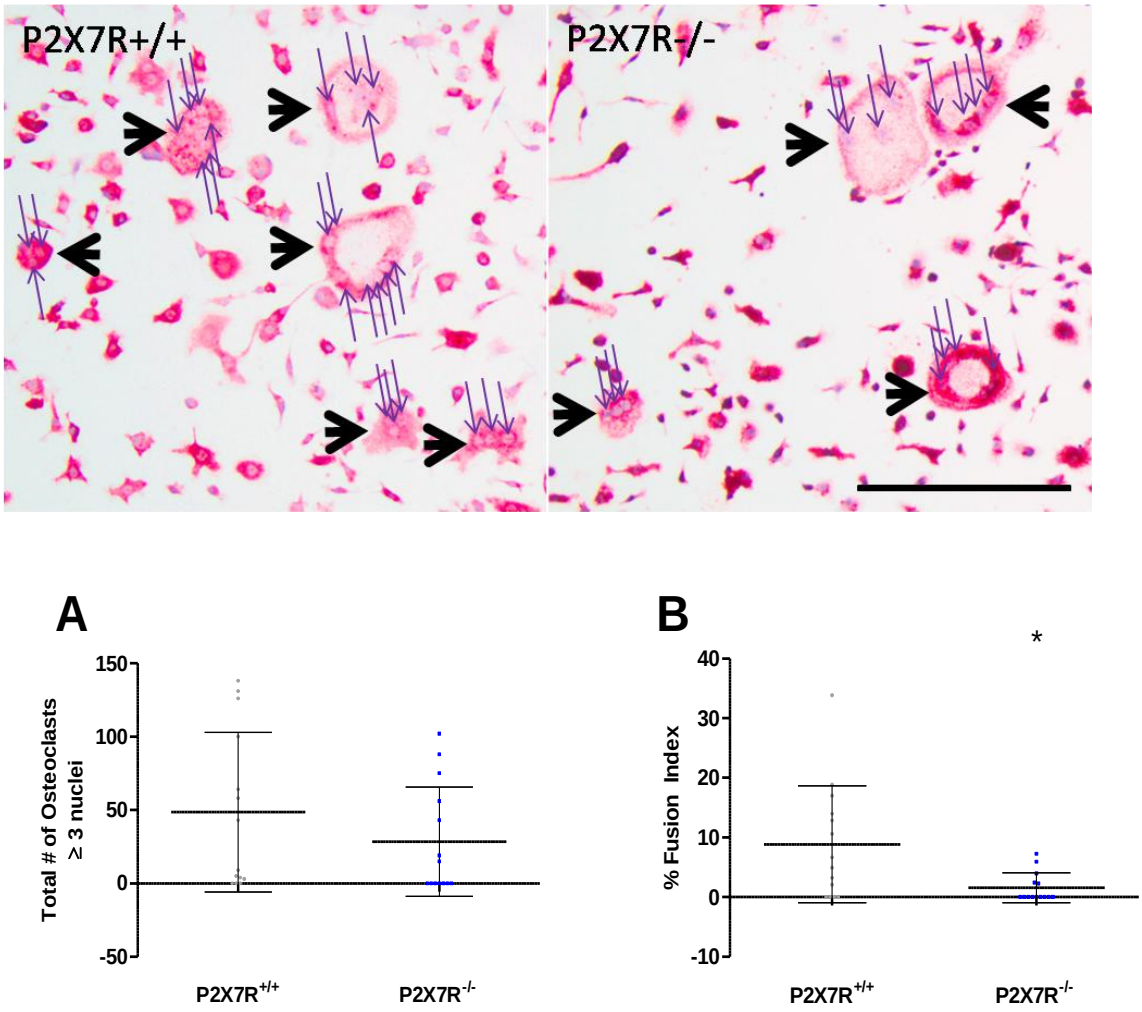

Figure 3-5 Formation of spleen derived osteoclasts *in vitro*

Spleens of P2X7R+/+ and P2X7R-/- mice were macerated to collect precursor cells which were seeded onto glass coverslips in the presence of M-CSF and RANKL for 7 days and TRAP stained. Gill's haematoxylin was used to counter stain nuclei and osteoclasts were defined as TRAP+ve (red, thick arrows), multi-nucleated (3 or more nuclei, thin arrows). Number of osteoclasts per coverslip (A) and fusion index (B) in splenic osteoclasts from P2X7R+/+ and P2X7R-/- mice. Values are mean ± SD, n = 2 mice osteoclast cultures, 7 replicate coverslips each culture (Univariate analysis of variance) Scale bar= 200µm.

3.2.3.2. Osteoclast function

Total number of BM osteoclasts, number of resorbing osteoclasts or the total amount of resorption on dentine discs were not significantly different between P2X7R+/+ and P2X7R-/- mice (145.4 versus 128.3, 63.93 versus 80.61 and $3.95x10^4$ μm^2 versus $4.41x10^4$ μm^2 in P2X7R+/+ and P2X7R-/- respectively). However, the resorption ability of P2X7R-/- BM osteoclasts was significantly reduced by a third compared to that of P2X7R+/+ (6.42 versus 8.92, p=0.016) (Figure 3-6).

On the contrary, the resorption ability of spleen derived P2X7R-/- osteoclasts was significantly enhanced by greater than 2 fold compared to P2X7R+/+ (25.65 versus 10.38, p=0.003). Additionally, the total number of splenic osteoclasts were 3 fold significantly higher in P2X7R-/- (184.2 versus 57.75 respectively, p=0.016) compared to P2X7R+/+. The number of resorbing osteoclast and total resorption in P2X7R-/- was also enhanced by 2 and 3 fold respectively but it did not reach statistical significance (17.75 in P2X7R-/- versus 7.37 in P2X7R+/+ resorbing osteoclasts, p=0.090; $3.2x10^4$ μm^2 resorption in P2X7R-/- versus $1.12x10^4$ μm^2 in P2X7R+/+, p=0.069). Moreover, P2X7R/- osteoclasts showed lesser TRAP stain compared to the P2X7R+/+ cells on dentine (Figure 3-7).

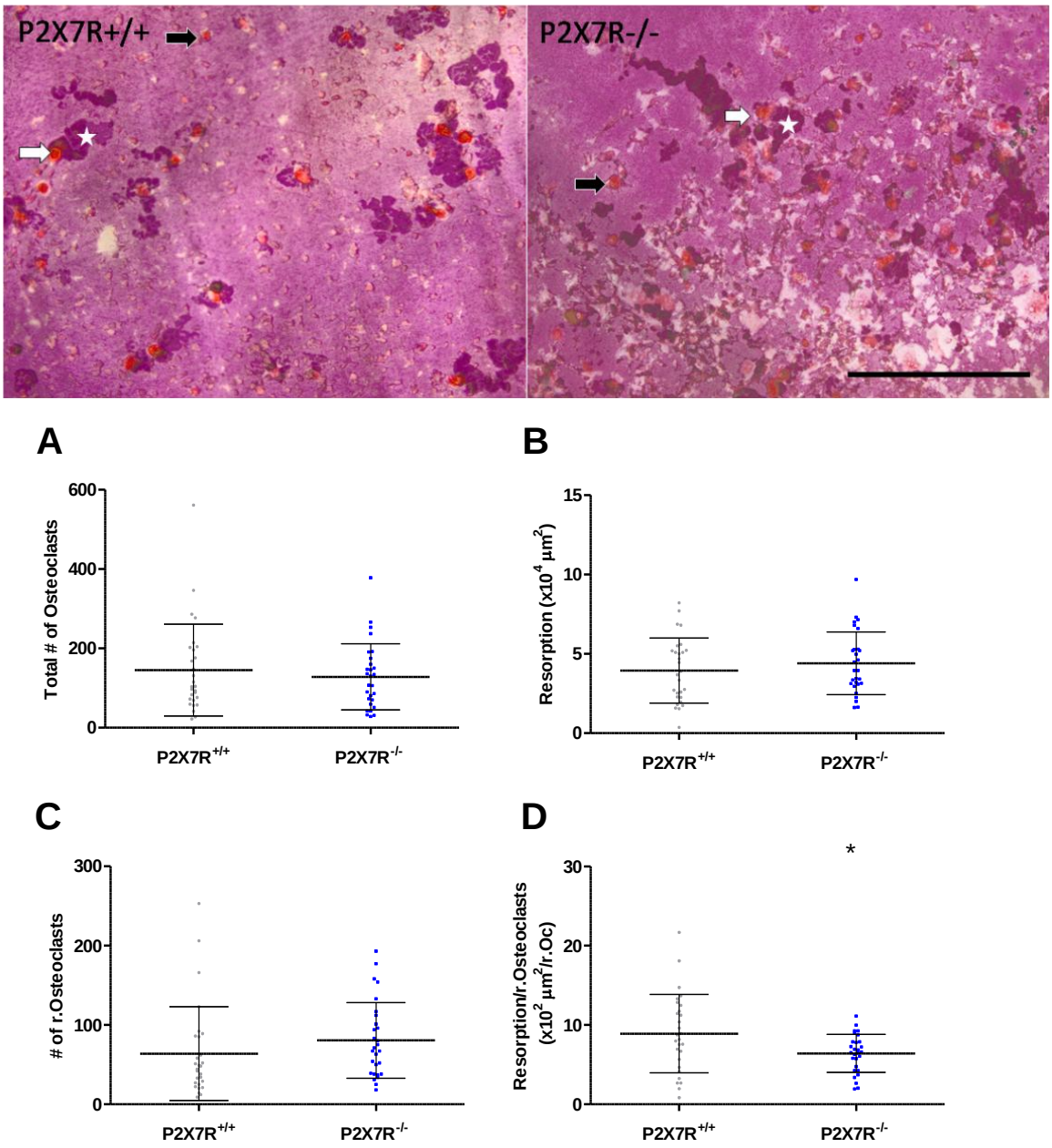

Figure 3-6 Osteoclast function of BM derived osteoclasts *in vitro*

Long bone aspirates of P2X7R+/+ and P2X7R-/- mice were collected and seeded on dentine discs for 17 days and TRAP stained. All TRAP+ve cells were counted as mature osteoclasts (black arrows) and were classed as resorbing (white arrows) if they lay in close proximity to resorption pits (white stars). Gill's hematoxylin was used to highlight the resorption trails created by osteoclasts and area was counted to assess total resorption. Total number of osteoclasts (A), resorption (B), number of resorbing osteoclasts (C) and resorptive ability (resorption/resorbing osteoclast) (D) was analysed. Values are mean ± SD, n=4 mice osteoclast cultures, 7 replicate discs each culture *$p < 0.05$ (Univariate analysis of variance). Scale bar = 500µm.

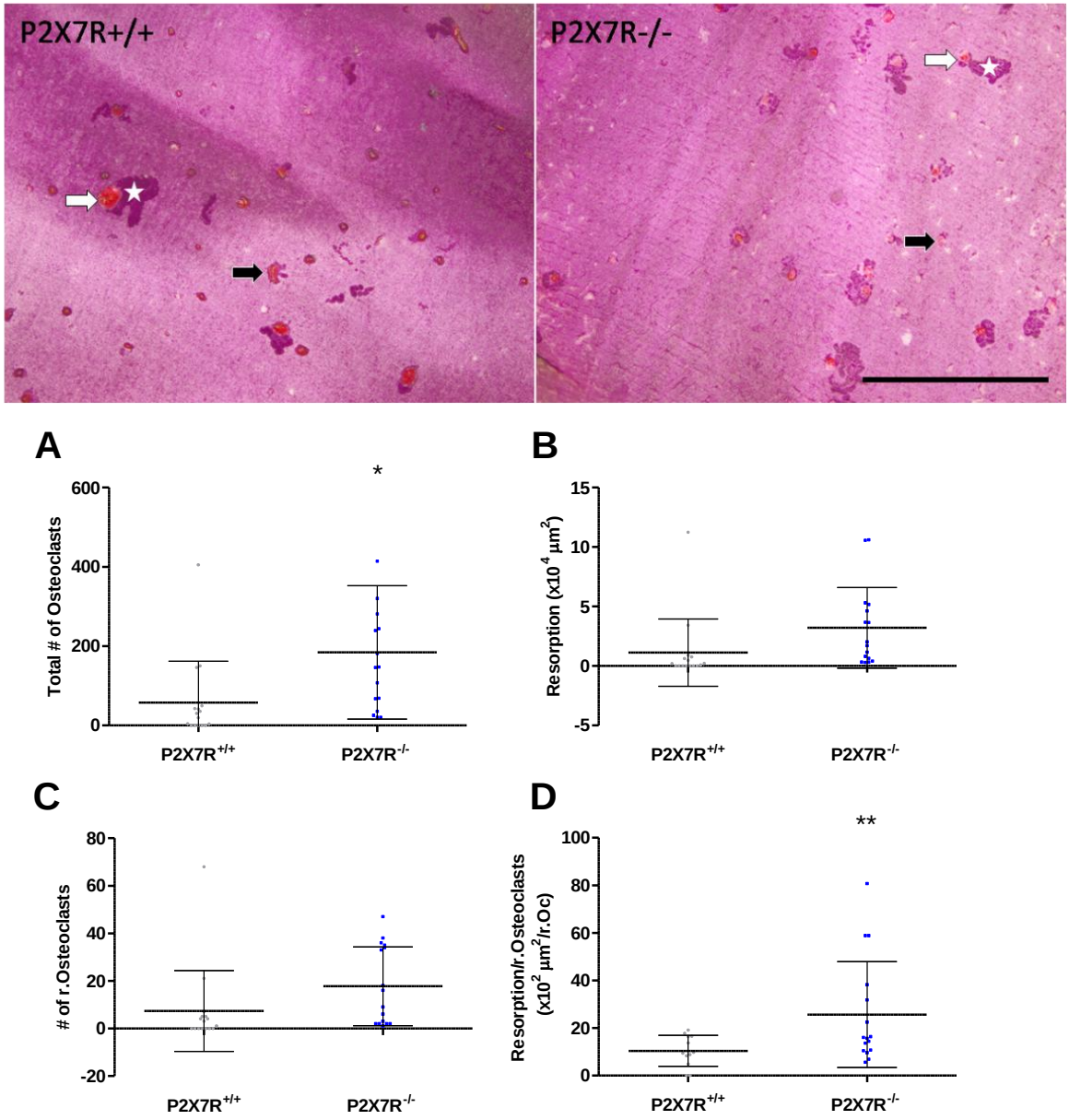

Figure 3-7 Osteoclast function of spleen derived osteoclasts *in vitro*

Splenic precursors from P2X7R+/+ and P2X7R-/- were differentiated on dentine discs for 9 days and TRAP stained. All TRAP+ve cells were counted as mature osteoclasts (black arrows) and were classed as resorbing (white arrows) if they lay in close proximity to resorption pits (white stars). Gill's hematoxylin was used to highlight the resorption trails created by osteoclasts and area was counted to assess total resorption. Total number of osteoclasts (A), resorption (B), number of resorbing osteoclasts (C) and resorptive ability (resorption/resorbing osteoclast) (D) was analysed. values are mean ± SD, n=2 mice osteoclast cultures, 8 replicate discs each culture, *p < 0.05, **p<0.01 (Univariate analysis of variance) Scale bar = 500µm.

Table 3-2 *In vitro* osteoclastogenesis.
Summary of parameters from osteoclast cultures from bone marrow and spleen of P2X7R+/+ and P2X7R-/- mice.

Parameter	**P2X7R+/+ Mean ± SD**	**P2X7R-/- Mean ± SD**	**p-value**	**P2X7R+/+ Mean ± SD**	**P2X7R-/- Mean ± SD**	**p-value**
	Bone Marrow derived			Spleen derived		
Total Osteoclasts (≥ 3 nuclei) glass coverslips	216.1± 50.90	254.7± 83.43	0.245	48.64± 54.35	28.43± 37.24	0.261
Fusion Index	22.92± 4.30	23.30± 2.98	0.828	8.86± 9.8	1.56± 2.49	0.012 *
Total Osteoclasts (dentine)	145.4± 115.7	128.3± 83.55	0.532	57.75± 104.2	184.2± 168.6	0.016 *
Resorbing Osteoclasts	63.93± 59.08	80.61± 47.68	0.239	7.37± 17.00	17.75± 16.53	0.090
Resorption ($x10^4$ μm^2)	3.95± 2.04	4.41± 1.98	0.384	1.12± 2.83	3.2± 3.39	0.069
Resorption Ability ($x10^2$ μm^2/r.Oc)	8.92± 4.96	6.42± 2.4	0.016 *	10.38± 6.54	25.65± 22.31	0.003 **

p- values were calculated using Univariate analysis of Variance

$$\text{Fusion Index} = \frac{(\text{number of nuclei within osteoclasts})}{(\text{total number of nuclei counted})} \times 100$$

3.2.4. Effect of P2X7R deletion on gene expression in BM aspirates and mature osteoclasts

3.2.4.1. Gene expression in BM aspirates.

3.2.4.1.1. ΔCT based gene expression analysis

To determine gene expression changes due to *P2rx7* gene deletion, bone marrow aspirate was collected from P2X7R+/+ and P2X7R-/- mice and cDNA was analysed using TaqMan® Array Custom Micro Fluidic cards. Delta CT (ΔCT) values were calculated by normalising target templates in all samples β-actin (*Actb*) as $\Delta CT = CT_{target} - CT_{Actb}$. A heatmap was composed using the reciprocal values of ΔCT (1/ΔCT) showing the pattern of gene expression, with a gradient of expression levels ranging from low expression (blue) to high expression (Figure 3-8).

Results confirmed a low expression of *P2rx7* gene in P2X7R-/- BM aspirates confirming the attenuated P2X7R in the BALB/c mice. Downregultaion of *Csf1* (macrophage colony stimulating factor 1), *Traf-6* (TNF receptor-associated factor 6), *Itga5* (integrin alpha 5), *Il-6* (IL-6) and *Il1r2* (IL-1 type II receptor and upregulated *Sparc* (osteonectin), *Ctsk* (cathepsin-K), *Col1a2* (collagen, type I, alpha 2) and *Col2a1* (collagen, type II, alpha 1) was detected in bone marrows of P2X7R-/- mice (Figure 3-8).

Additionally, within the P2R family, deletion of P2X7R showed a down regulation of *P2rx4* in the mice bone marrow aspirates.

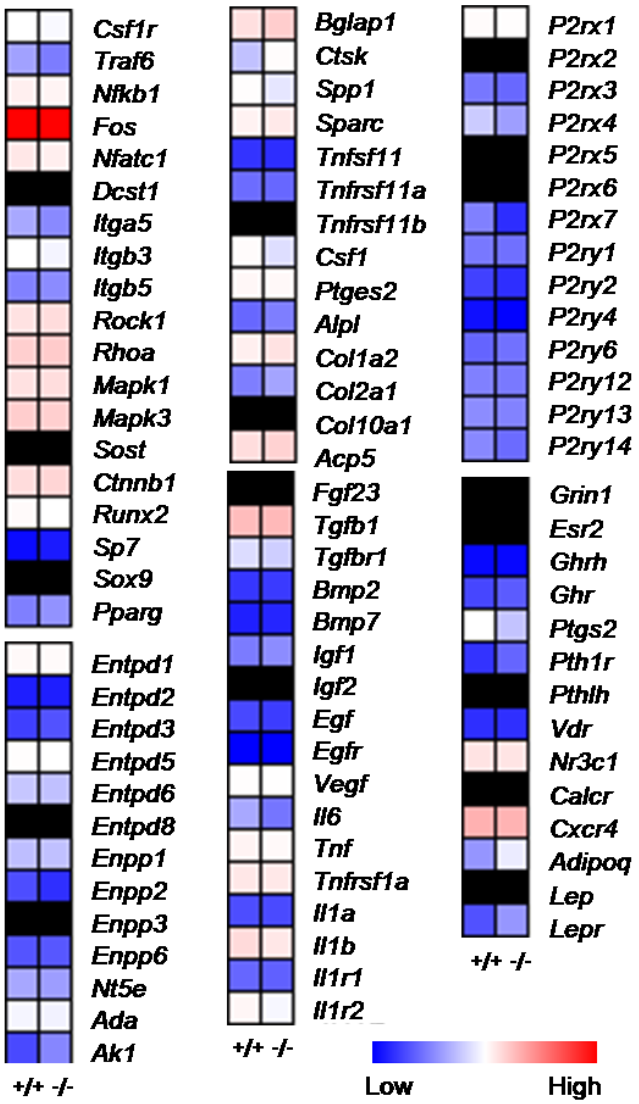

Figure 3-8 Heatmap showing gene expression in BM aspirates of P2X7R+/+ and P2X7R-/- mice.

cDNA obtained from bone marrows was run on TaqMan Array cards and relative quantification of all target templates was performed by normalizing to endogenous control β-actin (*Actb*) to obtain ΔCT. A heatmap showing differential expression of genes in P2RX7+/+ and P2RX7-/- BM was generated from the reciprocal value of ΔCT (ΔCT^{-1}). Legend shows a gradient of genes expression ranging from lowest (blue) to highest. Missing values are shown in black.

3.2.4.1.2. Fold changes in BM aspirates

Fold changes in difference in expression of target genes was expressed as ΔΔCT (ΔΔCT = $\Delta CT_{P2X7R+/+}$ - $\Delta CT_{P2X7R-/-}$) and was calculated by taking 2 to the power of ΔΔCT ($2^{-\Delta\Delta CT}$). A fold change of more than ±2 were considered significantly different as they represent doubling (>2) or halving (<-2) in the template copy numbers.

Significant reductions in *Csf1* (macrophage colony stimulating factor 1, 2 fold), *Ptgs2* (prostaglandin-endoperoxide synthase 2, 2.1 fold) and interleukin cytokine *Il6* (Interleukin 6, 2.2 fold) and an interleukin receptor *Il1r2* (Interleukin 1 receptor, type II, 2.1 fold).

Moreover, significant upregulation in *Bglap1* (Osteocalcin, 3.2 fold), *Ctsk* (Cathepsin K, 4.3 fold), *Sparc* (Osteonectin, 2.3 fold), *Col1a2* (Collagen, type I, alpha 2, 3.5 fold), *Col2a1* (Collagen, type II, alpha 1, 4.6 fold), *Pth1r* (Parathyroid hormone I receptor, 4.0 fold), *Adipoq* (Adiponectin, 3.6), *Lepr* (leptin receptor, 4.2), *Ak1* (adenylate kinase 1, 4.8 fold) in *P2rx7* deficient cells (Table 3-3).

Table 3-3 Fold changes in gene expression between BM aspirate of P2X7R+/+ and P2X7R-/- mice

Gene	BM aspirate	Gene	BM aspirate	Gene	BM aspirate
Csf1r	-1.1	*Bglap1*	**3.2**	*P2rx1*	-1.1
Traf6	-1.6	*Ctsk*	**4.3**	*P2rx2*	ND
Nfkb1	-1.4	*Spp1*	-1.6	*P2rx3*	-1.0
Fos	-1.1	*Sparc*	**2.3**	*P2rx4*	-1.9
Nfatc1	-1.4	*Tnfsf11*	-1.0	*P2rx5*	ND
Dcst1	ND	*Tnfrsf11a*	-1.0	*P2rx6*	ND
Itga5	-1.6	*Tnfrsf11b*	ND	*P2rx7*	**-5.9**
Itgb3	-1.2	*Csf1*	**-2.0**	*P2ry1*	-1.1
Itgb5	1.3	*Ptges2*	-1.0	*P2ry2*	-1.5
Rock1	1.3	*Alpl*	1.8	*P2ry4*	-1.3
Rhoa	1.1	*Col1a2*	**3.5**	*P2ry6*	1.4
Mapk1	1.1	*Col2a1*	**4.6**	*P2ry12*	-1.0
Mapk3	-1.1	*Col10a1*	ND	*P2ry13*	-1.1
Sost	ND	*Acp5*	1.6	*P2ry14*	-1.6
Ctnnb1	1.3	*Fgf23*	ND	*Grin1*	ND
Runx2	-1.4	*Tgfb1*	1.0	*Esr2*	ND
Sp7	1.9	*Tgfbr1*	-1.2	*Ghrh*	1.3
Sox9	ND	*Bmp2*	1.3	*Ghr*	1.8
Pparg	1.5	*Bmp7*	1.5	*Ptgs2*	**-2.1**
Entpd1	-1.0	*Igf1*	1.5	*Pth1r*	**4.0**
Entpd2	1.2	*Igf2*	ND	*Pthlh*	ND
Entpd3	1.8	*Egf*	-1.2	*Vdr*	1.3
Entpd5	-1.2	*Egfr*	1.2	*Nr3c1*	-1.0
Entpd6	-1.1	*Vegfa*	-1.1	*Calcr*	ND
Entpd8	ND	*Il6*	**-2.2**	*Cxcr4*	-1.1
Enpp1	1.1	*Tnf*	-1.5	*Adipoq*	**3.6**
Enpp2	-1.5	*Tnfrsf1a*	-1.1	*Lep*	ND
Enpp3	ND	*Il1a*	1.0	*Lepr*	**4.2**
Enpp6	1.2	*Il1b*	-1.7		
Nt5e	-1.1	*Il1r1*	-1.0		
Ada	-1.0	*Il1r2*	**-2.1**		
Ak1	**4.8**				

Significant fold changes are shown in bold. ND: The gene was not amplified.

3.2.4.1.3. Relative expression of P2 receptors in BM aspirates

In order to determine whether deletion of *P2rx7* gene lead to changes in expression of other P2 receptors, all ΔCT values were calibrated using the most highly expressed P2R (calibrator). Calibrator was chosen as the gene with highest expression in P2X7R+/+ samples and relative expression was determined as $2^{-\Delta\Delta CT}$ where $\Delta\Delta CT = \Delta CT_{calibrator} - \Delta CT_{target}$.

Expression of *P2rx2*, *P2rx5* and *P2rx6* was not detected in BM aspirates of BALB/c mice. Results showed no significant differences in relative expression of either P2X or P2Y receptors due to *P2rx7* gene deletion (Figure 3-9).

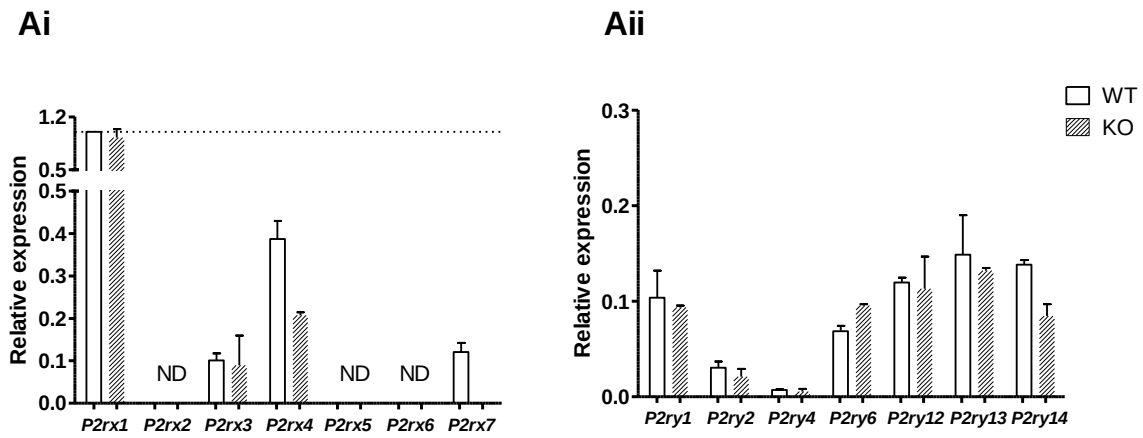

Figure 3-9 Relative expression of P2 receptors following P2X7R deletion

cDNA from BM aspirates was run on TaqMan Array cards and gene expression changes upon P2rx7 gene deletion were calculated relative to a calibrator gene (*P2rx1* in P2X7R+/+). Relative expression was calculated as $2^{-\Delta\Delta CT}$, where $\Delta\Delta CT = \Delta CT_{calibrator} - \Delta CT_{target}$. (A) Relative gene expression changes of P2X (Ai) and P2Y (Aii) receptors in P2X7R+/+ and P2X7R-/- in whole BM aspirates, values are mean ± SD, n=2 mice in each genotype.

3.2.4.2. Gene expression in osteoclasts.

3.2.4.2.1. ΔCT based gene expression analysis

Results confirmed the deleted *P2rx7* gene in both BM and splenic osteoclasts and expression of genes was different between osteoclasts from both lineages. BM osteoclasts showed an overall higher expression (red) of all genes despite the genotype compared to the splenic osteoclasts (blue) from both genotypes (Figure 3-10).

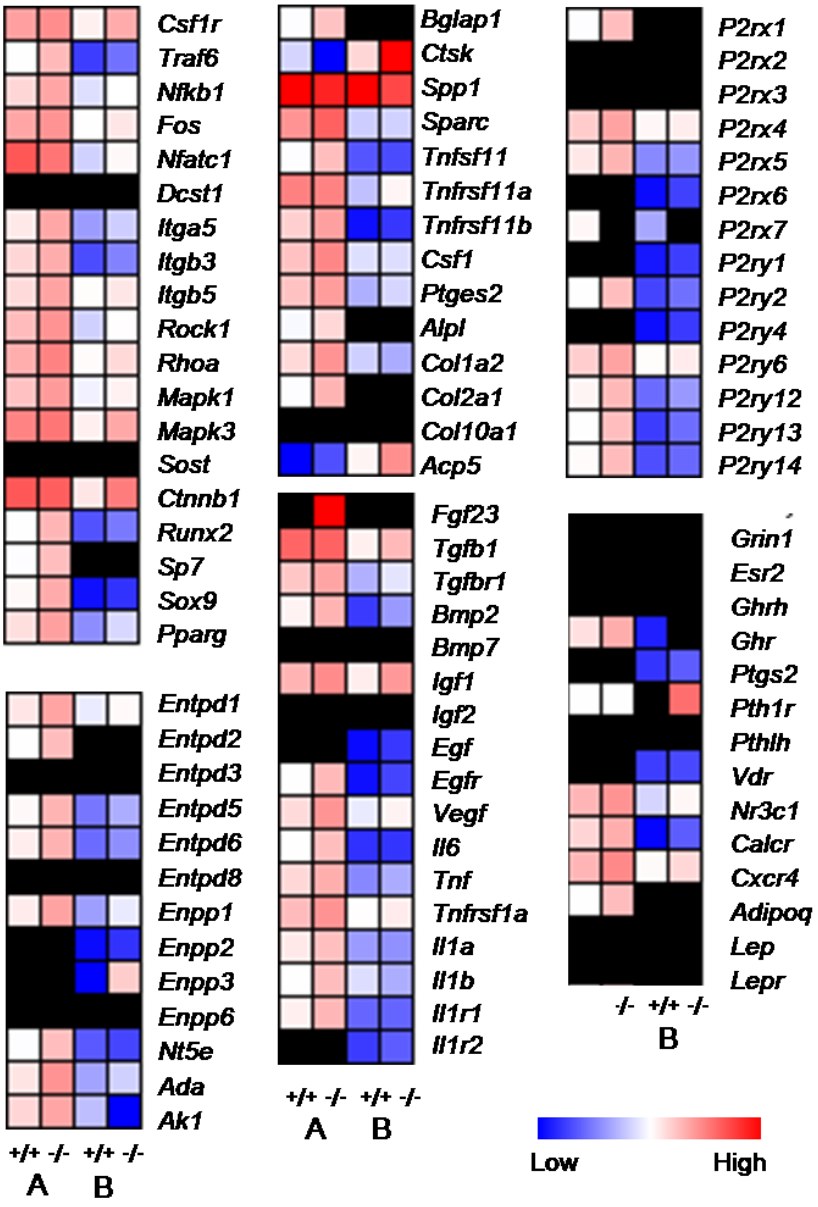

Figure 3-10 Heatmap showing gene expression in osteoclasts from P2X7R+/+ and P2X7R-/- mice.

cDNA obtained from primary osteoclasts was run on TaqMan Array cards and relative quantification of all target templates was performed by normalizing to endogenous control β-actin (*Actb*) to obtain ΔCT. A heatmap showing differential expression of genes in P2RX7+/+ and P2RX7-/- BM osteoclasts (A) and splenic osteoclasts (B) was generated from the reciprocal value of ΔCT (ΔCT^{-1}). Legend shows a gradient of genes expression ranging from lowest (blue) to highest. Missing values are shown in black.

3.2.4.2.2. Fold changes in osteoclasts

Significant changes in *Runx2* (osteoblast-specific transcription factor 2; 2.1 fold), *Sox9* (transcription factor SOX2, 3.7 fold), *Sparc* (osteonectin, 3.3 fold), *Csf1* (M-CSF, 2.8 fold), *Col1a2* (collagen type I α2, 3.1 fold), *Col2a*1 (collagen type II α1, 4.2 fold), *Acp5* (TRAP, -2.1 fold), *Vegfa* (vascular endothelial growth factor A, 3.8 fold) and *P2rx5* (-2.2 fold) were observed in P2X7R-/- BM osteoclasts.

However, genes for *Nt5e* (ecto5'nucleotidase, -5.7 fold), *Spp1* (osteopontin, -5.0 fold), *Sparc* (-2.0 fold), *Tnfsf11* (RANKL, -3.5 fold), *Col1a2* (-4.0 fold), *Bmp2* (bone morphogenetic protein 2, 2.9 fold), *Il6* (Interleukin-6, -4.5 fold), *Il1a* (interleukin 1, alpha , IL-1α, -2.9 fold), *Il1b* (interleukin 1, beta, IL-1β, -4.3 fold), *Il1r1* (IL-1 receptor type I, -4.2 fold), *Vdr* (Vitamin D receptor, -3.2 fold), *Calcr* (Calcitonin receptor, 4.3 fold) *P2rx4* (-2.7 fold) and *P2rx5* (-2.2 fold) were significantly dysregulated in *P2rx7* gene knockout splenic osteoclasts (Table 3-4).

Table 3-4 Fold changes in gene expression of osteoclasts from P2X7R+/+ and P2X7R-/- mice

Gene	BM	Splenic	Gene	BM	Splenic	Gene	BM	Splenic
Csf1r	-1.3	-1.1	*Bglap1*	1.3	ND	*P2rx1*	1.5	ND
Traf6	-1.1	1.0	*Ctsk*	-1.2	1.2	*P2rx2*	ND	ND
Nfkb1	-1.1	-1.3	*Spp1*	1.5	**-5.0**	*P2rx3*	ND	ND
Fos	-1.4	1.1	*Sparc*	**3.3**	**-2.0**	*P2rx4*	-1.2	**-2.7**
Nfatc1	-1.5	1.2	*Tnfsf11*	1.9	**-3.5**	*P2rx5*	**-2.2**	**-2.2**
Dcst1	ND	ND	*Tnfrsf11a*	-1.4	1.6	*P2rx6*	ND	1.4
Itga5	1.9	-1.1	*Tnfrsf11b*	1.2	-1.6	*P2rx7*	ND	ND
Itgb3	-1.6	1.1	*Csf1*	**2.8**	-1.8	*P2ry1*	ND	-1.5
Itgb5	1.4	-1.2	*Ptges2*	-1.2	-1.3	*P2ry2*	-1.3	-1.2
Rock1	1.4	-1.0	*Alpl*	ND	ND	*P2ry4*	ND	-1.1
Rhoa	1.7	1.0	*Col1a2*	**3.1**	**-4.0**	*P2ry6*	-1.2	-1.5
Mapk1	-1.1	1.1	*Col2a1*	**4.1**	ND	*P2ry12*	-1.6	-1.2
Mapk3	1.1	-1.2	*Col10a1*	ND	ND	*P2ry13*	1.3	-1.1
Sost	ND	ND	*Acp5*	**-2.1**	1.7	*P2ry14*	-1.8	-2.0
Ctnnb1	1.1	-1.1	*Fgf23*	ND	ND	*Grin1*	ND	ND
Runx2	**2.1**	-1.4	*Tgfb1*	1.2	-1.5	*Esr2*	ND	ND
Sp7	ND	ND	*Tgfbr1*	-1.3	-1.1	*Ghrh*	ND	ND
Sox9	**3.3**	-1.7	*Bmp2*	-1.0	**2.9**	*Ghr*	-1.4	ND
Pparg	2.0	1.3	*Bmp7*	ND	ND	*Ptgs2*	ND	-1.4
Entpd1	2.0	-1.2	*Igf1*	1.3	-1.1	*Pth1r*	ND	ND
Entpd2	-1.6	ND	*Igf2*	ND	ND	*Pthlh*	ND	ND
Entpd3	ND	ND	*Egf*	ND	-1.1	*Vdr*	ND	**-3.2**
Entpd5	1.2	1.0	*Egfr*	-1.2	1.3	*Nr3c1*	-1.0	1.2
Entpd6	-1.5	-1.5	*Vegfa*	**3.8**	1.1	*Calcr*	-1.9	**4.3**
Entpd8	ND	ND	*Il6*	1.6	**-4.5**	*Cxcr4*	1.8	1.2
Enpp1	**3.7**	1.3	*Tnf*	-1.3	-1.4	*Adipoq*	1.2	ND
Enpp2	ND	-1.4	*Tnfrsf1a*	1.2	-1.2	*Lep*	ND	ND
Enpp3	ND	ND	*Il1a*	-1.4	**-2.9**	*Lepr*	ND	ND
Enpp6	ND	ND	*Il1b*	1.5	**-4.3**			
Nt5e	1.4	**-5.7**	*Il1r1*	-1.6	**-4.2**			
Ada	ND	-1.1	*Il1r2*	ND	-1.6			
Ak1	-1.1	ND						

Significant fold changes are shown in bold. ND: The gene was not amplified.

3.2.4.2.3. Relative expression of P2 receptors in osteoclasts

In order to determine whether deletion of *P2rx7* gene lead to changes in expression of other P2 receptors in mature osteoclasts, all ΔCT values were calibrated using the most highly expressed P2R (calibrator). Calibrator was chosen as *P2ry6* in BM osteoclasts and *P2rx4* in splenic osteoclasts.

P2rx3 expression in BM osteoclasts and *P2rx1, P2rx2* and *P2rx3* in splenic osteoclasts could not be detected (ND). In BM osteoclasts, there was a >2 fold downregulation in genes for *P2rx5* (P2RX7+/+ at 0.3499 versus P2RX7-/- at 0.1479) and *P2ry12* (P2RX7+/+ at 0.1590 versus P2RX7-/- at 0.0967) in the absence of *P2rx7* gene. Moreover, splenic osteoclasts from P2X7R-/- mice showed a >2 fold downregulation in genes for *P2rx4* (P2RX7+/+ at 1.000 versus P2RX7-/- at 0.3731), *P2rx5* (P2RX7+/+ at 0.0733 versus P2RX7-/- at 0.0308) and *P2ry14* (P2RX7+/+ at 0.0201 versus P2RX7-/- at 0.0097) (Figure 3-11).

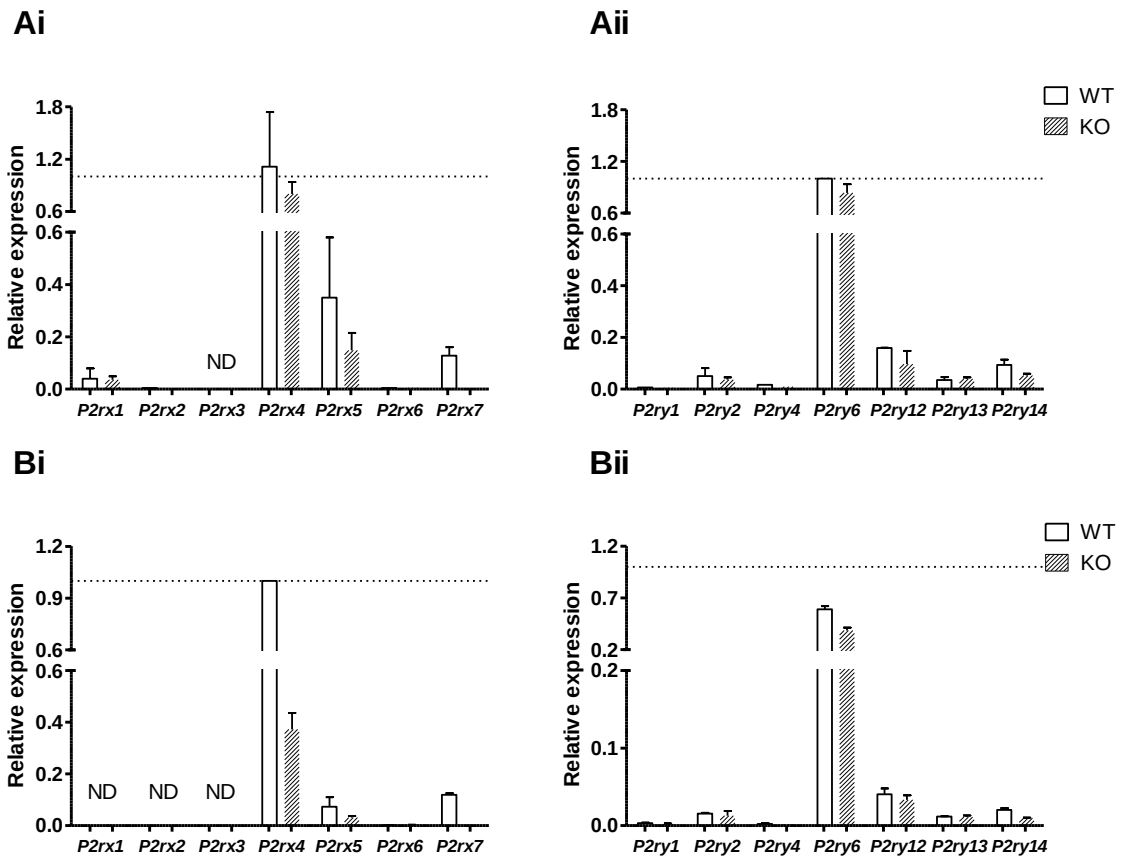

Figure 3-11 Relative expression of P2 receptors following P2X7R deletion

cDNA from primary osteoclasts was run on TaqMan Array cards and gene expression changes were calculated relative to a calibrator gene (highest expression in P2X7R+/+). Calibrator was chosen as *P2ry6* in BM osteoclasts and *P2rx4* in splenic osteoclasts and relative expression was calculated as $2^{-\Delta\Delta CT}$, where $\Delta\Delta CT = \Delta CT_{calibrator} - \Delta CT_{target}$. (A) Relative expression of P2X (Ai) and P2Y (Aii) genes in BM osteoclasts. (B) Relative expression of P2X (Bi) and P2Y (Bii) genes in splenic osteoclasts following *P2rx7* gene deletion, values are mean ± SEM, n=2 mice in each genotype.

3.3. Discussion

Previous studies to establish the role of P2X7R on development of bone phenotype have had contradictory findings. Despite their expression on human osteoblasts (Gartland et al., 2001; Nakamura et al., 2000) and osteoclasts (Buckley et al., 2002; Gartland et al., 2003a), murine osteoblasts (Ke et al., 2003; Li et al., 2005), osteoclasts (Gartland et al., 2003c; Ke et al., 2003) and osteocytes (Li et al., 2005), conflicting reports to establish the role of P2X7R on skeletal maintenance have been described. Mice knockout models to determine the effect of *P2rx7* gene deletion on bone remodelling had discrepancies that were attributed to a natural mutation in the P2X7R due to the different genetic backgrounds of inbred strain. In light of the recent re-evaluation of existing P2X7R KO mice models (Adriouch et al., 2002; Masin et al., 2012; Nicke et al., 2009), a new P2X7R-/- mouse model was investigated. Mice were obtained by backcrossing the Glaxo KO mice onto the BALB/c background the findings from this chapter indicate that the P2X7(k) variant is expressed in their osteoclast precursors but not in mature osteoclasts differentiated *in vitro*. Results from histological analysis suggest that osteoclast numbers are enhanced with deletion of the receptor, although, bone resorption was altered *in vitro* in P2X7R-/-. There appears to be an intrinsic defect in bone cell function following receptor deletion and genetic analysis is suggestive of impairment of key osteogenic events in P2X7R-/- which may prevent normal bone turnover.

3.3.1. P2X7R-/- mice have increased osteoclast numbers on trabecular and endocortical area

In vivo histological analysis showed an enhanced osteoclastogenesis in P2X7R-/- mice as seen in their numbers and cell size. The Pfizer KO mice used by Ke et al., showed a similar age-independent increase in the osteoclast surface in their female mice (Ke et al., 2003). However, the original Glaxo KO did not show a change in their number of osteoclasts compared to the strain matched WT (Gartland et al., 2003c) despite a change in their cortical bone phenotype. The authors suggested the absence of

osteoblastic apoptosis contributed to the increased cortical thickening, rather than any affect on their osteoclasts. Interestingly, osteoblast numbers and size on endocortical and trabecular surfaces respectively were reduced in our P2X7R-/- mice and in combination with increased osteoclasts are suggestive of a phenotype with severe bone loss.

Despite the changes in bone cell characteristics, P2X7R deletion did not show significant alterations in their trabecular bone architecture. However, they have significantly lower tibial cortical bone mineral density (BMD) but higher bone volume (unpublished findings). The group that generated these KO mice showed an increase in serum alkaline phosphatase activity and increased BMD following P2X7R deletion (Syberg et al., 2012a). This difference in the bone phenotype findings could be attributed to a site-specific response in the absence of P2X7R. Syberg et al., used DEXA for their total BMD measurements and observed a positive balance towards bone formation in these P2X7R-/- mice. On the other hand Wang et al., findings are based on a detailed analysis of the tibial metaphysical architecture however information from serum bone turnover markers is missing from this study and would be better suggestive of an altered bone turnover in P2X7R-/- mice.

3.3.2. Osteoclast precursor cells, but not mature osteoclasts express P2X7(k) variant.

A P2X7(k) variant, which is more sensitive to ATP, is known to have escaped gene deletion in Glaxo KO mice as its been detected in their organs such as spleen, liver, lung (Nicke et al., 2009) and in T-lymphocytes (Xu et al., 2012). In this study, P2X7(k) transcripts were detected in bone marrow cells containing a heterogeneous cell population but also in their splenic buffy layer containing monocytes from hematopoietic lineage. Mature osteoclasts did not show P2X7(k) expression suggesting the successful deletion of P2X7R in the bone resorbing cells in the P2X7R-/- model. However, the stage at which the loss of P2X7(k) variant occurred is unclear as the osteoclasts were isolated at the end of the culture period. Investigating the cells at different time points is needed to identify whether the loss is due to

their culture duration *in vitro* or a characteristic of mature osteoclasts in the mouse model.

3.3.3. P2X7R deletion alters the resorption ability of osteoclasts *in vitro*, dependent upon precursor cell lineage.

Despite the complete absence of P2X7R in both BM and splenic osteoclasts, their function *in vitro* was contradictory and seemed dependent on the site of precursor cell origin. Both Pfizer and Glaxo KO maintained their ability to generate multinucleated osteoclasts *in vitro* (Gartland et al., 2003c; Ke et al., 2003) suggesting a dispensible role of P2X7R for fusion of osteoclastic precursors. In our P2X7R-/- mice, osteoclasts were indeed capable of fusion whether they are generated from the murine BM or spleen, however they were less multinucleated from the P2X7R-/- splenic precursors. Although BM is an established source of (pro)monocytes (van Furth and Cohn, 1968), mouse spleen harbours large quantities of bona fide monocytes (Swirski et al., 2009). It is possible that the mouse spleen acts as a reservoir of extramedullary monocytes capable of contributing to the demands of bone turnover under challenging conditions. A compartment specific P2X7R regulation is speculated and differences in the intrinsic culture conditions for instance, the type of accessory cells, could contribute to the apparent differences in the regulatory mechanism.

This was further supported by the differences in the osteoclastic resorption abilities in the absence of P2X7R. While the P2X7R-/- BM osteoclasts showed significantly reduced resorption abilities, the splenic osteoclasts had a more aggressive osteoclastogenesis reflected by their significantly increased cell numbers and resorptive ability. Despite the conflicting results from the two different *in vitro* models, findings point to an important role of P2X7R in osteoclastic resorption.

3.3.4. P2X7R deletion alters key osteogenic events and may prevent normal bone turnover.

Whole bone marrow aspirates from P2X7R-/- mice showed downregulation of *Csf1* (gene for M-CSF) which is needed in early stages of osteoclast development. M-CSF is secreted by osteoblasts and affects the proliferation, differentiation and survival of the monocytes, macrophages and their progenitors. Murine mutation in the gene for M-CSF results in osteopetrosis due to smaller osteoclasts with impaired bone resorption abilities (Marks and Lane, 1976). This is counter intuitive since not only did the histological analysis show TRAP+ve osteoclasts on bone sections in P2X7R-/- mice, but they were more numerous and larger than P2X7R+/+ controls. It is possible that despite the osteoclast morphology on bone sections, there is a defect in their bone resorbing ability. Serum analysis of BALB/c P2X7R-/- mice showed an almost 50% reduction in CTX (collagen type 1 cross-linked C-telopeptide, a bone resorption biomarker) concentration in P2X7R-/- mice confirming an altered osteoclast activity due to P2X7R deletion (Syberg et al., 2012a). Interestingly, media supplementation was seen to reverse the inability of precursors to differentiate into mature cells of monocyte-macrophage lineage (Wiktor-Jedrzejczak et al., 1982). Therefore, the defect was attributed to lack of M-CSF production *in vivo* rather than an abnormal precursor cell population. P2X7R-/- BM derived osteoclasts *in vitro* maintained their reduced resorption ability despite M-CSF supplementation potentially due to the lack of a P2X7R mediated co-stimulus.

Another pro-osteoclastic cytokine is IL-6 as evidence shows its presence in diseases involving excessive bone resorption and targeting its receptor, IL-6R, is currently prescribed for the treatment of RA (Smolen et al., 2010). Increased IL-6 results in an increased osteoclast activity and similar to M-CSF, the main source of IL-6 are osteoblasts and stromal cells (De Benedetti et al., 2006; Ishimi et al., 1990). A downregulated IL-6 mRNA in P2X7R-/- bone marrow cells suggests their inability to sufficiently stimulate osteoclasts and an eventual dysregulation in osteoclastic intracellular signalling events. Other than the independent action of IL-6 by supporting events that promote

bone resorption, IL-6 is capable of acting synergistically with RANKL and enhance the precursor cell sensitivity to RANKL (Menaa et al., 2000). Release of IL-6 is in part, induced by IL-1 (Rothe et al., 1998) and P2X7R activation has been demonstrated to be upstream of IL-6 release (Solini et al., 1999). Moreover, processing and release of bioactive of IL-1 is a well studied phenomenon induced by extracellular ATP. Therefore, a change in one of these key immunomodulatory factors, that are regulated by P2X7R, can amplify the effect of the other. Additionally, reduction in *Il1r2* (decoy receptor for IL-1) could disrupt the complex interactions between IL-1 factors (IL-1α, IL-1β, IL-1Ra, IL-1 receptors, and IL-1 receptor accessory protein) essential for osteoclast formation and activity.

Another important downregulation in P2X7R-/- bone marrow was in the gene coding for COX-2 protein, *Ptgs2*. Importance of COX-2 in bone cells function was demonstrated when specific inhibitors prevented differentiation and resorption by osteoclasts along with osteoblast differentiation from their precursors (Kellinsalmi et al., 2007). Its increased levels were recently shown in differentiated RAW264.7 cells alongside activation of osteoclast related genes such as RANK, TRAF6 and MAPK (Hou et al., 2013). These data suggest that the BM microenvironment might be unable to adequately drive the precursors into functional osteoclasts.

In addition to the seemingly intrinsic defects in osteoclastic differentiation and activity, P2X7R-/- BM cells showed upregulated *Bglap1* (Osteocalcin), *Sparc* (Osteonectin), *Col1a2* (Collagen type I alpha-2), *Col2a1* (Collagen type II alpha-1) which are known osteoblast-specific genes. Whilst osteocalcin limits bone formation without compromising mineralisation (Ducy et al., 1996), osteonectin is needed for normal bone turnover by maintaining cell survival (Delany et al., 2000). *Col1a1* produces pro-alpha1(I) chain and in combination with product of *Col1a2*, result in maturation of collagen fibres by osteoblasts. Increased collagen production will increase the volume of the bone but not its density and therefore deregulation of these genes is suggestive of a phenotype with altered bone mass. Due to the importance of each of the genes during specific osteoblastic events, identifying the effects

of P2X7R deletion on osteoblastic bone formation and mineralisation will help determine the contribution of the receptor in bone formation.

Nevertheless, this P2X7R-/- model suggests a tendency towards development of a bone phenotype with higher bone formation and µCT analysis showing high cortical bone volume (Wang et al., in prep) at 4 months of age with increased femoral strength (Syberg et al., 2012a) and highlights the usefulness of the model in studying the events of bone remodelling.

On the contrary, an existing Pfizer KO model shows a suppressed expression of osteoblast markers in calvarial cells suggestive of an osteogenic role of P2X7R activation (Panupinthu et al., 2008). These seemingly different P2X7R mediated responses in bone formation could be due to the presence of splice variants. The Pfizer KO mice were recently reported to have a C-terminal truncated splice variant rendering a reduced function to the P2X7R (Masin et al., 2012) whereas the BALB/c KO mice retain a more sensitive variant, P2X7(k) (Nicke et al., 2009). It is likely that these functional changes in P2X7R affect the bone cell responses and contribute to these opposing findings. However more studies are needed to determine the role of P2X7(k) variant in regulating osteoblast differentiation and mediation in bone turnover.

Interestingly, the presence of P2X7(k) variant was detected in BM aspirates suggestive that the P2X7R mediated changes might not be fully abrogated but the extent to which the variant contributes to the development of each of the bone cells still needs to be investigated. Additionally, *Ak1* (adenylate kinase 1), gene responsible for maintaining the reversible conversion of 2 ADP ⇔ ATP + AMP in skeletal muscle was upregulated in P2X7R-/- mice. Excess production of the enzyme suggests a rapid inter-conversion of nucleotides, which could, potentially allow other purinoceptors to compensate for the loss of P2X7R.

3.3.5. Reduced resorption in P2X7R-/- could be partly due to a defect in TRAP secretion and in part due to a reduced sensitivity to cytokines of BM osteoclasts.

BM osteoclasts obtained from P2X7R-/- showed reduced resorptive ability per osteoclasts despite no changes in the cell numbers on dentine discs (Figure 3-6). To determine whether the genetic defects in the osteoclasts could be contributing to their failure to resorb as efficiently as P2X7R+/+ cells, TaqMan® Array was performed. A reduced expression of *Acp5* (gene coding for TRAP enzyme) could in part, be indicative of their inability to resorb similar to the BM osteoclasts from P2X7R+/+ mice. High amounts of TRAP is secreted by osteoclasts to aid the dissolution of bone protein, along with Cathepsin-K and MMPs (Bossard et al., 1996; Kusano et al., 1998; Saftig et al., 1998) and low TRAP is associated with an intrinsic defect in resorptive ability (Hayman et al., 1996). Moreover, *P2rx7* gene deletion led to production of osteoclasts with higher osteonectin expression with a slight reduction in *Csf1r* (receptor for M-CSF). This is rather interesting as osteonectin deficiency was demonstrated to increase the sensitivity of marrow cells to M-CSF and promote osteoclastogenesis (Machado do Reis et al., 2008; McCabe et al., 2011). A combination of potentially a reduced survival of mature osteoclasts to pro-osteoclastogenic cytokine M-CSF and a defective proteolysis due to insufficient TRAP production suggests a defect in bone resorptive ability of P2X7R-/- osteoclasts.

3.3.6. P2X7R deletion causes increased survival but reduced fusion of splenic osteoclasts.

Contradictory to BM osteoclasts, precursors derived from spleens of P2X7R-/- mice differentiated into more numerous and more aggressive bone resorbing cells compared to P2X7R+/+ cultures. In line with the significance of osteonectin deficiency in enhancing the sensitivity of osteoclastic precursors, a recent role of this non-collagenous bone protein was

documented in enhancing cancer induced osteolysis in *sparc* null mice (McCabe et al., 2011). The authors showed increase in the endogenous resorptive efficiency of osteoclast-like cells, similar to the findings *in vitro* in the splenic osteoclasts from P2X7R-/- mice. Significant higher osteoclast numbers towards the end of the culture period could be due to a prolonged cell survival (Figure 3-7).

Rather interestingly, *Bmp2* was overexpressed in splenic osteoclasts generated from P2X7R-/- mice. Osteoclastic BMP-2 has been detected by both mRNA and protein expression in previous studies (Anderson et al., 2000; Itoh et al., 2001), although its expression in osteoclasts at bone modelling/remodelling sites is debatable (Spector et al., 2001; Zoricic et al., 2003). It is speculated that osteoclastic expression of BMP-2 is limited to particular stages of their differentiation which could explain the discrepancies in the findings (Jensen et al., 2010). Since addition of BMP-2 stimulates murine osteoclastic formation and survival in the presence of RANKL (Itoh et al., 2001; Kaneko et al., 2000) and Jensen et al., suggest that BMP-2 signalling could be under autocrine regulation by osteoclasts (Jensen et al., 2010) enhanced *Bmp2* expression could be an additional cause for heightened resorption and survival by P2X7R-/- osteoclasts.

Expression of *Calcr* (gene for calcitonin receptor) supports the findings of enhanced maturation and activity by P2X7R-/- splenic osteoclasts. Receptor expression is long known to be a hallmark of a mature, resorbing osteoclast (Nicholson et al., 1986), and its ligand, calcitonin, inhibits resorption and is the basis of using it as a therapeutic target in diseases with excessive bone loss.

Involvement of interleukins has been extensively studied in regulation of bone physiology and maintenance of a healthy skeleton. Osteoclasts containing the *P2rx7* gene deletion showed aberrant expression of genes for IL-6, IL1α, IL1β, Interleukin 1 receptor, type I, suggesting loss of orchestration of osteoclast activity by cytokines. Presumably, loss of homeostatic control by the cytokines could be caused by the absence of P2X7R. Activation of P2X7R in interleukin-1 maturation and release and higher receptor

expression during inflammatory response has been extensively reviewed in the literature (Ferrari et al., 2006; Miller et al., 2011a; Wiley et al., 2011). Both Pfizer and Glaxo KO mice show defective cytosolic and cellular LPS-induced IL-1β levels (Chessell et al., 2005; Labasi et al., 2002; Solle et al., 2001). IL-1 in turn modulates IL-6 release and it is possible that loss of P2X7R led to crumbling of this cytokine cascade and abruption in homeostatic control of osteoclastogenesis. The extent to which the loss of *P2rx7* gene could be the causal or affect of the downregulation of the IL-1 family and its receptors in osteoclasts would be interesting to investigate.

Another important finding was the downregulation of *Nt5e* (gene for ecto5′-nucleotidase) in P2RX7-/- splenic osteoclasts, the enzyme which catalysis the conversion of nucleotides to adenosine. Extracellular adenosine results in increased fusion of osteoclasts (Pellegatti et al., 2011) during their *in vitro* differentiation from precursors. This fusion is reversible since adenosine degradation, despite enough substrate for the activity of plasma membrane 5′-nucleotidase, completely abolished the fusion. It is possible that despite the ability of precursors to initiate fusion, adenosine generation could be a limiting factor and restrict, but not completely abolish, their fusion ability. Results from splenic cultures show that deletion of *P2rx7* gene lead to reduced fusion index in splenic osteoclasts despite the presence of multinucleated cells on glass coverslips confirming that P2X7R does not exclusively mediate fusion. Pellegatti et al., suggested that P2X7R in combination with adenosine receptor, A2A are needed for fusion whereby P2X7R mediated ATP release acts as a source of adenosine, which eventually drives the process (Pellegatti et al., 2011).

3.3.7. P2X7R deletion reduced *P2ry12* gene expression in BM osteoclasts and reduced *P2rx4* expression in splenic osteoclasts.

Receptor redundancy is often cited as a reason why knockout models of single genes from larger closely related gene families do not show severe phenotypes/effects. In both cell lineages there was no upregulation of other

P2R genes ruling out a compensatory mechanism. However, mature osteoclasts of BM lineage showed reduced *P2ry12* expression. P2Y12R-/- mice showed aberrant function in osteoclasts both in vivo and during pathological bone remodelling (Su et al., 2012). Whether P2ry12 gene contributed to the defected resorption in *P2rx7* deficient osteoclasts *in vitro* was not investigated but a plausible connection resulting in overall reduced osteoclastic activity is interesting. In addition, splenic osteoclasts from P2X7R-/- mice showed reduced *P2rx4* gene expression. Expression of P2X4R on rat and rabbit osteoclasts has been demonstrated (Hoebertz et al., 2000; Naemsch et al., 1999) and it is speculated that activation could induce the membrane depolarization and therefore influence osteoclastic events such as formation of ruffled border along with gene transcription following calcium entry.

3.4. Conclusion

In the BALB/c P2X7R-/- mice, the P2X7(k) variant was present in the precursor cells used to obtain the osteoclasts but was missing in the resorbing osteoclasts differentiated *in vitro* confirming the absence of P2X7R in mature osteoclasts. The behaviour of the mature osteoclasts from the two lineages was different and appeared regulated by the site of origin and dependent on the loss of P2X7R. Closer examination of the osteoclasts using the gene expression profile suggests that absence of receptor causes an alteration in key osteogenic and osteoclastogenic events. The P2X7R is dispensable for initiation of osteoclast fusion but could play an important role in osteoclast activity by influencing the rate of formation of osteoclasts as well as regulating cell survival.

Chapter 4. Can P2X7R blockade rescue OVX induced bone loss?

4.1. Introduction

Osteoclasts are multinucleated cells formed by the fusion of mononuclear precursors present in blood monocyte fraction, targeting their formation could prove to be beneficial for treatment of bone diseases with excessive osteoclast activity such as osteoporosis. Multinucleated osteoclast formation however, is a multistep process comprising of different stages and cell-cell interaction is crucial for their formation. It is still uncertain at which step P2X7R acts in the process, but literature suggests that blockade of receptor activity reduces bone resorption *in vitro*, preceded by a loss of osteoclast fusion (Agrawal et al., 2010). As shown in 0, absence of P2X7R resulted in impaired osteoclast formation and subsequent alteration in resorption. Also, a dysregulation in osteoclastogenic genes either causing an intrinsic defect in the osteoclasts or an impairment in the process due to an altered microenvironment were observed in the absence of *P2rx7* gene. Therefore, the hypothesis of this chapter is that pharmacological blockade of P2X7R will result in rescue of OVX induced bone loss via a decline in osteoclastic resorption.

The aim of this chapter is to determine the effects of a novel P2X7R antagonist (compound CPH1) on murine osteoclast formation and function *in vitro* and determine whether OVX induced bone loss could be reversed by antagonising P2X7R in a mouse model of osteoporosis. Finally, determine the effects of compound CPH1 on human osteoclastogenesis *in vitro*. CPH1 is a small molecule P2X7R antagonist with an IC50 30 nM on mouse P2X7R. In monocytes, it was seen to inhibit BzATP induced IL-1 production and in HEK293 cells over expressing P2X7R, addition of compound blocks Ca^{2+} intake. It has a poor metabolic stability with an *in vivo* t½ of 0.69 hours in mice and therefore has to be administered with PEG as vehicle.

4.2. Results

4.2.1. Effect of P2X7R antagonist on differentiation of murine osteoclasts *in vitro*

CPH1 was introduced throughout the 17 day culture period to differentiating bone marrow precursors obtained from long bone flushes of 3 month old BALB/c female mice. As is clearly established, the definitive marker for osteoclast activity is their ability to form resorption lacunae on bone substrates. The precursors were seeded onto dentine discs, results demonstrate that treatment with CPH1 reduced the area of resorption lacunae excavated by the osteoclasts in a dose dependent manner (Figure 4-1 A). CPH1 had no significant effect on the number of resorbing osteoclasts that remained at the end of the culture period or a change in their resorption ability (Figure 4-1 C).

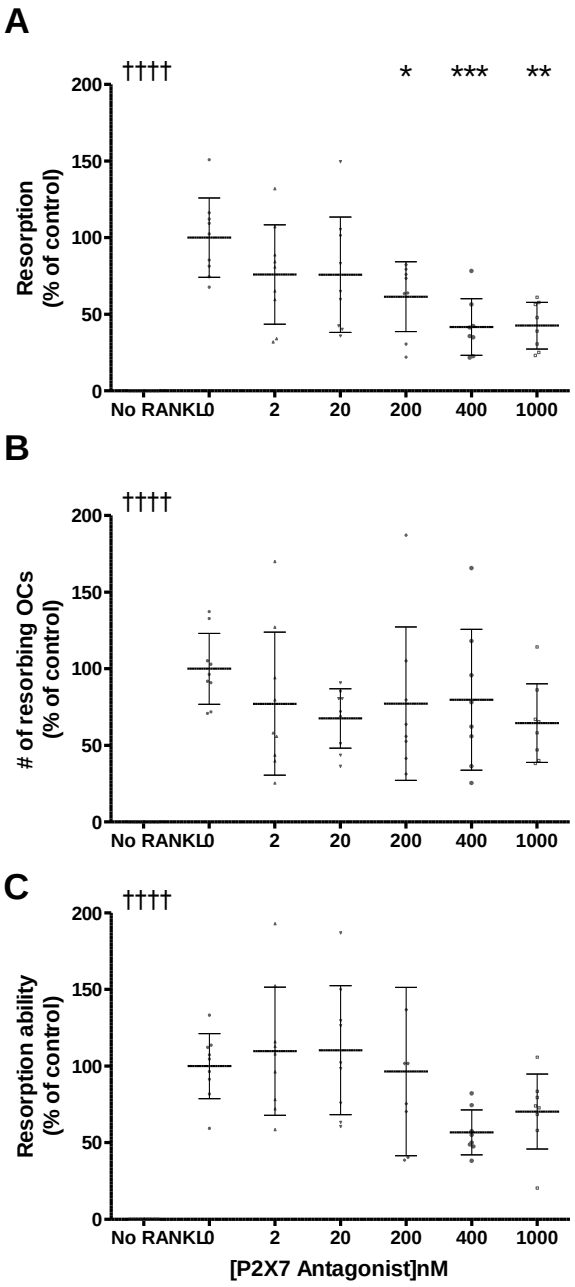

Figure 4-1 Effect of CPH1 on murine osteoclast formation.

CPH1 was added with every culture medium change to differentiating murine osteoclasts *in vitro* and TRAP stained. Resorption (A), number of resorbing osteoclasts (B) and resorptive ability (resorption/resorbing osteoclast) (C) was determined. Values are mean ± SD, n = 3 mice osteoclast cultures containing a total of 9 replicate dentine discs. *p < 0.05, **p<0.01, ***p<0.001 (One-Way ANOVA), ††††P<0.0001 (Student's t-test) significance from vehicle

4.2.1.1. Confirmation of bone loss in OVX mice

4.2.1.2. Effect on vertebral bone

BALB/c mice clearly respond to OVX induced bone loss and show pronounced changes in the trabecular bone architecture following surgery (Bouxsein et al., 2005). To confirm whether there manifestation of osteoporosis in our model, bone microarchitecture was analysed using µCT.

Trabecular changes in L4 were assessed by µCT in both SHAM and OVX animals 4 weeks post surgery. OVX resulted in non-significant trends towards decreased BV/TV and Tb.Th. No increase in Tb.Sp or reduction in DA were observed following OVX in L4 vertebrae of the animals compared to those of SHAM. Moreover, the length of L4 was not altered due to surgery. However, Tb.N were reduced with concomitant increase in Tb.Pf (increase in disconnectivity) and increased SMI (transition to rod-like structures) in OVX (↓14%, p=0.0383, ↑295%, p=0.0207, ↑44%, p=0.0133 respectively) compared to SHAM (Figure 4-2).

OVX parameters are expressed as percentage of mean of SHAM and t-test was used to compare the parameters.

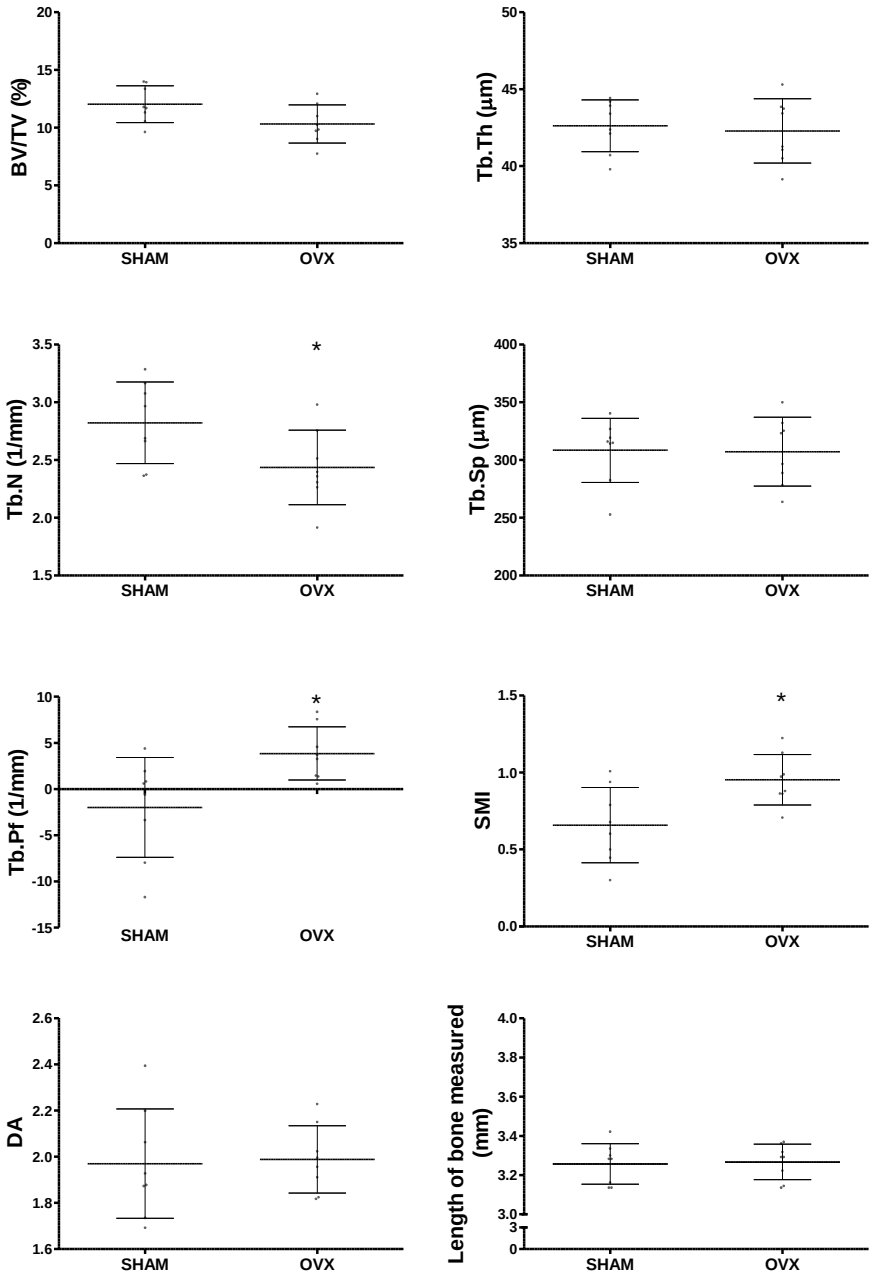

Figure 4-2 Vertebral trabecular morphology following OVX

Female mice at 16 weeks underwent either SHAM or OVX surgery. Four weeks were allowed for the induction of osteoporosis and mice were sacrificed and L4 vertebrae scanned at a resolution of 4.3µm through 360° rotation. ROI spanned 30% of the height of each vertebra. Y-axis parameters are Percent bone volume (BV/TV), Trabecular thickness (Tb.Th), Trabecular number (Tb.N), Trabecular separation (Tb.Sp), Trabecular bone pattern factor (Tb.Pf), Structure model index (SMI) and Degree of anisotropy (DA). Graphs Mean±SD, n=8 mice each group. *p<0.05 (Student's t-test)

4.2.1.3. Effect on tibial bone

Left tibia of all mice was collected and proximal metaphysis was scanned at 4.3µ as described in Section 2.2.5.2. Trabecular changes were assessed and a statistically significant reduction in BV/TV (↓22%, p=0.0020), Tb.N (↓18%, p=0.0204) and increased DA (↑11%, p=0.0137) were obtained in OVX compared to SHAM mice 4 weeks post surgery. No significant reductions in total BV, Tb.Th or increase in Tb.Sp, Tb.Pf or SMI were observed (Figure 4-3)

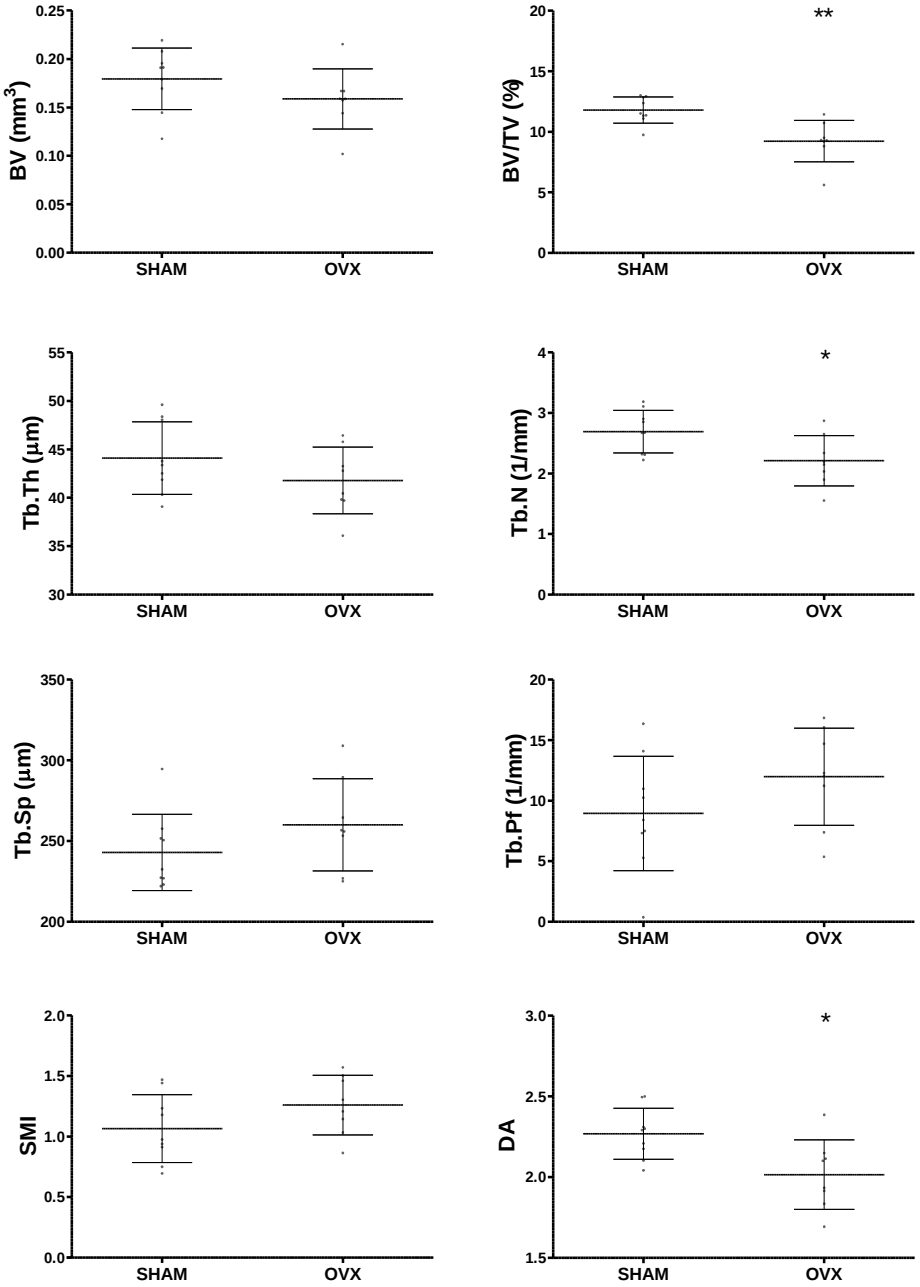

Figure 4-3 Tibial trabecular morphology following OVX.

Female mice at 16 weeks underwent either SHAM or OVX surgery. Four weeks were allowed for the induction of osteoporosis and mice were sacrificed and left tibiae scanned at a resolution of 4.3µm through 180° rotation. ROI spanned 1mm height 0.5mm distal to first break in growth plate bridge. Y-axis parameters are Percent bone volume (BV/TV), Trabecular thickness (Tb.Th), Trabecular number (Tb.N), Trabecular separation (Tb.Sp), Trabecular bone pattern factor (Tb.Pf), Structure model index (SMI) and Degree of anisotropy (DA). Graphs Mean±SD, n=9 mice in SHAM, 8 mice in OVX. *p<0.05, **p<0.01(Student's t-test).

4.2.1.4. Effect on femoral bone

Left femur of mice were analysed at distal metaphysis to measure the changes in trabecular bone compartment. Significant reductions in total BV (↓13%, p=0.0030), BV/TV (↓24%, p<0.0001), Tb.Th (↓5%, p=0.0018), Tb.N (↓20%, p<0.0001) were observed. Additionally, trabeculae architecture was also significantly altered as increased Tb.Sp (↑8%, p=0.0083), Tb.Pf (↑77%, p=0.0038) and SMI (↑26%, p=0.0014) were measured in OVX femur compared to SHAM. No alteration in DA was observed between SHAM and OVX. (Figure 4-4)

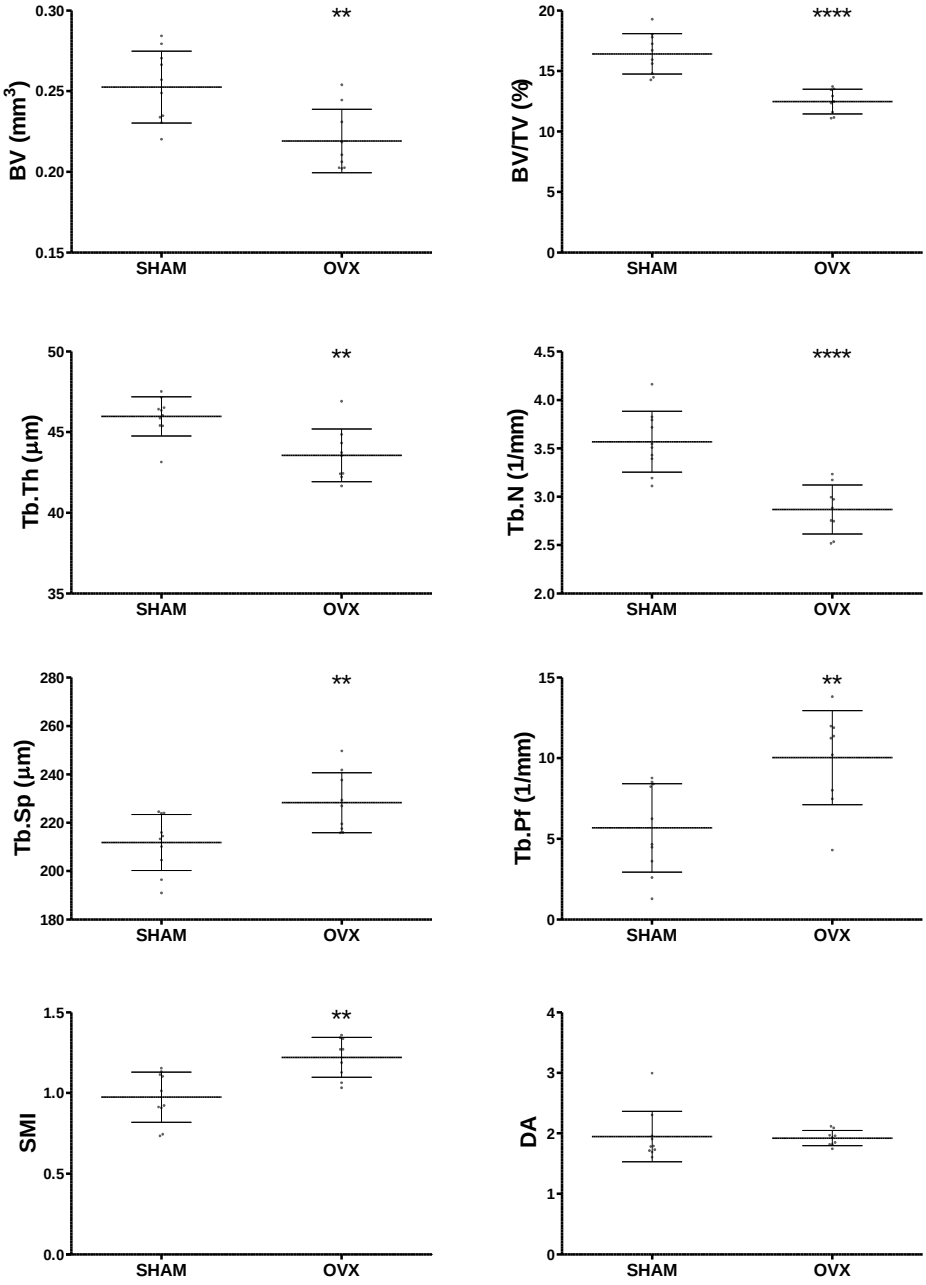

Figure 4-4 Femoral trabecular morphology following OVX.

Female mice at 16 weeks underwent either SHAM or OVX surgery. Four weeks were allowed for the induction of osteoporosis and mice were sacrificed and femur scanned at a resolution of 4.3µm through 180° rotation. ROI spanned 1mm height 0.6mm distal to first break in growth plate bridge. Y-axis parameters are Percent bone volume (BV/TV), Trabecular thickness (Tb.Th), Trabecular number (Tb.N), Trabecular separation (Tb.Sp), Trabecular bone pattern factor (Tb.Pf), Structure model index (SMI) and Degree of anisotropy (DA). Graphs Mean±SD, n=10 mice in SHAM, 9 mice in OVX. **p<0.01, ****p<0.0001 (Student's t-test)

4.2.2. Trabecular bone response post OVX and CPH1 administration

4.2.2.1. Effect on vertebral bone

Daily administration of CPH1 for 4 weeks to reverse OVX induced bone loss was measured by assessing the trabecular bone architecture in L4 vertebra of the mice. Treatment with PTH resulted in increased BV/TV (↑24%, p=0.0002), Tb.N (↑33%, p<0.0001) along with restoration of Tb.Pf (connectivity) (↓218%, p=0.0002), SMI (plate like trabeculae) (↓98%, p=0.0091) and DA (symmetry) (↓15%, p=0.0233) compared to vehicle (0) treated mice. CPH1 failed to induce a similar reversal of bone loss but there was a prominence of more rod like trabeculae with treatment (100) (↑100%, p<0.05) compared to vehicle (0) (Figure 4-5).

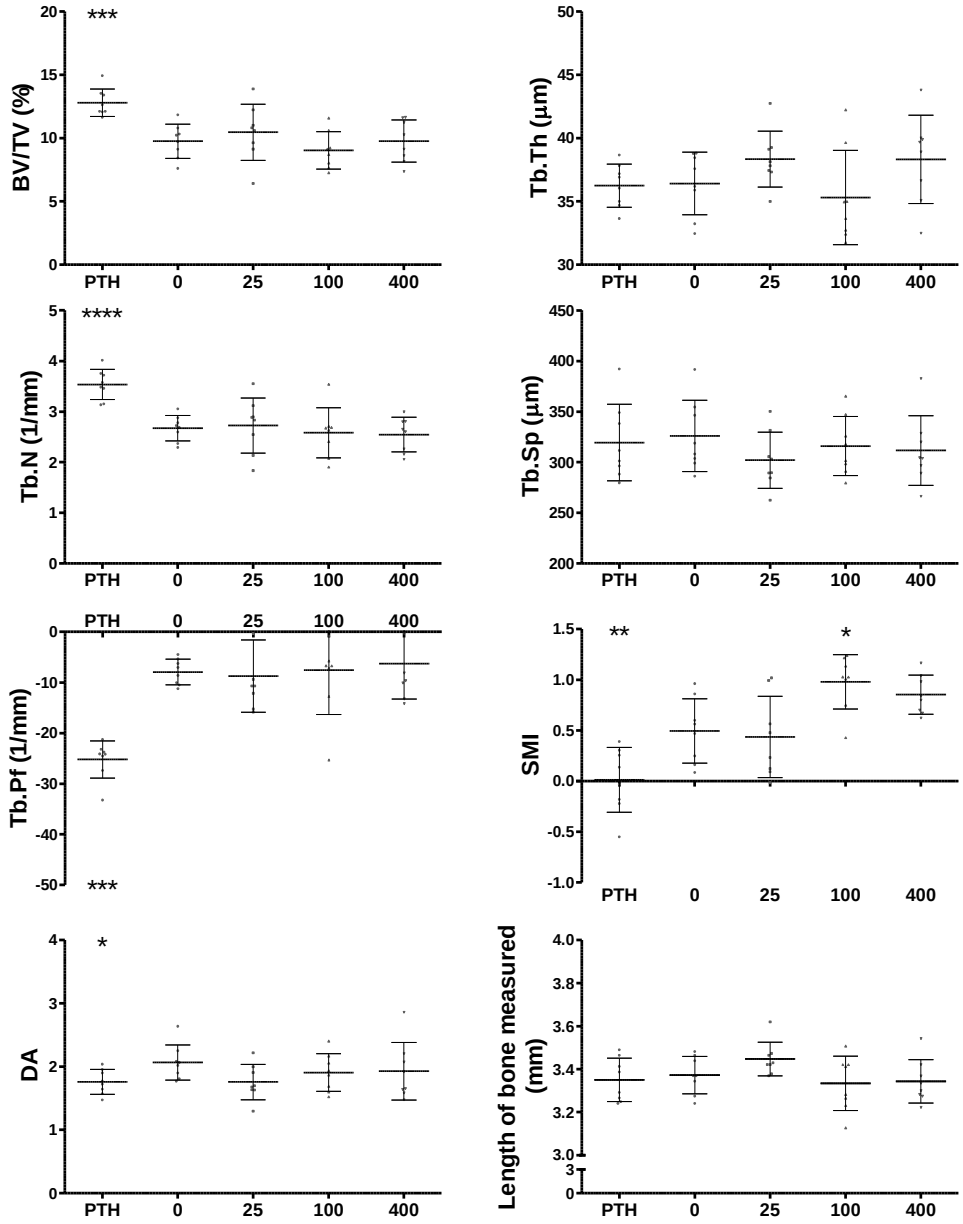

Figure 4-5 Vertebral trabecular bone response post OVX and CPH1 administration.

Female mice at 16 weeks underwent OVX surgery and were treated daily with PTH, vehicle (0) or CPH1 (25, 100, 400) between 20 and 24 weeks. Mice were sacrificed and L4 vertebrae were scanned at a resolution of 4.3µm through 360° rotation. ROI spanned 30% of the height of each vertebra. Y-axis parameters are Percent bone volume (BV/TV), Trabecular thickness (Tb.Th), Trabecular number (Tb.N), Trabecular separation (Tb.Sp), Trabecular bone pattern factor (Tb.Pf), Structure model index (SMI) and Degree of anisotropy (DA). Graphs Mean±SD, n=8 mice each group. *p<0.05 significance from vehicle (0).

4.2.2.2. Effect on tibial bone

Examination of trabecular bone architecture in the proximal metaphysis of all mice demonstrated no effect of CPH1 following the 4 week treatment regime. Effects of PTH were prominent with increase in BV (↑65%, $p=0.0005$), BV/TV (↑66%, $p<0.0001$), Tb.N (↑86%, $p<0.0001$) compared to vehicle (0). Moreover, restoration of tibial trabecular architecture was observed following PTH treatment as reduced Tb.Pf (↓419%, $p<0.0001$), SMI (↓203%, $p<0.0001$) was obtained in the bone compartment. Interestingly, Tb.Th showed a significant decline in PTH treated mice (↓11%, $p=0.0032$) compared to the vehicle treated group, suggestive of increase in number of trabeculae as opposed to any thickening of the existing ones causal for the observed increase in bone volume (Figure 4-6).

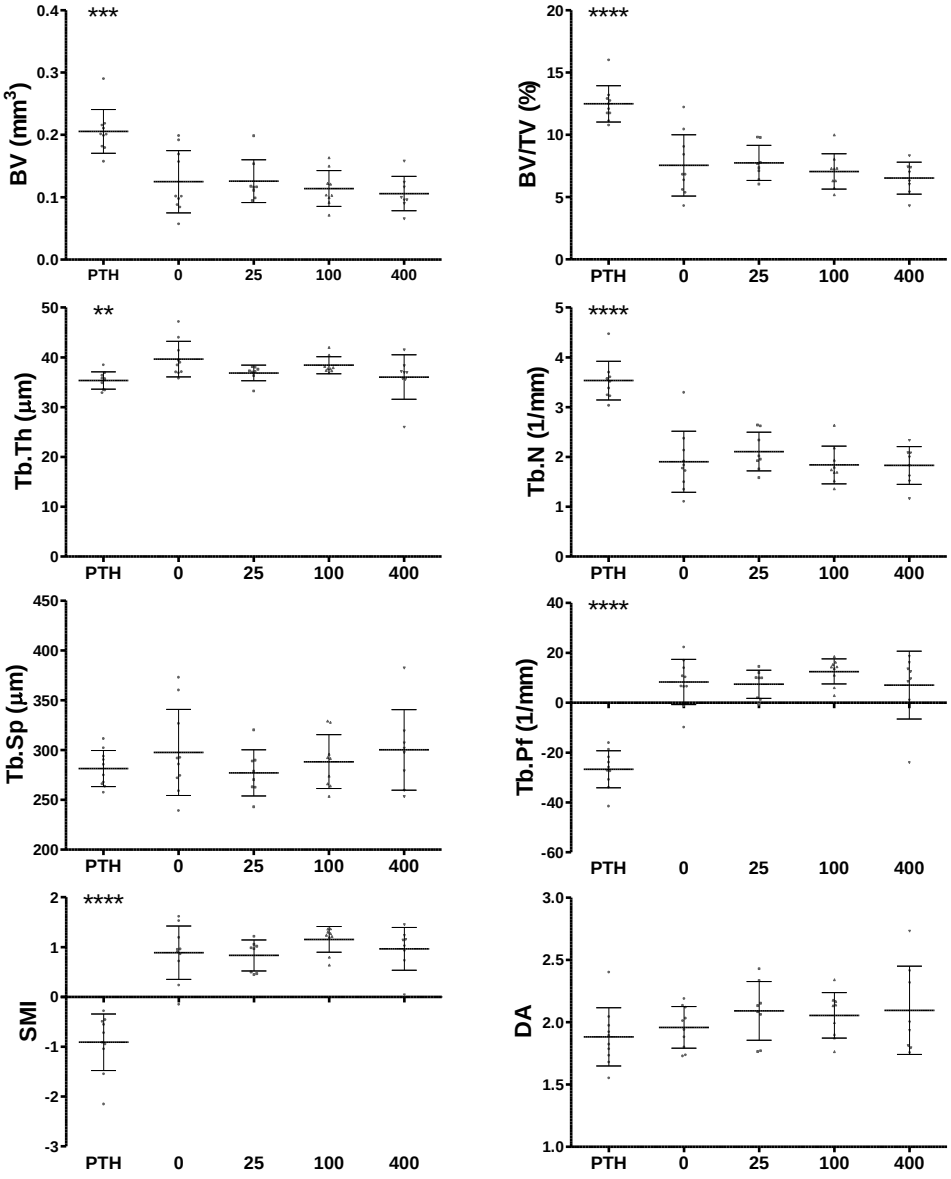

Figure 4-6 Tibial trabecular bone response post OVX and CPH1 administration.

Female mice at 16 weeks underwent OVX surgery and were treated daily with PTH, vehicle (0) or CPH1 (25, 100, 400) between 20 and 24 weeks. Mice were sacrificed and left tibiae scanned at a resolution of 4.3µm through 180° rotation. ROI spanned 1mm height, 0.5mm distal to first break in growth plate bridge. Y-axis parameters are Percent bone volume (BV/TV), Trabecular thickness (Tb.Th), Trabecular number (Tb.N), Trabecular separation (Tb.Sp), Trabecular bone pattern factor (Tb.Pf), Structure model index (SMI) and Degree of anisotropy (DA). Graphs Mean ±SD, n=8-10 mice in each group. **p<0.01, ***p<0.001, ****p<0.0001 significance from vehicle (0).

4.2.2.3. Effect on femoral bone

Femurs of all mice were examined at the distal metaphysis, CPH1 did not show any significant increase in BV, BV/TV or Tb.N after 4 weeks of treatment. Tb.Th was reduced in the presence of CPH1 at 100 (↓6%, p=0.0127) and 400 (↓7%, p=0.0115) which is a contrary effect to the increased Tb.Th following PTH treatment (9%, p=0.0008). Treatment with PTH also increased BV (↑73%, p<0.0001), BV/TV (↑72%, p<0.0001), Tb.N (↑58%, p<0.0001) in addition to restoration of femoral architecture as trabecular connectivity; Tb.Pf (↓142%, p<0.0001) and plate like structures; SMI (↓68%, p<0.0001) were significantly restored compared to vehicle (0) (Figure 4-7).

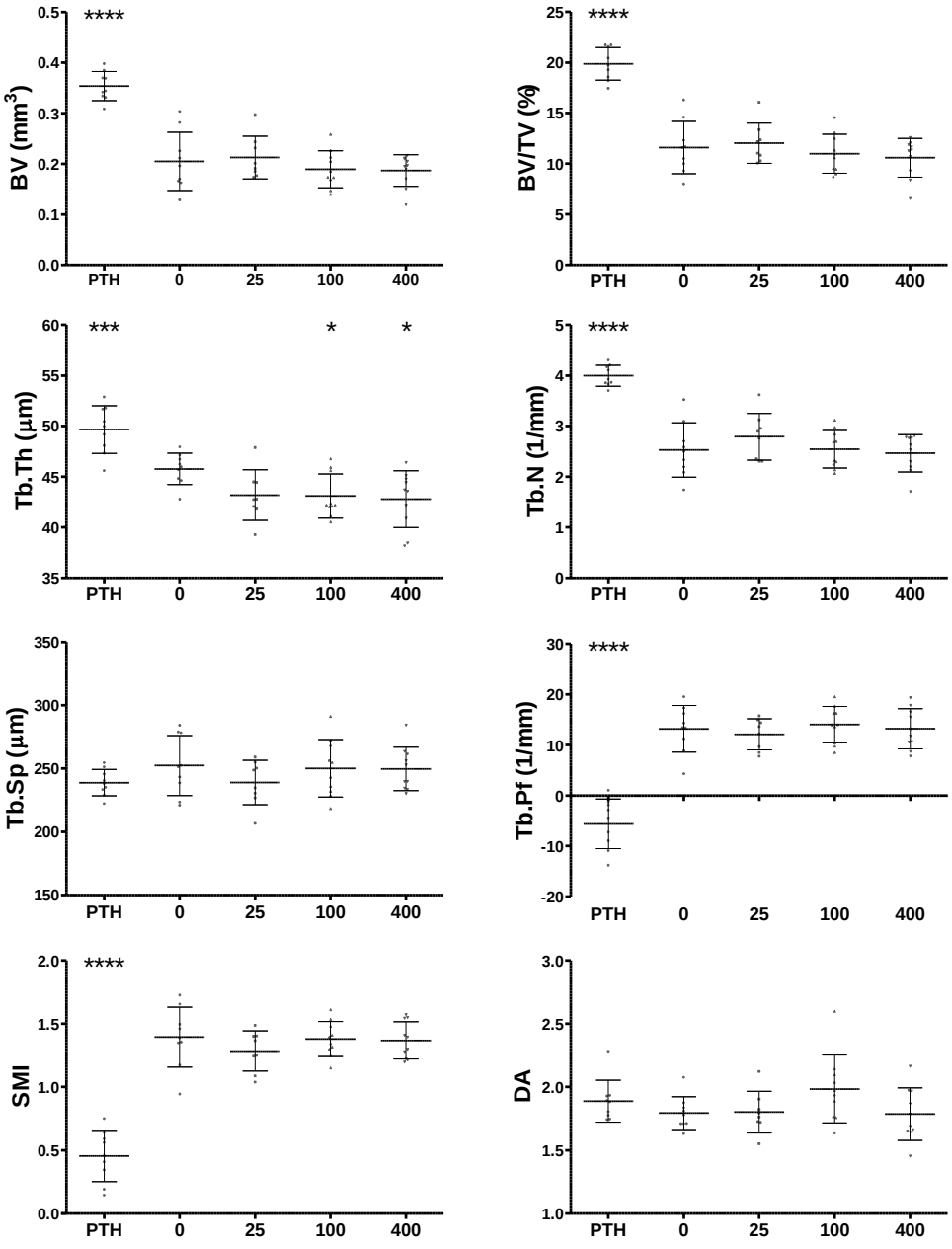

Figure 4-7 Femoral trabecular bone response post OVX and CPH1 administration.

Female mice at 16 weeks underwent OVX surgery and were treated daily with PTH, vehicle (0) or CPH1 (25, 100, 400) between 20 and 24 weeks. Mice were sacrificed and femora were scanned at a resolution of 4.3µm through 180° rotation. ROI spanned 1mm height 0.6mm distal to first break in growth plate bridge. Y-axis parameters are Percent bone volume (BV/TV), Trabecular thickness (Tb.Th), Trabecular number (Tb.N), Trabecular separation (Tb.Sp), Trabecular bone pattern factor (Tb.Pf), Structure model index (SMI) and Degree of anisotropy (DA). Graphs Mean±SD, n=8-10 mice in each group. ***p<0.001, ****p<0.0001 significance from vehicle (0).

Table 4-1 Effect of OVX and CPH1 treatment on trabecular bone parameters

Parameter	**Treatment groups Mean±SD**						
Vertebra (L4)	SHAM	OVX	PTH	0	25	100	400
BV (mm^3)	0.142± 0.018	0.141± 0.028	0.179± 0.020†††	0.132± 0.020	0.146± 0.038	0.123± 0.025	0.134± 0.025
BV/TV (%)	12.03± 1.60	10.33± 1.66	12.80± 1.09†††	9.76± 1.35	10.46± 2.21	9.03± 1.47	9.76± 1.67
Tb.Th (µm)	42.62± 1.69	42.29± 2.09	36.25± 1.71	36.42± 2.48	38.35± 2.21	35.31± 3.73	38.33± 3.48
Tb.N (1/mm)	2.82± 0.35	2.44± 0.32*	3.54± 0.30††††	2.67± 0.25	2.73± 0.54	2.58± 0.49	2.54± 0.34
Tb.Sp (µm)	308.4± 27.7	307.2± 29.8	319.5± 37.8	326.0± 35.3	302.0± 27.8	316.0± 29.2	311.6± 34.4
Tb.Pf	-1.98± 5.40	3.86± 2.87*	-25.21± 3.66†††	-7.93± 2.53	-8.74± 7.13	-7.57± 8.75	-6.28± 6.98
SMI	0.66± 0.24	0.95± 0.16*	0.01± 0.32††	0.49± 0.32	0.44± 0.40	0.98± 0.27†	0.85± 0.19
DA	1.97± 0.23	1.99± 0.15	1.76± 0.20†	2.07± 0.28	1.76± 0.28	1.91± 0.30	1.93± 0.45
Tibia							
BV (mm^3)	0.179± 0.032	0.159± 0.031	0.206± 0.035†††	0.125± 0.050	0.126± 0.034	0.114± 0.029	0.106± 0.028
BV/TV (%)	11.80± 1.08	9.23± 1.71**	12.50± 1.46††††	7.55± 2.47	7.75± 1.40	7.06± 1.42	6.53± 1.29
Tb.Th (µm)	44.10± 3.73	41.78± 3.44	35.37± 1.74††	39.65± 3.59	36.86± 1.56	38.41± 1.69	36.06± 4.46
Tb.N (1/mm)	2.69± 0.35	2.21± 0.42*	3.54± 0.39††††	1.90± 0.61	2.11± 0.39	1.84± 0.38	1.83± 0.38
Tb.Sp (µm)	242.9± 23.6	260.1± 28.5	281.4± 18.1	297.6± 43.2	277.1± 23.2	288.3± 26.9	300.2± 40.5
Tb.Pf	8.95± 4.73	11.98± 4.02	-26.67± 7.45††††	8.35± 9.08	7.44± 5.66	12.55± 5.04	7.07± 13.62
SMI	1.07± 0.28	1.26± 0.25	-0.91± 0.57††††	0.88± 0.54	0.83± 0.31	1.16± 0.26	0.96± 0.43
DA	2.27± 0.15	2.02± 0.22*	1.88± 0.23	1.96± 0.17	2.09± 0.24	2.06± 0.18	2.09± 0.35
Femur							
BV (mm^3)	0.253± 0.022	0.219± 0.020**	0.354± 0.029††††	0.205± 0.058	0.212± 0.043	0.189± 0.037	0.187± 0.031
BV/TV (%)	16.42± 1.68	12.48± 1.02****	19.86± 1.62††††	11.59± 2.59	12.02± 1.99	10.98± 1.93	10.58± 1.91
Tb.Th (µm)	45.98± 1.21	43.57± 1.64**	49.66± 2.35†††	45.77± 1.54	43.19± 2.51	43.09± 2.18†	42.78± 2.80†
Tb.N (1/mm)	3.57± 0.32	2.87± 0.25****	3.99± 0.21††††	2.53± 0.54	2.79± 0.46	2.54± 0.37	2.46± 0.37
Tb.Sp (µm)	211.8± 11.6	228.3± 12.4**	238.9± 10.5	252.4± 23.7	239.0± 17.6	250.2± 22.7	249.8± 17.2
Tb.Pf	5.68± 2.74	10.03± 2.92**	-5.59± 4.92††††	13.18± 4.61	12.11± 3.01	14.03± 3.59	13.21± 3.96
SMI	0.97± 0.15	1.22± 0.12**	0.45± 0.20††††	1.39± 0.24	1.29± 0.16	1.38± 0.14	1.37± 0.15
DA	1.95± 0.42	1.92± 0.13	1.88± 0.17	1.79± 0.13	1.80± 0.17	1.98± 0.27	1.79± 0.21

*p<0.05, **p<0.01, ***p<0.001, ****p<0.0001 of SHAM or †p<0.05, ††p<0.01, †††p<0.001, ††††p<0.0001 of vehicle (0).

4.2.3. Cortical bone morphology following OVX

4.2.3.1. Effect on tibial bone

Left tibia was examined at the diaphysis to determine cortical bone parameters with the exclusion of all trabeculae. OVX induced bone loss was absent in tibial cortical compartment as BMD, BV, BV/TV and Ma.V were non-significantly altered in OVX mice compared to SHAM (Figure 4-8).

Entire tibiae were also examined and BV/TV was 4% less in OVX animals ($p=0.0303$) (Table 4-2).

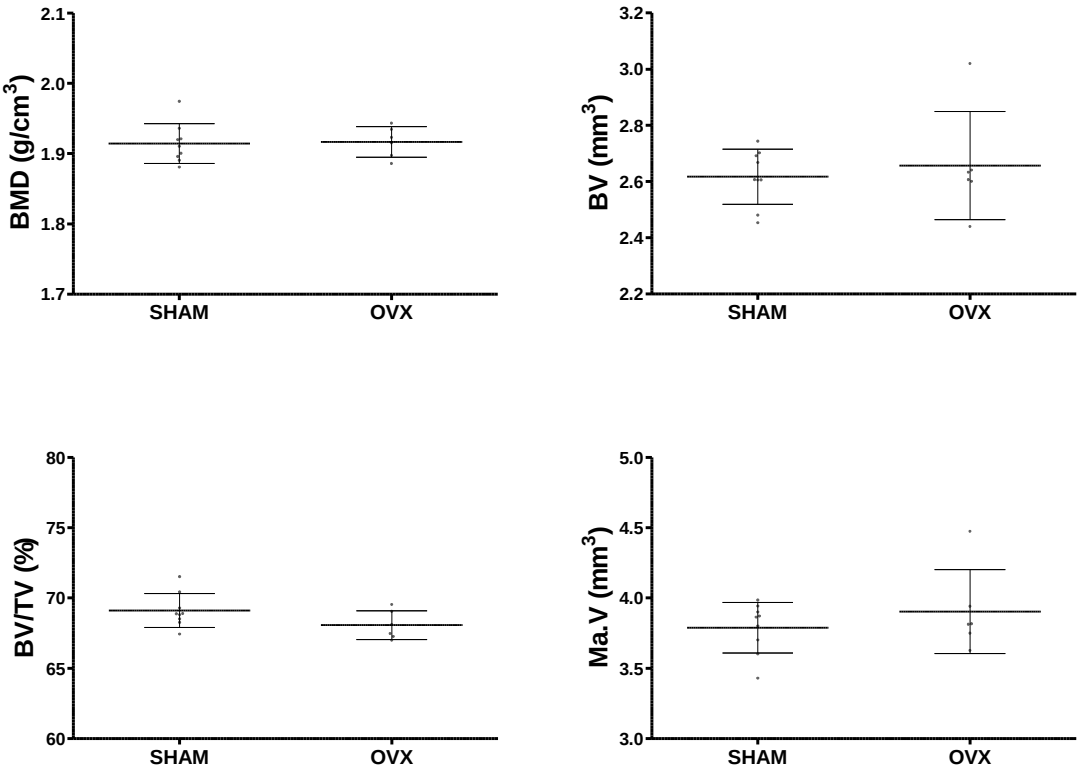

Figure 4-8 Tibial cortical bone morphology following OVX.

Female mice at 16 weeks underwent either SHAM or OVX surgery. Four weeks were allowed for the induction of osteoporosis and mice were sacrificed and tibiae scanned at a resolution of 17µm through 360° rotation. ROI were selected at the diaphysis, through 1/3rd the length between joining of the triangular structures at the proximal end to the distal end where fibula split from the tibia. Fibula were excluded. Y-axis parameters are Bone mineral density (BMD), Bone volume (BV), Percent bone volume (BV/TV) and Marrow volume (Ma.V). Graphs Mean±SD, n=9 mice in SHAM and 6 mice in OVX.

4.2.3.2. Effect on femoral bone

BV and BMD showed a non-significant reduction in the femoral cortices 4 weeks post surgery. Femoral diaphysis were compared in OVX and SHAM mice and neither BMD, BV, BV/TV nor Ma.V were altered between the groups (Figure 4-9).

Upon examination of entire femur, a 10% reduction in BV/TV was observed in OVX mice ($p=0.0024$) compared to SHAM (Table 4-2).

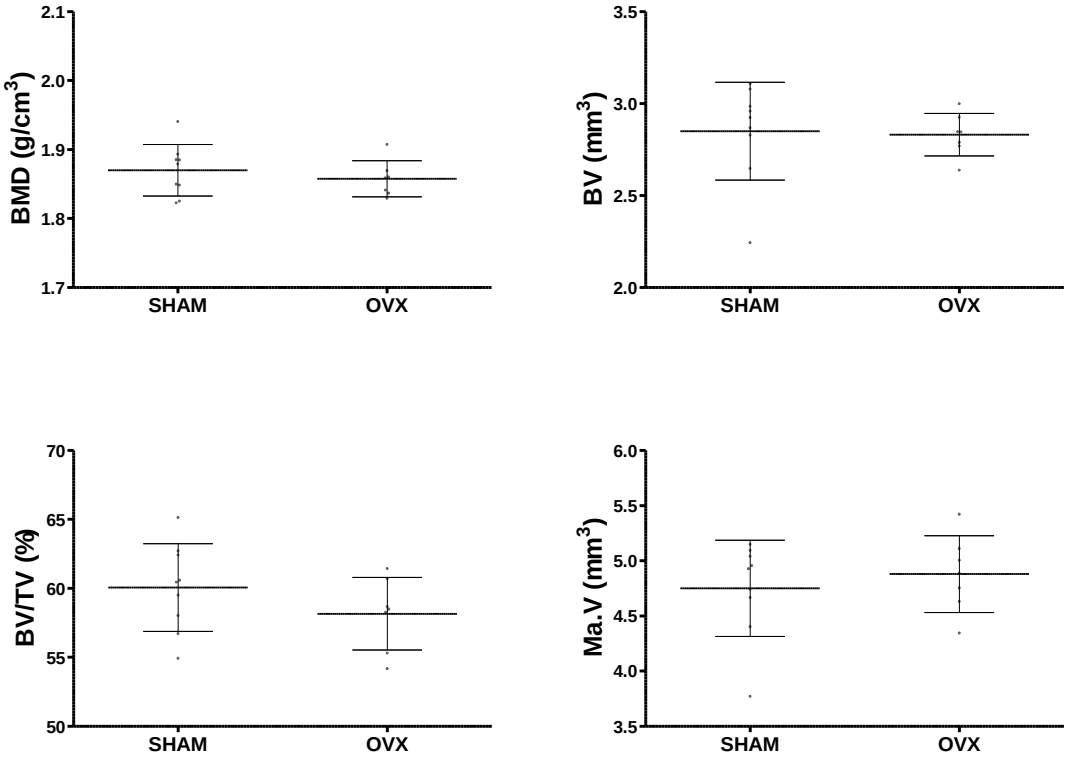

Figure 4-9 Femoral cortical bone morphology following OVX.

Female mice at 16 weeks underwent either SHAM or OVX surgery. Mice were sacrificed 4 weeks later and femur scanned at a resolution of 17µm through 360° rotation. ROI were considered at the diaphysis, through 1/3rd the length between joining of triangular structures at the distal end until the appearance of femoral head at the proximal. Y-axis parameters are Bone mineral density (BMD), Bone volume (BV), Percent bone volume (BV/TV) and Marrow volume (Ma.V). Graphs Mean±SD, n=9 mice in SHAM and 7 mice in OVX.

4.2.4. Cortical bone response post OVX and CPH1 administration

4.2.4.1. Effect on tibial bone

Daily administration of CPH1 via oral gavage did not alter the tibial cortical bone parameters in comparison to vehicle (0). This could be due to the absence of a response in the cortical compartment following OVX. However, PTH led to an increase in BV (↑9%, p=0096) and enlargement of Ma.V (7%, p=0.0442) CPH1 (Figure 4-10).

Examination of entire tibia revealed a significant reduction of BMD in PTH treated group (↓2%, p=0.0062) with an increased BV (↑11%, p=0.0018) and BV/TV (↑5%, p=0.0012) (Table 4-2).

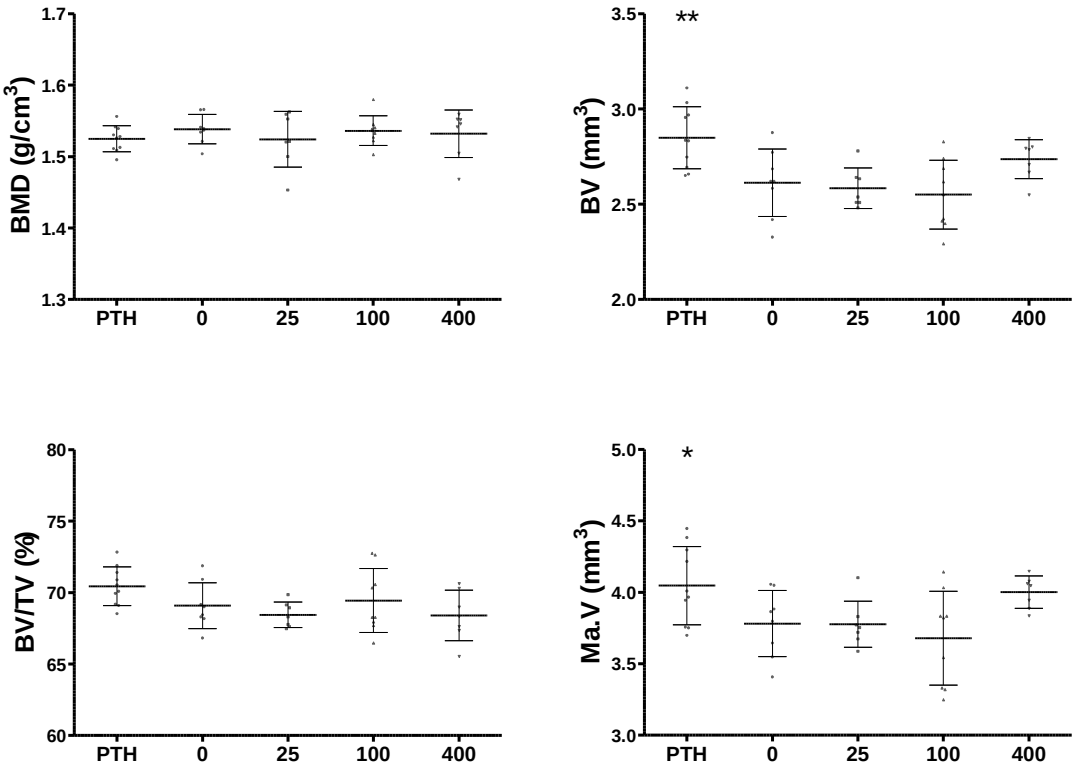

Figure 4-10 Tibial cortical bone response post OVX and CPH1 administration.

Female mice at 16 weeks underwent OVX surgery and were treated daily with PTH, vehicle (0) or CPH1 (25, 100, 400) between 20 and 24 weeks. Mice were sacrificed and left tibiae were scanned at a resolution of 17µm through 360° rotation. ROI were considered at the diaphysis, through 1/3rd length between joining of the triangular structures at the proximal end to the distal end where fibula split from the tibia. Fibula were excluded. Y-axis parameters are Bone mineral density (BMD), Bone volume (BV), Percent bone volume (BV/TV) and Marrow volume (Ma.V). Graphs Mean ±SD, n=7-10 mice in each group. *p<0.05, **p<0.01 significance from vehicle (0)

4.2.4.2. Effect on femoral bone

Femur cortical region revealed interesting findings about CPH1. Mice with 400mg dosage (400) had significantly reduced BMD in diaphysis (↓2.5%, $p<0.01$) and entire femur (↓1.9%, $p<0.05$) compared to vehicle (0) (Figure 4-11). The effects of PTH administration manifested in improvement of BV in diaphysis (↑7%, $p=0.0404$) and entire femur (↑9%, $p=0.0136$), in addition to significant increase in BV/TV (↑6%, $p=0.0009$) in entire femoral cortical bone compared to vehicle (0) (Table 4-2).

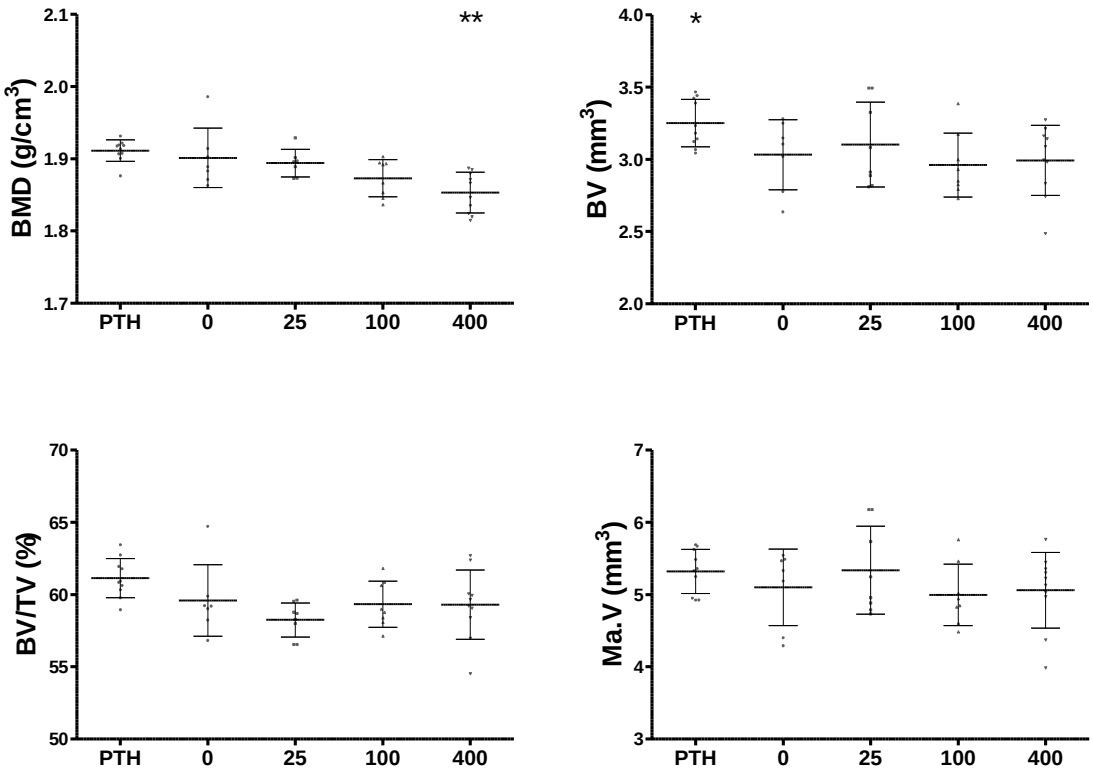

Figure 4-11 Femoral cortical bone response post OVX and CPH1 administration.

Female mice at 16 weeks underwent OVX surgery and were treated daily with PTH, vehicle (0) or CPH1 (25, 100, 400) between 20 and 24 weeks. Mice were sacrificed and femora scanned at a resolution of 17µm through 360° rotation. ROI were considered at the diaphysis, through 1/3rd length between joining of triangular structures at the distal end until the appearance of femoral head at the proximal. Y-axis parameters are Bone mineral density (BMD), Bone volume (BV), Percent bone volume (BV/TV) and Marrow volume (Ma.V). Graphs Mean±SD, n=7-10 mice in each group. *p<0.05, **p<0.01 significance from vehicle (0)

Table 4-2 Effect of OVX and CPH1 treatment on cortical bone (diaphyses) or entire long bone parameters.

Parameter	Treatment groups Mean±SD						
	SHAM	OVX	PTH	0	25	100	400
Tibia (diaphysis)							
BMD (g/cm^3)	1.914± 0.028	1.917± 0.022	1.525± 0.018	1.539± 0.021	1.524± 0.039	1.536± 0.021	1.532± 0.033
BV (mm^3)	2.62± 0.10	2.66± 0.19	2.85± 0.16††	2.61± 0.18	2.59± 0.11	2.55± 0.18	2.74± 0.10
BV/TV (%)	69.12± 1.21	68.07± 1.03	70.45± 1.35	69.09± 1.61	68.44± 0.90	69.45± 2.24	68.40± 1.77
Ma.V (mm^3)	3.79± 0.18	3.90± 0.30	4.05± 0.27†	3.78± 0.23	3.78± 0.16	3.68± 0.33	4.00± 0.11
Entire tibia							
BMD (g/cm^3)	1.835± 0.021	1.841± 0.007	1.987± 0.015††	2.028± 0.050	1.998± 0.029	2.009± 0.012	2.011± 0.019
BV (mm^3)	12.00± 0.64	11.64± 0.80	13.08± 0.67††	11.80± 0.79	11.74± 0.77	11.47± 0.88	12.32± 0.53
BV/TV (%)	57.67± 2.20	55.26± 1.22*	58.38± 0.57††	55.70± 2.09	55.89± 1.33	56.07± 1.63	55.70± 1.68
Femur (diaphysis)							
BMD (g/cm^3)	1.870± 0.037	1.858± 0.026	1.911± 0.015	1.901± 0.041	1.894± 0.019	1.873± 0.026	1.853± 0.028††
BV (mm^3)	2.85± 0.27	2.83± 0.12	3.25± 0.16†	3.03± 0.24	3.10± 0.29	2.96± 0.22	2.99± 0.24
BV/TV (%)	60.05± 3.18	58.15± 2.63	61.14± 1.36	59.59± 2.47	58.25± 1.18	59.34± 1.60	59.30± 2.39
Ma.V (mm^3)	4.75± 0.44	4.88± 0.35	5.32± 0.31	5.10± 0.53	5.34± 0.61	4.99± 0.43	5.06± 0.52
Entire femur							
BMD (g/cm^3)	1.739± 0.029	1.736± 0.018	1.758± 0.012	1.768± 0.033	1.763± 0.012	1.745± 0.017	1.734± 0.024†
BV (mm^3)	13.80± 1.56	13.31± 0.61	15.20± 0.74†	13.97± 1.08	13.95± 1.04	13.42± 1.20	13.28± 1.03
BV/TV (%)	50.61± 3.34	45.80± 0.78**	51.34± 1.20†††	48.35± 1.81	48.08± 0.83	47.87± 1.20	47.34± 1.76

*p<0.05, **p=0.01 of SHAM or †p<0.05, ††p=0.01, †††p<0.001 of vehicle (0). n=6 to 10 mice per treatment group.

4.2.5. Effect of P2X7R antagonism on human osteoclasts *in vitro*

4.2.5.1. Effect of CPH1 on osteoclast formation

CPH1 (0.1 µM-1.5 µM) was introduced throughout the 21-day culture period to peripheral blood monocytes and TRAP stained at the end of the culture period. Dentine discs were assessed for the amount of resorption lacunae excavated by the osteoclasts as a measure of their function and number of resorbing osteoclasts were counted along with their resorption ability.

Results show that osteoclastic resorption showed a significant reduction in the presence of 0.1 µM and 1 µM CPH1 (34% and 36% respectively of 100% in vehicle; $p<0.05$). Interestingly, 1.5 µM CPH1 did not reduce the osteoclastic resorption on dentine but enhanced by 153% although the data did not reach statistical significance ($p=0.0906$) (Figure 4-12 A). CPH1 significantly reduced the numbers of resorbing osteoclasts at 0.1 µM (33%, $p<0.05$) but this effect was not observed at any of the higher concentrations (Figure 4-12 B). Osteoclast resorption ability was not significantly affected in the presence of CPH1 when present throughout their differentiation (Figure 4-12 C).

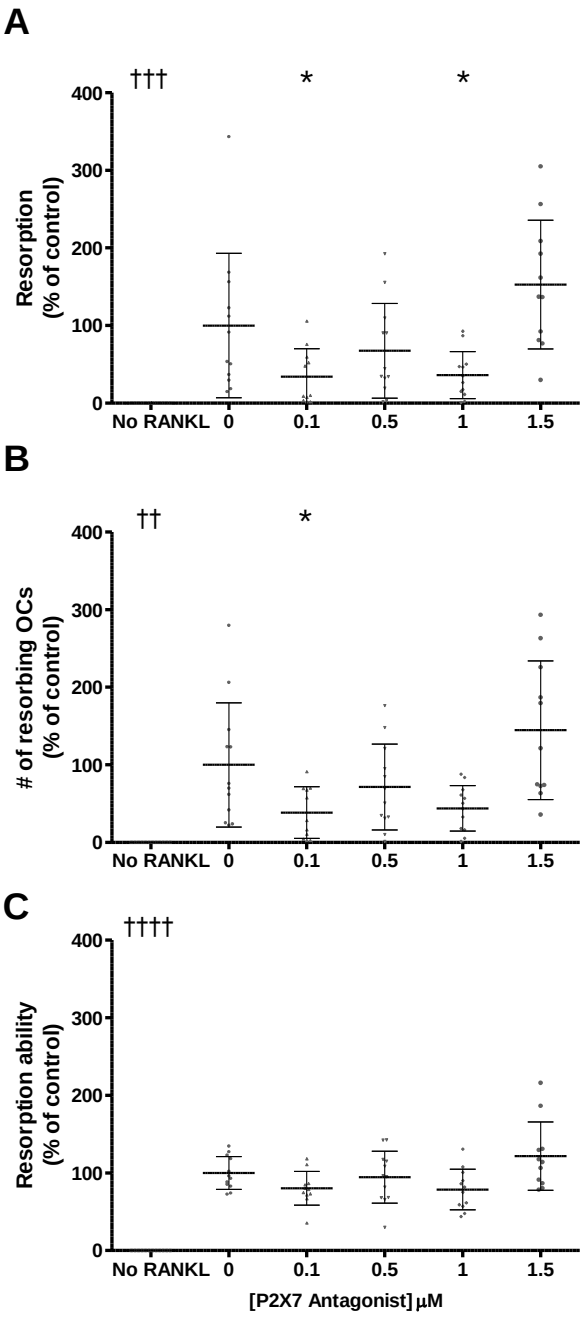

Figure 4-12 Effect of CPH1 on human osteoclast formation

CPH1 was added with every culture medium change to differentiating human osteoclasts *in vitro* and TRAP stained. Resorption (A), number of resorbing osteoclasts (B) and resorptive ability (resorption/resorbing osteoclast) (C) was determined. Values are mean ± SD, n = 2 human donors containing a total of 12 replicate dentine discs. *p < 0.05 (One-Way ANOVA). ††p<0.01, †††P<0.001, ††††p<0.0001 (Student's t-test) significance from vehicle (0).

4.2.5.2. Effect of CPH1 on mature osteoclasts

CPH1 (0.1 µM-1.5 µM) was introduced in the last 1 week of culture by its inclusion in media changes. This was done to determine whether blocking P2X7R affects the resorption by mature osteoclasts as the majority of osteoclasts in these cultures are fully differentiated by 14 days. At the end of the culture period dentine discs were assessed for the area of resorption pits excavated by the mature osteoclasts and the number of resorbing osteoclasts was determined as a measure of their survival.

Neither osteoclastic resorption nor the number of mature osteoclasts were significantly altered in the presence of CPH1. Resorption at 0.5 µM and 1 µM CPH1 was reduced to 47% and 50% respectively with a concomitant decline in the number of resorbing osteoclasts (50% at 0.5 µM and 59% at 1 µM) however these reductions were non-significant and showed a reversal at 1.5 µM (resorption to 79% and number of osteoclasts to 84%). CPH1 had no effect on the resorption abilities at any of the concentrations used (Figure 4-13).

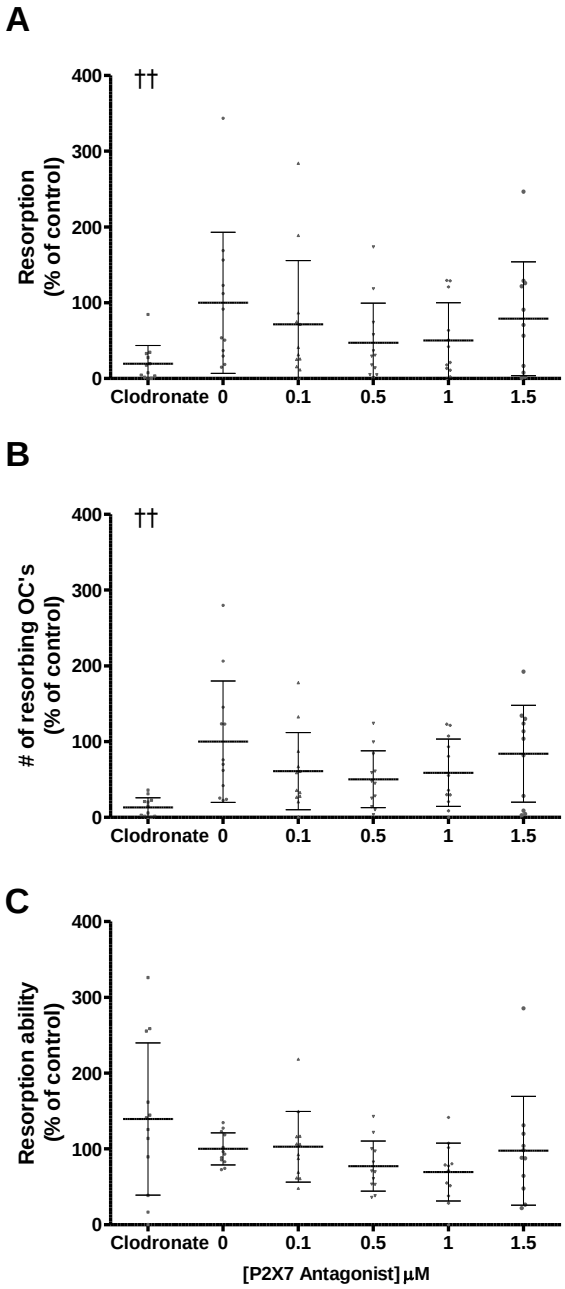

Figure 4-13 Effect of CPH1 on mature human osteoclasts

CPH1 was added with every culture medium change to mature human osteoclasts *in vitro* and TRAP stained. Resorption (A), number of resorbing osteoclasts (B) and resorptive ability (resorption/resorbing osteoclast) (C) was determined. Values are mean ± SD, n = 2 human donors containing a total of 12 replicate dentine discs. *$p < 0.05$ (One-Way ANOVA). ††$p<0.01$ (Student's t-test) significance from vehicle (0).

4.3. Discussion

The activity of bone resorbing osteoclasts is important in the process of bone remodelling as their coordination with the bone forming osteoblasts results in a synergist process of bone regeneration. A specific and potent P2X7R antagonist) was kindly donated by Dr.Niklas Rye Jørgensen to determine its effect on osteoclast formation and activity. Moreover, it was determined whether administration of CPH1 could rescue OVX induced bone loss via down-regulating osteoclast activity. Findings showed that CPH1 reduced the *in vitro* resorption by murine BM precursors when present throughout the 17 day culture period. However, it did not reverse the bone loss associated with OVX in a mouse model of osteoporosis. Additionally, preliminary data using human blood monocytes suggests that introduction of CPH1 throughout the 3 week culture period affected their resorption however, this effect was not observed in a dose dependent manner. Presence of CPH1 also did not inhibit mature osteoclast numbers or bone resorption *in vitro*.

4.3.1. P2X7R antagonist dose-dependently reduced murine osteoclast resorption without altering cell numbers

Results suggest that CPH1 is able to dose-dependently reduce resorption by murine osteoclasts. As discussed in section 1.3.3.2.2 and section 1.3.3.2.3, P2X7R function regulates osteoclast signalling and activity. Key signalling molecules such as PKC, NF-κB and NFATc1 are dependent on rise of $[Ca^{2+}]_i$ an event downstream of P2X7 receptor activation and osteoclasts have been demonstrated as responsive to P2X7R mediated cytosolic calcium elevations (Naemsch et al., 2001). It is likely that pharmacological blockade of P2X7R would prevent osteoclast formation via loss of calcium dependent signalling. Previous studies using mice osteoclasts have shown that *P2rx7* deletion caused loss of agonist induced membrane translocation of PKC (Armstrong et al., 2009) ,a signal essential for osteoclast survival (Pereverzev et al., 2008); loss of NF-κB activation (Korcok et al., 2004), a transcription factor essential for osteoclastogenesis (Iotsova et al., 1997). P2X7R signalling was

reported to couple to NFATc1 in human cells (Adinolfi et al., 2009), a master regulator of osteoclast differentiation (Takayanagi et al., 2002). It is likely that abolishing P2X7R activity would block these signalling events and result in reduction in resorption. Interestingly, in this study, no effect on the number of osteoclasts was obtained in CPH1 treated precursors which is consistent with previous findings using mouse KO models showing that absence of P2X7R function is not imperative to osteoclast formation (Gartland et al., 2003c; Ke et al., 2003). These findings are suggestive of an alternate mechanism of osteoclast formation in the absence of the P2X7R but implicate a role of receptor function in bone resorption.

4.3.2. OVX led to altered trabecular bone architecture and reduced cortical bone volume after 4 weeks of surgery

Having identified CPH1 mediated changes at cellular level using murine osteoclasts *in vitro*, its effect on regulation of bone loss was determined *in vivo*. Firstly, success of bone loss in OVX model was confirmed and bone micro architecture was analysed in SHAM and OVX groups. Trabecular numbers were reduced in all regions analysed following OVX. Additionally, trabecular bone volume was reduced in long bones of OVX mice (Table 4-1). Long bone cortices (diaphyseal region) did not show a change in bone loss due to removal of ovaries suggesting that trabecular compartment is more sensitive to OVX induced bone loss compared to the cortical. This observation is consistent with previous findings on the BALB/c strain as a model of osteoporosis (Bouxsein et al., 2005; Klinck and Boyd, 2008). These studies have demonstrated that despite a manifestation of OVX-induced bone loss in mice bones, the extent of bone loss varies with site. They found that changes in the trabecular compartment were particularly noticeable compared to the cortices, in all the inbred strains of mice that underwent the surgery. Moreover, Klinck and Boyd did not find significant changes in cortical femoral midshaft following OVX in BALB/c mice similar to these observations following 4 weeks of surgery.

Therefore, although the uterine weight post surgery was not measured to establish the success of OVX, results of structural analysis using µCT are in line with previously reported findings shown using the BALB/c model of OVX.

4.3.3. CPH1 failed to reverse OVX induced bone loss and trabecular architecture and showed a continual deterioration of bone architecture

To reverse the effects of OVX, CPH1 was added after 4 weeks of surgery and bone structure analysed following a further 4 weeks of treatment. PTH was used as a positive control in the treatment regime as its role as bone anabolic agent is widely established (Dobnig and Turner, 1995). Bone parameters were compared in 3 trabecular sites- lumbar vertebra, proximal tibia metaphysis and distal femur metaphysis. Despite a reversal of trabecular micro-architecture in PTH treated mice, no reversal of bone loss was observed in trabecular bone parameters in any of the 3 sites following CPH1 treatment. OVX led to increased prevalence of rod-like trabeculae compared to SHAM group and PTH administration reversed the changed structures into a more plate-like morphology. However, there remained a prevalence of rod-like morphology in antagonist treated mice and this was more evident in the vertebrae. Trabecular transition from plate to rod- like structures is documented in post-menopausal women and with aging (Borah et al., 2004; Parfitt et al., 1983) and along with thinning trabeculae are dominant mechanisms during osteoporotic bone loss. This pattern of bone loss was observed in femur trabeculae where P2X7R antagonism led to reduction in trabeculae thickness compared to vehicle treated mice. Interestingly, these architectural changes are consistent with excessive bone resorption (Parfitt, 1992) and high turnover (Parfitt, 2002). This is counter intuitive as *in vitro* treatment reduced osteoclastic resorption and histomorphometric analysis is needed to ascertain the effect of receptor antagonism on bone formation and resorption.

Results show that CPH1 did not reverse the OVX induced bone loss in a manner similar to that of an anabolic agent, PTH. Contrarily, there appears to

be a continual bone loss as shown by persistence of rod like trabeculae in lumbar and thinning of trabeculae in femoral regions.

4.3.4. CPH1 treatment led to increased tibial cortical bone volume but reduced femoral cortical BMD

Examination of cortical region of tibia did not show any response to CPH1 treatment presumably because the surgery in itself did not manifest into any significant changes in cortical bone architecture. Interestingly, a non-significant anabolic effect of CPH1 was noticed in the cortical bone volume of BALB/c tibiae with an increase in diameter (Marrow volume), similar to the bone anabolic PTH effect (Table 4-2). Cortical periosteal and endosteal surfaces are active bone remodelling sites with both bone cell activity higher in the former than the latter. Periosteal bone formation exceeds bone resorption and endosteal bone resorption is greater than the bone formation, leading to marrow expansion which is typical with aging. An overall increase in bone volume suggests a positive balance towards bone formation presumably due to decline in resorption (either due to shorter osteoclast activity or due to shallower excavation pits) or enhanced bone deposition.

Femur cortices showed significant decline in BMD in the presence of CPH1 in both the diaphysis and entire bone compared to vehicle treated mice. This is indicative of an aggressive bone remodelling replacing densely mineralised old bone with new bone yet to undergo secondary mineralisation. This is particularly interesting as OVX did not reduce the cortical BMD after 4 weeks of surgery in either of the long bones. Whether these are direct effects on bone cells resulting in the reduction of bone turnover events or indirect by attenuation of mineral mobilisation or deposition still needs to be investigated. Intriguingly, PTH failed to restore cortical BMD in long bones of the mice in either the whole bones or diaphysis (Table 4-2).This loss of PTH effect could be due to a reported recovery phase post-OVX in BALB/c strain (Klinck and Boyd, 2008). Klinck and Byod showed by a longitudinal study that between 2 and 5 weeks, the OVX induced bone changes were time sensitive and

showed a levelling out despite large losses immediately after the surgery. It is tempting to speculate that a similar recovery could have occurred in the mice and therefore prevented PTH from showing a further additive effect. Similarly, it is therefore also possible that the effects of CPH1 could be underestimated and a time course study might prove to be more sensitive to the effects of the treatment.

An overall osteoporotic phenotype was observed in the presence of CPH1 and it failed to reverse the effects of OVX induced bone loss.

4.3.5. CPH1 did not affect human osteoclast formation and function dose dependently

Addition of CPH1 to forming osteoclasts resulted in the inhibition of resorption and number of resorbing osteoclasts. The highest concentration (1.5μM), however, did not inhibit the area of resorption lacunae and number of resorbing osteoclasts *in vitro*. Therefore, the compound did not affect the formation of osteoclasts in a dose-dependent manner but showed an apparent biphasic response. The observed effect at the highest dose could be attributed to a non-specific binding of CPH1 and more studies are needed to understand the properties and potency of CPH1 on human P2X7R and other P2 receptors. Additionally, a bigger dosage, spanning over a range of log units, is needed to calculate a dose-response curve and ascertain the effect of CPH1 on human osteoclasts.

Previous findings have associated blockade of P2X7R with a dose-dependent inhibition of osteoclastogenesis (Agrawal et al., 2010; Gartland et al., 2003a). However, pharmacologic blockade using different antagonists shows a variable degree of inhibition of bone resorption, and a different rank order of potency at P2X7R (Agrawal et al., 2010). It is likely that CPH1 demonstrates conditional antagonism and is responsible for activating different signalling events depending on the presence of the agonist. Previous conditional antagonists have been demonstrated and in one well documented case, Tamoxifen, which was developed as an antagonist against breast cancer could agonise bone cells and endometrium (Grilli, 2006; Krum

et al., 2008; Nakamura et al., 2007). Understanding the structural and molecular composition of CPH1 would help describe the underlying basis of a potential agonism/antagonism switching.

The differences in human and murine osteoclast resorption due to P2X7R antagonism could be attributed to the species specific differences in potency of CPH1. The limitation in this chapter is the lack on another antagonist to compare and verify the findings obtained using CPH1. While various P2X7R antagonists are commerically available, their potency and selectivity is variable with the species tested. For instance, P2X7R antagonists such as Brilliant Blue G (BBG), calcium/calmodulin-dependent protein kinase II such as the isoquinoline, (1-[*N*,*O*-bis(5-isoquinoline-sulfonyl)-*N*-methyl-l-tyrosyl]-4-phenylpiperazine) (KN62), AZ1111645373 and A-438079, have shown species differences in *in vitro* assays with preferential affinity towards one species or the other (Humphreys et al., 1998; Nelson et al., 2006; Stokes et al., 2006). Additionally, some inhibitors display non-selective pharmacological activity including blockade of P2X1R and P2X2R (oxidised-ATP) (Evans et al., 1995) and P2X2R and P2X4R (Decavanadate) (Michel et al., 2006) when P2X7R function when assessed on cells expressing other P2Rs. Moreover, analysis of antagonism is complicated by the end point that is measured with different agonist incubation times required. Abbott Laboratories disclosed a novel compound, A-438079, which was shown to potently block BzATP-stimulated intracellular calcium concentration changes at rate and human P2X7R, IL-1*β* release and pore formation in human THP-1 cells differentiated with LPS and IFN-*γ* into a macrophage-like phenotype with little or no activity at other P2 receptors (Nelson et al., 2006). However, fusion of human peripheral blood derived monocytes into osteoclatsts remains unaffected in the presence of A-438079 when added throughout culture, in addition to an absence of effect on osteoclastic bone resorption *in vitro* (Agrawal et al., 2010). Thus, the usefulness of A-438079 as a tool for P2X7R function in bone cells is limited. An alternative commercially available P2X7R antagonist is a second Abbot compound, A-740003, with specific and potent antagonism at rat and human P2X7R (Nelson et al., 2006) and sufficient bioavailability in

in vivo investigations (Honore et al., 2006). However, its activity on mouse P2X7R and in context to bone cells has not yet been explored.

Additionally, variations in human P2X7R due to SNPs could interfere with the binding of the antagonist and affect physiological responses, as has been demonstrated by differences in ATP-mediated ethidium uptake and IL-1β production in individuals with altered P2X7R function (McHugh et al., 2012).

Nevertheless, these data provide evidence for the involvement of the P2X7R in the complex chain of events leading to the formation of human osteoclasts. A delicate balance between osteoclastic bone resorption and osteoblastic bone formation is paramount for the maintenance of a functional skeleton. The availability of selective P2X7R antagonists may prove helpful in the management of bone diseases however, the precise mechanism underlying the action of CPH1 needs to be investigated further.

4.4. Conclusion

Murine osteoclastic resorption could be inhibited by the addition of small molecule inhibitor of P2X7R but similar results could not be obtained by preliminary investigation using human osteoclasts. This reflects a potential species specific action of CPH1 however, OVX-induced bone loss could not be treated by P2X7R antagonism and a decline towards continual bone loss was observed. More studies are needed to determine the potency of CPH1 and confirm these findings by utilising commercially available P2X7R antagonists.

Chapter 5. P2 receptor deletion augments the effect of oestrogen loss and regulates osteoclastogenesis *in vitro*

5.1. Introduction

According to National Osteoporosis Society, in the UK, 1 in 2 women and 1 in 5 men over the age of 50 will break a bone mainly because of poor bone health with almost 3 million people estimated to have osteoporosis (National Osteoporosis Society, 2012). Due to this, it costs the government more than £2.3 billion per year in hospital and social care for patients with fractures. Therefore, osteoporosis represents an important public health issue and an understanding of the role of age-related changes upon bone cells, which in turn influence the overall bone turnover, is warranted. Bone loss associated with oestrogen deficiency is a result of accelerated depletion of bone mineral density with resorption exceeding the rate of formation despite an up-regulation of both osteoblastogenesis and osteoclastogenesis (Parfitt, 2002). The knowledge that both osteoclasts and osteoblasts are responsive to purine signalling at all stages of their development and that levels of oestrogen can disturb the equilibrium needed to maintain a healthy skeleton, it is important to determine whether targeting P2 receptors alters the skeletal response to oestrogen deficiency.

As part of the EU Framework 7 funded project "ATPBone: Fighting osteoporosis by blocking nucleotides: purinergic signalling in bone formation and homeostasis," the P2X7, $P2Y_6$ and $P2Y_{13}$ receptor knock out (KO) (P2X7R-/-, $P2Y_6$R-/- and $P2Y_{13}$R-/-) mice were made available to our lab and their roles in maintenance of skeletal homeostasis studied (unpublished findings) (Wang et al., 2012; Wang et al., 2013). Activation of $P2Y_6$R has been demonstrated to increase osteoclast formation and expectedly, osteoclasts derived from $P2Y_6$R-/- mice show reduced resorption (Orriss et al., 2011b). Studies in our lab suggest that when the bone remodelling cycle is challenged *in vivo* (OVX induced bone loss), $P2Y_6$R-/- mice show heightened loss of bone volume, suggestive of an enhanced resorption in oestrogen deplete conditions (unpublished findings). In addition, Wang et al., report a reduced oestrogen deficiency-induced bone loss in $P2Y_{13}R^{-/-}$ mice suggestive of a preventative role of $P2Y_{13}$R deletion in mice model of osteoporosis (Wang et al., 2012).

Above studies reveal the role of these P2 receptors on osteoclastogenesis and that bone turnover is altered in KO mice following OVX. Moreover P2X7R mediated loss of apoptosis was observed in oestrogen-responsive tissues suggesting a purinoceptors modulation of oestrogen loss (Gorodeski, 2004; Wang et al., 2004a). The hypothesis of this chapter is that purinoceptors augments the effect of oestrogen loss dependent osteoclastogenesis *in vitro*. To investigate this *in vitro*, precursor cells were obtained from KO mice and osteoclasts were differentiated and their function assessed while oestrogen deficient conditions were achieved by manipulation of culture media components. The aims were 1) Investigate the combined effect of P2R deletion and oestrogen depletion on BM derived osteoclasts and 2) Investigate the combined effect of P2R deletion and oestrogen depletion on spleen derived osteoclasts.

5.2. Results

5.2.1. Combined effect of P2R deletion and oestrogen depletion on BM derived osteoclasts

5.2.1.1. P2X7R

Precursor cells from the BM of 12 week old P2X7R+/+ and P2X7R-/- were obtained and cultured under pro-osteoclastic conditions for 17 days to generate functional osteoclasts *in vitro*. Media components were manipulated to mimic oestrogen depletory conditions in culture. Results showed significant increases in all parameters measured to assess osteoclastogenesis in both P2X7R+/+ and P2X7R-/-, in the absence of oestrogen (-E) compared to oestrogen containing conditions (+E) (Figure 5-1, Table 5-1).

However, the fold change in resorption ability of P2X7R-/- osteoclasts was significantly higher compared to the change in resorption ability of P2X7R+/+ osteoclasts (10 fold versus 4 fold, p=0.0104) upon oestrogen depletion (Figure 5-3). No significant differences were observed between change in total and resorbing osteoclast number or total resorption in -E compared to +E in either genotype (Figure 5-3, Table 5-1).

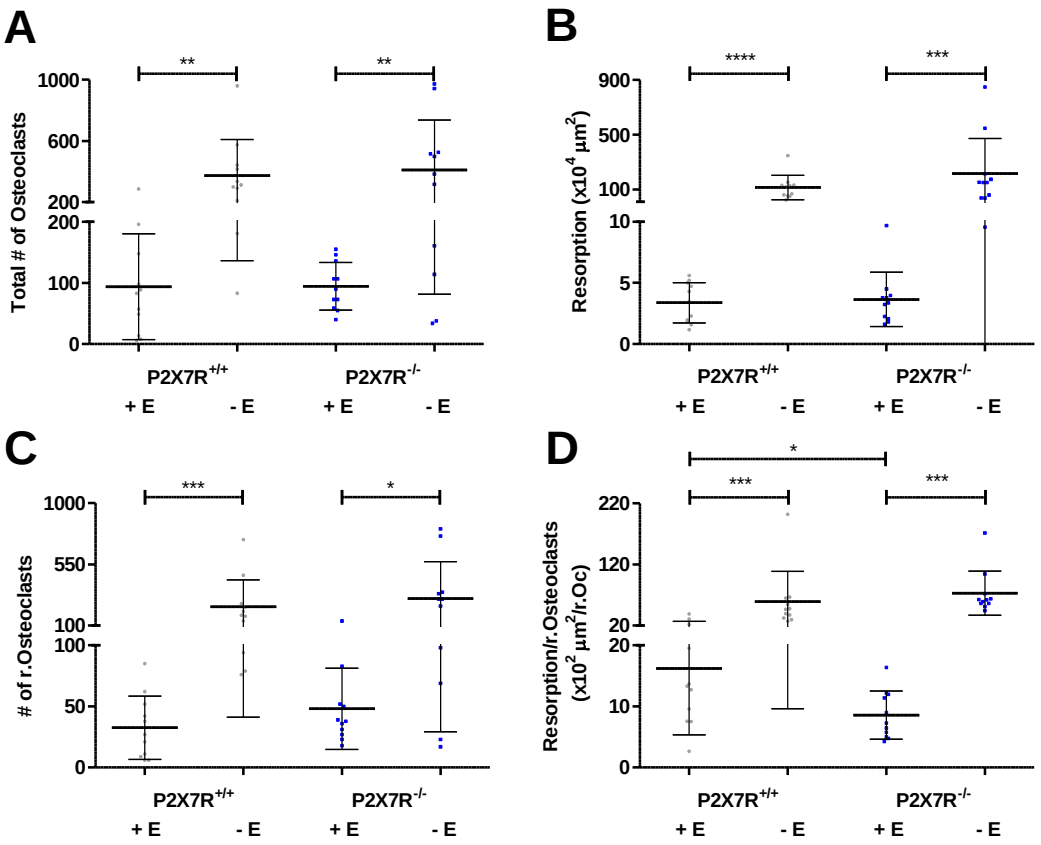

Figure 5-1 Effect of oestrogen depletion on BM osteoclasts from P2X7R+/+ and P2X7R-/- mice

Precursor cells from BM aspirates were differentiated on dentine and TRAP stained to analyse total number of osteoclasts (A), total resorption (B), number of resorbing osteoclasts (C) and the resorptive ability (resorption/resorbing osteoclast) (D), values are mean ± SD, n=3 repeat cultures containing a total of 11 dentine discs. *p<0.05 **p<0.01, ***p<0.001, ****p<0.0001 indicates statistical significance compared to +E (Student's t-test).

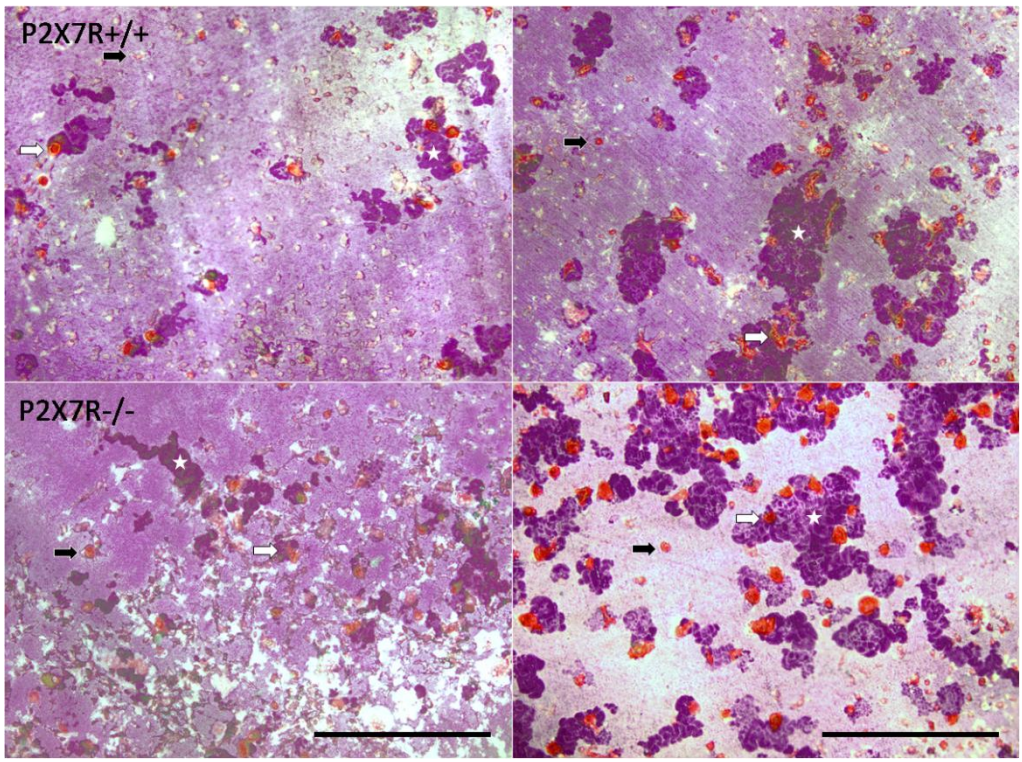

Figure 5-2 Representative images showing effect of oestrogen depletion on BM osteoclasts of P2X7R+/+ and P2X7R-/- mice.

Precursor cells from BM aspirates of P2X7R+/+ and P2X7R-/- were differentiated on dentine in oestrogen containing (+E) and oestrogen depletory (-E) conditions and TRAP stained. Images show non-resorbing (black arrows) and resorbing (white arrows) osteoclasts and resorption trails (white stars) excavated by the cells on dentine. Scale bar= 500µm.

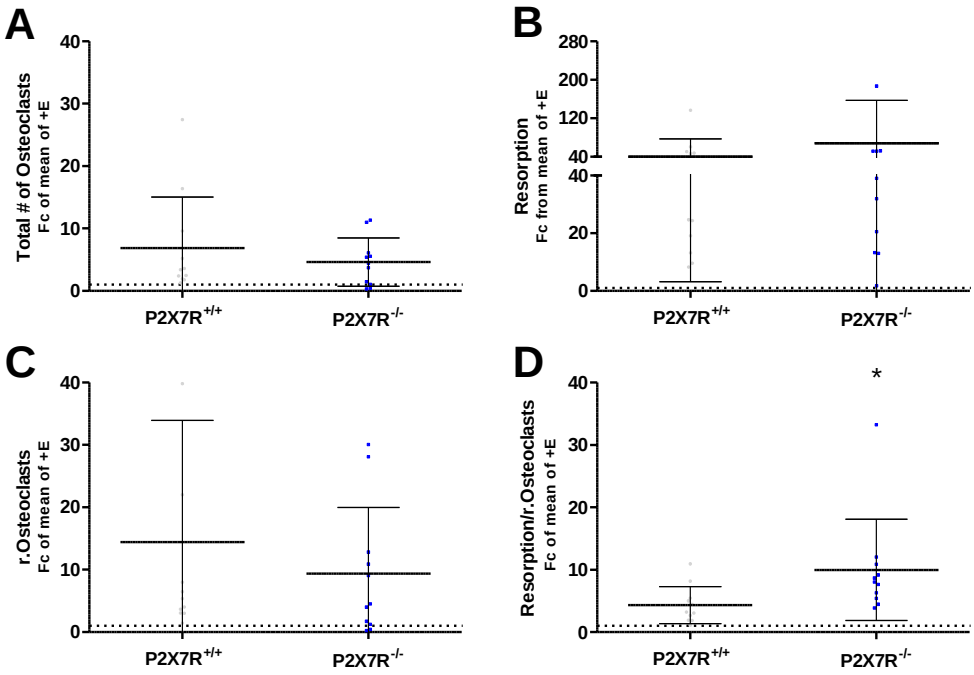

Figure 5-3 Response to oestrogen depletion on BM osteoclasts from P2X7R+/+ and P2X7R-/- mice

Response to oestrogen depletion (-E) was expressed as a fold change of the mean of +E in either genotype. Change in total number of osteoclasts (A), total resorption (B), number of resorbing osteoclasts (C) and the resorptive ability (resorption/resorbing osteoclast) (D) was analysed, values are mean ± SD, n=3 repeat cultures containing a total of 11 dentine discs. *$p<0.05$ indicates statistical significance compared to P2X7R+/+ (Univariate analysis of variance).

5.2.1.2. $P2Y_6R$

Cells from the long bone marrows of 5- 6 week old female $P2Y_6R+/+$ and $P2Y_6R-/-$ were seeded onto dentine discs for 11 days to obtain mature osteoclasts *in vitro* under oestrogen depletory conditions. The number of osteoclasts derived from $P2Y_6R-/-$ in response to loss of oestrogen (-E), compared to normal complete media (+E) *in vitro* were significantly higher ($p=0.0010$), so were the number of resorbing osteoclasts ($p<0.0001$). However, they showed a significantly reduced resorption ability ($p=0.0326$) (Figure 5-4). Interestingly, this change could not be measured in osteoclasts derived from $P2Y_6R+/+$ as no TRAP +ve cells remained on the dentine discs at the end of the culture period. The total resorption obtained from $P2Y_6R-/-$ was significantly enhanced following oestrogen depletion ($p<0.0001$) compared to a significant reduction ($p=0.0149$) by $P2Y_6R+/+$ osteoclasts.

Expressing –E parameters as a change from +E to determine the effect of oestrogen depletion, $P2Y_6R-/-$ showed a 7 fold increase in resorption compared to a 0.43 fold reduction by $P2Y_6R+/+$ ($p<0.0001$) (Figure 5-6)

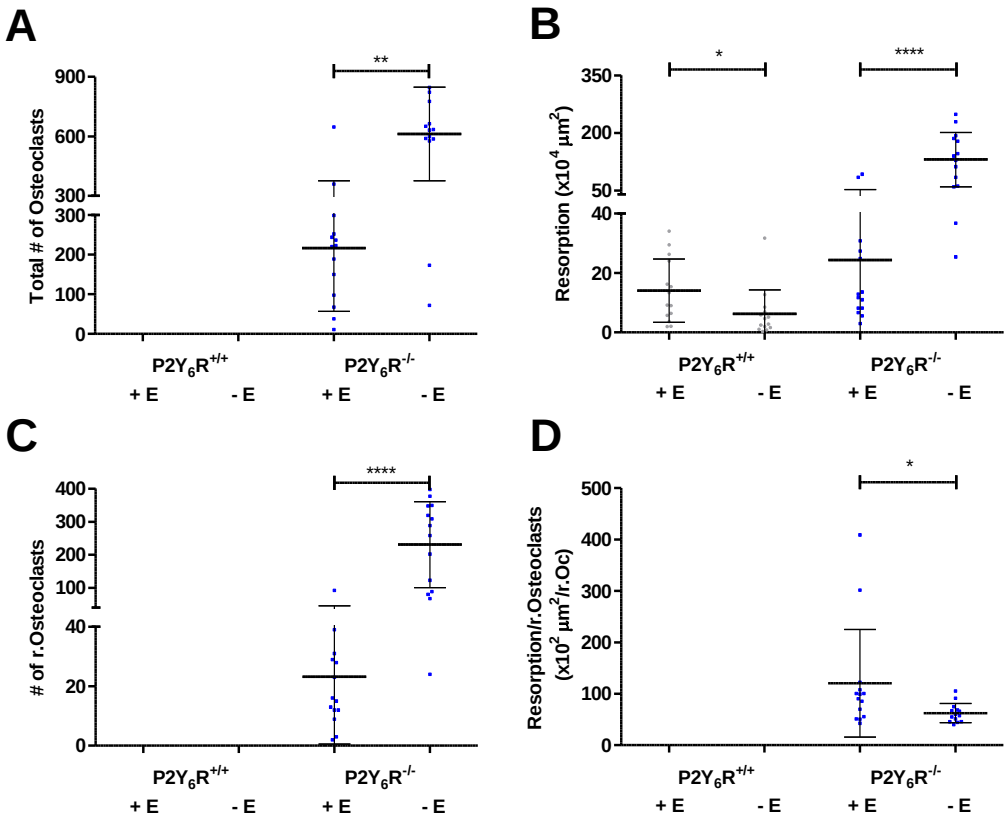

Figure 5-4 Effect of oestrogen depletion on BM osteoclasts from P2Y$_6$R+/+ and P2Y$_6$R-/- mice

Precursor cells from BM aspirates were differentiated on dentine and stained to analyse total number of osteoclasts (A), total resorption (B), number of resorbing osteoclasts (C) and resorptive ability (resorption/resorbing osteoclast) (D), values are mean ± SD, n=3 repeat cultures containing a total of 14 dentine discs. *p<0.05 **p<0.01, ***p<0.001, ****p<0.0001 indicates statistical significance compared to +E (Student's t-test).

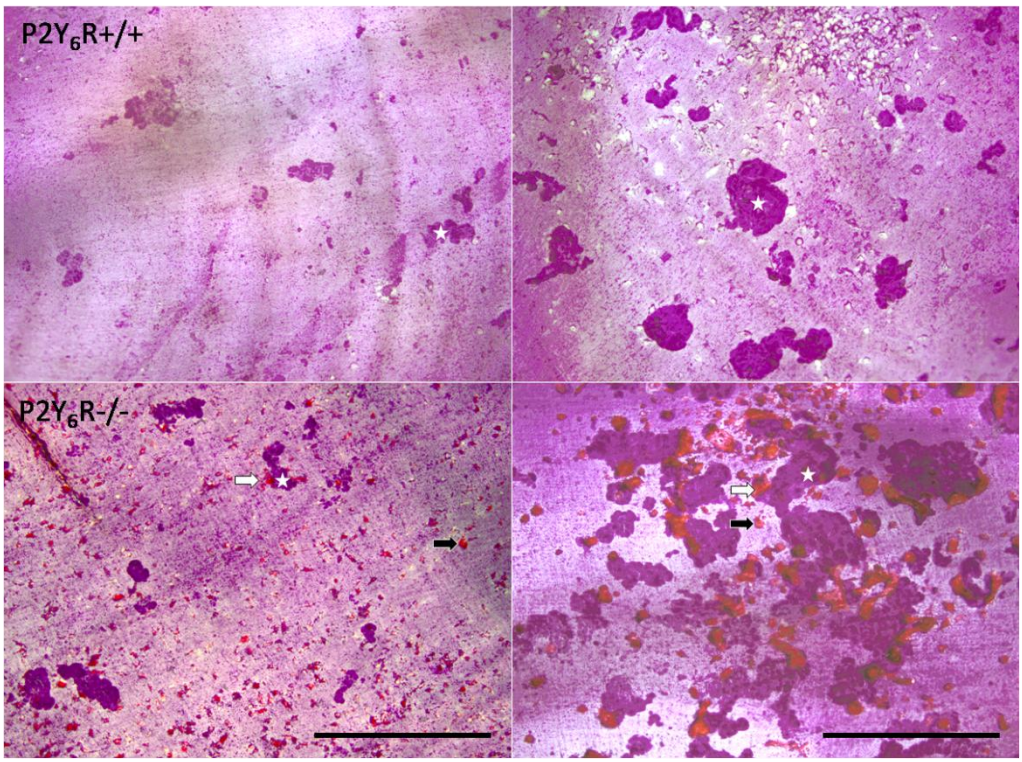

Figure 5-5 Representative images showing effect of oestrogen depletion on BM osteoclasts of $P2Y_6R+/+$ and $P2Y_6R-/-$ mice.

Precursor cells from BM aspirates of $P2Y_6R+/+$ and $P2Y_6R-/-$ were differentiated on dentine in oestrogen containing (+E) and oestrogen depletory (-E) conditions and TRAP stained. Images show non-resorbing (black arrows) and resorbing (white arrows) osteoclasts and resorption trails (white stars) excavated by the cells on dentine. Scale bar= 500µm.

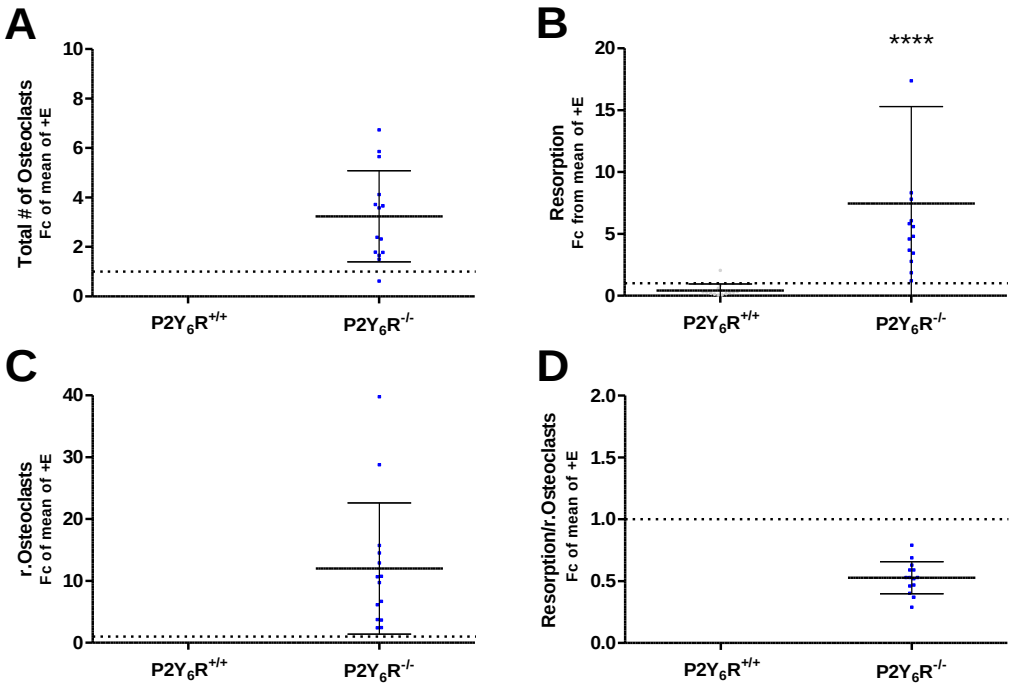

Figure 5-6 Response to oestrogen depletion on BM osteoclasts from $P2Y_6R$+/+ and $P2Y_6R$-/- mice

Response to oestrogen depletion (-E) was expressed as a fold change of the mean of +E. Change in total number of osteoclasts (A), total resorption (B), number of resorbing osteoclasts (C) and the resorptive ability (resorption/resorbing osteoclast) (D) was analysed, values are mean ± SD, n= 3 repeat cultures containing a total of 14 dentine discs ****p<0.0001 indicates statistical significance compared to $P2Y_6R$+/+(Univariate analysis of variance).

5.2.1.3. $P2Y_{13}R$

Cells from long bone marrows of 6- 7 week old $P2Y_{13}R+/+$ and $P2Y_{13}R-/-$ mice were seeded onto dentine discs for 17 days and differentiated under pro-osteoclastogenic and oestrogen depletory conditions *in vitro*. Osteoclasts derived from $P2Y_{13}R-/-$ in response to loss of oestrogen (-E), compared to normal complete media (+E) *in vitro* were significantly enhanced in their total numbers ($p=0.0229$). However, this change could not be detected in osteoclasts derived from $P2Y_{13}R+/+$ as no TRAP +ve cells remained on the surface of dentine discs in any of the culture media conditions. Increases in total resorption were obtained from both $P2Y_{13}R+/+$ and $P2Y_{13}R-/-$ osteoclasts following oestrogen depletion but the data failed to reach statistical significance (Figure 5-7).

Moreover, fold change in resorption from $P2Y_{13}R-/-$ osteoclasts was higher compared to change in resorption in $P2Y_{13}R+/+$ (1.68 fold versus 1.35 fold; $p=0.0768$) although this was not statistically significant (Figure 5-9).

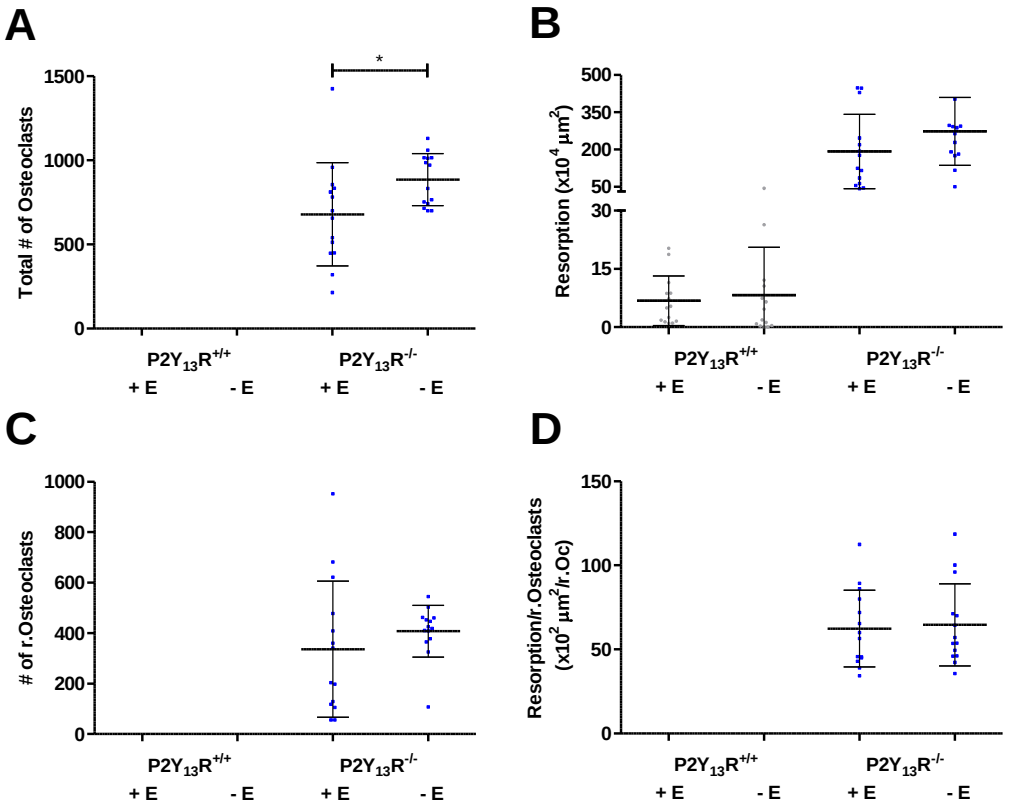

Figure 5-7 Effect of oestrogen depletion in BM osteoclasts from $P2Y_{13}R+/+$ and $P2Y_{13}R-/-$ mice

Precursor cells from BM aspirates were differentiated on dentine and stained to analyse total number of osteoclasts (A), total resorption (B), number of resorbing osteoclasts (C) and the resorptive ability (resorption/resorbing osteoclast) (D), values are mean ± SD, n=3 repeat cultures containing a total of 14 dentine discs. *p<0.05 indicates statistical significance compared to +E (Student's t-test).

.

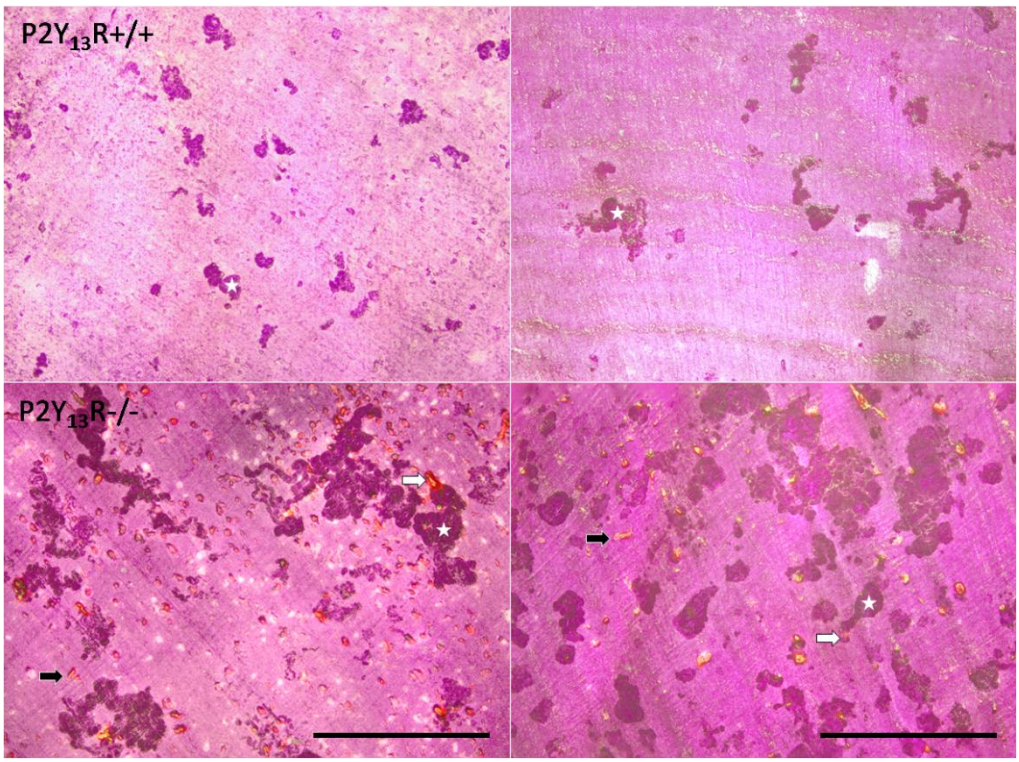

Figure 5-8 Representative images showing effect of oestrogen depletion on BM osteoclasts of $P2Y_{13}R+/+$ and $P2Y_{13}R-/-$ mice.

Precursor cells from BM aspirates of $P2Y_{13}R+/+$ and $P2Y_{13}R-/-$ were differentiated on dentine in oestrogen containing (+E) and oestrogen depletory (-E) conditions and TRAP stained. Images show non-resorbing (black arrows) and resorbing (white arrows) osteoclasts and resorption trails (white stars) excavated by the cells on dentine. Scale bar= 500µm.

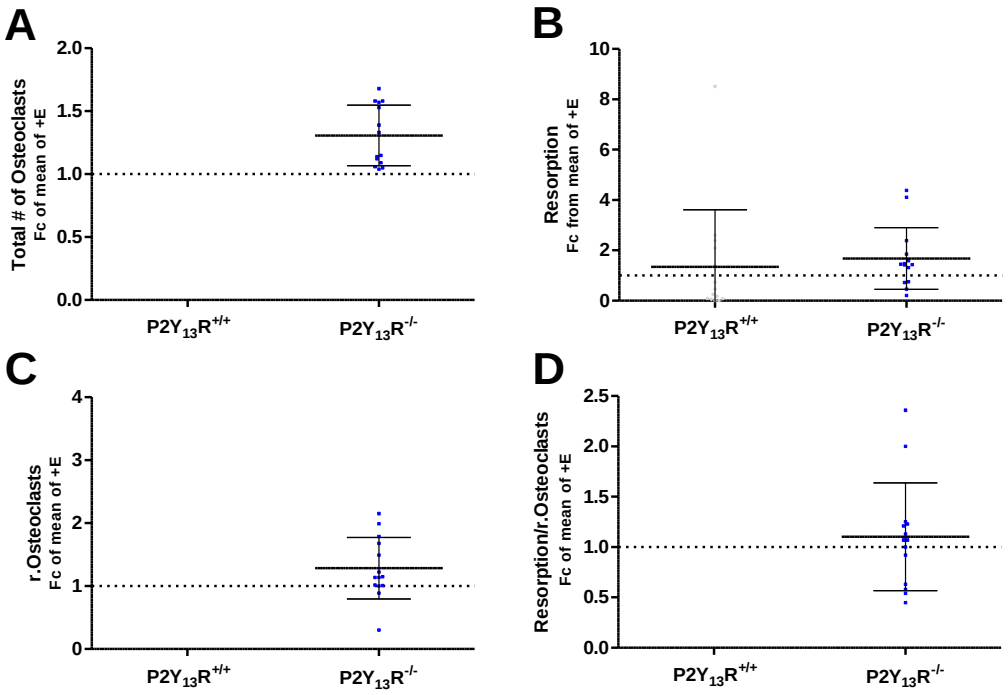

Figure 5-9 Response to oestrogen depletion on BM osteoclasts from $P2Y_{13}R+/+$ and $P2Y_{13}R-/-$ mice.

Response to oestrogen depletion (-E) was expressed as a fold change of the mean of +E. Change in total number of osteoclasts (A), total resorption (B), number of resorbing osteoclasts (C) and the resorptive ability (resorption/resorbing osteoclast) (D) was analysed, values are mean ± SD, n=3 repeat cultures containing a total of 14 dentine discs (Univariate analysis of variance).

Table 5-1 Effect of oestrogen depletion on bone marrow derived osteoclasts from P2R mice (+E versus –E)

Parameters	+/+ (+E) Mean± SD	+/+ (-E) Mean± SD	p-value	-/- (+E) Mean± SD	-/- (-E) Mean± SD	p-value
P2X7						
Total Osteoclasts	94.00± 86.76	372.7± 236.2	0.0015 **	94.64± 38.84	409.3± 327.6	0.0049 **
Resorption ($x10^4$ μm^2)	3.37± 1.65	115.6± 88.05	<0.0001 ****	3.64± 2.23	216.8± 255.1	0.0001 ***
Resorbing Osteoclasts (r.Oc)	32.64± 25.90	238.8± 197.6	0.0001 ***	48.18± 33.24	299.1± 269.9	0.0165 *
Resorption Ability ($x10^2$ μm^2/r.Oc)	16.20± 10.83	58.96± 49.34	0.0004 ***	8.59± 3.92	73.02± 36.19	<0.0001 ****
$P2Y_6$						
Total Osteoclasts	no cells	no cells	ND	216.9± 159.6	611.7± 236.6	0.0010 **
Resorption ($x10^4$ μm^2)	14.07± 10.63	6.21± 8.13	0.0149 *	24.34± 28.47	130.5± 70.89	<0.0001 ****
Resorbing Osteoclasts (r.Oc)	no cells	no cells	ND	23.14± 22.59	230.7± 130.1	<0.0001 ****
Resorption Ability ($x10^2$ μm^2/r.Oc)	ND	ND	ND	120.6± 104.6	62.45± 18.67	0.0326 *
$P2Y_{13}$						
Total Osteoclasts	no cells	no cells	ND	679.2± 306.1	885.8± 154.4	0.0229*
Resorption ($x10^4$ μm^2)	6.78± 6.36	8.22± 12.33	0.4483	191.5± 149.8	272.4± 136.7	0.1475
Resorbing Osteoclasts (r.Oc)	no cells	no cells	ND	336.4± 269.4	407.8± 102.7	0.1542
Resorption Ability ($x10^2$ μm^2/r.Oc)	ND	ND	ND	62.46± 22.90	64.63± 24.44	0.8101

p- values were calculated using Student's t test

Table 5-2 Response of oestrogen depletion on osteoclasts derived from BM of P2R mice (Fc of +E)			
Parameters **Mean±SEM**	**+/+** **Mean±SD**	**-/-** **Mean±SD**	**p-value**
P2X7			
Total Osteoclasts	6.85± 8.12	4.60± 3.86	0.8438
Resorption ($x10^4$ µm^2)	40.06± 36.86	68.24± 88.69	0.5545
Resorbing Osteoclasts (r.Oc)	14.42± 19.50	9.35± 10.64	0.5994
Resorption Ability ($x10^2$ µm^2/r.Oc)	4.36± 2.96	9.99± 8.12	0.0104*
$P2Y_6$			
Total Osteoclasts	ND	3.2± 1.85	ND
Resorption ($x10^4$ µm^2)	0.43± 0.51	7.4± 7.8	<0.0001****
Resorbing Osteoclasts (r.Oc)	ND	12.0± 10.63	ND
Resorption Ability ($x10^2$ µm^2/r.Oc)	ND	0.53± 0.13	ND
$P2Y_{13}$			
Total Osteoclasts	ND	1.31± 0.24	ND
Resorption ($x10^4$ µm^2)	1.35± 2.27	1.68± 1.23	0.0768
Resorbing Osteoclasts (r.Oc)	ND	1.28± 0.49	ND
Resorption Ability ($x10^2$ µm^2/r.Oc)	ND	1.10± 0.54	ND
p- values were calculated using Univariate analysis of Variance			

5.2.2. Combined effect of P2R deletion and oestrogen depletion on splenic osteoclasts

5.2.2.1. P2X7R

Osteoclast precursors located in the spleens of 12 week old P2X7R+/+ and P2X7R-/- were isolated and driven for 9 days in oestrogen depletory conditions to obtain functional osteoclasts *in vitro*. Both P2X7R+/+ and P2X7R-/- osteoclasts had a significant increases in their total number of osteoclasts, number of resorbing osteoclasts, total resorption and the resorbing ability in the absence of oestrogen (-E) compared to oestrogen containing conditions (Figure 5-10).

However, no statistical difference in change in resorption ability in –E conditions was obtained from P2X7R-/- osteoclasts (4 fold) compared to the change in P2X7R+/+ (6 fold). Moreover, the change in resorbing osteoclasts in P2X7R-/- in -E was significantly lower than the change obtained from P2X7R+/+ (20 fold versus 72 fold, p=0.0111) similar to a reduced change in resorption (32 fold in P2X7R-/- versus 396 fold in P2X7R+/+; p=0.0006) (Figure 5-12).

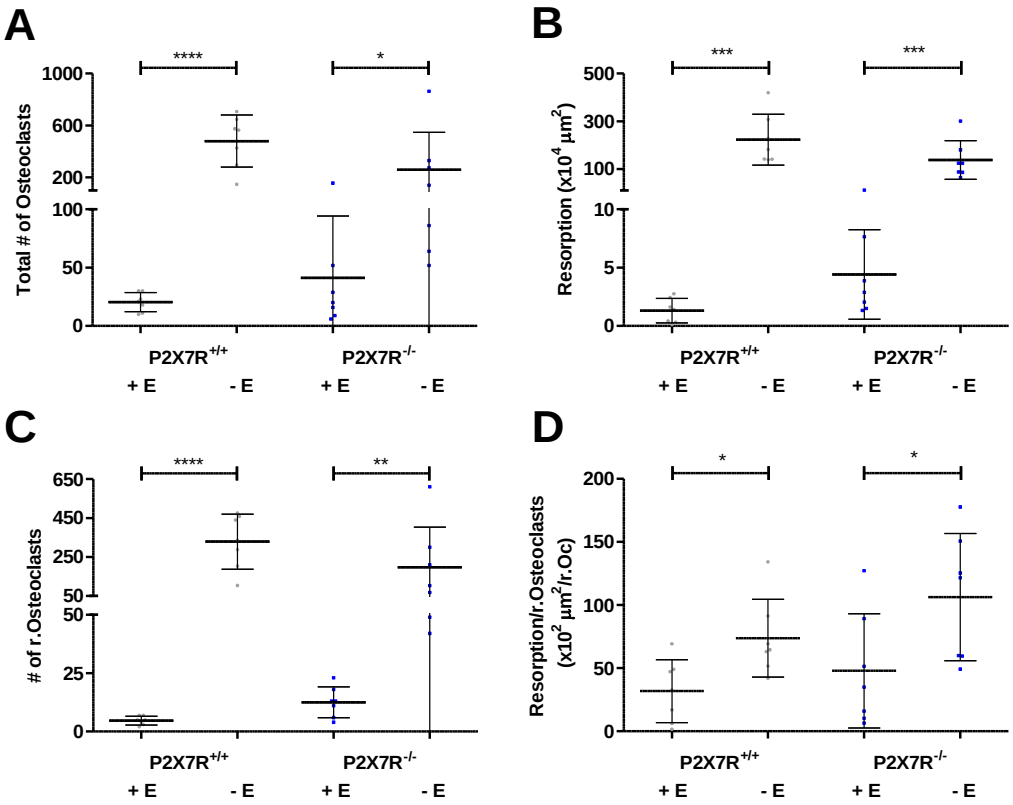

Figure 5-10 Effect of oestrogen depletion on spleen derived osteoclasts from P2X7R+/+ and P2X7R-/- mice

Precursor cells residing in murine spleens were differentiated on dentine and stained to analyse total number of osteoclasts (A), total resorption (B), number of resorbing osteoclasts (C) and resorptive ability (resorption/resorbing osteoclast) (D), values are mean ± SD, n=2 repeat cultures containing a total of 7 dentine discs. *p<0.05, **p<0.01, ***p<0.001, ****p<0.0001 0001 indicates statistical significance compared to +E (Student's t-test).

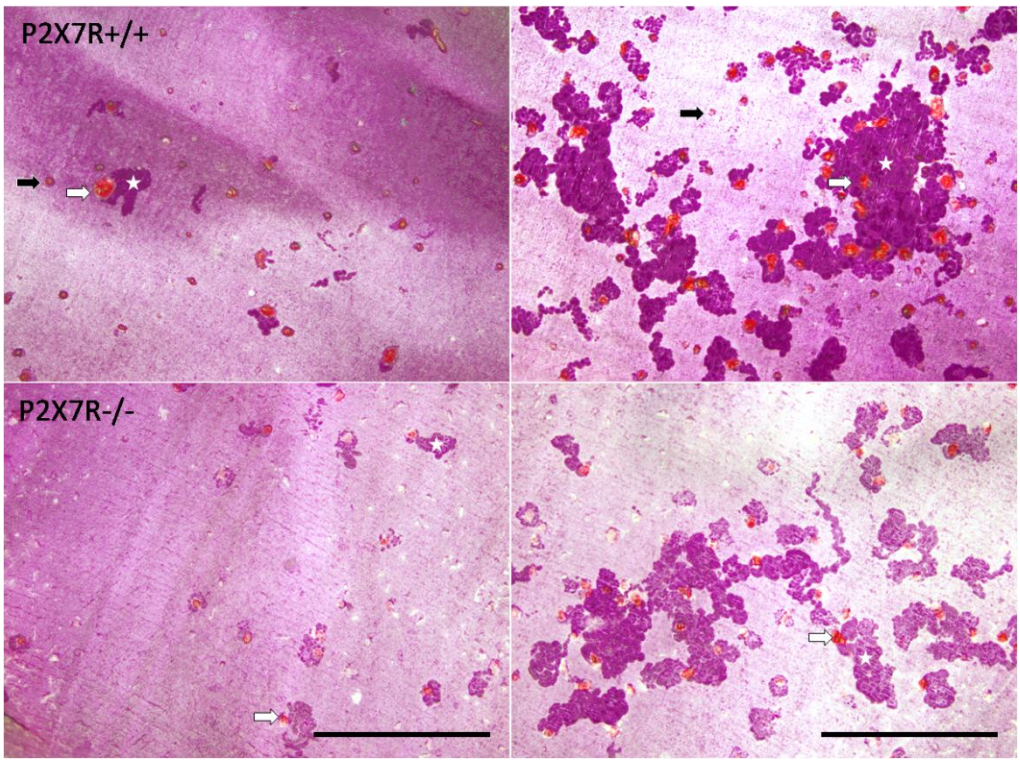

Figure 5-11 Representative images showing effect of oestrogen depletion on spleen derived osteoclasts of P2X7R+/+ and P2X7R-/- mice.

Precursor cells from splenic precursors of P2X7R+/+ and P2X7R-/- were differentiated on dentine in oestrogen containing (+E) and oestrogen depletory (-E) conditions and TRAP stained. Images show non-resorbing (black arrows) and resorbing (white arrows) osteoclasts and resorption trails (white stars) excavated by the cells on dentine. Scale bar= 500µm.

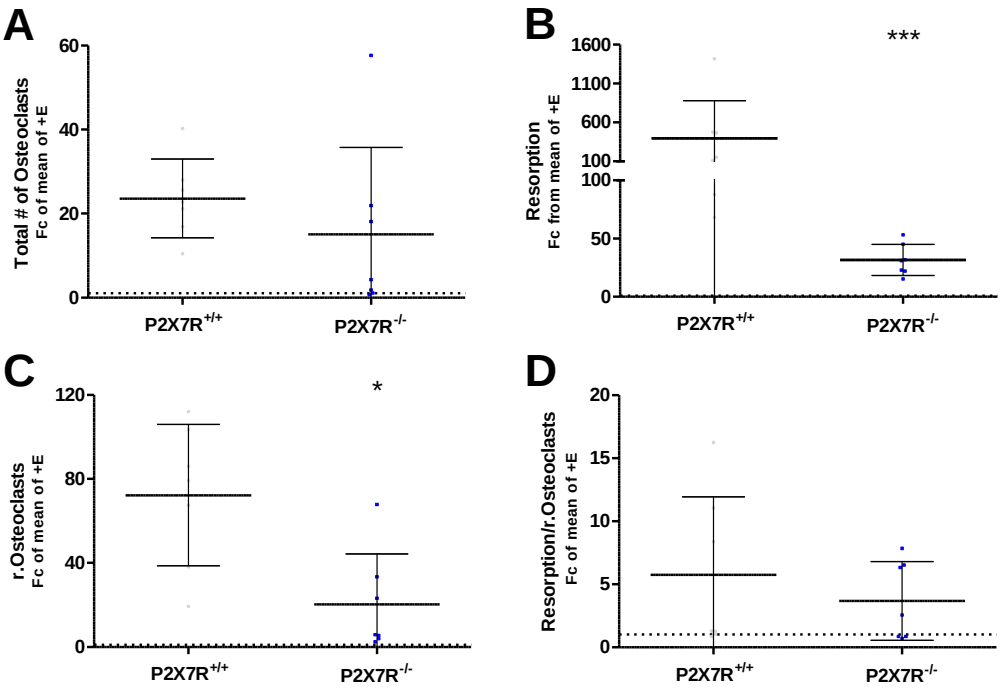

Figure 5-12 Response to oestrogen depletion on spleen derived osteoclasts of P2X7R+/+ and P2X7R-/- mice

Response to oestrogen depletion (-E) was expressed as a fold change of the mean of +E. Change in total number of osteoclasts (A), total resorption (B), number of resorbing osteoclasts (C) and the resorptive ability (resorption/resorbing osteoclast) (D) was analysed, values are mean ± SD, n= 2 repeat cultures containing a total of 7 dentine discs *p<0.05, ***p<0.001 indicates statistical significance compared to P2X7R+/+ (Univariate analysis of variance).

5.2.2.2. $P2Y_6R$

Splenic precursors of 5- 6 week old $P2Y_6R$+/+ and $P2Y_6R$-/- were seeded onto dentine discs for 9 days under oestrogen depletory conditions to obtain osteoclasts *in vitro*. Both $P2Y_6R$-/- and $P2Y_6R$+/+ showed a reduction in the total osteoclast number, number of resorbing osteoclasts, resorption and resorbing ability following loss of oestrogen (Figure 5-13) compared to the oestrogen containing media although the data did not reach statistical significance.

However, fold change in the total number of osteoclasts from $P2Y_6R$-/- was significantly higher in –E conditions compared to the change in $P2Y_6R$+/+ (1.3 fold versus 0.41 fold; p=0.0499). Moreover, the change in resorption ability was significantly altered in $P2Y_6R$-/- where it showed a 0.25 fold reduction in –E compared to 2 fold increase in the change in resorptive ability in $P2Y_6R$+/+ (p=0.0164) (Figure 5-15). No significant differences were obtained in the change in number of resorbing osteoclasts or total resorption in –E compared to +E in either genotype.

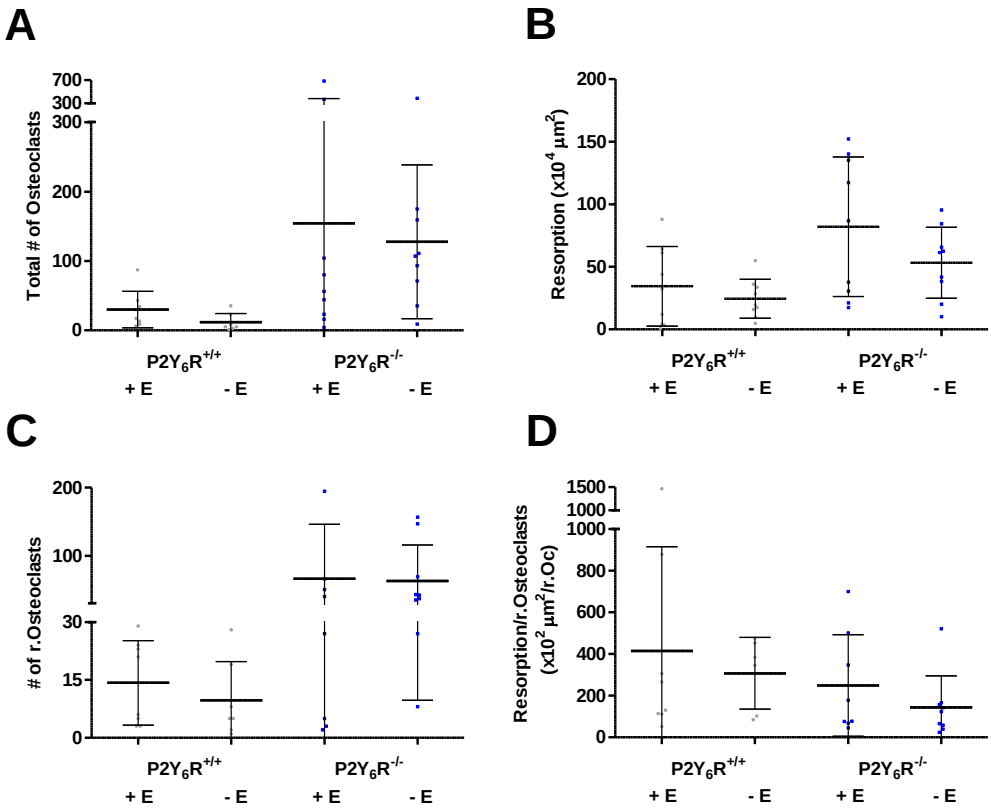

Figure 5-13 Effect of oestrogen depletion on spleen derived osteoclasts of P2Y$_6$R+/+ and P2Y$_6$R-/- mice

Precursor cells residing in murine spleens were differentiated on dentine and stained to analyse total number of osteoclasts (A), total resorption (B), number of resorbing osteoclasts (C) and resorptive ability (resorption/resorbing osteoclast) (D), values are mean ± SD, n= 2 repeat cultures containing a total of 9 dentine discs (Student's t-test).

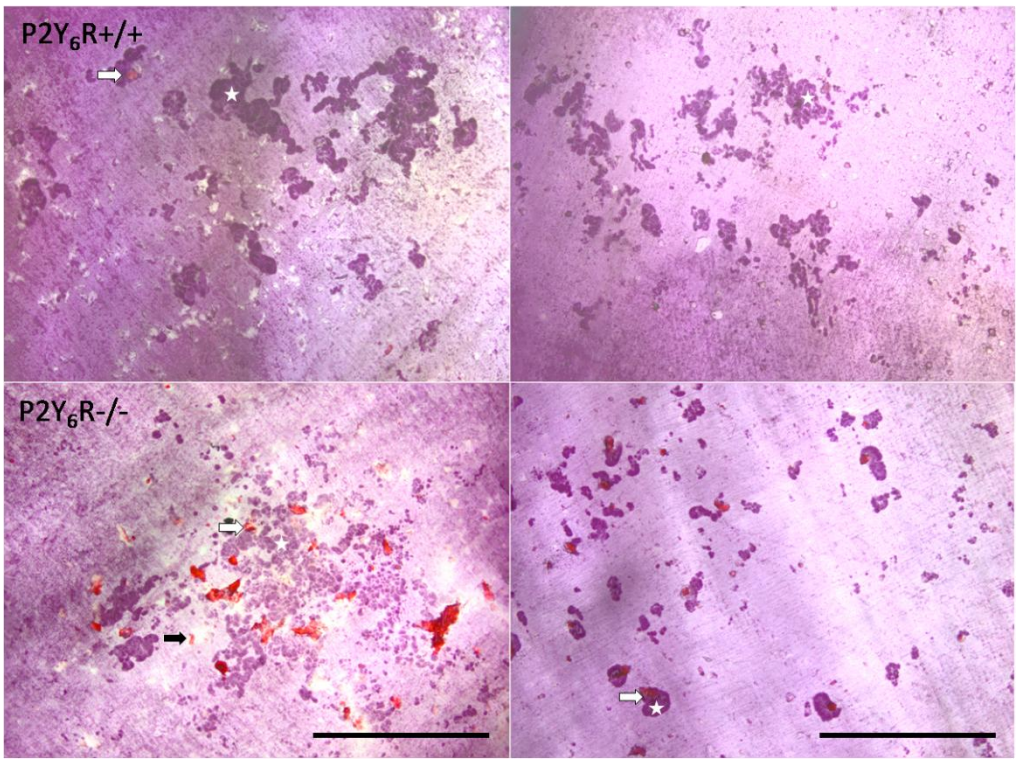

Figure 5-14 Representative images showing effect of oestrogen depletion on spleen derived osteoclasts of $P2Y_6R+/+$ and $P2Y_6R-/-$ mice.

Precursor cells from splenic precursors of $P2Y_6R+/+$ and $P2Y_6R-/-$ were differentiated on dentine in oestrogen containing (+E) and oestrogen depletory (-E) conditions and TRAP stained. Images show non-resorbing (black arrows) and resorbing (white arrows) osteoclasts and resorption trails (white stars) excavated by the cells on dentine. Scale bar= 500µm.

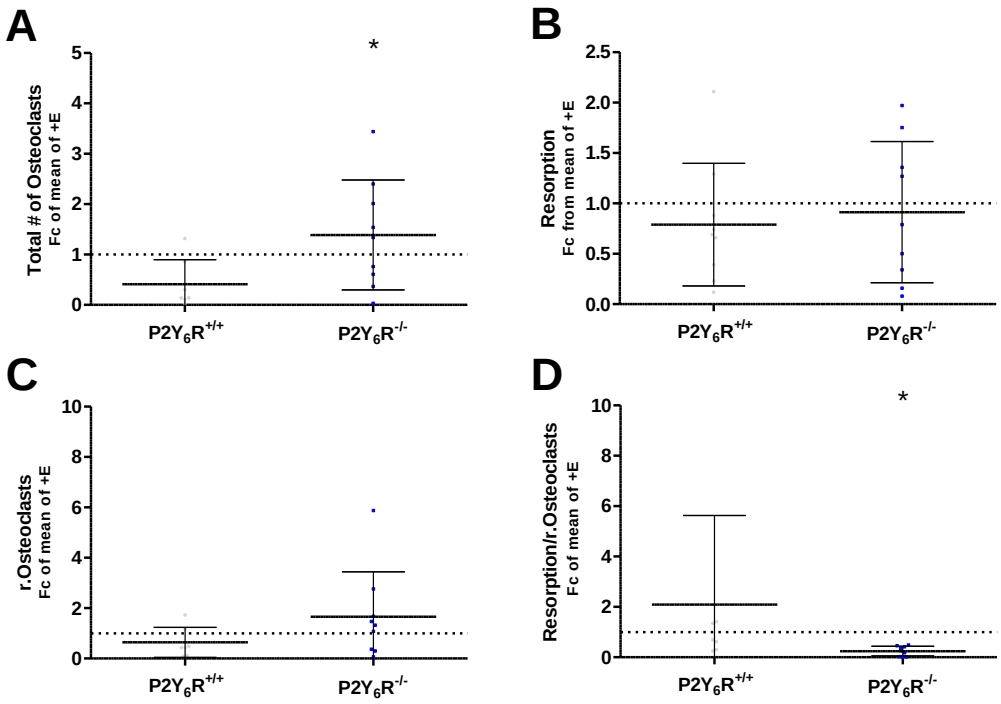

Figure 5-15 Response to oestrogen depletion on spleen derived osteoclasts of P2Y$_6$R+/+ and P2Y$_6$R-/- mice

Response to oestrogen depletion (-E) was expressed as a fold change of the mean of +E. Change in total number of osteoclasts (A), total resorption (B), number of resorbing osteoclasts (C) and the resorptive ability (resorption/resorbing osteoclast) (D) was analysed, values are mean ± SD, n= 2 repeat cultures containing a total of 9 dentine. *p<0.05 indicates statistical significance compared to P2Y$_6$R+/+ (Univariate analysis of variance).

5.2.2.3. $P2Y_{13}R$

Female 6- 7 week old $P2Y_{13}R+/+$ and $P2Y_{13}R-/-$ were obtained to isolate their spleens and precursors were seeded onto dentine discs for 17 days to generate osteoclasts *in vitro*. Osteoclasts derived from $P2Y_{13}R-/-$ in response to loss of oestrogen (-E), compared to normal complete media (+E) *in vitro* were significantly enhanced in their total numbers, ($p=0.0020$), numbers of resorbing osteoclast ($p=0.0002$) and their resorption ability ($p=0.2005$). These changes could not be measured in $P2Y_{13}R+/+$ osteoclasts as no TRAP +ve cells remained on the dentine discs following oestrogen loss. Following oestrogen depletion, total resorption obtained from $P2Y_{13}R-/-$ was significantly enhanced ($p<0.0001$) compared to a non-significant reduction ($p=0.0939$) obtained from $P2Y_{13}R+/+$ (Figure 5-16).

Expressing parameters as a fold change from +E, $P2Y_{13}R-/-$ showed an 11 fold change in resorption compared to the change in resorption from $P2Y_{13}R+/+$, which was reduced to 0.41 fold ($p<0.0001$) (Figure 5-18).

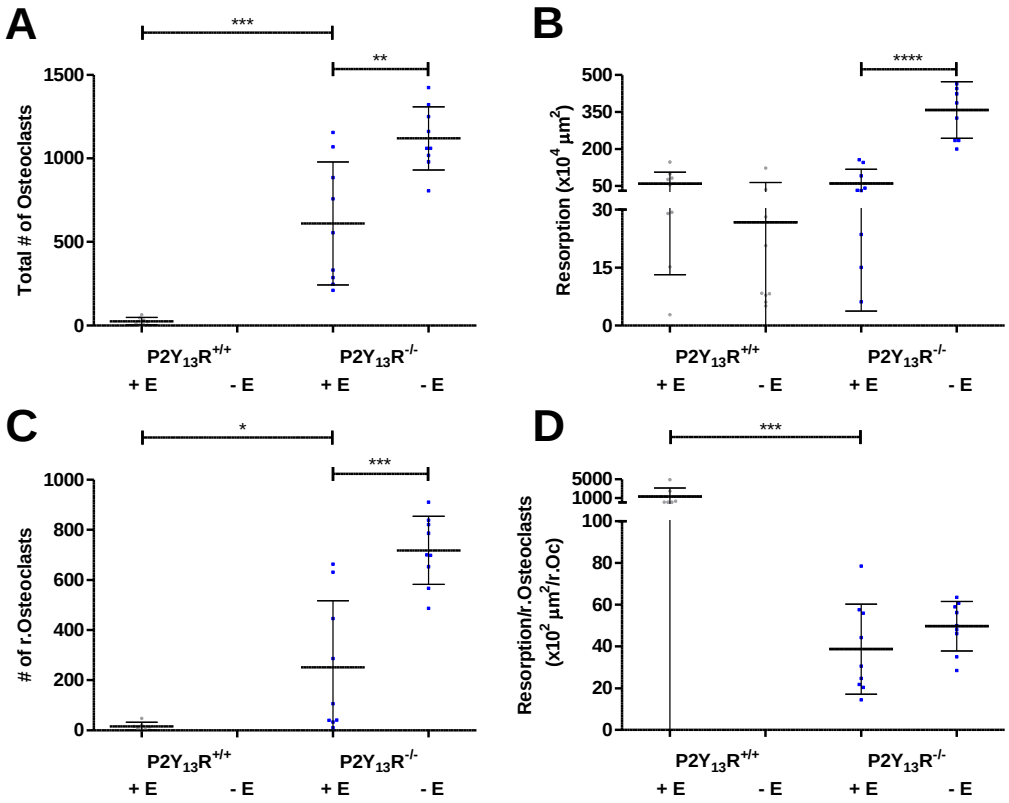

Figure 5-16 Effect of oestrogen depletion on spleen derived osteoclasts from P2Y$_{13}$R+/+ and P2Y$_{13}$R-/- mice

Splenic precursors were differentiated on dentine and stained to analyse total number of osteoclasts (A), total resorption (B), number of resorbing osteoclasts (C) and resorptive ability (resorption/resorbing osteoclast) (D), values are mean ± SD, n= 2 repeat cultures containing a total of 9 dentine discs. *p<0.05, **p<0.01, ***p<0.001, ****p<0.0001 indicates statistical significance compared to +E. (Student's t-test).

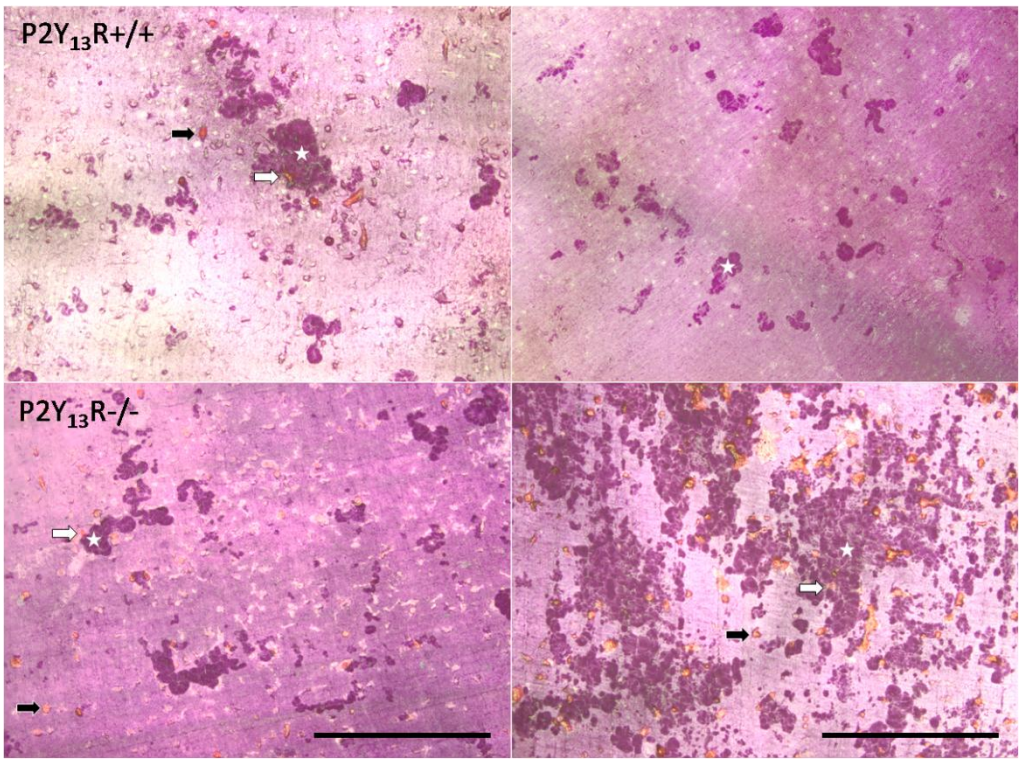

Figure 5-17 Representative images showing effect of oestrogen depletion on spleen derived osteoclasts of $P2Y_{13}R+/+$ and $P2Y_{13}R-/-$ mice.

Precursor cells from splenic precursors of $P2Y_{13}R+/+$ and $P2Y_{13}R-/-$ were differentiated on dentine in oestrogen containing (+E) and oestrogen depletory (-E) conditions and TRAP stained. Images show non-resorbing (black arrows) and resorbing (white arrows) osteoclasts and resorption trails (white stars) excavated by the cells on dentine. Scale bar= 500µm.

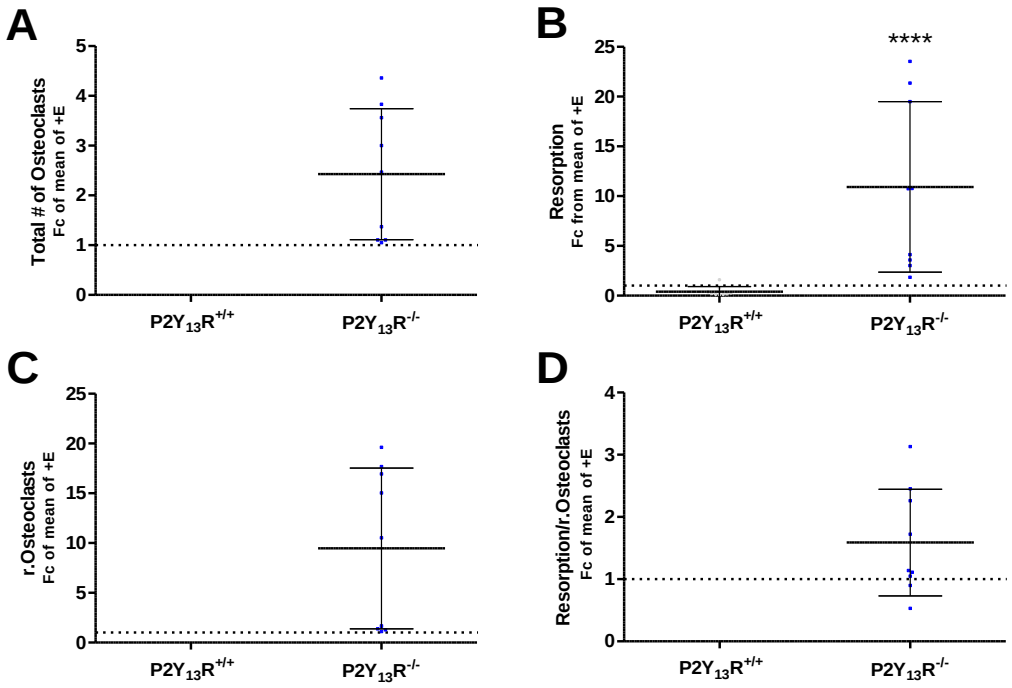

Figure 5-18 Response to oestrogen depletion on spleen derived osteoclasts from $P2Y_{13}R+/+$ and $P2Y_{13}R-/-$ mice

Response to oestrogen depletion (-E) was expressed as a fold change of the mean of +E. Change in total number of osteoclasts (A), total resorption (B), number of resorbing osteoclasts (C) and the resorptive ability (resorption/resorbing osteoclast) (D) was analysed, values are mean ± SD, n= 2 repeat cultures containing a total of 9 dentine discs. ****$p<0.0001$ indicates statistical significance compared to $P2Y_{13}R+/+$ (Univariate analysis of variance)

Table 5-3 Effect of oestrogen depletion on spleen derived osteoclasts from P2R mice (+E versus –E)

Parameters	+/+ (+E) Mean± SD	+/+ (-E) Mean± SD	p-value	-/- (+E) Mean± SD	-/- (-E) Mean± SD	p-value
P2X7						
Total Osteoclasts	20.43± 8.10	480.1± 201.7	<0.0001 ****	41.14± 52.92	258.3± 287.9	0.0126 *
Resorption ($x10^4$ µm^2)	1.31± 1.06	222.2± 106.6	0.0001 ***	4.41± 3.83	137.96± 81.21	0.0010 ***
Resorbing Osteoclasts (r.Oc)	4.71± 1.89	329.3± 141.2	<0.0001 ****	12.57± 6.55	197.3± 205.6	0.0021 **
Resorption Ability ($x10^2$ µm^2/r.Oc)	31.84± 24.90	73.72± 30.80	0.0161 *	47.98± 45.30	106.4± 50.45	0.0418 *
$P2Y_6$						
Total Osteoclasts	29.88± 26.48	11.43± 12.67	0.0560	154.1± 229.4	127.4± 110.8	0.3865
Resorption ($x10^4$ µm^2)	34.39± 31.86	24.44± 15.56	0.4126	82.06± 55.85	53.26± 28.26	0.1865
Resorbing Osteoclasts (r.Oc)	14.25± 10.96	9.71± 10.03	0.4208	66.22± 79.88	62.78± 53.09	0.6910
Resorption Ability ($x10^2$ µm^2/r.Oc)	415.3± 500.5	307.2± 172.8	0.8518	248.7± 244.0	143.6± 151.1	0.3213
$P2Y_{13}$						
Total Osteoclasts	25.86± 23.13	no cells	ND	611.1± 367.7	1120± 189.5	0.0020 **
Resorption ($x10^4$ µm^2)	59.17± 45.98	26.71± 37.14	0.0939	60.13± 56.37	357.9± 114.6	<0.0001 ****
Resorbing Osteoclasts (r.Oc)	16.14± 15.69	no cells	ND	250.9± 266.4	717.7± 135.7	0.0002 ***
Resorption Ability ($x10^2$ µm^2/r.Oc)	1350± 1790	ND	ND	38.68± 21.61	49.65± 11.86	0.2005

p-values were calculated using Student's t test

Table 5-4 Response of oestrogen depletion on osteoclasts derived from splenic precursors of P2R mice (Fc of +E)			
Parameters **Mean±SEM**	**+/+** **Mean±SD**	**-/-** **Mean±SD**	**p-value**
P2X7			
Total Osteoclasts	23.59± 9.38	15.09± 20.67	0.1282
Resorption ($x10^4$ µm^2)	396.1± 482.8	31.65± 13.39	0.0006***
Resorbing Osteoclasts (r.Oc)	72.25± 33.65	20.30± 24.01	0.0111*
Resorption Ability ($x10^2$ µm^2/r.Oc)	5.73± 6.21	3.67± 3.12	0.4428
$P2Y_6$			
Total Osteoclasts	0.41± 0.48	1.6± 1.07	0.0499*
Resorption ($x10^4$ µm^2)	0.79± 0.61	0.91± 0.70	0.8633
Resorbing Osteoclasts (r.Oc)	0.64± 0.60	1.66± 1.79	0.3404
Resorption Ability ($x10^2$ µm^2/r.Oc)	2.10± 3.53	0.25±0.20	0.0164*
$P2Y_{13}$			
Total Osteoclasts	ND	2.4± 1.32	ND
Resorption ($x10^4$ µm^2)	0.41± 0.49	10.94± 8.57	<0.0001****
Resorbing Osteoclasts (r.Oc)	ND	9.4± 8.1	ND
Resorption Ability ($x10^2$ µm^2/r.Oc)	ND	1.59± 0.86	ND
p- values were calculated using Univariate analysis of variance			

5.3. Discussion

Bone turnover is under an orchestrated control of local stimulus such as mechanical forces and systemic factors such as oestrogen. Oestrogen deficiency affects the survival of functional osteoclasts (Hughes et al., 1996; Kameda et al., 1997) and therefore the amount of bone that they can resorb, thereby affecting the overall rate of bone turnover. Purinergic signalling is known to synergise with the bone hormone PTH and is thought to provide a mechanism for integrating local and systemic responses in the activation of bone remodelling (Bowler et al., 2001) Considering the varied purinoceptor expression on osteoclasts and evidence suggesting an interaction of oestrogen with purinoceptors (Gartland et al., 2012b; Husted et al., 2013; Jorgensen et al., 2012; Ohlendorff et al., 2007b; Wesselius et al., 2013) potentiating osteoclastic resorption, in this chapter, the effect of oestrogen loss on osteoclastogenesis in the absence of P2R models was assessed *in vitro*. Results indicate that combined absence of oestrogen and P2X7R led to an enhanced resorption ability by osteoclasts. However, oestrogen depletion seemed to regulate P2X7R mediated responses dependent on the lineage of the osteoclast precursor cells. The later finding was supported by the origin-dependent effect of oestrogen withdrawal on osteoclast function via other purinoceptors (i.e.$P2Y_6R$ and $P2Y_{13}R$).

5.3.1. Absence of oestrogen enhances the resorption ability in P2X7R-/- BM osteoclasts

Results demonstrate that there was an overall increase in the resorption abilities under oestrogen deplete conditions in both genotypes, however, the resorptive ability was aggravated in P2X7R-/- osteoclasts Interestingly, this was independent of a change in osteoclast numbers suggesting the formation of osteoclasts was not affected in the combined absence of P2X7R and oestrogen. From 0, it is indicative that deletion of P2X7R causes reduced resorption abilities of BM osteoclasts and interestingly, oestrogen loss rescued the reduced resorption ability by BM osteoclasts as seen in this chapter. Oestrogen deficiency is a powerful catabolic stimulus, one that is

possibly overpowering any impairment in resorptive abilities due to P2X7R deletion. Not only that, there appears to be a synergistic effect of oestrogen withdrawal-mediated enhancement in osteoclastic resorption in the absence of P2X7R. It is possible that part of this regulation is via the loss of P2X7R mediated cytotoxicity (Gartland et al., 2003b) and part due to increased osteoclast development after oestrogen loss (Jilka et al., 1992). In 2001, Naemsch et al showed that ATP acts via P2X7R causing ligand-gated calcium influx in rabbit osteoclasts (Naemsch et al., 2001). The authors showed that P2X7R activation led to inhibition of resorption and P2X7R-/- deletion in osteoclasts could prevent the negative regulation of resorption by extracellular ATP, thereby enhancing resorption abilities. It is tempting to speculate that P2X7R might be acting as a 'control switch' following oestrogen loss and its absence resulted in an exacerbated osteoclastogenesis.

Bone phenotype following OVX results in a loss of bone volume in both trabecular and cortical compartment of P2X7R-/- mice (unpublished findings). *In vitro* results suggest that increased osteoclastic resorption may be responsible for the development of the murine phenotype following OVX. Moreover, in post-menopausal women, loss of P2X7R function results in an accelerated loss of their lumbar BMD over 6-7 year period (Gartland et al., 2012b) and increased fracture risk over 10 year period (Jorgensen et al., 2012). These findings along with the OVX induced bone loss in P2X7R-/- *in vivo* and potentiation of osteoclastic resorption abilities *in vitro* ascertain the role of P2X7R in regulation of bone mass following oestrogen loss. It will be informative to assess oestrogen's effect on osteoblasts derived from P2X7R-/- mice, to confirm whether this aggravated bone loss is exclusively mediated by lack of oestrogen's influence on osteoclasts.

5.3.2. Oestrogen depletion increased resorption in $P2Y_6R$-/- BM osteoclasts

Given that $P2Y_6R$ is the highest expressed of all the purinoceptors on both early and mature murine osteoclasts (Orriss et al., 2011b) and evidence of a role in prolonging osteoclast survival (Korcok et al., 2005), deletion of $P2Y_6R$

suggested interesting roles of the receptor in regulation of bone physiology. Orriss et al., showed that activating $P2Y_6R$ increased osteoclast formation and that osteoclasts derived from KO mice showed reduced resorption (Orriss et al., 2011b). The bone remodelling cycle was challenged *in vivo* following OVX induced bone loss and $P2Y_6R$-/- mice showed heightened loss of bone volume, reduction in trabecular number with increase in trabecular separation in both tibial and vertebral cancellous bone compartments representative of appendicular and axial skeleton respectively (unpublished findings). These results are consistent with *in vitro* findings that osteoclasts from $P2Y_6R$-/- mice demonstrate enhanced resorption in oestrogen deplete conditions.

Previous studies in our lab on female mice using the same colony as Orriss et al., showed an increased osteoclastogenesis *in vitro* in $P2Y_6R$-/- cultures (unpublished findings). The differences in these findings were attributed to the age of mice and different concentrations of cytokines in the culture media. Gupta et al., speculate that increasing RANKL concentrations rescues the defective survival and resorptive capacity in $P2Y_6R$-/- osteoclasts. Indeed, loss of oestrogen can augment RANKL induced osteoclastogenesis by increased engagement of other cell surface receptors. For instance, enhanced activation of TNF-α receptor, p55, augmented RANKL-dependent osteoclast formation and bone loss following OVX (Cenci et al., 2003). It can be argued that $P2Y_6R$-/- defects in osteoclasts is rescued in a similar manner either directly by stimulation of osteoclast precursors or indirectly by action on other cell types contained in the heterogeneous culture *in vitro*. Additionally, oestrogen blocks key osteoclastogenic transcription factors (Srivastava et al., 1999) and thus another mechanism could be an increased responsiveness of precursors thereby enhanced resorption in its absence.

The data suggest that $P2Y_6R$+/+ osteoclasts underwent an accelerated maturation but shortened life and deletion of $P2Y_6R$ resulted in their enhanced survival. Due to the limitation of analysis to a single time point in these osteoclast cultures, it cannot be confirmed whether osteoclasts from either genotype exhibit early maturation with enhanced survival or normal maturation with delayed death. More studies are needed to determine the life

span of the osteoclasts and the influence of oestrogen in the absence of $P2Y_6R$.

5.3.3. $P2Y_{13}R$ deletion and oestrogen loss did not affect the resorption of BM osteoclasts

Oestrogen loss did not result in heightened osteoclastogenesis in either $P2Y_{13}R+/+$ or $P2Y_{13}R-/-$ cultures *in vitro*. Despite an increased number of osteoclasts in oestrogen deplete conditions in $P2Y_{13}R-/-$ cultures, no change in resorption was detected. This is contradictory to *in vivo* findings in which $P2Y_{13}R−/−$ mice were shown to have a reduced oestrogen deficiency-induced bone loss (Wang et al., 2012). The preventative role of $P2Y_{13}R$ deletion in bone loss following OVX is partly due to the defect in their bone formation abilities. It is speculated that the improper mineralisation and reduced bone forming rates in the absence of $P2Y_{13}R$ could contribute to the development of the phenotype in mice model of osteoporosis. Interestingly, Ning et al., observed a reduced resorption by $P2Y_{13}R−/−$ osteoclasts *in vitro* however results obtained in this chapter show an increased cumulative resorption compared to $P2Y_{13}R+/+$ osteoclasts. The differences in findings could be due to two reasons. Firstly, the age of mice used in their study were >2 month old compared to <2 month old mice in this chapter. C57BL/6 mice are known to be skeletally immature until 4 months of age (Beamer et al., 2001). There is still acquisition of peak bone mass in the mice and they show steep growth spurts between 1 and 2 months of age and again between 2-4 months of age (Beamer et al., 2001). It is possible that the precursors obtained from mice during their growth spurt might be controlled by different sets of genes at each age. Their controlled and timely regulation would help attain their peak bone mass and maybe under epigenetic control. Another reason could be the differences in the RANKL concentrations between the studies. Ning et al., showed that the bone marrow cells from $P2Y_{13}R−/−$ mice had an intrinsic defect resulting in a downregulated *Tnfsf11* (RANKL) (Wang et al., 2012). Therefore, a 10-fold increase in RANKL, used in this chapter could have rescued the defective osteoclast survival and function in $P2Y_{13}R-/-$ cultures.

These results suggest that resorption obtained in $P2Y_{13}R$-/- osteoclasts was not affected by the loss of oestrogen. Moreover, the supplementation with RANKL could have rescued the defect in $P2Y_{13}R$-/- osteoclasts which was not potentiated following oestrogen loss.

5.3.4. Oestrogen mediated effects on osteoclasts depends on precursor cell origin.

It was interesting to find differences in responses both absolute and receptor dependent, in osteoclasts derived from two different murine sources. Literature suggests organ specific microenvironments in mice containing pools of progenitors different in both their size and colonizing abilities (Ghinassi et al., 2009). Existence of a lineage-dependent regulation is speculated. Bone forming osteoblasts showed variable development and function dependent on the lineage of the precursors (Declercq et al., 2004). In light of this, it is possible that osteoclast precursors are regulated in a lineage dependent manner and could develop into mature cells with different osteoclastogenic abilities.

In P2X7R-/- osteoclasts, despite a pro-osteoclastic effect of oestrogen depletion the change in resorptive ability remained unaffected between the P2X7R+/+ or P2X7R-/- splenic cells unlike the effects observed from BM lineage. Splenic osteoclasts did not show a heightened osteoclastogenesis when precursors were obtained from either the $P2Y_6R$+/+ or $P2Y_6R$-/- mice. There seemed no difference in the change in resorption in either genotype which is different to the enormous effect following oestrogen loss obtained from BM osteoclasts. On similar lines, oestrogen depletion led to more profound changes on osteoclast survival, development and function when cells were derived from spleens of $P2Y_{13}R$-/- compared to the BM. These findings suggest a lineage dependent regulation of both oestrogen and P2Rs on osteoclasts within the two compartments.

Effects of molecules like TNF-α, IL-6, p38 and NF-κB (Azuma et al., 2000; Jilka et al., 1992; Li et al., 2002; Vaira et al., 2008) on osteoclastogenesis have been demonstrated using murine bone marrow derived cells and

whether a different mechanism in spleen monocytes converging in common key osteoclastogenetic events, needs to be investigated.

One could argue that BM are a better and bigger pool of less differentiated monocytes (van Furth and Cohn, 1968), compared to precursors from an organ with a primary function of removal of aging cells and filtering iron (Mebius and Kraal, 2005) and therefore a better model to study *in vitro* osteoclastogenesis. The results from these experiments demonstrate that the changes in BM osteoclasts mimic the effects of oestrogen loss *in vitro* to the development of oestrogen withdrawal mediated bone phenotype and therefore, are a good model for osteoclast function *in vitro*. However, splenic precursors are an active and ready-to-be-deployed source of monocytes, at least in response to tissue injury (Swirski et al., 2009). The injection of normal spleen cells into osteopetrotic mice is able to cure the bone phenotype *in situ* (Walker, 1975) suggesting their capability to differentiate into fully-functional bone resorbing osteoclasts. It is likely that a co-ordinated contribution by both bone marrow and splenic precursors in mice, might be responsible for the bone resorption *in vivo* and the development of their overall bone phenotype. Moreover, as observed in 0, P2R regulation appears to be cell-type dependent. Nevertheless, evidence points towards an important role of P2 receptors in regulation of bone resorption as shown by the BM osteoclasts *in vitro* but a similar change in combined absence of oestrogen and P2 receptors was not obtained from splenic osteoclasts.

5.4. Conclusion

Despite the arguments regarding the value of murine OVX as a model to understand post menopausal osteoporosis considering there is gradual decline of the hormone in latter compared to the abrupt loss in the former, oestrogen withdrawal influences osteoclast generation and activity via P2Rs. These results highlight the existence of different osteoclastic lineages capable of regulation by both oestrogen and purinoceptors albeit to different extents. More work is needed to conclusively determine the involvement of oestrogen on bone forming osteoblasts in the presence of purine signalling. This is critical for accomplishing the goal of fighting both post menopausal and senile osteoporosis.

Chapter 6. Non-synonymous SNPs in human P2RX7 gene cause altered osteoclastogenesis.

6.1. Introduction

The human *P2RX7* gene lies on chromosome 12q24.3 and codes for a P2X7R subunit 595 amino acid in length containing two membrane-spanning domains and a 240 amino acid long intracellular C-terminus. P2X7R splice isoforms have been reported, known to alter receptor function leading to alteration of signalling properties downstream of receptor activation. In addition, reported SNPs in the *P2RX7* gene which contribute to further variation in receptor-mediated signalling between individuals. Currently, 197 SNPs lie in the coding region and 8 have been functionally characterised to impart either gain or loss of function to the receptor. Consequently, these variations in the highly polymorphic *P2RX7* gene have been associated with various human diseases in several population based cohorts. For instance, p.Gln460Arg, known to impart an increased dye uptake and ATP-induced currents (Stokes et al., 2010) has been associated with an increased susceptibility to mood disorders (Barden et al., 2006; Lucae et al., 2006; McQuillin et al., 2009). The 1513A>C polymorphism is strongly associated with an increased risk of tuberculosis due to a loss of mycobacterial killing by the macrophages in patients with 1513C allele (Fernando et al., 2007; Sharma et al., 2010; Tekin et al., 2010).

Functional P2X7R SNPs have also been associated with changes in bone turnover and thereby influencing bone quality. Recently, loss of function (LOF) SNP p.Arg307Gln was associated with higher bone loss (Gartland et al., 2012b; Jorgensen et al., 2012) whilst both men and women containing the gain of function (GOF) SNPs p.Gln460Arg and p.Ala348Thr were protected against bone loss in addition to a reduced fracture risk (Jorgensen et al., 2012; Wesselius et al., 2013). The bone phenotype was seen to be influenced by loss of osteoclast apoptosis via the LOF SNP, p.Glu496Ala, which therefore, could contribute to an increased fracture risk (Ohlendorff et al., 2007b). These studies suggest that detecting non-synonymous SNPs within the P2RX7 gene could prove helpful in identifying people at a greater risk of developing diseases and bone disorders. The aim of this chapter was to 1) Determine P2X7R expression on mature osteoclasts bearing receptor

SNPs. 2) Determine whether P2X7R function is altered on monocytic precursors and mature osteoclasts due to GOF or LOF SNPs and 3) Determine the effect of P2X7R SNPs on osteoclastogenesis *in vitro*.

6.2. Results

6.2.1. Polymorphisms in the P2X7R gene

Description of non-synonymous SNPs with their functional relevance is given in Table 6-1. All DOPS donors were genotyped for all 12 SNPs using TaqMan allelic discrimination assays as previously described in (Jorgensen et al., 2012).

Table 6-1 List of P2X7R SNPs with their reported functions. [Adapted from (Wesselius et al., 2011) with permission from Frontiers in Bioscience)]

SNP ID	Base change	Amino Acid change	Functional Effect	References
rs35933842	151+1g→t	Null allele	No expression of receptor mRNA	(Fernando et al., 2005; Skarratt et al., 2005)
rs17525809	253T→C	Val76Ala	Loss-of-function	(Roger et al., 2009)
rs28360447	474G→A	Gly150Arg	Loss-of-function SNP	(Roger et al., 2009)
rs208294	489C→T	His155Tyr	Gain-of-function SNP	(Cabrini et al., 2005; Roger et al., 2009)
rs7958311	809G→A	His270Arg	Gain-of-function SNP	(Stokes et al., 2010)
rs7958316	853G→A	Arg276His	Loss-of-function SNP	(Stokes et al., 2010)
rs28360457	946G→A	Arg307Gln	Loss-of-function	(Fernando et al., 2005; Gu et al., 2004a)
rs1718119	1068G→A	Ala348Thr	Gain-of-function SNP	(Cabrini et al., 2005; Roger et al., 2009; Sun et al., 2009)
rs2230911	1096C→G	Thr357Ser	Loss-of-function	(Cabrini et al., 2005; Roger et al., 2009; Shemon et al., 2006)
rs2230912	1405A→C	Gln460Arg	Minor loss-of-function Marker of gain-of-function	(Cabrini et al., 2005; Roger et al., 2009; Stokes et al., 2010)
rs3751143	1513A→C	Glu496Ala	Loss-of-function SNP (pore formation)	(Boldt et al., 2003; Fernando et al., 2007; Gu et al., 2004a; Gu et al., 2001; Ohlendorff et al., 2007a; Wiley et al., 2002)
rs1653624	1729T→A	Ile568Asn	Loss-of-function SNP (trafficking defect)	(Roger et al., 2009; Wiley et al., 2003)

6.2.2. Details of the study population

Description of DOPS donors that were used to obtain CD14+ precursors and mature osteoclasts *in vitro* is given in Table 6-2. All donors were post-menopausal women and no significant differences were measured in their percentage change in BMD per year in lumbar spine (LS; L2-L4) total hip (TH) and femoral neck (FN). Donors who were smokers, on bone treatment or on anti-inflammatory drugs were excluded from analyses for P2X7R function or osteoclastogenesis.

The P2X7R genotype distribution of donors who were included in the study is shown in Table 6-3. Donors will be referred to as P2X7-WT, without any P2X7R SNPs except heterozygous allele at His155Tyr. All P2X7-GOF donors, contain homozygous allele at His155Tyr, Ala348Thr and Gln460Arg. All the 3 donors classed as P2X7-LOF (heterozygous at Arg307Gln), showed several non-synonymous SNPs in the P2RX7 gene.

Table 6-2 Details of DOPS donors at the time of peripheral blood donation			
	P2X7-WT	**P2X7-GOF**	**P2X7-LOF**
Mean Age (years)	70.8	69.8	69.6
Annualised change in BMD (LS, TH, FN) (%)	(-0.40, -0.71, -0.50)	(-0.76, -0.53, -0.46)	(-0.09, -0.51, -1.03)
Current smoker (no, yes) (%)	83.3, 16.7	100.0, 0.0	80.0, 20.0
Current bone treatment (no, yes) (%)	100.0, 0.0	100.0, 0.0	60.0, 40.0
Current NSAID use (no, yes) (%)	100.0, 0.0	80.0, 20.0	100.0, 0.0

Data from 6 P2X7-WT, 6 P2X7-GOF and 5 P2X7-GOF donors.
Abbreviations: BMD, Bone Mineral Density; LS, Lumbar spine L2-L4; TH, Total Hip; FN, Femoral neck; NSAID, Non-steroidal anti-inflammatory drugs.
NB All donors were post-menopausal women from DOPS, Danish Osteoporosis Prevention Study.

Table 6-3 P2X7R genotype distribution for donors from DOPS study

Post menopausal women used to obtain CD14+ monocytes and osteoclasts *in vitro* are shown with their DOPS IDs (rows) and the corresponding SNPs (columns).

SNPs →	Null allele	p.Val 76Ala	p.Gly 150Arg	p.Tyr 155His	p.His 270Arg	p.Arg 276His	p.Arg 307Gln	p.Ala 348Thr	p.Thr 357Ser	p.Gln 460Arg	p.Glu 496Ala	p.Ile 568Asn
DOPS ID↓												
P2X7-WT												
1973	WT	WT	WT	WT	**HET**	WT	WT	WT	WT	WT	WT	WT
1562	WT	WT	WT	WT	**HET**	WT	WT	WT	WT	WT	WT	WT
1180	WT	WT	WT	WT	**HET**	WT	WT	WT	WT	WT	WT	WT
1151	WT	WT	WT	WT	**HET**	WT	WT	WT	WT	WT	WT	WT
1252	WT	WT	WT	WT	**HET**	WT	WT	WT	WT	WT	WT	WT
P2X7-GOF												
1193	WT	WT	WT	**HOMO**	WT	WT	WT	**HOMO**	WT	**HOMO**	WT	WT
1879	WT	WT	WT	**HOMO**	WT	WT	WT	**HOMO**	WT	**HOMO**	WT	WT
1751	WT	WT	WT	**HOMO**	WT	WT	WT	**HOMO**	WT	**HOMO**	WT	WT
1931	WT	WT	WT	**HOMO**	WT	WT	WT	**HOMO**	WT	**HOMO**	WT	WT
P2X7-LOF												
1782	WT	WT	WT	**HET**	**HET**	WT	**HET**	**HET**	WT	WT	WT	WT
1095	WT	WT	WT	WT	**HET**	WT	**HET**	**HET**	WT	WT	WT	WT
1830	WT	WT	WT	WT	**HOMO**	WT	**HET**	WT	WT	WT	WT	WT

Allelic changes are highlighted in bold.
HOMO: Homozygous for the variant allele.
HET: Heterozygous.
WT: Wild-type.

6.2.3. P2X7R expression in osteoclasts bearing functional SNPs

Osteoclasts generated on glass coverslips were stained using a monoclonal antibody against P2X7R as described in Section 2.2.2.10. Staining was done with or without permeabilisation to detect both surface and intracellular expression of P2X7R respectively.

As expected in P2X7-WT osteoclasts, P2X7R expression was detected when stained without permeabilisation suggesting surface expression. Expression was also detected in P2X7-GOF but not in P2X7-LOF osteoclasts (Figure 6-1). Receptor expression could be detected in P2X7-LOF upon permeabilisation (Figure 6-2).

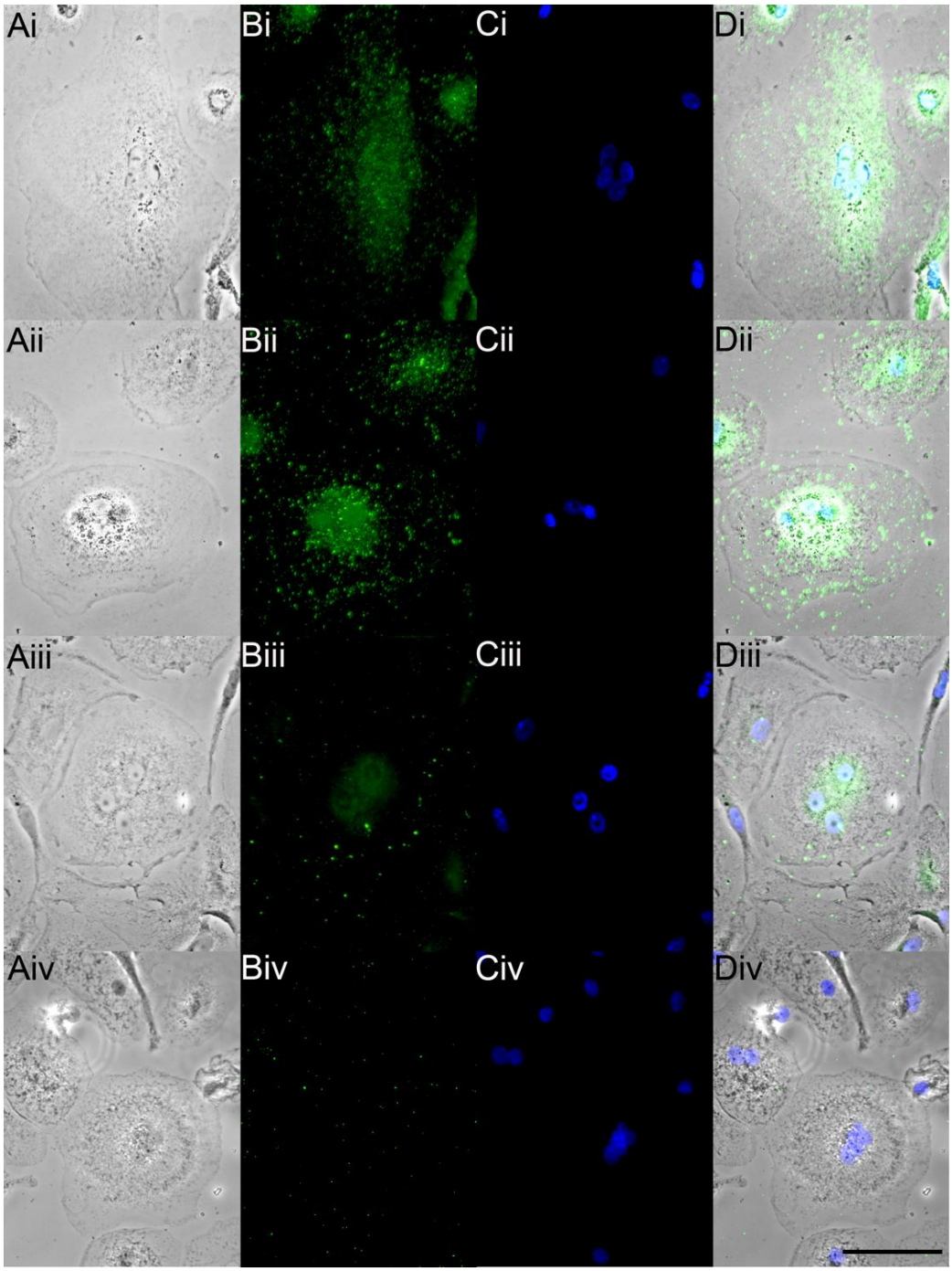

Figure 6-1 Representative images showing surface expression of P2X7R

Panels on the left show the bright field image of multinucleated osteoclasts on glass coverslips (A). Cells were stained for hP2X7R expression (B, green) using a monoclonal antibody and nuclei (C, blue) using Hoechst. Panels on the right are merged images showing localisation of P2X7R on osteoclasts surface (D). Osteoclasts were generated from P2X7-WT (i), P2X7-GOF (ii) P2X7-LOF (iii) donors *in vitro*. Control for staining was performed by replacing mAb with isotype antibody (mouse IgG1) (iv). Scale bar = 25 μm.

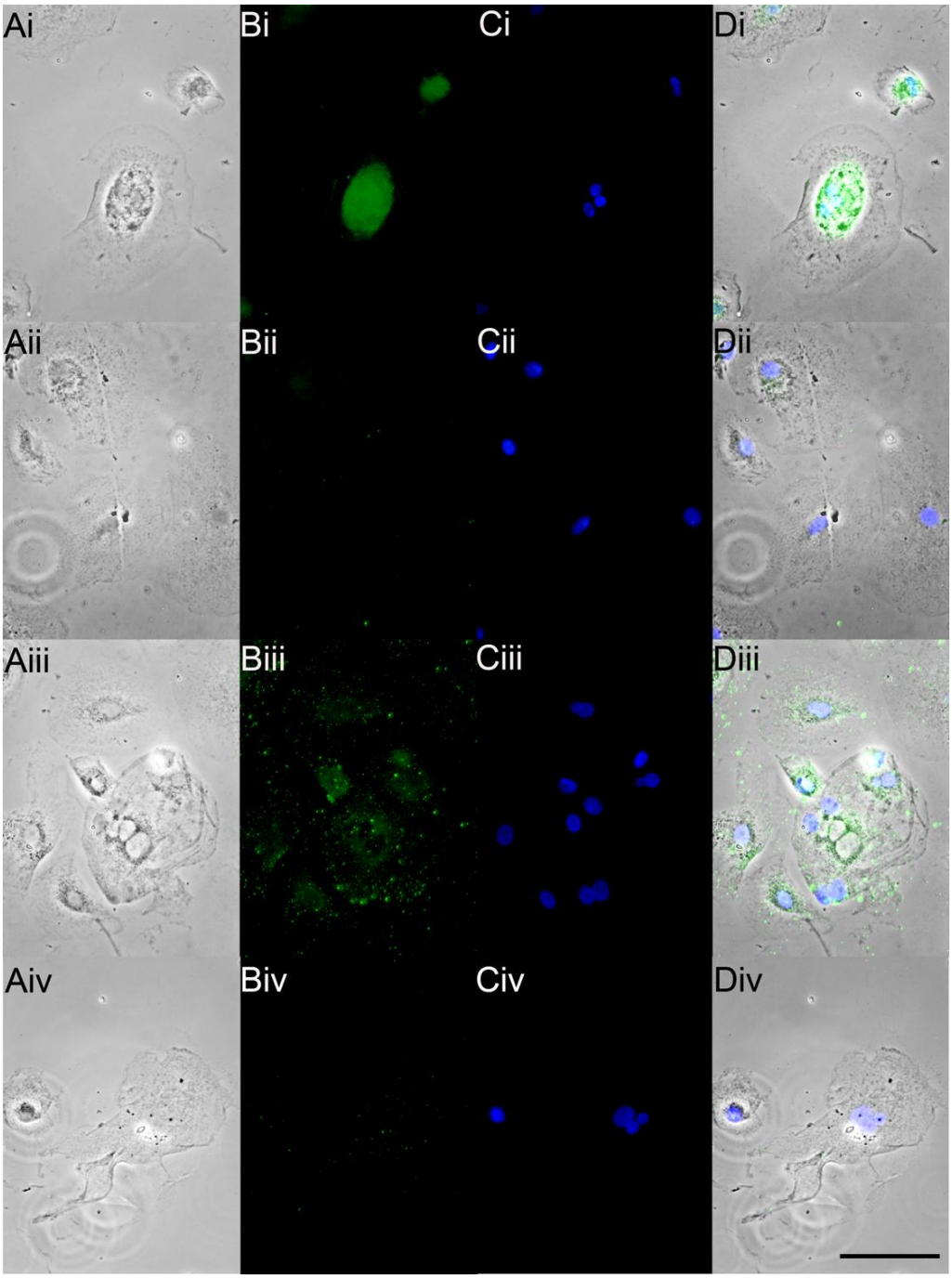

Figure 6-2 Representative images showing intracellular P2X7R expression

Panels on the left show the bright field image of multinucleated osteoclasts on glass coverslips (A). Cells were permeabilised using 0.1% Triton X-100 and stained for hP2X7R expression (B, green) using a monoclonal antibody and nuclei (C, blue) using Hoechst. Panels on the right are merged images showing intracellular P2X7R expression of osteoclasts (D). Osteoclasts were generated from P2X7-WT (i), P2X7-GOF (ii) and P2X7-LOF (iii) donors *in vitro*. Control for staining was performed by replacing mAb with isotype antibody (mouse IgG1) (iv). Scale bar = 25 μm.

6.2.4. Effect of SNPs on P2X7R function

6.2.4.1. Calcium influx

P2X7R is an ion channel with two transmembrane domains that allows entry of cations like Ca^{2+} and K^{+} following brief activation (Rassendren et al., 1997). To test whether the SNPs resulted in functional changes in the Ca^{2+} influx on CD14+ monocytes or osteoclasts, cells from P2X7-WT, P2X7-GOF and P2X7-LOF donors were assessed for P2X7R mediated Ca^{2+} influx. Fluorescence due to binding of free calcium to intracellular Fluo-4 was measured after BzATP stimulus.

Ca^{2+} influx in P2X7-GOF precursors was significantly higher following BzATP stimulus (1218%, p=0.0080) compared to non-stimulated cells (basal). This response was significantly higher than the response by P2X7-WT (243%, p=0.0022). Interestingly, BzATP failed to illicit a significant increase in calcium influx in P2X7-LOF precursors (253%, p=0.3869) compared to no stimulus as well as compared to P2X7-WT (p=0.9529) (Figure 6-3). Pre-treatment with P2X7R antagonist did not change the BzATP mediated Ca^{2+} influx following stimulus in either precursors despite the genotype.

Similar to precursors, osteoclasts generated from P2X7-GOF showed significantly increased Ca^{2+} influx following BzATP stimulation (2262%, p=0.0029). Additionally, osteoclasts from P2X7-WT and P2X7-LOF showed significant influx compared to basal albeit to a smaller extent (405% in P2X7-WT, p=0.0093 and 279% in P2X7-LOF, p=0.0498). Moreover, pre-incubation with antagonist resulted in significantly less channel activity in P2X7-WT osteoclasts (220%, p=0.0303) but not in osteoclasts with P2X7R SNPs (923% in P2X7-GOF, p=0.0722 and 177% in P2X7-LOF, p=2310).

The P2X7R mediated Ca^{2+} influx was significantly enhanced in P2X7-GOF osteoclasts compared to P2X7-WT (2262% versus 405%, p=0.0045). P2X7-LOF osteoclasts showed a non-significant reduction of Ca^{2+} influx compared to that of P2X7-WT osteoclasts (279% versus 405%, p=0.1024). (Figure 6-3).

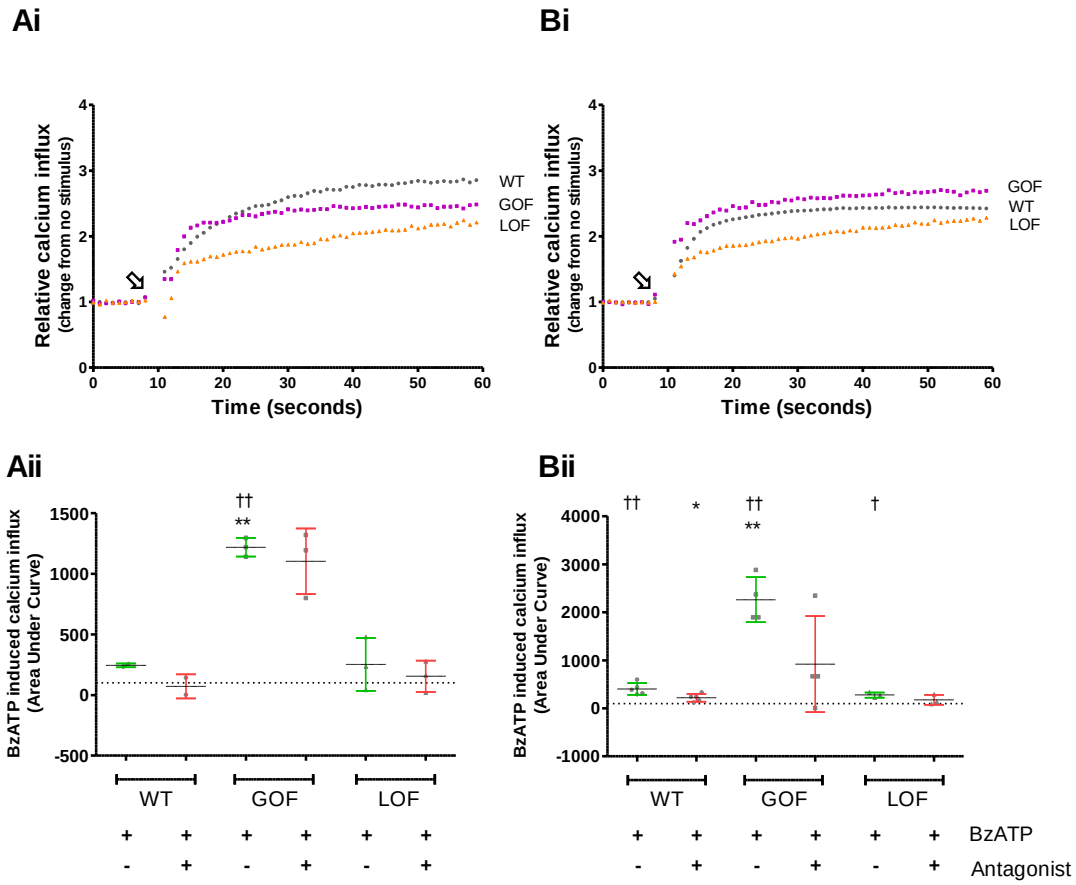

Figure 6-3 Ca^{2+} influx following BzATP stimulation

Ca^{2+} influx was measured in CD14 enriched monocyte precursors (A) or mature osteoclasts (B) from DOPS donors containing P2X7R SNPS. Baseline values were taken before injecting 300µM BzATP (arrow) in the absence or presence of P2X7R antagonist (1µM KN62). Curves show relative fluorescence due to binding of Fluo-4 with free calcium (i) and area under the curve (ii) was calculated and is shown as percentage change of no stimulus (dotted line). Values are mean ± SD, n = 2 P2X7-WT, 3 P2X7-GOF and 3 P2X7-LOF donors (precursors) and 5 P2X7-WT, 4 P2X7-GOF and 3 P2X7-LOF donors (osteoclasts) containing 8-10 glass coverslips per treatment. * p<0.05, ** p<0.01 significance from P2X7-WT BzATP, † p<0.05, †† p<0.01 from basal (Student's t-test)

6.2.4.2. Pore formation

Due to the 240 amino acid carboxyl terminal extension, sustained stimulation of the P2X7R causes membrane permeation of molecular weight solutes of up to 900 Da (Wiley et al., 1998). This property is widely exploited to determine the functional activity of the receptor in various cells types with the help of DNA intercalating fluorescent dyes such as ethidium bromide and YO-PRO. To determine the effects of SNPs on the pore-forming ability of the monocytic precursors or mature osteoclasts generated from P2X7-WT, P2X7-GOF and P2X7-LOF were assessed for YO-PRO-1 uptake following BzATP stimulation.

Dye uptake in P2X7-GOF precursors was significantly different to non-stimulated precursors (basal) (652%; p=0.0187) and a higher increase by P2X7-WT (11507%, p=0.4139) and P2X7-LOF precursors (2478%, p=0.0653) were also obtained following BzATP stimulation however, the data did not reach statistical significance. Treatment with antagonist failed to significantly reduce YO-PRO uptake by precursors of either genotype (Figure 6-4).

BzATP stimulation caused significant increase in dye uptake in P2X7-WT and P2X7-GOF in mature osteoclasts (716%; p=0002 and 1372%, p=0009 respectively from basal). Moreover, YO-PRO-1 uptake was significantly higher in P2X7-GOF osteoclasts compared to P2X7-WT (p=0.0027). P2X7-LOF osteoclasts also increase in pore formation (904%, p=0.0756) compared to basal but was not significantly different than P2X7-WT osteoclasts (p=0.5110).

YO-PRO-1 uptake was significantly inhibited in the presence of antagonist in P2X7-WT (570%, p=0.0352) but not in P2X7-GOF (1263%, p=0.5078) or P2X7-LOF (784%, p=0.7404) (Figure 6-4).

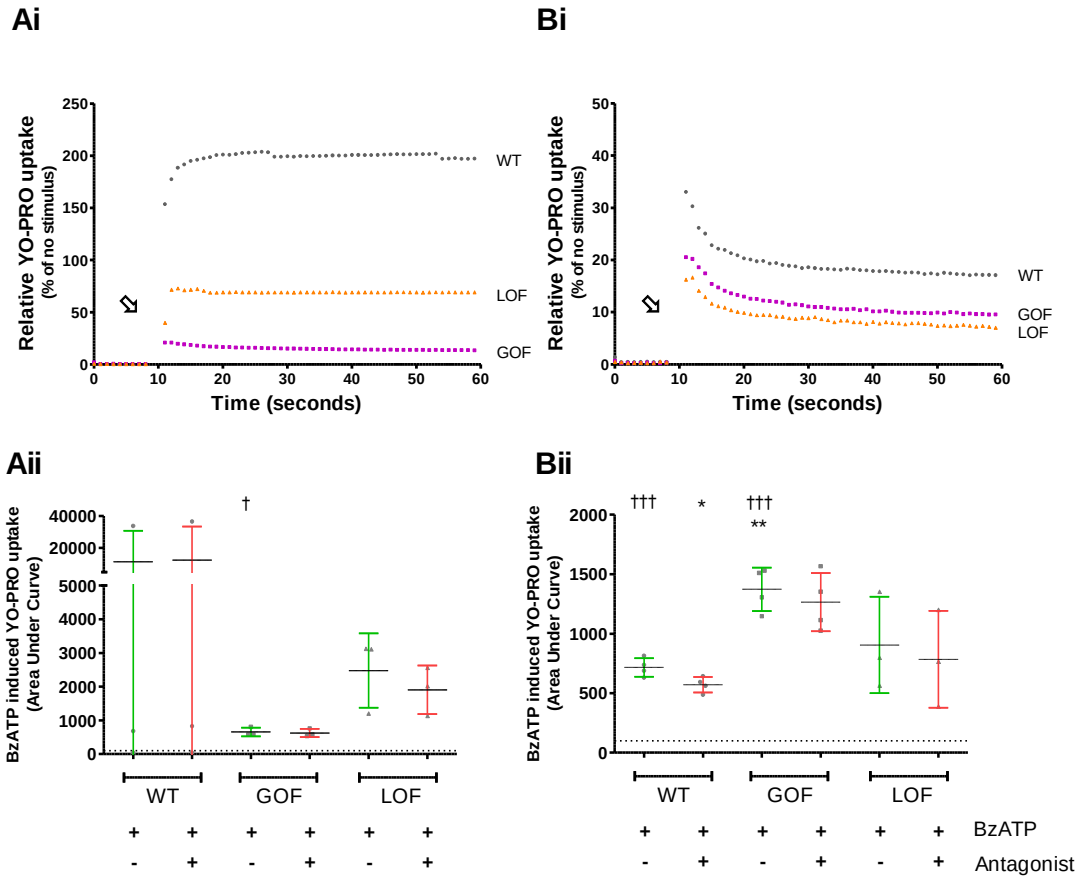

Figure 6-4 Pore formation following BzATP stimulation

CD14 enriched monocyte precursors (A) or mature osteoclasts (B) from DOPS donors containing P2X7R SNPS were assessed for their pore formation ability. Baseline values were taken before injecting 500µM BzATP (arrow) in the absence or presence of P2X7R antagonist (1µM KN62). Curves show relative fluorescence following YO-PRO-1 uptake (i) and area under the curve (ii) was calculated and is shown as percentage change of no stimulus (dotted line). Values are mean ± SD, n = 3 donors each (precursors) and 5 P2X7-WT, 4 P2X7-GOF and 3 P2X7-LOF donors (osteoclasts) containing 8-10 glass coverslips per treatment. * $p<0.05$, ** $p<0.01$ significance from P2X7-WT BzATP, † $p<0.05$, ††† $p<0.001$ from basal (Student's t-test)

6.2.4.3. Cytokine release

Several possible physiological roles have been suggested for the P2X7R. Evidence suggests that activation of P2X7R causes IL-1β maturation and release (Ferrari et al., 1997; Wilson et al., 2007) which is an important mediator during inflammatory response. Other pro-inflammatory cytokines like IL-6, IL-18 and TNF-α can also be produced by P2X7R activation (Lister et al., 2007). Monocytes are the known primary cytokine producing cells but human osteoclasts have also been shown to secrete these cytokines which can be enhanced by LPS stimulus (Li et al., 2010) and high levels of IL-8 (Rothe et al., 1998). To determine the effects of P2X7R stimulation on cytokine prediction by CD14+ enriched monocytes and osteoclasts generated from them *in vitro*, as well as the potential effects of P2X7R SNPs, cytokine release following LPS stimulation (1μg/ml for 2 hours) was measured in cell supernatants. All values are expressed as fold change of no LPS to adjust for the differences in cell numbers between donors.

6.2.4.3.1. Effect on IL-1β release in response to BzATP

No difference in basal IL-1β release was obtained between monocytes of P2X7-WT, P2X7-GOF and P2X7-LOF donors and treatment with BzATP did not significantly alter the basal IL-1β release independent of the P2X7R SNPs. However, osteoclasts generated from P2X7-WT donors showed significant enhancement in the basal IL-1β level following BzATP stimulation (3.7 fold, p=0.0500). This could be successfully reversed by pre-treatment with P2X7R antagonist however, it did not reach statistical significance (3.5 fold, p=0.0539). P2X7-LOF osteoclasts showed a 5.5 fold heightened basal levels of IL-1β release compared to P2X7-WT (2.16 versus 0.39, p=0.0903) however, the data did not reach statistical significance (Figure 6-5).

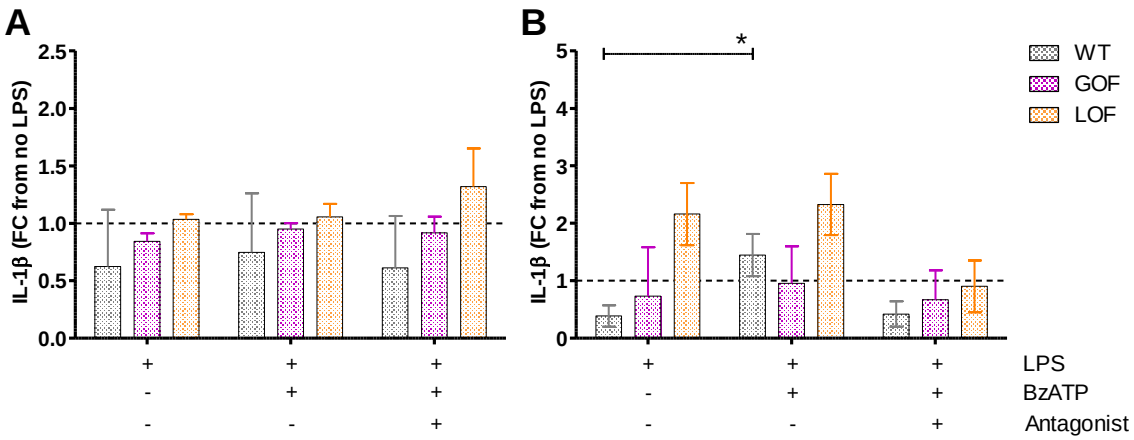

Figure 6-5 IL-1β release from monocytic precursors and osteoclasts

Cell supernatant was collected from CD14+ enriched monocyte precursors (A) or osteoclasts generated *in vitro* (B) from the peripheral blood of DOPS donors. LPS-induced (1µg/ml for 2 hours) IL-1β release in response to 30 minute stimulation by BzATP with or without the antagonist (1µM KN62) in cell supernatant collected from P2X7-WT, P2X7-GOF and P2X7-LOF cells was measured. Results are expressed as fold change of no LPS (no LPS stimulation) and show mean ± SD. n = 3 donors in precursors and 5 P2X7-WT, 4 P2X7-GOF and 3 P2X7-LOF donors for osteoclasts. * $p<0.05$ (Student's t-test)

6.2.4.3.2. Effect on IL-6 release in response to BzATP

Monocytes from P2X7-LOF showed 2.1 fold heightened LPS stimulated IL-6 release compared to P2X7-WT, however this was not statistically significant (p=0.1146). The trend between the genotypes remained the same with the least IL-6 release in P2X7-WT and highest release in P2X7-LOF (P2X7-WT<P2X7-GOF<P2X7-LO) however the data failed to reach statistical significance.

Similar trend in IL-6 release was observed in mature osteoclasts with a 2.3 fold increase by P2X7-LOF compared to P2X7-WT, although data did reach statistical significance (p=0.4520). Levels were not altered in either genotype in the presence of BzATP stimulation or pre-treatment with P2X7R antagonist (Figure 6-6).

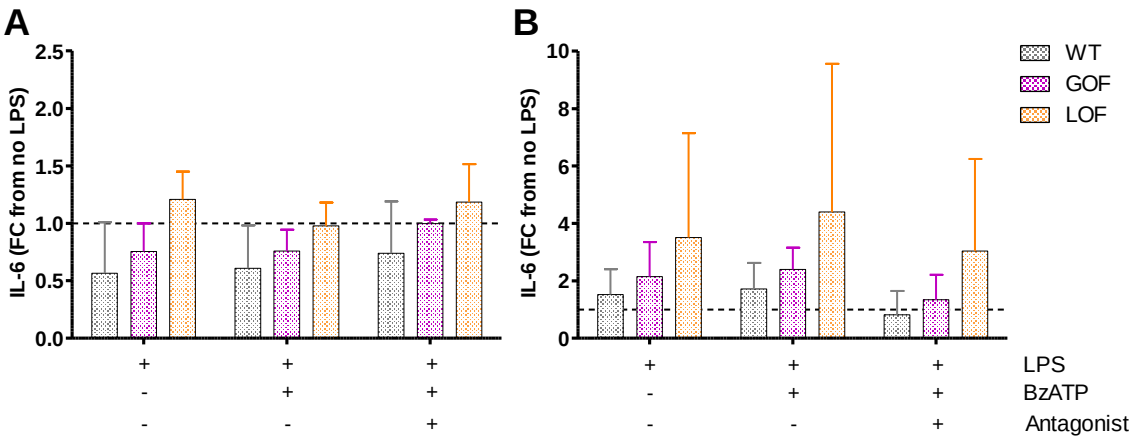

Figure 6-6 IL-6 release in monocytic precursors and osteoclasts

Cell supernatant was collected from CD14+ enriched monocyte precursors (A) or osteoclasts generated *in vitro* (B) from the peripheral blood of DOPS donors. LPS-induced (1µg/ml for 2 hours) IL-6 release in response to 30 minute stimulation by BzATP with or without the antagonist (1µM KN62) in cell supernatant collected from P2X7-WT, P2X7-GOF and P2X7-LOF cells was measured. Results are expressed as fold change of no LPS (no LPS stimulation) and show mean ± SD. n = 3 donors in precursors and 5 P2X7-WT, 4 P2X7-GOF and 3 P2X7-LOF donors for osteoclasts.

6.2.4.3.3. Effect on IL-10 release in response to BzATP

Incubation with LPS did not alter IL-10 release by monocytes with P2X7R SNPs compared to WT monocytes. However, BzATP stimulation in the presence of LPS resulted in significantly higher IL-10 release by monocytes with P2X7-GOF (2.03 fold, p=0.0374) and P2X7-LOF (1.97 fold, p=0.0403) compared to P2X7-WT. Monocytes pre-treated with KN62 did not show the BzATP mediated heightened IL-10 release with P2X7-GOF and P2X7-LOF SNPs.

Mature osteoclasts from P2X7-LOF showed a 2 fold enhanced basal IL-10 release compared to P2X7-WT (p=0.3958) however this was not statistically significant. IL-10 in P2X7-WT was prevented by a significant 5 fold with KN62 incubation (p=0.0119) and 4 fold in P2X7-LOF osteoclasts (p=0.2544) however the data failed to achieve significance. No effect of BzATP stimulation or KN62 incubation was observed IL-10 release by P2X7-GOF osteoclasts (Figure 6-7).

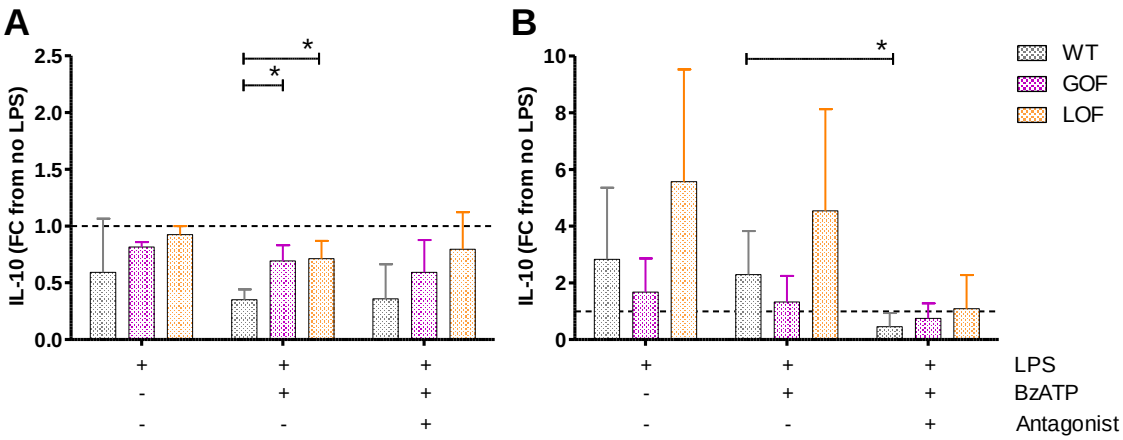

Figure 6-7 IL-10 release in monocytic precursors and osteoclasts

Cell supernatant was collected from CD14+ enriched monocyte precursors (A) or osteoclasts generated *in vitro* (B) from the peripheral blood of DOPS donors. LPS-induced (1µg/ml for 2 hours) IL-10 release in response to 30 minute stimulation by BzATP with or without the antagonist (1µM KN62) in cell supernatant collected from P2X7-WT, P2X7-GOF and P2X7-LOF cells was measured. Results are expressed as fold change of no LPS (no LPS stimulation) and show mean ± SD. n = 3 donors in precursors and 5 P2X7-WT, 4 P2X7-GOF and 3 P2X7-LOF donors for osteoclasts * $p<0.05$ (Student's t-test)

6.2.4.3.4. Effect on TNF release in response to BzATP

Monocytes showed a reduction in TNF levels after P2X7R activation using BzATP. P2X7-WT cells showed a 2.7 fold decrease in TNF release ($p=0.0985$) however this failed to reach statistical significance. Moreover, P2X7-LOF monocytes showed a significant 3.2 fold reduction in TNF release ($p=0.0073$) following BzATP stimulation. BzATP stimulus did not impair TNF release in P2X7-GOF monocytes and presence of P2X7R antagonist prevented a BzATP mediated modulation of TNF release in P2X7-GOF monocytes.

Osteoclasts from P2X7-LOF released 5.7 fold higher basal TNF in comparison to a 1.06 fold release by P2X7-GOF osteoclasts compared to the P2X7-WT cells. BzATP stimulation did not alter the TNF release by osteoclasts from either genotype but incubation with KN62 abrogated TNF release by P2X7-LOF osteoclasts however this failed to reach statistical significance ($p=0.0626$) (Figure 6-8).

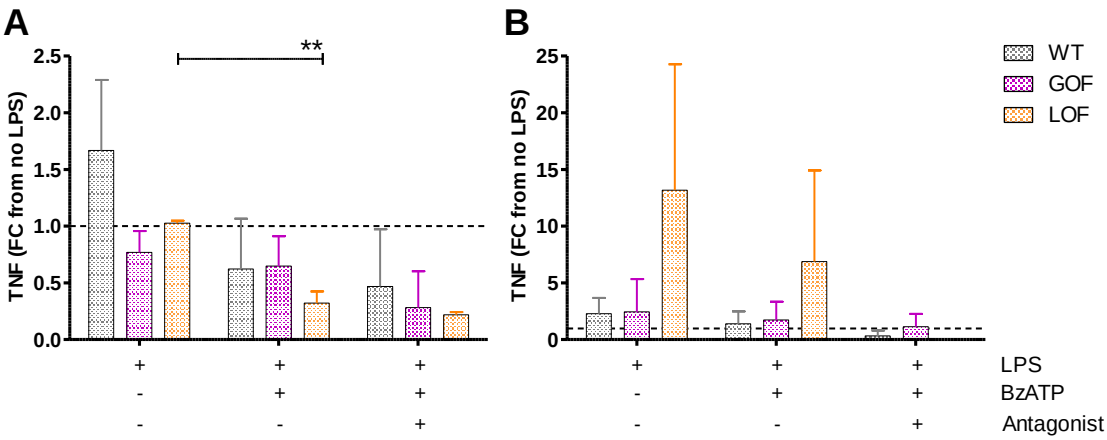

Figure 6-8 TNF release in monocytic precursors and osteoclasts

Cell supernatant was collected from CD14+ enriched monocyte precursors (A) or osteoclasts generated *in vitro* (B) from the peripheral blood of DOPS donors. LPS-induced (1µg/ml for 2 hours) TNF release in response to 30 minute stimulation by BzATP with or without the antagonist (1µM KN62) in cell supernatant collected from P2X7-WT, P2X7-GOF and P2X7-LOF cells was measured. Results are expressed as fold change of no LPS (no LPS stimulation) and show mean ± SD. n = 3 donors in precursors and 5 P2X7-WT, 4 P2X7-GOF and 3 P2X7-LOF donors for osteoclasts ** $p<0.01$ (Student's t-test)

6.2.4.3.5. Effect on IL-8 release in response to BzATP

Monocytes did not show significant changes in LPS mediated IL-8 release in the presence of P2X7R SNPs. BzATP stimulation or pre-treatment with KN62 failed to alter the basal IL-8 levels independent of the SNPs.

Similarly, basal IL-8 levels were not different between osteoclasts in either genotype and remained unchanged following BzATP stimulation in P2X7-WT cells. Osteoclasts showed a non-statistical reduction in IL-8 levels when they were obtained from P2X7-GOF (2.12 fold, p=0.1948) and P2X7-LOF (2.04 fold, p=0.2082) compared to the levels in P2X7-WT cells following P2X7R activation. Incubation with KN62 prevented BzATP mediated IL-8 release by 6.4 fold (p=0.0636) and 2.28 fold in P2X7-GOF (p= 0.0780) but not in P2X7-LOF osteoclasts, although the data did not reach statistical significance (Figure 6-9).

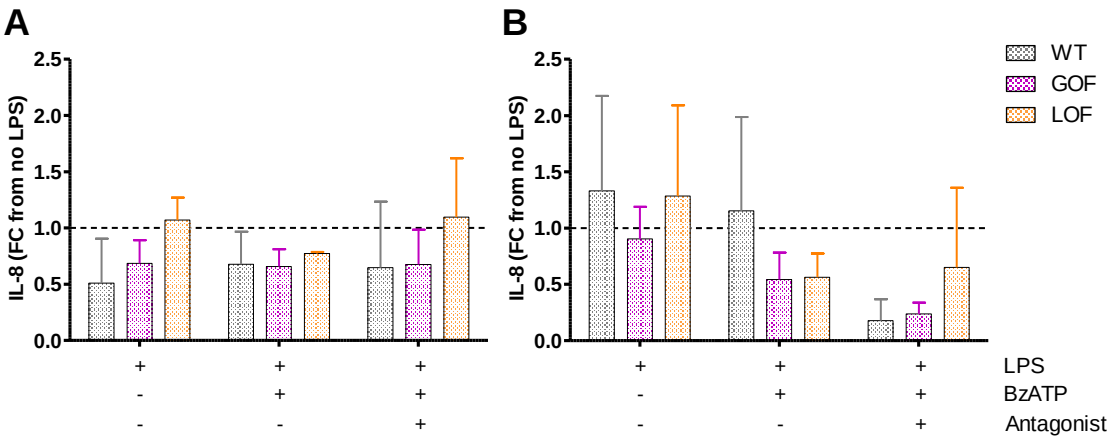

Figure 6-9 IL-8 release in monocytic precursors and osteoclasts

Cell supernatant was collected from CD14+ enriched monocyte precursors (A) or osteoclasts generated *in vitro* (B) from the peripheral blood of DOPS donors. LPS-induced (1µg/ml for 2 hours) IL-8 release in response to 30 minute stimulation by BzATP with or without the antagonist (1µM KN62) in cell supernatant collected from P2X7-WT, P2X7-GOF and P2X7-LOF cells was measured. Results are expressed as fold change of no LPS (no LPS stimulation) and show mean ± SD. n = 3 donors in precursors and 5 P2X7-WT, 4 P2X7-GOF and 3 P2X7-LOF donors for osteoclasts

6.2.5. Effect of SNPs on osteoclastogenesis

6.2.5.1. Number and area of osteoclasts

To determine the effect of P2X7R SNPs on osteoclast formation, precursors from P2X7-WT, P2X7-GOF and P2X7-LOF donors were cultured in the presence of M-CSF and RANKL for 14 days on glass coverslips. Osteoclasts were fixed using 10% formalin at day 14 when the majority of the cells were multinucleated and mature. Cells were TRAP stained and analysed to determine total numbers and area of TRAP+ve multinucleated osteoclasts.

The number of TRAP+ve cells was significantly high in P2X7-GOF cultures compared to P2X7-WT (128 versus 70 respectively, p=0.0363). Osteoclast numbers in P2X7-LOF cultures were higher than those in P2X7-GOF, however results failed to achieve statistical significance (163 osteoclasts in P2X7-LOF, p=0.0739) (Figure 6-10 A).

The size of the multinucleated, TRAP+ve cells from each donor was analysed and osteoclasts from both P2X7-GOF and P2X7-LOF cultures were significantly bigger compared to P2X7-WT cultures (7172 μm^2 in P2X7-GOF, p=<0.0001 and 6915 μm^2 in P2X7-LOF, p= 0.0067 versus 4975 μm^2 in P2X7-WT) (Figure 6-10 B).

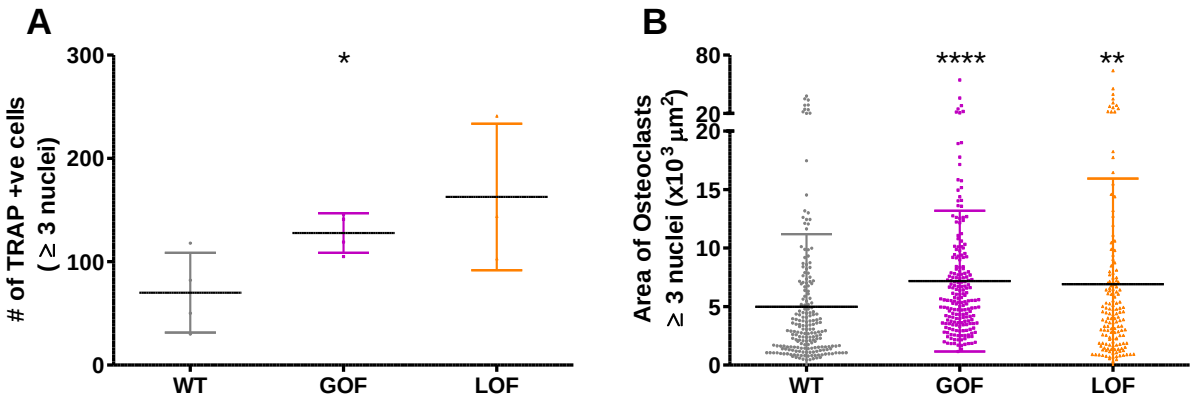

Figure 6-10 Effect of P2X7R SNPs on number and area of TRAP+ve osteoclasts

Osteoclasts generated from DOPS donors were TRAP stained and analysed to obtain total numbers (A) and area of multinucleated, TRAP+ve cells from each donor (B). Values are mean ± SD *p<0.05, **p<0.001, ****p<0.0001 significance from P2X7-WT. n = 4 P2X7-WT, 4 P2X7-GOF and 3 P2X7-LOF donors (Student's t-test)

6.2.5.2. Resorption by osteoclasts

The hallmark of a bona fide osteoclast is its ability to resorb calcified substrates. Precursors from P2X7-WT, P2X7-GOF and P2X7-LOF donors were cultured in the presence of M-CSF and RANKL for 21 days on dentine discs and osteoclasts were fixed using 10% formalin. Discs were analysed to determine osteoclast numbers and resorption pits excavated on dentine discs.

Resorption was obtained in 2 P2X7-WT cultures (DOPS ID 1973, 30% and 1252, 15%) and 1 P2X7-GOF culture (DOPS ID 1879, 10%). Dentine discs in other cultures showed TRAP+ve cells but did not show any resorption pits.

6.2.5.3. Calcium release by osteoclasts

Precise regulation of calcium concentration, both extracellular $[Ca^{2+}]_e$ and intracellular $[Ca^{2+}]_i$, is imperative for osteoclastic resorption. High $[Ca^{2+}]_e$ induces osteoclastic apoptosis thereby inhibiting resorption (Mentaverri et al., 2006). To determine whether osteoclast activity was affected due to P2X7R SNPs, the levels of calcium in the osteoclast environment were measured in culture media obtained from osteoclasts growing on dentine.

Results showed that osteoclasts generated from P2X7-GOF donors showed significantly higher $[Ca^{2+}]_e$ compared to P2X7-WT cells (0.6378 mmol/L versus 0.5280 mmol/L, p=0.0294). Moreover, osteoclasts from P2X7-LOF donors showed reduction in $[Ca^{2+}]_e$ but it did not reach statistical significance in comparison to P2X7-WT (0.4657 mmol/L, p=0.0785) (Figure 6-11).

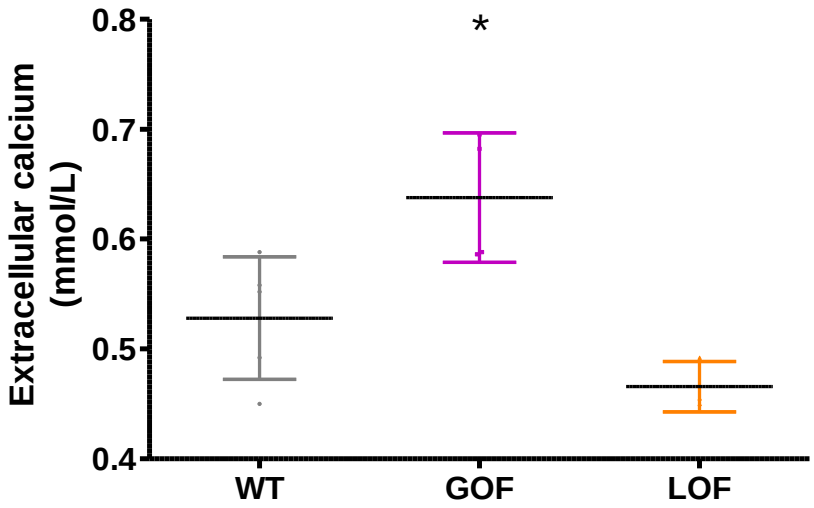

Figure 6-11 Extracellular calcium concentration in osteoclasts with P2X7R SNPs

Osteoclasts generated from DOPS donors were cultured till 21 days on dentine discs and cell supernatant was collected to measure $[Ca^{2+}]_e$. Values are mean ± SD *p<0.05, significance from P2X7-WT. n = 5 P2X7-WT, 4 P2X7-GOF and 3 P2X7-LOF donors (Student's t-test).

6.3. Discussion

Non synonymous SNPs in the human *P2RX7* gene have been associated with an increased risk of several human disorders. LOF SNP, p.Arg307Gln, contributes to an accelerated bone loss in post menopausal women whereas both men and women with GOF SNPs, p.Ala348Thr and pGln460Arg are associated with a reduced fracture risk and increased bone strength (Jorgensen et al., 2012; Wesselius et al., 2013). This chapter looked at whether P2X7R expression and function was altered on osteoclastic precursors and mature osteoclasts from donors with P2X7R GOF or LOF SNPs. Moreover, it was determined whether the changed function in P2X7R could potentially impair osteoclast formation *in vitro*. The main finding of the chapter is that SNP causing a reduced channel function in the receptor may cause a loss of P2X7R mediated 'danger signals' and promote the development of inflammatory response. Differences in the response to BzATP induced receptor function and physiological effects were obtained between monocytic precursors and mature osteoclasts with SNPs. However, SNPs have been reported previously to alter receptor function with cell differentiation causing an eventual alteration in receptor mediated response (Gu et al., 2004b).

6.3.1. P2X7-LOF osteoclasts show reduced surface reactivity to P2X7R antibody

A monoclonal antibody raised against the external domain of the P2X7R was utilised to determine the P2X7R protein expression on osteoclasts (Buell et al., 1998). As shown by immunofluorescence, the anti-human P2X7mAb (clone L4) showed strong surface reactivity to the osteoclasts generated from P2X7-WT donors. Osteoclasts from P2X7-GOF donors also showed robust P2X7R expression, in comparison, osteoclasts with P2X7-LOF showed decreased binding to the antibody. The latter is consistent with existing evidence in the literature where reduced antibody binding in lymphocytes from Arg307Gln heterozygotes was shown (Gu et al., 2004b). Considering the Arg307Gln SNP affects one of the amino acids essential for ATP binding,

an abolished function of P2X7R due to loss of ATP binding residue was confirmed in the osteoclasts. Interestingly, permeabilisation of osteoclasts with P2X7-LOF leads to a stronger binding of the mAb. This was surprising as the antibody is raised to recognise an epitope in the extracellular loop of P2X7R. However, hematopoietic cells retain large amounts of intracellular P2X7R protein and are capable of reacting to the P2X7mAb once receptor access is allowed (Gu et al., 2000). The authors speculate that the cells have intracellular pool of the receptor capable of being recruited to the surface following cellular activation. Considering a similar pool of P2X7R protein in osteoclasts with Arg307Gln, it would be interesting to measure the extent to which the SNP affects the ability of osteoclasts to recruit P2X7R protein from the intracellular reserves following agonist stimulation.

6.3.2. Enhanced receptor function in GOF and reduced function in LOF precursors and osteoclasts

Each of these polymorphisms, His155Tyr, Ala348Thr and Gln460Arg have been demonstrated to impart a high receptor function when present either in isolation or as a part of an inherited haplotype (Cabrini et al., 2005; Roger et al., 2009; Stokes et al., 2010; Sun et al., 2009). It is speculated that a combination of residue changes would have more profound effects on channel activation compared to single changes. In line with the current literature, both ion channel function and pore formation was enhanced in monocytic precursors and osteoclasts homozygous for the polymorphisms compared to the WT P2X7R. Pre-treatment with KN62 caused significant reduction in receptor function by wildtype osteoclasts. KN62 slightly blocked the channel function in GOF osteoclasts but did not prevent BzATP stimulated dye uptake. It is possible that GOF polymorphisms caused a change in KN62 reactivity whereby it was less effective on the pore form of the receptor. Similar selective activity has been demonstrated previously where KN62 antagonism was differential towards channel and pore forms of P2X7R (Chessell et al., 1998). Similar loss of KN62 activity was observed on P2X7-LOF cells suggesting presumably caused due to a change in the binding site of the receptor due to Arg307Gln polymorphism. Interestingly,

stimulation with BzATP caused both calcium influx and dye uptake in P2X7-LOF cells. However, the channel function was not as efficient as in P2X7-WT cells as measure by the fluorescence curves. This is in line with previous findings which have reported that agonist stimulation causes reduced dye uptake and cell apoptosis in macrophages and lymphocytes heterozygous for the polymorphism (Fernando et al., 2005; Gu et al., 2001). Given that the residue change (Arg307Gln) alters the ATP-binding motif in the extracellular domain of P2X7R (Gu et al., 2004b), a complete abolishment in P2X7R function in cells homozygous for the residue change. None of the 3 P2X7-LOF donors were homozygous for Arg307Gln SNP and contained various combinations of gain of function SNPs. While one donor was heterozygous at GOF Ala348Thr, the second donor contained GOF His155Tyr in addition to change at Ala348Thr. The third donor was homozygous at His270Arg position and although the functional role of this polymorphism is understudied, Stokes et al., showed increased ATP-induced ethidium uptake in cells transfected with His270 to 270Arg mutation compared to wild-type P2X7R expressing cells (Stokes et al., 2010). The authors also showed that residue change has a slight additive effect to an existing GOF in the haplotype. These findings suggest that residue change, His270Arg, could cause alteration in P2X7R function and potentially contribute to a BzATP mediated receptor function in P2X7-LOF donors. More studies are needed to assess the effect of Arg307Gln SNP on P2X7R function in cells of osteoclast lineage.

6.3.3. IL-1β release in precursors is not augmented following P2X7R activation but LOF osteoclasts show enhanced basal IL-1β release

ATP (and other nucleotides) which is normally contained within the cytosol are believed to act as ‘danger’ signals following their release in the extracellular milieu. These molecules upregulate the expression of inflammatory cytokines such as Interleukins and TNF-α and growing amount of data shows that P2X7R activation has an impact on immune cell functions (la Sala et al., 2003).

The mechanism of IL-1β production and maturation is a multi- step process where its release requires consecutive stimuli (Lister et al., 2007). Despite an induction of pro-IL-1β synthesis by bacterial LPS, it has been demonstrated that P2X7R activation is needed to mediate its maturation and release (Chin and Kostura, 1993; Ferrari et al., 1997; Sanz and Di Virgilio, 2000). Extracellular ATP caused shedding of microvesicles from monocytes containing mature IL-1β, a process mediated via P2X7R activation (MacKenzie et al., 2001). The involvement of P2X7R was confirmed when IL-1β secretion was absent in P2X7R knockout mice despite LPS priming and ATP stimulus (Labasi et al., 2002; Solle et al., 2001).

Contradictory to the literature, CD14+ monocytes from P2X7-WT DOPS donors did not show enhanced IL-1β release following BzATP stimulation. Additionally, IL-1β release could not be blocked by P2X7R antagonist. There are several possible explanations for this. Firstly, the absence of P2X7R mediated IL-1β release could be attributed to shorter LPS-priming in the experiments compared to other studies (Elssner et al., 2004; Grahames et al., 1999). Insufficient inflammatory response will cause an inadequate accumulation of pro-IL-1β which might fail to release active IL-1β in a P2X7R dependent manner. Another explanation could be a P2X7R independent mechanism of IL-1β release in monocytes as suggested by Grahames et al., when human monocytes showed no effect of P2X7R blockade on LPS-induced IL-1β release (Grahames et al., 1999). Loss of cytosolic K+ causes caspase-1 activation, which catalyses the reaction that converts pro-IL-1β to its mature form, and P2X7R is widely accepted to cause this activation (Ferrari et al., 2006; Perregaux and Gabel, 1994). Evidence for existence of receptor independent IL-1β release was provided by Ward et al., when P2X7R antagonist did not alter LPS-induced cytokine release (Ward et al., 2010). The authors demonstrated that prolonged LPS stimulus caused sufficient IL-1β release independent of P2X7R involvement but was dependent on the activity of caspase-1, inhibition of which caused an accumulation of unprocessed IL-1β.

Interestingly, mature osteoclasts from P2X7-WT donors showed an enhanced IL-1β release following BzATP stimulation. Despite a heightened

basal IL-1β by P2X7-LOF compared to P2X7-WT osteoclasts, P2X7R activation failed to augment IL-1β release in P2X7-LOF. It is possible that Arg307Gln heterozygosity caused a delayed P2X7R activation as a second LOF SNP (Glu496Ala) has been shown to be less sensitive to P2X7R mediated IL-1β release (Gu et al., 2004a).

Surprisingly, P2X7-GOF osteoclasts also failed to show P2X7R dependent LPS mediated IL-1β release. One explanation is that GOF polymorphisms that alter receptor function impairs inflammasome assembly, a cytosolic complex of proteins, needed for caspase-1 activation (Mariathasan et al., 2006; Piccini et al., 2008). These studies showed that autocrine stimulus of P2X7R is needed to activate inflammasome and caspase-1 maturation and potentially, a SNP causing an altered function could affect the cascade of events leading to inflammasome activation and subsequesnt Il-1β secretion.

6.3.4. LOF SNPs causes higher IL-6, IL-10 and TNF release by osteoclasts

Role of P2X7R in IL-6 production has been explained in inflammatory disorders such as RA. Activation of P2X7R in cells treated with bacterial endotoxin or in RA-associated cells has been linked to enhanced IL-6 secretion (Caporali et al., 2008; Solini et al., 1999) suggesting a P2X7R dependent mechanism of IL-6 release. However, neither the monocytes nor osteoclasts generated from DOPS donors showed a P2X7R activation dependent IL-6 release. Whether this is due to insufficient stimuli needs to be explored by investigating IL-6 levels at different time points. However cells with LOF, Arg307Gln appeared to generate higher LPS-induced IL-6 compared to cells with GOF or WT alleles. This suggests a heightened inflammatory response in the presence of the LOF SNP. Mouse knockout have reduced IL-6 production due to an impairment in IL-1β release (Solle et al., 2001) but whether these are species specific differences in cytokine signalling cascade need to be determined. Since IL-6 in concert with other cytokines, stimulates osteoclastogenesis and promotes bone resorption, enhanced levels of the cytokine could affect bone homeostasis and cause reduce bone strength. Interestingly, post-menopausal women with Arg307Gln

LOF SNP have increased bone loss and increased risk of fracture (Gartland et al., 2012b; Jorgensen et al., 2012; Wesselius et al., 2013), which could be an inflammation induced response. Further research to determine the effects of P2X7R SNPs on ATP induced IL-6 release is therefore needed to understand the patho-physiology of osteoporosis and potentially even inflammation associated bone loss.

IL-10 has a potent inhibitory effect on osteoclastogenesis and is also secreted by osteoclasts following LPS stimulus (Li et al., 2010). SNPs causing a reduced pore activity to P2X7R were shown to release significantly higher amounts of IL-10 compared to high pore controls in human blood samples (Denlinger et al., 2005). In this chapter, P2X7R activation appears to cause a reduction in IL-10 levels from wild type monocytes but sustained high levels in cells with altered P2X7R function. Additionally, basal levels were elevated in osteoclasts with LOF SNP which was not augmented further following BzATP stimulation. Moreover, IL-10 release could be prevented by antagonist addition in WT osteoclasts suggesting a P2X7R signalling mechanism of osteoclastic IL-10 release. Interestingly, P2X7R KO mice show delayed IL-10 production via p38 activation (Miller et al., 2011b) confirming a P2X7R mediated function of IL-10 release. IL-10 inhibits RANKL induced NFATc1 activation in osteoclasts (Evans and Fox, 2007) and therefore understanding the role of P2X7R would help target bone loss associated with receptor polymorphisms.

Addition of extracellular ATP inhibits TNF secretion by whole blood cells, a response independent of a P2X7R SNP (Swennen et al., 2005; Wesselius et al., 2012). A similar reduction in TNF release was seen in both monocytes and osteoclasts however, osteoclasts with LOF SNP showed enhanced TNF release in comparison to WT and GOF SNP. Considering that TNF is a potent osteoclastic stimulus and drives inflammation, accumulation of the cytokine in the cellular microenvironment might aggravate bone resorption and aid the development of osteoporotic phenotype.

6.3.5. LOF SNP in P2X7R may prevent IL-8 down regulation by osteoclasts

Human osteoclasts have also been shown to secrete high levels of IL-8 and its release can be stimulated by pro inflammatory signals such as LPS, IL-1β, Il-6 and TNF (Rothe et al., 1998). Given the enhanced release of the latter cytokines by the osteoclasts with LOF Arg307Gln, it was determined whether the IL-8 concentration was also altered in the presence of the polymorphism. LPS stimulated IL-8 production was not augmented by BzATP stimulus in WT osteoclasts; however, pre-treatment with KN62 caused impaired cytokine release despite the presence of LPS. KN62 is a highly potent P2X7R non-competitive antagonist (Chessell et al., 1998) but is also a specific inhibitor of Ca^{2+}/Calmodulin protein kinase II (CAMKII) (Tokumitsu et al., 1990). CAMKII inhibition is being investigated as a therapy for RA and the authors recently showed an inhibition of LPS stimulated IL-8 release in the presence of another inhibitor belonging to the same family as KN-62 (Westra et al., 2009; Westra et al., 2010). The concentration of KN62 used in the experiments could have affected the enzyme activity since the half maximal value for enzyme inhibition is approximately 1 μM (Wenham et al., 1992), and is a possible cause of IL-8 down regulation. Interestingly, cytokine release was halved in cells with altered function of P2X7R and osteoclasts with LOF Arg307Gln maintained the IL-8 levels despite the presence of KN-62. These findings suggest a receptor mediated release of IL-8 in the presence of LPS and that LOF SNP may have reduced the sensitivity to P2X7R blockade thereby maintaining higher levels of IL-8. This is of particular interest as elevation in IL-8 levels have been associated with not only inflammatory diseases such as RA, but also to increased osteolysis in bone metastasis and increased failure of osteo-integration of hip implants (Bendre et al., 2003; Lassus et al., 2000). All of which are caused due to an increased bone resorptive activity which is similar to the acceleration of post-menopausal bone loss with LOF Arg307Gln (Gartland et al., 2012b). These findings could help us move one step forward in determining the complex process of how P2X7R polymorphisms could affect skeletal homeostasis, and related conditions.

6.3.6. Osteoclasts are larger due to altered P2X7R function but may be less active with GOF SNP

More osteoclasts were obtained from both P2X7-GOF and P2X7-LOF donors and were also significantly bigger in size compared to P2X7-WT donors. Increased size and number of osteoclasts is a hallmark in conditions with higher osteoclast activity such as Paget's disease (Roodman and Windle, 2005). These findings suggest a higher resorptive activity in osteoclasts with P2X7R SNPs compared to those with WT receptor. Interestingly, osteoclasts with higher function P2X7R showed enhanced extracellular calcium $[Ca^{2+}]_e$. A higher P2X7R channel function due to GOF SNPs was expected to cause a rise $[Ca^{2+}]_i$, thereby reducing the free calcium in the medium. Therefore, an increase $[Ca^{2+}]_e$ was counter intuitive and is a likely result of excessive Ca^{2+} efflux via either transcytosis (Yamaki et al., 2005) or calcium ionophores to maintain balanced cytosolic levels. While $[Ca^{2+}]_i$ causes membrane depolarization and could potentially influence the formation of ruffled border and actin cytoskeleton (Kajiya, 2012; Miyazaki et al., 2012; Reyes et al., 2011), high $[Ca^{2+}]_e$ can induce apoptosis speculated via promotion of NF-κB mediated programmed cell death in mature osteoclasts (Mentaverri et al., 2006). $[Ca^{2+}]_e$ also induces $[Ca^{2+}]_i$ increase (Malgaroli et al., 1989) and therefore the overall result is inhibition of osteoclastic activity presumably in an autocrine manner. Moreover, lower $[Ca^{2+}]_e$ were measured in osteoclasts with LOF SNP which will necessitate the need for increased osteoclastic resorption to maintain calcium homeostasis.

6.4. Conclusion

These studies suggest that genetic variation in the human P2RX7 gene could affect the P2X7R mediated signalling in human osteoclasts. Although underpowered, the data suggests important roles of P2X7R SNPs in mediating receptor function and physiological roles. Accelerated bone loss in women with LOF Arg307Gln polymorphism could be due to a combined loss of receptor mediated cytotoxicity affecting the release of inflammatory cytokines and an enhanced osteoclastic activity. Reduced fracture risk in individuals with GOF Ala348Thr and pGln460Arg could be in part due to an accumulation of $[Ca^{2+}]_e$ causing an inhibition of osteoclastic resorption.

Chapter 7. Discussion

Release of extracellular ATP has been extensively studied to mediate NANC signal transmission via the abundant subtypes of cell surface purinoceptors. Each purinoceptor family has a cell specific response and there is growing body of data to indicate their role in the patho-physiology of various diseases. Purinoceptors can respond directly to extracellular ATP and other nucleotides and initiate signalling cascades or could involve protein interactions with other regulatory agents to achieve a threshold neither one of the stimulus could cause in isolation (North, 2002; Surprenant and North, 2009). Post menopausal osteoporosis is caused due to a loss of oestrogen and is associated with a high mortality rate. Compared to the rapid increase in life expectancy due to advanced in public health measures, the treatment options for osteoporosis have been slow with only a few anabolic agents (such as PTH, vitamin D) and antiresorptive therapies (such as bisphosphonates, calcitonin). These treatments have been associated with complications and in recent years, signalling via the P2X7R has been identified in the pathophysiology of normal and inflammation induced bone remodelling (Baroja-Mazo and Pelegrin, 2012).

Until now, findings from mice models assessing the role of P2X7R in the development of bone phenotype have been compromised due to the structural variation in the murine receptor protein (Masin et al., 2012; Nicke et al., 2009). In 0, the effect of osteoclast development was assessed using the P2X7R knockout mice generated on BALB/c background. This novel knockout model does not harbour the natural mutation, P451L (Adriouch et al., 2002) and although a restricted variant, P2X7(k), was detected in BM aspirate and spleen buffy layer, it was not detected in mature osteoclasts generated *in vitro*. This is consistent with another study where loss of P2X7(k) variant was described with *in vitro* differentiation of macrophages (Boumechache et al., 2009). Both macrophages and osteoclasts are multinuclear and although the P2X7R function is imperative for the fusion of these cells, it appears to be dispensable in the multinuclear cells. Further studies are needed to identify the stage at which the P2X7(k) variant was lost and its role in mediating cell fusion. It would be interesting to identify whether loss of P2X7(k) and the C-truncated isoforms (13b and 13c) affect the fusion

ability of multinuclear cells and determine the part of receptor imperative to the process. *In vivo*, receptor deletion caused a significant enhancement in the number of osteoclasts and this increase is a likely consequence of a prolonged osteoclast survival following a loss of P2X7R mediated apoptotic signal (Gartland et al., 2003b). Since the function of P2X7R negative osteoclasts could not be assessed by histology, resorption was assessed using an *in vitro* model. In the absence of P2X7R, osteoclasts showed a reduced bone resorbing ability, with two probable explanations. Firstly, the presence of highly sensitive P2X7(k) variant may have caused P2X7R mediated apoptosis, selecting for cells with a reduced receptor function. Subsequently, this loss of P2X7R channel activity may restrict ATP release and limit osteoclast fusion (Pellegatti et al., 2011) generating smaller sized osteoclasts with a reduced bone resorbing ability. A second reason could be that P2X7R deletion may have caused an intrinsic defect in the osteoclast precursors, and genetic analysis showed that the bone marrow microenvironment was altered and may have been less efficient in driving the precursors into functional osteoclasts. This is in line with the reduced bone resorption marker with an increased BMD and bone strength in these BALB/c P2X7R-/- mice (Syberg et al., 2012a). In conclusion, loss of P2X7R activity reduces osteoclast function *in vitro* and potentially regulates bone resorption *in vivo*.

A P2X7R antagonist was explored as a potential therapeutic target, in the development of bone phenotype associated with loss of oestrogen in Chapter 4. Surprisingly, P2X7R blockage did not rescue the bone loss as predicted by findings in 0, and instead a continual development to an osteoporotic phenotype was observed. Although contrary to the effect of loss of P2X7R function on osteoclastic resorption *in vitro*, these were interesting findings as they suggest a role of oestrogen mediated P2X7R response in bone resorption. The major physiological effect of oestrogen is inhibition of formation, activity and survival of osteoclasts (Manolagas, 2000; Manolagas et al., 2002; Nakamura et al., 2007; Piva et al., 2005). Loss of oestrogen directly mediates osteoclast activity or indirectly by production osteoclastogenic factors such as (IL-1, IL-6, TNF-α, M-CSF, and RANKL)

(Table 1-7). It would be interesting to investigate the serum cytokine levels in the mice and assess whether treatment with CPH1 altered any of the oestrogen mediated pro-osteoclastic responses by altering P2X7R mediated cytokine release (Hughes et al., 2007). Current findings are based solely on bone micro-architecture analysis using μCT and detailed information by histomorphometry, both static to determine bone cell numbers *in vivo* and dynamic to ascertain bone remodelling at the level of individual events are needed. Serum samples from mice (to quantify circulating bone turnover markers i.e. P1NP and ALP for bone formation and CTX and TRAcP 5 for bone resorption) would provide valuable information regarding bone remodelling rates following CPH1 treatment. Additionally, bone strength measurements are missing from the current study as change in bone geometry to rod like trabeculae are associated with increased accumulation of micro-damage and reduced energy to failure.

To investigate the regulation of P2X7R by oestrogen loss, osteoclasts were derived in their combined absence *in vitro* (Chapter 5). Interestingly, loss of oestrogen caused more aggressive bone resorption in the absence of P2X7R compared to when the receptor was present. These results are in line with an associated fracture risk due to a reduced P2X7R function in women cohorts (Gartland et al., 2012b; Jorgensen et al., 2012; Wesselius et al., 2013) . Moreover, women with SNP associated with loss of plasma membrane trafficking of P2X7R do not respond to hormone replacement therapy (Ohlendorff et al., 2007b) further strengthening the case for a P2X7R dependent modulation of oestrogen on bone loss.

Findings from this study indicate an interplay of oestrogen and purinoceptors, specifically, oestrogen depletion in the absence of P2X7R aggravated resorption *in vitro*. Presence of oestrogen has been shown to obliterate calcium influx and rise of $[Ca^{2+}]_i$ (Gorodeski, 2004) and rescue epithelial cells apoptosis (Gorodeski, 2004; Wang et al., 2004a; Wang et al., 2004b) suggestive of an oestrogen withdrawal induction in rise of $[Ca^{2+}]_i$. Oestrogen loss would induce the activation of $[Ca^{2+}]_i$ dependent transcription factors and therefore a potential mechanism behind the increased osteoporotic bone loss. Curiously, loss of P2X7R exacerbated the resorption following

oestrogen loss possibly due to an additive anti-apoptotic effect on the osteoclasts. It will be interesting to investigate the osteoclastogenic events downstream of P2X7R activation, particularly those associated with rise of $[Ca^{2+}]_{i,}$ such as NF-kb and NFATc1 (Adinolfi et al., 2009; Korcok et al., 2004) in isolation and under the regulation of oestrogen.

In Chapter 6, the direct effect of altered P2X7R function was assessed on osteoclastogenesis. Osteoclasts heterozygous for LOF SNP Arg307Gln showed reduced P2X7R surface expression and reduced calcium influx and pore formation. However, cells were still responsive to agonist mediated receptor activation possibly partly due to their heterozygous allelic change or presence of other non synonymous SNPs in their *P2RX7* gene. Enhanced pro- osteoclastogenic cytokine release was also measured by cells with LOF SNPs, suggestive of a dysregulation in cytokine cascade. In addition, the regulation of osteoclast activity due to P2X7R mediated $[Ca^{2+}]_i$ is possible. These findings address a potential physiology behind accelerated bone loss associated with functional changes in P2X7R. However, given the potential interaction between oestrogen and P2X7R mediated signalling, it is possible that the precursors were 'primed' due to oestrogen loss and these findings could be influenced by the post-menopausal condition of the DOPS women. Further studies are needed to address the role of each of the non-synonymous SNPs in osteoclast bone resorption. Assessing osteoclastogenesis and resorption in normal and oestrogen depleted conditions with precursors isolated from healthy men and women will help confirm these findings. These results will identify the cellular component of the associated bone phenotype and help ascertain whether screening for P2X7R SNPs could be used as a marker of osteoporosis.

Once established, it will be also interesting to investigate whether osteoclastic resorption is altered in patients with known pathological conditions. Given the association of P2X7R SNPs with an altered inflammatory cytokine release (Gu et al., 2004a; Shemon et al., 2006; Stokes et al., 2010; Wesselius et al., 2012); the role of P2X7R in driving the patho-physiology of inflammatory diseases (Di Virgilio, 1995; Goncalves et al., 2006; Hughes et al., 2007; Lister et al., 2007); and the regulation of cytokine

release in bone resorption (Manolagas, 2000), it is plausible that regulation of cytokine release due to P2X7R SNPs could drive the patho-physiology of inflammation induced bone loss. These results would be invaluable in predicting the progression of diseases such as rheumatoid arthritis and a new therapeutic approach targeting P2X7R involving a combination of anti-inflammatory, anti-resorptive could be adopted.

Appendix I

CT values obtained from TaqMan® Array Custom Micro Fluidic cards (LDA) analysis

Table showing the CT values (average of duplicates) obtained from TaqMan® Array Custom Micro Fluidic cards (LDA) analysis of BM aspirate of P2X7R+/+ and P2X7R-/- mice. *Actb* was the house keeping gene used for analysis in section 3.2.4.1.

Gene	Average Ct		Gene	Average Ct		Gene	Average Ct	
	P2X7R +/+	**P2X7R -/-**		**P2X7R +/+**	**P2X7R -/-**		**P2X7R +/+**	**P2X7R -/-**
**18S*	15.0	15.2	*Esr2*	ND	ND	*P2rx7*	27.3	30.1
Acp5	21.9	21.6	*Fgf23*	ND	ND	*P2ry1*	27.5	27.8
**Actb*	15.8	16.0	*Fos*	17.9	18.3	*P2ry12*	27.3	27.6
Ada	24.8	25.0	**Gapdh*	17.1	17.6	*P2ry13*	27.0	27.3
Adipoq	26.8	25.2	*Ghr*	29.1	28.5	*P2ry14*	27.1	28.0
Ak1	29.0	27.3	*Ghrh*	31.8	31.7	*P2ry2*	29.3	30.0
Alpl	28.0	27.5	*Grin1*	ND	ND	*P2ry4*	31.4	ND
Bglap1	22.3	21.4	**Hprt1*	21.9	22.3	*P2ry6*	28.1	27.8
Bmp2	29.7	29.5	*Igf1*	24.8	27.1	*Pparg*	27.3	27.0
Bmp7	30.7	30.4	*Igf2*	ND	ND	*Ptges2*	23.8	24.1
Calcr	ND	ND	*Il1a*	28.9	29.0	*Ptgs2*	24.6	25.9
Col10a1	ND	ND	*Il1b*	21.8	22.7	*Pth1r*	29.8	28.1
Col1a2	23.3	22.4	*Il1r1*	28.1	28.3	*Pthlh*	ND	ND
Col2a1	27.6	26.6	*Il1r2*	23.7	25.0	*Rhoa*	21.2	21.3
Csf1	24.1	25.4	*Il6*	26.3	27.7	*Rock1*	22.2	22.2
Csf1r	24.6	25.0	*Itga5*	26.3	27.2	*Runx2*	24.0	24.7
Ctnnb1	21.9	21.7	*Itgb3*	24.6	25.1	*Sost*	ND	ND
Ctsk	25.9	24.5	*Itgb5*	27.3	27.1	*Sox9*	ND	ND
Cxcr4	20.2	20.6	*Lep*	ND	ND	*Sp7*	31.6	30.9
Dcst1	ND	ND	*Lepr*	28.7	26.9	*Sparc*	23.5	22.8
Egf	29.0	29.5	*Mapk1*	22.1	22.2	*Spp1*	24.4	25.3
Egfr	32.2	32.1	*Mapk3*	21.2	21.4	**Tfrc*	21.3	21.4
Enpp1	25.9	25.9	*Nfatc1*	22.5	23.2	*Tgfb1*	20.5	20.6
Enpp2	28.9	30.2	*Nfkb1*	23.1	23.8	*Tgfbr1*	25.3	25.7
Enpp3	ND	31.9	*Nr3c1*	22.3	22.5	*Tnf*	23.4	24.1
Enpp6	28.6	28.6	*Nt5e*	26.3	26.7	*Tnfrsf11a*	27.9	28.1
Entpd1	24.0	24.3	*P2rx1*	24.2	24.5	*Tnfrsf11b*	ND	ND
Entpd2	30.7	30.7	*P2rx2*	ND	ND	*Tnfrsf1a*	22.5	22.8
Entpd3	29.4	28.7	*P2rx3*	27.5	28.2	*Tnfsf11*	29.8	30.1
Entpd5	24.4	24.8	*P2rx4*	25.6	26.7	*Traf6*	26.5	27.6
Entpd6	25.7	26.0	*P2rx5*	ND	ND	*Vdr*	30.0	30.0
Entpd8	ND	ND	*P2rx6*	ND	ND	*Vegfa*	24.4	24.7
*= house keeping gene. ND= Not detected.								

Table showing the CT values (average of duplicates) obtained from TaqMan® Array Custom Micro Fluidic cards (LDA) analysis of BM derived osteoclasts from P2X7R+/+ and P2X7R-/- mice. *Actb* was the house keeping gene used for analysis in section 3.2.4.2.

Gene	Average Ct		Gene	Average Ct		Gene	Average Ct	
	P2X7R +/+	**P2X7R -/-**		**P2X7R +/+**	**P2X7R -/-**		**P2X7R +/+**	**P2X7R -/-**
**18S*	16.0	15.9	*Esr2*	ND	ND	*P2rx7*	29.7	ND
Acp5	18.0	19.8	*Fgf23*	ND	28.4	*P2ry1*	32.2	32.1
**Actb*	18.6	19.0	*Fos*	25.0	26.0	*P2ry12*	29.3	30.7
Ada	28.1	26.3	**Gapdh*	19.4	19.5	*P2ry13*	31.6	31.8
Adipoq	31.3	31.6	*Ghr*	27.7	28.7	*P2ry14*	30.1	31.4
Ak1	27.2	27.8	*Ghrh*	33.6	ND	*P2ry2*	31.1	32.0
Alpl	30.1	30.0	*Grin1*	ND	ND	*P2ry4*	30.8	31.5
Bglap1	32.7	33.5	**Hprt1*	24.7	25.5	*P2ry6*	26.7	27.4
Bmp2	29.2	29.7	*Igf1*	25.5	25.5	*Pparg*	27.7	27.3
Bmp7	33.8	ND	*Igf2*	ND	32.8	*Ptges2*	26.2	26.8
Calcr	27.1	29.1	*Il1a*	30.0	32.7	*Ptgs2*	30.2	30.0
Col10a1	ND	ND	*Il1b*	31.6	31.5	*Pth1r*	31.3	22.4
Col1a2	27.4	26.3	*Il1r1*	28.9	30.4	*Pthlh*	ND	ND
Col2a1	31.7	30.1	*Il1r2*	31.4	30.4	*Rhoa*	25.4	25.0
Csf1	26.1	25.2	*Il6*	31.1	32.1	*Rock1*	25.8	26.1
Csf1r	24.9	25.9	*Itga5*	28.4	27.9	*Runx2*	30.7	30.1
Ctnnb1	23.2	23.5	*Itgb3*	27.1	28.9	*Sost*	ND	ND
Ctsk	18.8	19.5	*Itgb5*	27.5	27.5	*Sox9*	29.8	28.6
Cxcr4	25.6	25.3	*Lep*	ND	ND	*Sp7*	32.6	32.2
Dcst1	ND	ND	*Lepr*	32.9	31.9	*Sparc*	24.5	23.6
Egf	31.3	31.9	*Mapk1*	26.1	26.7	*Spp1*	22.3	22.2
Egfr	30.4	31.1	*Mapk3*	24.1	24.4	**Tfrc*	23.5	26.2
Enpp1	28.6	27.5	*Nfatc1*	23.2	24.7	*Tgfb1*	23.4	23.6
Enpp2	32.4	30.4	*Nfkb1*	27.2	27.9	*Tgfbr1*	26.3	28.1
Enpp3	32.4	32.1	*Nr3c1*	25.6	26.1	*Tnf*	27.4	28.9
Enpp6	33.5	32.1	*Nt5e*	31.9	31.9	*Tnfrsf11a*	24.0	25.0
Entpd1	28.1	27.6	*P2rx1*	31.8	32.0	*Tnfrsf11b*	26.8	27.2
Entpd2	30.4	31.6	*P2rx2*	32.6	ND	*Tnfrsf1a*	25.8	26.1
Entpd3	ND	ND	*P2rx3*	17.8	ND	*Tnfsf11*	32.3	31.8
Entpd5	29.8	30.0	*P2rx4*	26.7	27.5	*Traf6*	30.3	31.0
Entpd6	28.7	29.8	*P2rx5*	28.4	30.0	*Vdr*	31.7	29.6
Entpd8	ND	ND	*P2rx6*	33.0	32.4	*Vegfa*	27.4	26.2
*= house keeping gene. ND= Not detected.								

Table showing the CT values (average of duplicates) obtained from TaqMan® Array Custom Micro Fluidic cards (LDA) analysis of splenic osteoclasts from P2X7R+/+ and P2X7R-/- mice. *Actb* was the house keeping gene used for analysis in section 3.2.4.2.

Gene	Average Ct		Gene	Average Ct		Gene	Average Ct	
	P2X7R +/+	**P2X7R -/-**		**P2X7R +/+**	**P2X7R -/-**		**P2X7R +/+**	**P2X7R -/-**
18S	15.8	15.9	*Esr2*	ND	ND	*P2rx7*	25.3	ND
Acp5	21.8	21.3	*Fgf23*	32.0	26.7	*P2ry1*	30.5	31.3
Actb	17.1	17.3	*Fos*	23.5	23.5	*P2ry12*	26.9	27.3
Ada	25.4	25.9	*Gapdh*	18.1	18.7	*P2ry13*	28.6	28.9
Adipoq	ND	ND	*Ghr*	30.0	ND	*P2ry14*	27.9	29.1
Ak1	24.9	ND	*Ghrh*	ND	ND	*P2ry2*	28.3	28.8
Alpl	31.3	31.9	*Grin1*	ND	ND	*P2ry4*	31.2	31.5
Bglap1	ND	ND	*Hprt1*	23.8	23.6	*P2ry6*	23.0	23.8
Bmp2	28.7	27.3	*Igf1*	21.0	21.3	*Pparg*	25.9	25.7
Bmp7	30.9	ND	*Igf2*	ND	ND	*Ptges2*	25.2	25.7
Calcr	31.6	29.6	*Il1a*	25.7	27.6	*Ptgs2*	29.0	29.6
Col10a1	ND	ND	*Il1b*	24.3	26.7	*Pth1r*	31.8	21.4
Col1a2	24.6	26.7	*Il1r1*	27.1	29.3	*Pthlh*	ND	ND
Col2a1	ND	ND	*Il1r2*	28.7	29.7	*Rhoa*	22.9	23.0
Csf1	24.4	25.5	*Il6*	29.2	31.9	*Rock1*	24.5	24.7
Csf1r	21.4	21.8	*Itga5*	25.6	25.9	*Runx2*	27.8	28.4
Ctnnb1	20.6	20.9	*Itgb3*	28.0	28.1	*Sost*	ND	ND
Ctsk	19.8	19.7	*Itgb5*	23.1	23.6	*Sox9*	30.9	32.0
Cxcr4	22.7	23.0	*Lep*	ND	ND	*Sp7*	ND	ND
Dcst1	ND	ND	*Lepr*	ND	ND	*Sparc*	24.6	25.8
Egf	31.3	31.7	*Mapk1*	24.0	24.1	*Spp1*	17.8	20.3
Egfr	31.0	30.9	*Mapk3*	21.3	21.7	*Tfrc*	24.7	23.7
Enpp1	25.5	25.3	*Nfatc1*	24.5	24.5	*Tgfb1*	21.3	22.1
Enpp2	31.2	ND	*Nfkb1*	24.3	24.9	*Tgfbr1*	25.2	25.4
Enpp3	ND	22.6	*Nr3c1*	24.4	24.3	*Tnf*	26.1	26.7
Enpp6	ND	28.6	*Nt5e*	27.5	31.0	*Tnfrsf11a*	24.8	24.3
Entpd1	24.1	24.5	*P2rx1*	ND	ND	*Tnfrsf11b*	31.0	31.8
Entpd2	29.9	30.8	*P2rx2*	ND	ND	*Tnfrsf1a*	23.3	23.7
Entpd3	ND	29.6	*P2rx3*	ND	ND	*Tnfsf11*	27.8	30.6
Entpd5	26.6	26.7	*P2rx4*	22.3	23.8	*Traf6*	28.6	28.7
Entpd6	26.9	27.7	*P2rx5*	26.1	27.4	*Vdr*	28.6	30.7
Entpd8	ND	ND	*P2rx6*	31.3	31.2	*Vegfa*	24.1	24.1
*= house keeping gene. ND= Not detected.								

Appendix II

Publications and meeting abstracts

Publications during the PhD studies

Rumney RM, Wang N, **Agrawal A** and Gartland A (2012). Purinergic signalling in bone. Front. Endocrin. 3:116. doi: 10.3389/fendo.2012.00116

Agrawal A, Gallagher JA, Gartland A (2012). Human Osteoclast Culture and Phenotypic Characterisation. Methods in Molecular Biology 806(357-75).

Wang N, Robaye B, **Agrawal A**, Reilly G, Boeynaems JM, Gartland A (2012). Reduced bone turnover in mice lacking the P2Y13 receptor. Molecular Endocrinology 26(1):142-52.

Wesselius A, Bours MJ, **Agrawal A**, Gartland A, Dagnelie PC, Schwarz P, Jorgensen NR (2011). Role of purinergic receptor polymorphisms in human bone. Frontiers in Bioscience 16, 2572-2585.

Publications before starting the PhD studies

Agrawal A, Buckley KA, Bowers K, Furber M, Gallagher JA, Gartland A. The effects of P2X7 receptor antagonists on the formation and function of human osteoclasts *in vitro*. Purinergic Signalling (2010). 6(3):307-15.

Meeting abstracts produced during PhD studies

Agrawal A and Gartland A (2013). Augmentation of osteoclastogenesis in the absence of the P2X7 receptor in oestrogen deplete conditions *in vitro* is dependent on precursor cell origin. Bone Research Society and the British Orthopaedic Research Society, Oxford, UK. 4-5 September 2013. *Selected for Oral Presentation.*

Agrawal A and Gartland A (2013). Combined effects of depletion of P2X7R and oestrogen on murine osteoclast function and survival *in vitro*. Medical School Research Meeting 2013. Sheffield, UK. *Oral Presentation.*

Agrawal A and Gartland A (2012). Combined effects of depletion of P2X7R and oestrogen on murine osteoclast function and survival *in vitro*. UK Purine Club 2012 Symposium, Norwich, UK. *Poster Presentation.*

Agrawal A, Syberg S, Jørgensen NR and Gartland A (2012) Age-dependent changes in osteoclast formation in a new strain of P2X7 receptor knockout mice. UK Purine Club 2011 Symposium, Cardiff. UK. *Poster Presentation*. Purinergic Signalling 8:781–800.

Agrawal A, Syberg S, Jørgensen N and Gartland A (2011). Age-dependent changes in osteoclast formation in a new strain of P2X7 receptor knockout mice. Joint meeting of Bone Research Society & the British Orthopaedic Research Society, Cambridge. UK. *Poster Presentation*. Front. Endocrinol. doi: 10.3389/conf.fendo.2011.02.00001.

Wang N, Robaye B, **Agrawal A**, Reilly G, Boeynaems JM and Gartland A (2011). Bone phenotype of P2Y13 receptor knockout mice. UK Purine Club 2010, Nottingham. United Kingdom. *Oral presentation*. Purinergic Signalling 7:143–163.

Agrawal A, Gartland A. (2011). Expression of NFATc1 is inducible by P2X7 receptor activation in human osteoclasts. European Calcified Tissue Society

& International Bone and Mineral Society 2011, Athens. Greece. *Poster Presentation*. Bone 48 (2): S126.

Pacheco-Pantoja EL, Waring-Green V, Fraser WD, **Agrawal A**, Gallagher JA (2011). Adiponectin receptors in multinucleated osteoclast-like cells. European Calcified Tissue Society & International Bone and Mineral Society 2011, Athens. Greece. *Poster Presentation.* Bone 48 (2): S129.

Wang N, Robaye B, **Agrawal A**, Reilly G, Boeynaems JM and Gartland A. (2011) Deletion of the P2Y13 receptor leads to reduced bone turnover and protection from ovariectomy-induced bone loss. European Calcified Tissue Society & International Bone and Mineral Society 2011, Athens. Greece. *Poster Presentation* Bone 48(7): S227.

Agrawal A, Gartland A (2010). Expression of NFATc1 is inducible by P2X7 receptor activation in human osteoclasts. Medical School Research Meeting 2010. Sheffield, UK. *Poster Presentation*.

Bibliography

Abbracchio, M.P., and Burnstock, G. (1994). Purinoceptors: Are there families of P2X and P2Y purinoceptors? Pharmacology & Therapeutics *64*, 445-475.

Abbracchio, M.P., and Burnstock, G. (1998). Purinergic signalling: pathophysiological roles. Japanese journal of pharmacology *78*, 113-145.

Abbracchio, M.P., Burnstock, G., Boeynaems, J.M., Barnard, E.A., Boyer, J.L., Kennedy, C., Knight, G.E., Fumagalli, M., Gachet, C., Jacobson, K.A.*, et al.* (2006). International Union of Pharmacology LVIII: update on the P2Y G protein-coupled nucleotide receptors: from molecular mechanisms and pathophysiology to therapy. Pharmacological reviews *58*, 281-341.

Abbracchio, M.P., Burnstock, G., Boeynaems, J.M., Barnard, E.A., Boyer, J.L., Kennedy, C., Miras-Portugal, M.T., King, B.F., Gachet, C., Jacobson, K.A.*, et al.* (2005). The recently deorphanized GPR80 (GPR99) proposed to be the P2Y15 receptor is not a genuine P2Y receptor. Trends in pharmacological sciences *26*, 8-9.

Abbracchio, M.P., Burnstock, G., Verkhratsky, A., and Zimmermann, H. (2009). Purinergic signalling in the nervous system: an overview. Trends in neurosciences *32*, 19-29.

Adinolfi, E., Callegari, M.G., Cirillo, M., Pinton, P., Giorgi, C., Cavagna, D., Rizzuto, R., and Di Virgilio, F. (2009). Expression of the P2X7 receptor increases the Ca2+ content of the endoplasmic reticulum, activates NFATc1, and protects from apoptosis. The Journal of biological chemistry *284*, 10120-10128.

Adinolfi, E., Cirillo, M., Woltersdorf, R., Falzoni, S., Chiozzi, P., Pellegatti, P., Callegari, M.G., Sandona, D., Markwardt, F., Schmalzing, G.*, et al.* (2010). Trophic activity of a naturally occurring truncated isoform of the P2X7 receptor. FASEB journal : official publication of the Federation of American Societies for Experimental Biology *24*, 3393-3404.

Adriouch, S., Dox, C., Welge, V., Seman, M., Koch-Nolte, F., and Haag, F. (2002). Cutting edge: a natural P451L mutation in the cytoplasmic domain impairs the function of the mouse P2X7 receptor. Journal of immunology *169*, 4108-4112.

Agrawal, A., Buckley, K.A., Bowers, K., Furber, M., Gallagher, J.A., and Gartland, A. (2010). The effects of P2X7 receptor antagonists on the formation and function of human osteoclasts in vitro. Purinergic signalling *6*, 307-315.

Agrawal, A., Gallagher, J.A., and Gartland, A. (2012). Human Osteoclast Culture and Phenotypic Characterisation. In Methods in Molecular Biology, W. JM, ed. (Springer Protocols), pp. 357-375.

Al-Shukaili, A., Al-Kaabi, J., and Hassan, B. (2008). A comparative study of interleukin-1beta production and p2x7 expression after ATP stimulation by peripheral blood mononuclear cells isolated from rheumatoid arthritis patients and normal healthy controls. Inflammation *31*, 84-90.

Alzola, E., Perez-Etxebarria, A., Kabre, E., Fogarty, D.J., Metioui, M., Chaib, N., Macarulla, J.M., Matute, C., Dehaye, J.P., and Marino, A. (1998). Activation by P2X7 agonists of two phospholipases A2 (PLA2) in ductal cells of rat submandibular gland. Coupling of the calcium-independent PLA2 with kallikrein secretion. The Journal of biological chemistry *273*, 30208-30217.

Anderson, H.C., Hodges, P.T., Aguilera, X.M., Missana, L., and Moylan, P.E. (2000). Bone morphogenetic protein (BMP) localization in developing human and rat growth plate, metaphysis, epiphysis, and articular cartilage. The journal of histochemistry and cytochemistry : official journal of the Histochemistry Society *48*, 1493-1502.

Angel, N.Z., Walsh, N., Forwood, M.R., Ostrowski, M.C., Cassady, A.I., and Hume, D.A. (2000). Transgenic mice overexpressing tartrate-resistant acid

phosphatase exhibit an increased rate of bone turnover. Journal of bone and mineral research : the official journal of the American Society for Bone and Mineral Research *15*, 103-110.

Armstrong, A.P., Tometsko, M.E., Glaccum, M., Sutherland, C.L., Cosman, D., and Dougall, W.C. (2002). A RANK/TRAF6-dependent signal transduction pathway is essential for osteoclast cytoskeletal organization and resorptive function. The Journal of biological chemistry *277*, 44347-44356.

Armstrong, S., Pereverzev, A., Dixon, S.J., and Sims, S.M. (2009). Activation of P2X7 receptors causes isoform-specific translocation of protein kinase C in osteoclasts. Journal of cell science *122*, 136-144.

Asagiri, M., Sato, K., Usami, T., Ochi, S., Nishina, H., Yoshida, H., Morita, I., Wagner, E.F., Mak, T.W., Serfling, E.*, et al.* (2005). Autoamplification of NFATc1 expression determines its essential role in bone homeostasis. The Journal of experimental medicine *202*, 1261-1269.

Azuma, Y., Kaji, K., Katogi, R., Takeshita, S., and Kudo, A. (2000). Tumor necrosis factor-alpha induces differentiation of and bone resorption by osteoclasts. The Journal of biological chemistry *275*, 4858-4864.

Bar, I., Guns, P.J., Metallo, J., Cammarata, D., Wilkin, F., Boeynams, J.M., Bult, H., and Robaye, B. (2008). Knockout mice reveal a role for P2Y6 receptor in macrophages, endothelial cells, and vascular smooth muscle cells. Molecular pharmacology *74*, 777-784.

Barden, N., Harvey, M., Gagne, B., Shink, E., Tremblay, M., Raymond, C., Labbe, M., Villeneuve, A., Rochette, D., Bordeleau, L.*, et al.* (2006). Analysis of single nucleotide polymorphisms in genes in the chromosome 12Q24.31 region points to P2RX7 as a susceptibility gene to bipolar affective disorder. American journal of medical genetics Part B, Neuropsychiatric genetics : the official publication of the International Society of Psychiatric Genetics *141B*, 374-382.

Barka, T. (1960). A simple azo-dye method for histochemical demonstration of acid phosphatase. Nature *187*, 248-249.

Baroja-Mazo, A., and Pelegrin, P. (2012). Modulating P2X7 Receptor Signaling during Rheumatoid Arthritis: New Therapeutic Approaches for Bisphosphonates. Journal of osteoporosis *2012*, 408242.

Baron, R. (1989). Polarity and membrane transport in osteoclasts. Connective tissue research *20*, 109-120.

Barrera, N.P., Ormond, S.J., Henderson, R.M., Murrell-Lagnado, R.D., and Edwardson, J.M. (2005). Atomic force microscopy imaging demonstrates that P2X2 receptors are trimers but that P2X6 receptor subunits do not oligomerize. The Journal of biological chemistry *280*, 10759-10765.

Beamer, W.G., Shultz, K.L., Donahue, L.R., Churchill, G.A., Sen, S., Wergedal, J.R., Baylink, D.J., and Rosen, C.J. (2001). Quantitative trait loci for femoral and lumbar vertebral bone mineral density in C57BL/6J and C3H/HeJ inbred strains of mice. Journal of bone and mineral research : the official journal of the American Society for Bone and Mineral Research *16*, 1195-1206.

Bendre, M.S., Montague, D.C., Peery, T., Akel, N.S., Gaddy, D., and Suva, L.J. (2003). Interleukin-8 stimulation of osteoclastogenesis and bone resorption is a mechanism for the increased osteolysis of metastatic bone disease. Bone *33*, 28-37.

Berne, R.M. (1963). Cardiac nucleotides in hypoxia: possible role in regulation of coronary blood flow. The American journal of physiology *204*, 317-322.

Berthois, Y., Katzenellenbogen, J.A., and Katzenellenbogen, B.S. (1986). Phenol red in tissue culture media is a weak estrogen: implications concerning the

study of estrogen-responsive cells in culture. Proceedings of the National Academy of Sciences of the United States of America *83*, 2496-2500.

Bianco, F., Ceruti, S., Colombo, A., Fumagalli, M., Ferrari, D., Pizzirani, C., Matteoli, M., Di Virgilio, F., Abbracchio, M.P., and Verderio, C. (2006). A role for P2X7 in microglial proliferation. J Neurochem *99*, 745-758.

Boldt, W., Klapperstuck, M., Buttner, C., Sadtler, S., Schmalzing, G., and Markwardt, F. (2003). Glu496Ala polymorphism of human P2X7 receptor does not affect its electrophysiological phenotype. Am J Physiol Cell Physiol *284*, C749-756.

Borah, B., Dufresne, T.E., Chmielewski, P.A., Johnson, T.D., Chines, A., and Manhart, M.D. (2004). Risedronate preserves bone architecture in postmenopausal women with osteoporosis as measured by three-dimensional microcomputed tomography. Bone *34*, 736-746.

Bossard, M.J., Tomaszek, T.A., Thompson, S.K., Amegadzie, B.Y., Hanning, C.R., Jones, C., Kurdyla, J.T., McNulty, D.E., Drake, F.H., Gowen, M.*, et al.* (1996). Proteolytic activity of human osteoclast cathepsin K. Expression, purification, activation, and substrate identification. The Journal of biological chemistry *271*, 12517-12524.

Boumechache, M., Masin, M., Edwardson, J.M., Gorecki, D.C., and Murrell-Lagnado, R. (2009). Analysis of assembly and trafficking of native P2X4 and P2X7 receptor complexes in rodent immune cells. The Journal of biological chemistry *284*, 13446-13454.

Bouxsein, M.L., Myers, K.S., Shultz, K.L., Donahue, L.R., Rosen, C.J., and Beamer, W.G. (2005). Ovariectomy-induced bone loss varies among inbred strains of mice. Journal of bone and mineral research : the official journal of the American Society for Bone and Mineral Research *20*, 1085-1092.

Bowler, W.B., Buckley, K.A., Gartland, A., Hipskind, R.A., Bilbe, G., and Gallagher, J.A. (2001). Extracellular nucleotide signaling: a mechanism for integrating local and systemic responses in the activation of bone remodeling. Bone *28*, 507-512.

Boyce, B.F., Yoneda, T., Lowe, C., Soriano, P., and Mundy, G.R. (1992). Requirement of pp60c-src expression for osteoclasts to form ruffled borders and resorb bone in mice. The Journal of clinical investigation *90*, 1622-1627.

Brandle, U., Kohler, K., and Wheeler-Schilling, T.H. (1998). Expression of the P2X7-receptor subunit in neurons of the rat retina. Brain research Molecular brain research *62*, 106-109.

Browne, L.E., Jiang, L.H., and North, R.A. (2010). New structure enlivens interest in P2X receptors. Trends in pharmacological sciences *31*, 229-237.

Bucay, N., Sarosi, I., Dunstan, C.R., Morony, S., Tarpley, J., Capparelli, C., Scully, S., Tan, H.L., Xu, W., Lacey, D.L.*, et al.* (1998). osteoprotegerin-deficient mice develop early onset osteoporosis and arterial calcification. Genes & development *12*, 1260-1268.

Buckley, K.A., Hipskind, R.A., Gartland, A., Bowler, W.B., and Gallagher, J.A. (2002). Adenosine triphosphate stimulates human osteoclast activity via upregulation of osteoblast-expressed receptor activator of nuclear factor-kappa B ligand. Bone *31*, 582-590.

Buell, G., Chessell, I.P., Michel, A.D., Collo, G., Salazzo, M., Herren, S., Gretener, D., Grahames, C., Kaur, R., Kosco-Vilbois, M.H.*, et al.* (1998). Blockade of human P2X7 receptor function with a monoclonal antibody. Blood *92*, 3521-3528.

Burgess, T.L., Qian, Y., Kaufman, S., Ring, B.D., Van, G., Capparelli, C., Kelley, M., Hsu, H., Boyle, W.J., Dunstan, C.R.*, et al.* (1999). The ligand for

osteoprotegerin (OPGL) directly activates mature osteoclasts. The Journal of cell biology *145*, 527-538.

Burnstock, G. (1972). Purinergic nerves. Pharmacological reviews *24*, 509-581.

Burnstock, G. (1976). Do some nerve cells release more than one transmitter? Neuroscience *1*, 239-248.

Burnstock, G. (1978). A basis for distinguishing two types of purinergic receptor. In: Cell Membrane Receptors for Drugs and Hormones: A Multidisciplinary Approach (New York, Raven Press).

Burnstock, G. (2007). Purine and pyrimidine receptors. Cellular and molecular life sciences : CMLS *64*, 1471-1483.

Burnstock, G. (2009). Purinergic signalling: past, present and future. Brazilian journal of medical and biological research = Revista brasileira de pesquisas medicas e biologicas / Sociedade Brasileira de Biofisica [et al] *42*, 3-8.

Burnstock, G. (2012). Purinergic signalling: Its unpopular beginning, its acceptance and its exciting future. BioEssays : news and reviews in molecular, cellular and developmental biology *34*, 218-225.

Burnstock, G. (2013). Purinergic mechanisms and pain-An update. European journal of pharmacology.

Burnstock, G., Campbell, G., Satchell, D., and Smythe, A. (1970). Evidence that adenosine triphosphate or a related nucleotide is the transmitter substance released by non-adrenergic inhibitory nerves in the gut. British journal of pharmacology *40*, 668-688.

Burnstock, G., and Kennedy, C. (1985). Is there a basis for distinguishing two types of P2-purinoceptor? General Pharmacology: The Vascular System *16*, 433-440.

Burnstock, G., and Verkhratsky, A. (2010). Long-term (trophic) purinergic signalling: purinoceptors control cell proliferation, differentiation and death. Cell death & disease *1*, e9.

Cabrini, G., Falzoni, S., Forchap, S.L., Pellegatti, P., Balboni, A., Agostini, P., Cuneo, A., Castoldi, G., Baricordi, O.R., and Di Virgilio, F. (2005). A His-155 to Tyr polymorphism confers to gain-of-function to the human $P2X_7$ receptor of human leukemic lymphocytes. Journal of immunology *175*, 82-89.

Cao, L., Young, M.T., Broomhead, H.E., Fountain, S.J., and North, R.A. (2007). Thr339-to-serine substitution in rat P2X2 receptor second transmembrane domain causes constitutive opening and indicates a gating role for Lys308. The Journal of neuroscience : the official journal of the Society for Neuroscience *27*, 12916-12923.

Caporali, F., Capecchi, P.L., Gamberucci, A., Lazzerini, P.E., Pompella, G., Natale, M., Lorenzini, S., Selvi, E., Galeazzi, M., and Laghi Pasini, F. (2008). Human rheumatoid synoviocytes express functional P2X7 receptors. Journal of molecular medicine *86*, 937-949.

Cenci, S., Toraldo, G., Weitzmann, M.N., Roggia, C., Gao, Y., Qian, W.P., Sierra, O., and Pacifici, R. (2003). Estrogen deficiency induces bone loss by increasing T cell proliferation and lifespan through IFN-gamma-induced class II transactivator. Proceedings of the National Academy of Sciences of the United States of America *100*, 10405-10410.

Cenci, S., Weitzmann, M.N., Roggia, C., Namba, N., Novack, D., Woodring, J., and Pacifici, R. (2000). Estrogen deficiency induces bone loss by enhancing T-cell production of TNF-alpha. The Journal of clinical investigation *106*, 1229-1237.

Cheewatrakoolpong, B., Gilchrest, H., Anthes, J.C., and Greenfeder, S. (2005). Identification and characterization of splice variants of the human P2X7 ATP channel. Biochemical and biophysical research communications *332*, 17-27.

Chessell, I.P., Hatcher, J.P., Bountra, C., Michel, A.D., Hughes, J.P., Green, P., Egerton, J., Murfin, M., Richardson, J., Peck, W.L.*, et al.* (2005). Disruption of the P2X7 purinoceptor gene abolishes chronic inflammatory and neuropathic pain. Pain *114*, 386-396.

Chessell, I.P., Michel, A.D., and Humphrey, P.P. (1997). Properties of the pore-forming P2X7 purinoceptor in mouse NTW8 microglial cells. British journal of pharmacology *121*, 1429-1437.

Chessell, I.P., Michel, A.D., and Humphrey, P.P. (1998). Effects of antagonists at the human recombinant P2X7 receptor. British journal of pharmacology *124*, 1314-1320.

Chin, J., and Kostura, M.J. (1993). Dissociation of IL-1 beta synthesis and secretion in human blood monocytes stimulated with bacterial cell wall products. Journal of immunology *151*, 5574-5585.

Chomczynski, P. (1993). A reagent for the single-step simultaneous isolation of RNA, DNA and proteins from cell and tissue samples. Biotechniques *15*, 532-534, 536-537.

Clarke, B. (2008). Normal bone anatomy and physiology. Clinical journal of the American Society of Nephrology : CJASN *3 Suppl 3*, S131-139.

Collo, G., Neidhart, S., Kawashima, E., Kosco-Vilbois, M., North, R.A., and Buell, G. (1997). Tissue distribution of the P2X7 receptor. Neuropharmacology *36*, 1277-1283.

Dai, X.M., Ryan, G.R., Hapel, A.J., Dominguez, M.G., Russell, R.G., Kapp, S., Sylvestre, V., and Stanley, E.R. (2002). Targeted disruption of the mouse colony-stimulating factor 1 receptor gene results in osteopetrosis, mononuclear phagocyte deficiency, increased primitive progenitor cell frequencies, and reproductive defects. Blood *99*, 111-120.

De Benedetti, F., Rucci, N., Del Fattore, A., Peruzzi, B., Paro, R., Longo, M., Vivarelli, M., Muratori, F., Berni, S., Ballanti, P.*, et al.* (2006). Impaired skeletal development in interleukin-6-transgenic mice: a model for the impact of chronic inflammation on the growing skeletal system. Arthritis and rheumatism *54*, 3551-3563.

Declercq, H., Van den Vreken, N., De Maeyer, E., Verbeeck, R., Schacht, E., De Ridder, L., and Cornelissen, M. (2004). Isolation, proliferation and differentiation of osteoblastic cells to study cell/biomaterial interactions: comparison of different isolation techniques and source. Biomaterials *25*, 757-768.

Delany, A.M., Amling, M., Priemel, M., Howe, C., Baron, R., and Canalis, E. (2000). Osteopenia and decreased bone formation in osteonectin-deficient mice. The Journal of clinical investigation *105*, 1325.

Dell'Antonio, G., Quattrini, A., Cin, E.D., Fulgenzi, A., and Ferrero, M.E. (2002). Relief of inflammatory pain in rats by local use of the selective P2X7 ATP receptor inhibitor, oxidized ATP. Arthritis and rheumatism *46*, 3378-3385.

Dempster, D.W., Compston, J.E., Drezner, M.K., Glorieux, F.H., Kanis, J.A., Malluche, H., Meunier, P.J., Ott, S.M., Recker, R.R., and Parfitt, A.M. (2013). Standardized nomenclature, symbols, and units for bone histomorphometry: a 2012 update of the report of the ASBMR Histomorphometry Nomenclature Committee. Journal of bone and mineral research : the official journal of the American Society for Bone and Mineral Research *28*, 2-17.

Denlinger, L.C., Angelini, G., Schell, K., Green, D.N., Guadarrama, A.G., Prabhu, U., Coursin, D.B., Bertics, P.J., and Hogan, K. (2005). Detection of human P2X7 nucleotide receptor polymorphisms by a novel monocyte pore assay predictive of alterations in lipopolysaccharide-induced cytokine production. Journal of immunology *174*, 4424-4431.

Deuchars, S.A., Atkinson, L., Brooke, R.E., Musa, H., Milligan, C.J., Batten, T.F., Buckley, N.J., Parson, S.H., and Deuchars, J. (2001). Neuronal P2X7 receptors are targeted to presynaptic terminals in the central and peripheral nervous systems. The Journal of neuroscience : the official journal of the Society for Neuroscience *21*, 7143-7152.

Di Virgilio, F. (1995). The P2Z purinoceptor: an intriguing role in immunity, inflammation and cell death. Immunol Today *16*, 524-528.

Di Virgilio, F. (2007). Liaisons dangereuses: P2X(7) and the inflammasome. Trends in pharmacological sciences *28*, 465-472.

Di Virgilio, F., Falzoni, S., Chiozzi, P., Sanz, J.M., Ferrari, D., and Buell, G.N. (1999). ATP receptors and giant cell formation. J Leukoc Biol *66*, 723-726.

Dobnig, H., and Turner, R.T. (1995). Evidence that intermittent treatment with parathyroid hormone increases bone formation in adult rats by activation of bone lining cells. Endocrinology *136*, 3632-3638.

Donnelly-Roberts, D., McGaraughty, S., Shieh, C.C., Honore, P., and Jarvis, M.F. (2008). Painful purinergic receptors. The Journal of pharmacology and experimental therapeutics *324*, 409-415.

Downey, P.A., and Siegel, M.I. (2006). Bone biology and the clinical implications for osteoporosis. Physical therapy *86*, 77-91.

Drury, A.N., and Szent-Gyorgyi, A. (1929). The physiological activity of adenine compounds with especial reference to their action upon the mammalian heart. The Journal of physiology *68*, 213-237.

Ducy, P., Desbois, C., Boyce, B., Pinero, G., Story, B., Dunstan, C., Smith, E., Bonadio, J., Goldstein, S., Gundberg, C*., et al.* (1996). Increased bone formation in osteocalcin-deficient mice. Nature *382*, 448-452.

Duong, L.T., Lakkakorpi, P.T., Nakamura, I., Machwate, M., Nagy, R.M., and Rodan, G.A. (1998). PYK2 in osteoclasts is an adhesion kinase, localized in the sealing zone, activated by ligation of alpha(v)beta3 integrin, and phosphorylated by src kinase. The Journal of clinical investigation *102*, 881-892.

Eckert, R.L., and Katzenellenbogen, B.S. (1982). Effects of estrogens and antiestrogens on estrogen receptor dynamics and the induction of progesterone receptor in MCF-7 human breast cancer cells. Cancer Res *42*, 139-144.

Elssner, A., Duncan, M., Gavrilin, M., and Wewers, M.D. (2004). A novel P2X7 receptor activator, the human cathelicidin-derived peptide LL37, induces IL-1 beta processing and release. Journal of immunology *172*, 4987-4994.

Evans, K.E., and Fox, S.W. (2007). Interleukin-10 inhibits osteoclastogenesis by reducing NFATc1 expression and preventing its translocation to the nucleus. BMC cell biology *8*, 4.

Evans, R.J., Lewis, C., Buell, G., Valera, S., North, R.A., and Surprenant, A. (1995). Pharmacological characterization of heterologously expressed ATP-gated cation channels (P2x purinoceptors). Molecular pharmacology *48*, 178-183.

Fabre, A.C., Malaval, C., Ben Addi, A., Verdier, C., Pons, V., Serhan, N., Lichtenstein, L., Combes, G., Huby, T., Briand, F*., et al.* (2010). P2Y13 receptor is critical for reverse cholesterol transport. Hepatology *52*, 1477-1483.

Faccio, R., Takeshita, S., Zallone, A., Ross, F.P., and Teitelbaum, S.L. (2003). c-Fms and the alphavbeta3 integrin collaborate during osteoclast differentiation. The Journal of clinical investigation *111*, 749-758.

Falzoni, S., Chiozzi, P., Ferrari, D., Buell, G., and Di Virgilio, F. (2000). P2X(7) receptor and polykarion formation. Mol Biol Cell *11*, 3169-3176.

Falzoni, S., Munerati, M., Ferrari, D., Spisani, S., Moretti, S., and Di Virgilio, F. (1995). The purinergic P2Z receptor of human macrophage cells. Characterization and possible physiological role. The Journal of clinical investigation *95*, 1207-1216.

Feng, Y.H., Li, X., Wang, L., Zhou, L., and Gorodeski, G.I. (2006). A truncated P2X7 receptor variant (P2X7-j) endogenously expressed in cervical cancer cells antagonizes the full-length P2X7 receptor through hetero-oligomerization. The Journal of biological chemistry *281*, 17228-17237.

Fernando, S.L., Saunders, B.M., Sluyter, R., Skarratt, K.K., Goldberg, H., Marks, G.B., Wiley, J.S., and Britton, W.J. (2007). A polymorphism in the P2X7 gene increases susceptibility to extrapulmonary tuberculosis. American journal of respiratory and critical care medicine *175*, 360-366.

Fernando, S.L., Saunders, B.M., Sluyter, R., Skarratt, K.K., Wiley, J.S., and Britton, W.J. (2005). Gene dosage determines the negative effects of polymorphic alleles of the P2X7 receptor on adenosine triphosphate-mediated killing of mycobacteria by human macrophages. The Journal of infectious diseases *192*, 149-155.

Ferrari, D., Chiozzi, P., Falzoni, S., Hanau, S., and Di Virgilio, F. (1997). Purinergic modulation of interleukin-1 beta release from microglial cells stimulated with bacterial endotoxin. The Journal of experimental medicine *185*, 579-582.

Ferrari, D., Los, M., Bauer, M.K., Vandenabeele, P., Wesselborg, S., and Schulze-Osthoff, K. (1999a). P2Z purinoreceptor ligation induces activation of caspases with distinct roles in apoptotic and necrotic alterations of cell death. FEBS Lett *447*, 71-75.

Ferrari, D., Pizzirani, C., Adinolfi, E., Lemoli, R.M., Curti, A., Idzko, M., Panther, E., and Di Virgilio, F. (2006). The P2X7 receptor: a key player in IL-1 processing and release. Journal of immunology *176*, 3877-3883.

Ferrari, D., Stroh, C., and Schulze-Osthoff, K. (1999b). P2X7/P2Z purinoreceptor-mediated activation of transcription factor NFAT in microglial cells. The Journal of biological chemistry *274*, 13205-13210.

Franzoso, G., Carlson, L., Xing, L., Poljak, L., Shores, E.W., Brown, K.D., Leonardi, A., Tran, T., Boyce, B.F., and Siebenlist, U. (1997). Requirement for NF-kappaB in osteoclast and B-cell development. Genes & development *11*, 3482-3496.

Frattini, A., Orchard, P.J., Sobacchi, C., Giliani, S., Abinun, M., Mattsson, J.P., Keeling, D.J., Andersson, A.K., Wallbrandt, P., Zecca, L.*, et al.* (2000). Defects in TCIRG1 subunit of the vacuolar proton pump are responsible for a subset of human autosomal recessive osteopetrosis. Nature genetics *25*, 343-346.

Fredholm, B.B., Abbracchio, M.P., Burnstock, G., Daly, J.W., Harden, T.K., Jacobson, K.A., Leff, P., and Williams, M. (1994). Nomenclature and classification of purinoceptors. Pharmacological reviews *46*, 143-156.

Frost, H.M. (2001). From Wolff's law to the Utah paradigm: insights about bone physiology and its clinical applications. The Anatomical record *262*, 398-419.

Fuller, S.J., Stokes, L., Skarratt, K.K., Gu, B.J., and Wiley, J.S. (2009). Genetics of the P2X7 receptor and human disease. Purinergic signalling *5*, 257-262.

Garcia-Marcos, M., Pochet, S., Marino, A., and Dehaye, J.P. (2006). P2X7 and phospholipid signalling: the search of the "missing link" in epithelial cells. Cellular signalling *18*, 2098-2104.

Gartland, A. (2012). P2X receptors in bone. Wiley Interdisciplinary Reviews: Membrane Transport and Signaling *1*, 221-227.

Gartland, A., Buckley, K.A., Bowler, W.B., and Gallagher, J.A. (2003a). Blockade of the pore-forming P2X7 receptor inhibits formation of multinucleated human osteoclasts in vitro. Calcified tissue international *73*, 361-369.

Gartland, A., Buckley, K.A., Hipskind, R.A., Bowler, W.B., and Gallagher, J.A. (2003b). P2 receptors in bone--modulation of osteoclast formation and activity via P2X7 activation. Crit Rev Eukaryot Gene Expr *13*, 237-242.

Gartland, A., Buckley, K.A., Hipskind, R.A., Perry, M.J., Tobias, J.H., Buell, G., Chessell, I., Bowler, W.B., and Gallagher, J.A. (2003c). Multinucleated osteoclast formation in vivo and in vitro by P2X7 receptor-deficient mice. Crit Rev Eukaryot Gene Expr *13*, 243-253.

Gartland, A., Ginty, A.F., Gallagher, J.A., and Bowler, W.B. (1999). Activation of P2X7 receptors by human osteoclastoma modulates bone resorption. Calci Tissue Int *64*, abstract.

Gartland, A., Hipskind, R.A., Gallagher, J.A., and Bowler, W.B. (2001). Expression of a P2X7 receptor by a subpopulation of human osteoblasts. Journal of bone and mineral research : the official journal of the American Society for Bone and Mineral Research *16*, 846-856.

Gartland, A., Orriss, I.R., Rumney, R.M., Bond, A.P., Arnett, T., and Gallagher, J.A. (2012a). Purinergic signalling in osteoblasts. Frontiers in bioscience : a journal and virtual library *17*, 16-29.

Gartland, A., Skarratt, K.K., Hocking, L.J., Parsons, C., Stokes, L., Jorgensen, N.R., Fraser, W.D., Reid, D.M., Gallagher, J.A., and Wiley, J.S. (2012b). Polymorphisms in the P2X7 receptor gene are associated with low lumbar spine bone mineral density and accelerated bone loss in post-menopausal women. European journal of human genetics : EJHG *20*, 559-564.

Gelb, B.D., Shi, G.P., Chapman, H.A., and Desnick, R.J. (1996). Pycnodysostosis, a lysosomal disease caused by cathepsin K deficiency. Science *273*, 1236-1238.

Ghinassi, B., Martelli, F., Verrucci, M., D'Amore, E., Migliaccio, G., Vannucchi, A.M., Hoffman, R., and Migliaccio, A.R. (2009). Evidence for organ-specific stem cell microenvironments. J Cell Physiol *223*, 460-470.

Gidlof, O., Smith, J.G., Melander, O., Lovkvist, H., Hedblad, B., Engstrom, G., Nilsson, P., Carlson, J., Berglund, G., Olsson, S.*, et al.* (2012). A common missense variant in the ATP receptor P2X7 is associated with reduced risk of cardiovascular events. PloS one *7*, e37491.

Goncalves, R.G., Gabrich, L., Rosario, A., Jr., Takiya, C.M., Ferreira, M.L., Chiarini, L.B., Persechini, P.M., Coutinho-Silva, R., and Leite, M., Jr. (2006). The role of purinergic P2X7 receptors in the inflammation and fibrosis of unilateral ureteral obstruction in mice. Kidney international *70*, 1599-1606.

Gorodeski, G.I. (2004). Estrogen attenuates P2X7-R-mediated apoptosis of uterine cervical cells by blocking calcium influx. Nucleosides, nucleotides & nucleic acids *23*, 1287-1293.

Gowen, M., Lazner, F., Dodds, R., Kapadia, R., Feild, J., Tavaria, M., Bertoncello, I., Drake, F., Zavarselk, S., Tellis, I.*, et al.* (1999). Cathepsin K knockout mice develop osteopetrosis due to a deficit in matrix degradation but not

demineralization. Journal of bone and mineral research : the official journal of the American Society for Bone and Mineral Research *14*, 1654-1663.

Grahames, C.B., Michel, A.D., Chessell, I.P., and Humphrey, P.P. (1999). Pharmacological characterization of ATP- and LPS-induced IL-1beta release in human monocytes. British journal of pharmacology *127*, 1915-1921.

Greig, A.V., Linge, C., Healy, V., Lim, P., Clayton, E., Rustin, M.H., McGrouther, D.A., and Burnstock, G. (2003). Expression of purinergic receptors in non-melanoma skin cancers and their functional roles in A431 cells. The Journal of investigative dermatology *121*, 315-327.

Griffin, W.S. (2006). Inflammation and neurodegenerative diseases. Am J Clin Nutr *83*, 470S-474S.

Grigoriadis, A.E., Wang, Z.Q., Cecchini, M.G., Hofstetter, W., Felix, R., Fleisch, H.A., and Wagner, E.F. (1994). c-Fos: a key regulator of osteoclast-macrophage lineage determination and bone remodeling. Science *266*, 443-448.

Grilli, S. (2006). Tamoxifen (TAM): the dispute goes on. Annali dell'Istituto superiore di sanita *42*, 170-173.

Groschel-Stewart, U., Bardini, M., Robson, T., and Burnstock, G. (1999). P2X receptors in the rat duodenal villus. Cell Tissue Res *297*, 111-117.

Gu, B.J., Sluyter, R., Skarratt, K.K., Shemon, A.N., Dao-Ung, L.-P., Fuller, S.J., Barden, J.A., Clarke, A.L., Petrou, S., and Wiley, J.S. (2004a). An Arg^{307} to Gln polymorphism within the ATP-binding site causes loss of function of the human $P2X_7$ receptor. The Journal of biological chemistry *279*, 31287-31295.

Gu, B.J., Sluyter, R., Skarratt, K.K., Shemon, A.N., Dao-Ung, L.P., Fuller, S.J., Barden, J.A., Clarke, A.L., Petrou, S., and Wiley, J.S. (2004b). An Arg307 to Gln polymorphism within the ATP-binding site causes loss of function of the human P2X7 receptor. The Journal of biological chemistry *279*, 31287-31295.

Gu, B.J., Zhang, W., Worthington, R.A., Sluyter, R., Dao-Ung, P., Petrou, S., Barden, J.A., and Wiley, J.S. (2001). A Glu-496 to Ala polymorphism leads to loss of function of the human $P2X_7$ receptor. The Journal of biological chemistry *276*, 11135-11142.

Gu, B.J., Zhang, W.Y., Bendall, L.J., Chessell, I.P., Buell, G.N., and Wiley, J.S. (2000). Expression of P2X(7) purinoceptors on human lymphocytes and monocytes: evidence for nonfunctional P2X(7) receptors. Am J Physiol Cell Physiol *279*, C1189-1197.

Gudipaty, L., Humphreys, B.D., Buell, G., and Dubyak, G.R. (2001). Regulation of P2X(7) nucleotide receptor function in human monocytes by extracellular ions and receptor density. Am J Physiol Cell Physiol *280*, C943-953.

Hansen, R.R., Nielsen, C.K., Nasser, A., Thomsen, S.I., Eghorn, L.F., Pham, Y., Schulenburg, C., Syberg, S., Ding, M., Stojilkovic, S.S.*, et al.* (2011). P2X7 receptor-deficient mice are susceptible to bone cancer pain. Pain *152*, 1766-1776.

Harada, H., Chan, C.M., Loesch, A., Unwin, R., and Burnstock, G. (2000). Induction of proliferation and apoptotic cell death via P2Y and P2X receptors, respectively, in rat glomerular mesangial cells. Kidney international *57*, 949-958.

Harada, S., and Rodan, G.A. (2003). Control of osteoblast function and regulation of bone mass. Nature *423*, 349-355.

Hayato, R., Ohtubo, Y., and Yoshii, K. (2007). Functional expression of ionotropic purinergic receptors on mouse taste bud cells. The Journal of physiology *584*, 473-488.

Hayman, A.R., Jones, S.J., Boyde, A., Foster, D., Colledge, W.H., Carlton, M.B., Evans, M.J., and Cox, T.M. (1996). Mice lacking tartrate-resistant acid

phosphatase (Acp 5) have disrupted endochondral ossification and mild osteopetrosis. Development *122*, 3151-3162.

Hazama, R., Qu, X., Yokoyama, K., Tanaka, C., Kinoshita, E., He, J., Takahashi, S., Tohyama, K., Yamamura, H., and Tohyama, Y. (2009). ATP-induced osteoclast function: the formation of sealing-zone like structure and the secretion of lytic granules via microtubule-deacetylation under the control of Syk. Genes to cells : devoted to molecular & cellular mechanisms *14*, 871-884.

Hickman, S.E., el Khoury, J., Greenberg, S., Schieren, I., and Silverstein, S.C. (1994). P2Z adenosine triphosphate receptor activity in cultured human monocyte-derived macrophages. Blood *84*, 2452-2456.

Hiken, J.F., and Steinberg, T.H. (2004). ATP downregulates P2X7 and inhibits osteoclast formation in RAW cells. Am J Physiol Cell Physiol *287*, C403-412.

Hillman, K.A., Burnstock, G., and Unwin, R.J. (2005). The P2X7 ATP receptor in the kidney: a matter of life or death? Nephron Exp Nephrol *101*, e24-30.

Hoebertz, A., Townsend-Nicholson, A., Glass, R., Burnstock, G., and Arnett, T.R. (2000). Expression of P2 receptors in bone and cultured bone cells. Bone *27*, 503-510.

Hoffmann, C., Moro, S., Nicholas, R.A., Harden, T.K., and Jacobson, K.A. (1999). The role of amino acids in extracellular loops of the human P2Y1 receptor in surface expression and activation processes. The Journal of biological chemistry *274*, 14639-14647.

Hollberg, K., Hultenby, K., Hayman, A., Cox, T., and Andersson, G. (2002). Osteoclasts from mice deficient in tartrate-resistant acid phosphatase have altered ruffled borders and disturbed intracellular vesicular transport. Exp Cell Res *279*, 227-238.

Holton, P. (1959). The liberation of adenosine triphosphate on antidromic stimulation of sensory nerves. The Journal of physiology *145*, 494-504.

Honore, P., Donnelly-Roberts, D., Namovic, M.T., Hsieh, G., Zhu, C.Z., Mikusa, J.P., Hernandez, G., Zhong, C., Gauvin, D.M., Chandran, P.*, et al.* (2006). A-740003 [N-(1-{[(cyanoimino)(5-quinolinylamino) methyl]amino}-2,2-dimethylpropyl)-2-(3,4-dimethoxyphenyl)acetamide], a novel and selective P2X7 receptor antagonist, dose-dependently reduces neuropathic pain in the rat. The Journal of pharmacology and experimental therapeutics *319*, 1376-1385.

Hou, G.Q., Guo, C., Song, G.H., Fang, N., Fan, W.J., Chen, X.D., Yuan, L., and Wang, Z.Q. (2013). Lipopolysaccharide (LPS) promotes osteoclast differentiation and activation by enhancing the MAPK pathway and COX-2 expression in RAW264.7 cells. International journal of molecular medicine.

Hughes, D.E., Dai, A., Tiffee, J.C., Li, H.H., Mundy, G.R., and Boyce, B.F. (1996). Estrogen promotes apoptosis of murine osteoclasts mediated by TGF-beta. Nat Med *2*, 1132-1136.

Hughes, J.P., Hatcher, J.P., and Chessell, I.P. (2007). The role of P2X(7) in pain and inflammation. Purinergic signalling *3*, 163-169.

Humphreys, B.D., and Dubyak, G.R. (1998). Modulation of P2X7 nucleotide receptor expression by pro- and anti-inflammatory stimuli in THP-1 monocytes. J Leukoc Biol *64*, 265-273.

Humphreys, B.D., Virginio, C., Surprenant, A., Rice, J., and Dubyak, G.R. (1998). Isoquinolines as antagonists of the P2X7 nucleotide receptor: high selectivity for the human versus rat receptor homologues. Molecular pharmacology *54*, 22-32.

Husted, L.B., Harslof, T., Stenkjaer, L., Carstens, M., Jorgensen, N.R., and Langdahl, B.L. (2013). Functional polymorphisms in the P2X7 receptor gene are associated with osteoporosis. Osteoporos Int *24*, 949-959.

Insogna, K.L., Sahni, M., Grey, A.B., Tanaka, S., Horne, W.C., Neff, L., Mitnick, M., Levy, J.B., and Baron, R. (1997). Colony-stimulating factor-1 induces cytoskeletal reorganization and c-src-dependent tyrosine phosphorylation of selected cellular proteins in rodent osteoclasts. The Journal of clinical investigation *100*, 2476-2485.

Iotsova, V., Caamano, J., Loy, J., Yang, Y., Lewin, A., and Bravo, R. (1997). Osteopetrosis in mice lacking NF-kappaB1 and NF-kappaB2. Nat Med *3*, 1285-1289.

Ishii, K., Kaneda, M., Li, H., Rockland, K.S., and Hashikawa, T. (2003). Neuron-specific distribution of P2X7 purinergic receptors in the monkey retina. The Journal of comparative neurology *459*, 267-277.

Ishimi, Y., Miyaura, C., Jin, C.H., Akatsu, T., Abe, E., Nakamura, Y., Yamaguchi, A., Yoshiki, S., Matsuda, T., Hirano, T.*, et al.* (1990). IL-6 is produced by osteoblasts and induces bone resorption. Journal of immunology *145*, 3297-3303.

Itoh, K., Udagawa, N., Katagiri, T., Iemura, S., Ueno, N., Yasuda, H., Higashio, K., Quinn, J.M., Gillespie, M.T., Martin, T.J.*, et al.* (2001). Bone morphogenetic protein 2 stimulates osteoclast differentiation and survival supported by receptor activator of nuclear factor-kappaB ligand. Endocrinology *142*, 3656-3662.

Iwaniec, U.T., Moore, K., Rivera, M.F., Myers, S.E., Vanegas, S.M., and Wronski, T.J. (2007). A comparative study of the bone-restorative efficacy of anabolic agents in aged ovariectomized rats. Osteoporos Int *18*, 351-362.

Iwaniec, U.T., Yuan, D., Power, R.A., and Wronski, T.J. (2006). Strain-dependent variations in the response of cancellous bone to ovariectomy in mice. Journal of bone and mineral research : the official journal of the American Society for Bone and Mineral Research *21*, 1068-1074.

Jacobson, K.A., Balasubramanian, R., Deflorian, F., and Gao, Z.G. (2012). G protein-coupled adenosine (P1) and P2Y receptors: ligand design and receptor interactions. Purinergic signalling *8*, 419-436.

Jee, W. (1989). The skeletal tissues (Baltimore, Urban and Schwartzenberg).

Jensen, E.D., Pham, L., Billington, C.J., Jr., Espe, K., Carlson, A.E., Westendorf, J.J., Petryk, A., Gopalakrishnan, R., and Mansky, K. (2010). Bone morphogenic protein 2 directly enhances differentiation of murine osteoclast precursors. Journal of cellular biochemistry *109*, 672-682.

Jiang, L.H., Mackenzie, A.B., North, R.A., and Surprenant, A. (2000a). Brilliant blue G selectively blocks ATP-gated rat P2X(7) receptors. Molecular pharmacology *58*, 82-88.

Jiang, L.H., Rassendren, F., Mackenzie, A., Zhang, Y.H., Surprenant, A., and North, R.A. (2005). N-methyl-D-glucamine and propidium dyes utilize different permeation pathways at rat P2X(7) receptors. Am J Physiol Cell Physiol *289*, C1295-1302.

Jiang, L.H., Rassendren, F., Surprenant, A., and North, R.A. (2000b). Identification of amino acid residues contributing to the ATP-binding site of a purinergic P2X receptor. The Journal of biological chemistry *275*, 34190-34196.

Jiang, Q., Guo, D., Lee, B.X., Van Rhee, A.M., Kim, Y.C., Nicholas, R.A., Schachter, J.B., Harden, T.K., and Jacobson, K.A. (1997). A mutational analysis of residues essential for ligand recognition at the human P2Y1 receptor. Molecular pharmacology *52*, 499-507.

Jilka, R.L., Hangoc, G., Girasole, G., Passeri, G., Williams, D.C., Abrams, J.S., Boyce, B., Broxmeyer, H., and Manolagas, S.C. (1992). Increased osteoclast development after estrogen loss: mediation by interleukin-6. Science *257*, 88-91.

Jorgensen, N.R., Adinolfi, E., Orriss, I., and Schwarz, P. (2013). Purinergic signaling in bone. Journal of osteoporosis *2013*, 673684.

Jorgensen, N.R., Henriksen, Z., Sorensen, O.H., Eriksen, E.F., Civitelli, R., and Steinberg, T.H. (2002). Intercellular calcium signaling occurs between human osteoblasts and osteoclasts and requires activation of osteoclast P2X7 receptors. The Journal of biological chemistry *277*, 7574-7580.

Jorgensen, N.R., Husted, L.B., Skarratt, K.K., Stokes, L., Tofteng, C.L., Kvist, T., Jensen, J.E., Eiken, P., Brixen, K., Fuller, S.*, et al.* (2012). Single-nucleotide polymorphisms in the P2X7 receptor gene are associated with post-menopausal bone loss and vertebral fractures. European journal of human genetics : EJHG *20*, 675-681.

Kaczmarek-Hajek, K., Lorinczi, E., Hausmann, R., and Nicke, A. (2012). Molecular and functional properties of P2X receptors--recent progress and persisting challenges. Purinergic signalling *8*, 375-417.

Kajiya, H. (2012). Calcium signaling in osteoclast differentiation and bone resorption. Adv Exp Med Biol *740*, 917-932.

Kameda, T., Mano, H., Yuasa, T., Mori, Y., Miyazawa, K., Shiokawa, M., Nakamaru, Y., Hiroi, E., Hiura, K., Kameda, A.*, et al.* (1997). Estrogen inhibits bone resorption by directly inducing apoptosis of the bone-resorbing osteoclasts. The Journal of experimental medicine *186*, 489-495.

Kaneko, H., Arakawa, T., Mano, H., Kaneda, T., Ogasawara, A., Nakagawa, M., Toyama, Y., Yabe, Y., Kumegawa, M., and Hakeda, Y. (2000). Direct stimulation of osteoclastic bone resorption by bone morphogenetic protein (BMP)-2 and expression of BMP receptors in mature osteoclasts. Bone *27*, 479-486.

Kanis, J.A. (1996). Textbook of Osteoporosis (Wiley).

Ke, H.Z., Qi, H., Weidema, A.F., Zhang, Q., Panupinthu, N., Crawford, D.T., Grasser, W.A., Paralkar, V.M., Li, M., Audoly, L.P.*, et al.* (2003). Deletion of the P2X7 nucleotide receptor reveals its regulatory roles in bone formation and resorption. Mol Endocrinol *17*, 1356-1367.

Kellinsalmi, M., Parikka, V., Risteli, J., Hentunen, T., Leskela, H.V., Lehtonen, S., Selander, K., Vaananen, K., and Lehenkari, P. (2007). Inhibition of cyclooxygenase-2 down-regulates osteoclast and osteoblast differentiation and favours adipocyte formation in vitro. European journal of pharmacology *572*, 102-110.

Khakh, B.S., Bao, X.R., Labarca, C., and Lester, H.A. (1999). Neuronal P2X transmitter-gated cation channels change their ion selectivity in seconds. Nat Neurosci *2*, 322-330.

Kimble, R.B., Srivastava, S., Ross, F.P., Matayoshi, A., and Pacifici, R. (1996). Estrogen deficiency increases the ability of stromal cells to support murine osteoclastogenesis via an interleukin-1and tumor necrosis factor-mediated stimulation of macrophage colony-stimulating factor production. The Journal of biological chemistry *271*, 28890-28897.

Kitazawa, R., Kimble, R.B., Vannice, J.L., Kung, V.T., and Pacifici, R. (1994). Interleukin-1 receptor antagonist and tumor necrosis factor binding protein decrease osteoclast formation and bone resorption in ovariectomized mice. The Journal of clinical investigation *94*, 2397-2406.

Klinck, J., and Boyd, S.K. (2008). The magnitude and rate of bone loss in ovariectomized mice differs among inbred strains as determined by longitudinal in vivo micro-computed tomography. Calcified tissue international *83*, 70-79.

Koga, T., Inui, M., Inoue, K., Kim, S., Suematsu, A., Kobayashi, E., Iwata, T., Ohnishi, H., Matozaki, T., Kodama, T.*, et al.* (2004). Costimulatory signals mediated by the ITAM motif cooperate with RANKL for bone homeostasis. Nature *428*, 758-763.

Kong, Y.Y., Yoshida, H., Sarosi, I., Tan, H.L., Timms, E., Capparelli, C., Morony, S., Oliveira-dos-Santos, A.J., Van, G., Itie, A.*, et al.* (1999). OPGL is a key regulator of osteoclastogenesis, lymphocyte development and lymph-node organogenesis. Nature *397*, 315-323.

Korcok, J., Raimundo, L.N., Du, X., Sims, S.M., and Dixon, S.J. (2005). P2Y6 nucleotide receptors activate NF-kappaB and increase survival of osteoclasts. The Journal of biological chemistry *280*, 16909-16915.

Korcok, J., Raimundo, L.N., Ke, H.Z., Sims, S.M., and Dixon, S.J. (2004). Extracellular nucleotides act through P2X7 receptors to activate NF-kappaB in osteoclasts. Journal of bone and mineral research : the official journal of the American Society for Bone and Mineral Research *19*, 642-651.

Kornak, U., Kasper, D., Bosl, M.R., Kaiser, E., Schweizer, M., Schulz, A., Friedrich, W., Delling, G., and Jentsch, T.J. (2001). Loss of the ClC-7 chloride channel leads to osteopetrosis in mice and man. Cell *104*, 205-215.

Koshi, R., Coutinho-Silva, R., Cascabulho, C.M., Henrique-Pons, A., Knight, G.E., Loesch, A., and Burnstock, G. (2005). Presence of the P2X(7) purinergic receptor on immune cells that invade the rat endometrium during oestrus. J Reprod Immunol *66*, 127-140.

Koshimizu, T.A., Van Goor, F., Tomic, M., Wong, A.O., Tanoue, A., Tsujimoto, G., and Stojilkovic, S.S. (2000). Characterization of calcium signaling by purinergic receptor-channels expressed in excitable cells. Molecular pharmacology *58*, 936-945.

Krum, S.A., Miranda-Carboni, G.A., Hauschka, P.V., Carroll, J.S., Lane, T.F., Freedman, L.P., and Brown, M. (2008). Estrogen protects bone by inducing Fas ligand in osteoblasts to regulate osteoclast survival. The EMBO journal *27*, 535-545.

Kumagai, H., Sacktor, B., and Filburn, C.R. (1991). Purinergic regulation of cytosolic calcium and phosphoinositide metabolism in rat osteoblast-like osteosarcoma cells. Journal of bone and mineral research : the official journal of the American Society for Bone and Mineral Research *6*, 697-708.

Kusano, K., Miyaura, C., Inada, M., Tamura, T., Ito, A., Nagase, H., Kamoi, K., and Suda, T. (1998). Regulation of matrix metalloproteinases (MMP-2, -3, -9, and -13) by interleukin-1 and interleukin-6 in mouse calvaria: association of MMP induction with bone resorption. Endocrinology *139*, 1338-1345.

la Sala, A., Ferrari, D., Di Virgilio, F., Idzko, M., Norgauer, J., and Girolomoni, G. (2003). Alerting and tuning the immune response by extracellular nucleotides. J Leukoc Biol *73*, 339-343.

Labasi, J.M., Petrushova, N., Donovan, C., McCurdy, S., Lira, P., Payette, M.M., Brissette, W., Wicks, J.R., Audoly, L., and Gabel, C.A. (2002). Absence of the P2X7 receptor alters leukocyte function and attenuates an inflammatory response. Journal of immunology *168*, 6436-6445.

Lacey, D.L., Timms, E., Tan, H.L., Kelley, M.J., Dunstan, C.R., Burgess, T., Elliott, R., Colombero, A., Elliott, G., Scully, S.*, et al.* (1998). Osteoprotegerin ligand is a cytokine that regulates osteoclast differentiation and activation. Cell *93*, 165-176.

Lakkakorpi, P., Tuukkanen, J., Hentunen, T., Jarvelin, K., and Vaananen, K. (1989). Organization of osteoclast microfilaments during the attachment to bone surface in vitro. Journal of bone and mineral research : the official journal of the American Society for Bone and Mineral Research *4*, 817-825.

Lassus, J., Waris, V., Xu, J.W., Li, T.F., Hao, J., Nietosvaara, Y., Santavirta, S., and Konttinen, Y.T. (2000). Increased interleukin-8 (IL-8) expression is related to aseptic loosening of total hip replacement. Archives of orthopaedic and trauma surgery *120*, 328-332.

Le Mouellic, H., Lallemand, Y., and Brulet, P. (1990). Targeted replacement of the homeobox gene Hox-3.1 by the Escherichia coli lacZ in mouse chimeric embryos. Proceedings of the National Academy of Sciences of the United States of America *87*, 4712-4716.

Leipziger, J. (2003). Control of epithelial transport via luminal P2 receptors. American journal of physiology Renal physiology *284*, F419-432.

Lenertz, L.Y., Gavala, M.L., Zhu, Y., and Bertics, P.J. (2011). Transcriptional control mechanisms associated with the nucleotide receptor P2X7, a critical regulator of immunologic, osteogenic, and neurologic functions. Immunol Res *50*, 22-38.

Li, H., Hong, S., Qian, J., Zheng, Y., Yang, J., and Yi, Q. (2010). Cross talk between the bone and immune systems: osteoclasts function as antigen-presenting cells and activate CD4+ and CD8+ T cells. Blood *116*, 210-217.

Li, J., Liu, D., Ke, H.Z., Duncan, R.L., and Turner, C.H. (2005). The P2X7 nucleotide receptor mediates skeletal mechanotransduction. The Journal of biological chemistry *280*, 42952-42959.

Li, J., Meyer, R., Duncan, R.L., and Turner, C.H. (2009). P2X7 nucleotide receptor plays an important role in callus remodeling during fracture repair. Calcified tissue international *84*, 405-412.

Li, X., Udagawa, N., Itoh, K., Suda, K., Murase, Y., Nishihara, T., Suda, T., and Takahashi, N. (2002). p38 MAPK-mediated signals are required for inducing osteoclast differentiation but not for osteoclast function. Endocrinology *143*, 3105-3113.

Lister, M.F., Sharkey, J., Sawatzky, D.A., Hodgkiss, J.P., Davidson, D.J., Rossi, A.G., and Finlayson, K. (2007). The role of the purinergic P2X7 receptor in inflammation. Journal of inflammation *4*, 5.

Livak, K.J., and Schmittgen, T.D. (2001). Analysis of relative gene expression data using real-time quantitative PCR and the 2(-Delta Delta C(T)) Method. Methods *25*, 402-408.

Lomaga, M.A., Yeh, W.C., Sarosi, I., Duncan, G.S., Furlonger, C., Ho, A., Morony, S., Capparelli, C., Van, G., Kaufman, S.*, et al.* (1999). TRAF6 deficiency results in osteopetrosis and defective interleukin-1, CD40, and LPS signaling. Genes & development *13*, 1015-1024.

Lorenzo, J.A., Naprta, A., Rao, Y., Alander, C., Glaccum, M., Widmer, M., Gronowicz, G., Kalinowski, J., and Pilbeam, C.C. (1998). Mice lacking the type I interleukin-1 receptor do not lose bone mass after ovariectomy. Endocrinology *139*, 3022-3025.

Lucae, S., Salyakina, D., Barden, N., Harvey, M., Gagne, B., Labbe, M., Binder, E.B., Uhr, M., Paez-Pereda, M., Sillaber, I.*, et al.* (2006). P2RX7, a gene coding for a purinergic ligand-gated ion channel, is associated with major depressive disorder. Human molecular genetics *15*, 2438-2445.

Luxenburg, C., Geblinger, D., Klein, E., Anderson, K., Hanein, D., Geiger, B., and Addadi, L. (2007). The architecture of the adhesive apparatus of cultured osteoclasts: from podosome formation to sealing zone assembly. PloS one *2*, e179.

Machado do Reis, L., Kessler, C.B., Adams, D.J., Lorenzo, J., Jorgetti, V., and Delany, A.M. (2008). Accentuated osteoclastic response to parathyroid hormone undermines bone mass acquisition in osteonectin-null mice. Bone *43*, 264-273.

MacKenzie, A., Wilson, H.L., Kiss-Toth, E., Dower, S.K., North, R.A., and Surprenant, A. (2001). Rapid secretion of interleukin-1beta by microvesicle shedding. Immunity *15*, 825-835.

Malgaroli, A., Meldolesi, J., Zallone, A.Z., and Teti, A. (1989). Control of cytosolic free calcium in rat and chicken osteoclasts. The role of extracellular calcium and calcitonin. The Journal of biological chemistry *264*, 14342-14347.

Manolagas, S.C. (2000). Birth and death of bone cells: basic regulatory mechanisms and implications for the pathogenesis and treatment of osteoporosis. Endocr Rev *21*, 115-137.

Manolagas, S.C., Kousteni, S., and Jilka, R.L. (2002). Sex steroids and bone. Recent progress in hormone research *57*, 385-409.

Mariathasan, S., Weiss, D.S., Newton, K., McBride, J., O'Rourke, K., Roose-Girma, M., Lee, W.P., Weinrauch, Y., Monack, D.M., and Dixit, V.M. (2006). Cryopyrin activates the inflammasome in response to toxins and ATP. Nature *440*, 228-232.

Marin-Garcia, P., Sanchez-Nogueiro, J., Gomez-Villafuertes, R., Leon, D., and Miras-Portugal, M.T. (2008). Synaptic terminals from mice midbrain exhibit functional P2X7 receptor. Neuroscience *151*, 361-373.

Marks, S.C., Jr., and Lane, P.W. (1976). Osteopetrosis, a new recessive skeletal mutation on chromosome 12 of the mouse. The Journal of heredity *67*, 11-18.

Martin-Millan, M., Almeida, M., Ambrogini, E., Han, L., Zhao, H., Weinstein, R.S., Jilka, R.L., O'Brien, C.A., and Manolagas, S.C. (2010). The estrogen receptor-alpha in osteoclasts mediates the protective effects of estrogens on cancellous but not cortical bone. Mol Endocrinol *24*, 323-334.

Masin, M., Young, C., Lim, K., Barnes, S.J., Xu, X.J., Marschall, V., Brutkowski, W., Mooney, E.R., Gorecki, D.C., and Murrell-Lagnado, R. (2012). Expression, assembly and function of novel C-terminal truncated variants of the mouse P2X7 receptor: re-evaluation of P2X7 knockouts. British journal of pharmacology *165*, 978-993.

McCabe, N.P., Kerr, B.A., Madajka, M., Vasanji, A., and Byzova, T.V. (2011). Augmented osteolysis in SPARC-deficient mice with bone-residing prostate cancer. Neoplasia *13*, 31-39.

McHugh, K.P., Hodivala-Dilke, K., Zheng, M.H., Namba, N., Lam, J., Novack, D., Feng, X., Ross, F.P., Hynes, R.O., and Teitelbaum, S.L. (2000). Mice lacking beta3 integrins are osteosclerotic because of dysfunctional osteoclasts. The Journal of clinical investigation *105*, 433-440.

McHugh, S.M., Roman, S., Davis, B., Koch, A., Pickett, A.M., Richardson, J.C., Miller, S.R., Wetten, S., Cox, C.J., Karpe, F.*, et al.* (2012). Effects of genetic variation in the P2RX7 gene on pharmacodynamics of a P2X(7) receptor antagonist: a prospective genotyping approach. British journal of clinical pharmacology *74*, 376-380.

McQuillin, A., Bass, N.J., Choudhury, K., Puri, V., Kosmin, M., Lawrence, J., Curtis, D., and Gurling, H.M. (2009). Case-control studies show that a non-

conservative amino-acid change from a glutamine to arginine in the P2RX7 purinergic receptor protein is associated with both bipolar- and unipolar-affective disorders. Molecular psychiatry *14*, 614-620.

Mebius, R.E., and Kraal, G. (2005). Structure and function of the spleen. Nat Rev Immunol *5*, 606-616.

Mellstrom, D., Vandenput, L., Mallmin, H., Holmberg, A.H., Lorentzon, M., Oden, A., Johansson, H., Orwoll, E.S., Labrie, F., Karlsson, M.K.*, et al.* (2008). Older men with low serum estradiol and high serum SHBG have an increased risk of fractures. Journal of bone and mineral research : the official journal of the American Society for Bone and Mineral Research *23*, 1552-1560.

Melton, L.J., 3rd, Atkinson, E.J., O'Connor, M.K., O'Fallon, W.M., and Riggs, B.L. (1998). Bone density and fracture risk in men. Journal of bone and mineral research : the official journal of the American Society for Bone and Mineral Research *13*, 1915-1923.

Menaa, C., Reddy, S.V., Kurihara, N., Maeda, H., Anderson, D., Cundy, T., Cornish, J., Singer, F.R., Bruder, J.M., and Roodman, G.D. (2000). Enhanced RANK ligand expression and responsivity of bone marrow cells in Paget's disease of bone. The Journal of clinical investigation *105*, 1833-1838.

Mentaverri, R., Yano, S., Chattopadhyay, N., Petit, L., Kifor, O., Kamel, S., Terwilliger, E.F., Brazier, M., and Brown, E.M. (2006). The calcium sensing receptor is directly involved in both osteoclast differentiation and apoptosis. FASEB journal : official publication of the Federation of American Societies for Experimental Biology *20*, 2562-2564.

Michel, A.D., Xing, M., Thompson, K.M., Jones, C.A., and Humphrey, P.P. (2006). Decavanadate, a P2X receptor antagonist, and its use to study ligand interactions with P2X7 receptors. European journal of pharmacology *534*, 19-29.

Miller, C.M., Boulter, N.R., Fuller, S.J., Zakrzewski, A.M., Lees, M.P., Saunders, B.M., Wiley, J.S., and Smith, N.C. (2011a). The role of the P2X(7) receptor in infectious diseases. PLoS pathogens *7*, e1002212.

Miller, C.M., Zakrzewski, A.M., Ikin, R.J., Boulter, N.R., Katrib, M., Lees, M.P., Fuller, S.J., Wiley, J.S., and Smith, N.C. (2011b). Dysregulation of the inflammatory response to the parasite, Toxoplasma gondii, in P2X7 receptor-deficient mice. Int J Parasitol *41*, 301-308.

Mio, K., Kubo, Y., Ogura, T., Yamamoto, T., and Sato, C. (2005). Visualization of the trimeric P2X2 receptor with a crown-capped extracellular domain. Biochemical and biophysical research communications *337*, 998-1005.

Miras-Portugal, M.T., Diaz-Hernandez, M., Giraldez, L., Hervas, C., Gomez-Villafuertes, R., Sen, R.P., Gualix, J., and Pintor, J. (2003). P2X7 receptors in rat brain: presence in synaptic terminals and granule cells. Neurochem Res *28*, 1597-1605.

Miyazaki, T., Iwasawa, M., Nakashima, T., Mori, S., Shigemoto, K., Nakamura, H., Katagiri, H., Takayanagi, H., and Tanaka, S. (2012). Intracellular and extracellular ATP coordinately regulate the inverse correlation between osteoclast survival and bone resorption. The Journal of biological chemistry *287*, 37808-37823.

Modderman, W.E., Weidema, A.F., Vrijheid-Lammers, T., Wassenaar, A.M., and Nijweide, P.J. (1994). Permeabilization of cells of hemopoietic origin by extracellular ATP4-: elimination of osteoclasts, macrophages, and their precursors from isolated bone cell populations and fetal bone rudiments. Calcified tissue international *55*, 141-150.

Monif, M., Burnstock, G., and Williams, D.A. (2010). Microglia: proliferation and activation driven by the P2X7 receptor. The international journal of biochemistry & cell biology *42*, 1753-1756.

Moores, T.S., Hasdemir, B., Vega-Riveroll, L., Deuchars, J., and Parson, S.H. (2005). Properties of presynaptic P2X7-like receptors at the neuromuscular junction. Brain research *1034*, 40-50.

Naemsch, L.N., Dixon, S.J., and Sims, S.M. (2001). Activity-dependent development of P2X7 current and Ca2+ entry in rabbit osteoclasts. The Journal of biological chemistry *276*, 39107-39114.

Naemsch, L.N., Weidema, A.F., Sims, S.M., Underhill, T.M., and Dixon, S.J. (1999). P2X(4) purinoceptors mediate an ATP-activated, non-selective cation current in rabbit osteoclasts. Journal of cell science *112 (Pt 23)*, 4425-4435.

Naito, A., Azuma, S., Tanaka, S., Miyazaki, T., Takaki, S., Takatsu, K., Nakao, K., Nakamura, K., Katsuki, M., Yamamoto, T.*, et al.* (1999). Severe osteopetrosis, defective interleukin-1 signalling and lymph node organogenesis in TRAF6-deficient mice. Genes to cells : devoted to molecular & cellular mechanisms *4*, 353-362.

Nakamura, E., Uezono, Y., Narusawa, K., Shibuya, I., Oishi, Y., Tanaka, M., Yanagihara, N., Nakamura, T., and Izumi, F. (2000). ATP activates DNA synthesis by acting on P2X receptors in human osteoblast-like MG-63 cells. Am J Physiol Cell Physiol *279*, C510-519.

Nakamura, T., Imai, Y., Matsumoto, T., Sato, S., Takeuchi, K., Igarashi, K., Harada, Y., Azuma, Y., Krust, A., Yamamoto, Y.*, et al.* (2007). Estrogen prevents bone loss via estrogen receptor alpha and induction of Fas ligand in osteoclasts. Cell *130*, 811-823.

Nelson, D.W., Gregg, R.J., Kort, M.E., Perez-Medrano, A., Voight, E.A., Wang, Y., Grayson, G., Namovic, M.T., Donnelly-Roberts, D.L., Niforatos, W.*, et al.* (2006). Structure-activity relationship studies on a series of novel, substituted 1-benzyl-5-phenyltetrazole P2X7 antagonists. Journal of medicinal chemistry *49*, 3659-3666.

Nicholson, G.C., Moseley, J.M., Sexton, P.M., Mendelsohn, F.A., and Martin, T.J. (1986). Abundant calcitonin receptors in isolated rat osteoclasts. Biochemical and autoradiographic characterization. The Journal of clinical investigation *78*, 355-360.

Nicke, A., Baumert, H.G., Rettinger, J., Eichele, A., Lambrecht, G., Mutschler, E., and Schmalzing, G. (1998). P2X1 and P2X3 receptors form stable trimers: a novel structural motif of ligand-gated ion channels. The EMBO journal *17*, 3016-3028.

Nicke, A., Kuan, Y.H., Masin, M., Rettinger, J., Marquez-Klaka, B., Bender, O., Gorecki, D.C., Murrell-Lagnado, R.D., and Soto, F. (2009). A functional P2X7 splice variant with an alternative transmembrane domain 1 escapes gene inactivation in P2X7 knock-out mice. The Journal of biological chemistry *284*, 25813-25822.

North, R.A. (2002). Molecular physiology of P2X receptors. Physiological reviews *82*, 1013-1067.

Novack, D.V., and Teitelbaum, S.L. (2008). The osteoclast: friend or foe? Annual review of pathology *3*, 457-484.

Ohlendorff, S.D., Tofteng, C.L., Jensen, J.-E.B., Petersen, S., Civitelli, R., Fenger, M., Abrahamsen, B., Hermann, A.P., Eiken, P., and Jorgensen, N.R. (2007a). Single nucleotide polymorphisms in the $P2X_7$ gene are associated to

fracture risk and to effect estrogen treatment. Pharmacogenetics and genomics *17*, 555-567.

Ohlendorff, S.D., Tofteng, C.L., Jensen, J.E., Petersen, S., Civitelli, R., Fenger, M., Abrahamsen, B., Hermann, A.P., Eiken, P., and Jorgensen, N.R. (2007b). Single nucleotide polymorphisms in the P2X7 gene are associated to fracture risk and to effect of estrogen treatment. Pharmacogenetics and genomics *17*, 555-567.

Orriss, I., Syberg, S., Wang, N., Robaye, B., Gartland, A., Jorgensen, N., Arnett, T., and Boeynaems, J.M. (2011a). Bone phenotypes of P2 receptor knockout mice. Frontiers in bioscience *3*, 1038-1046.

Orriss, I.R., Burnstock, G., and Arnett, T.R. (2010). Purinergic signalling and bone remodelling. Current opinion in pharmacology *10*, 322-330.

Orriss, I.R., Wang, N., Burnstock, G., Arnett, T.R., Gartland, A., Robaye, B., and Boeynaems, J.M. (2011b). The P2Y(6) receptor stimulates bone resorption by osteoclasts. Endocrinology *152*, 3706-3716.

Orwoll, E.S., and Klein, R.F. (1995). Osteoporosis in men. Endocr Rev *16*, 87-116.

Pacifici, R., Brown, C., Puscheck, E., Friedrich, E., Slatopolsky, E., Maggio, D., McCracken, R., and Avioli, L.V. (1991). Effect of surgical menopause and estrogen replacement on cytokine release from human blood mononuclear cells. Proceedings of the National Academy of Sciences of the United States of America *88*, 5134-5138.

Panupinthu, N., Rogers, J.T., Zhao, L., Solano-Flores, L.P., Possmayer, F., Sims, S.M., and Dixon, S.J. (2008). P2X7 receptors on osteoblasts couple to production of lysophosphatidic acid: a signaling axis promoting osteogenesis. The Journal of cell biology *181*, 859-871.

Parfitt, A.M. (1992). Implications of architecture for the pathogenesis and prevention of vertebral fracture. Bone *13 Suppl 2*, S41-47.

Parfitt, A.M. (1994). Osteonal and hemi-osteonal remodeling: the spatial and temporal framework for signal traffic in adult human bone. Journal of cellular biochemistry *55*, 273-286.

Parfitt, A.M. (2002). High bone turnover is intrinsically harmful: two paths to a similar conclusion. The Parfitt view. Journal of bone and mineral research : the official journal of the American Society for Bone and Mineral Research *17*, 1558-1559; author reply 1560.

Parfitt, A.M., Mathews, C.H., Villanueva, A.R., Kleerekoper, M., Frame, B., and Rao, D.S. (1983). Relationships between surface, volume, and thickness of iliac trabecular bone in aging and in osteoporosis. Implications for the microanatomic and cellular mechanisms of bone loss. The Journal of clinical investigation *72*, 1396-1409.

Passeri, G., Girasole, G., Jilka, R.L., and Manolagas, S.C. (1993). Increased interleukin-6 production by murine bone marrow and bone cells after estrogen withdrawal. Endocrinology *133*, 822-828.

Pellegatti, P., Falzoni, S., Donvito, G., Lemaire, I., and Di Virgilio, F. (2011). P2X7 receptor drives osteoclast fusion by increasing the extracellular adenosine concentration. FASEB journal : official publication of the Federation of American Societies for Experimental Biology *25*, 1264-1274.

Pereverzev, A., Komarova, S.V., Korcok, J., Armstrong, S., Tremblay, G.B., Dixon, S.J., and Sims, S.M. (2008). Extracellular acidification enhances osteoclast

survival through an NFAT-independent, protein kinase C-dependent pathway. Bone *42*, 150-161.

Perregaux, D., and Gabel, C.A. (1994). Interleukin-1 beta maturation and release in response to ATP and nigericin. Evidence that potassium depletion mediated by these agents is a necessary and common feature of their activity. The Journal of biological chemistry *269*, 15195-15203.

Piccini, A., Carta, S., Tassi, S., Lasiglie, D., Fossati, G., and Rubartelli, A. (2008). ATP is released by monocytes stimulated with pathogen-sensing receptor ligands and induces IL-1beta and IL-18 secretion in an autocrine way. Proceedings of the National Academy of Sciences of the United States of America *105*, 8067-8072.

Piscopiello, M., Sessa, M., Anzalone, N., Castellano, R., Maisano, F., Ferrero, E., Chiesa, R., Alfieri, O., Comi, G., Ferrero, M.E.*, et al.* (2013). P2X7 receptor is expressed in human vessels and might play a role in atherosclerosis. International journal of cardiology.

Piva, R., Penolazzi, L., Lambertini, E., Giordano, S., and Gambari, R. (2005). Induction of apoptosis of human primary osteoclasts treated with a transcription factor decoy mimicking a promoter region of estrogen receptor alpha. Apoptosis : an international journal on programmed cell death *10*, 1079-1094.

Puthussery, T., and Fletcher, E.L. (2004). Synaptic localization of P2X7 receptors in the rat retina. The Journal of comparative neurology *472*, 13-23.

Ralevic, V., and Burnstock, G. (1998). Receptors for purines and pyrimidines. Pharmacological reviews *50*, 413-492.

Rassendren, F., Buell, G.N., Virginio, C., Collo, G., North, R.A., and Surprenant, A. (1997). The permeabilizing ATP receptor, P2X7. Cloning and expression of a human cDNA. The Journal of biological chemistry *272*, 5482-5486.

Reyes, J.P., Sims, S.M., and Dixon, S.J. (2011). P2 receptor expression, signaling and function in osteoclasts. Frontiers in bioscience *3*, 1101-1118.

Riggs, B.L., Khosla, S., and Melton, L.J., 3rd (1998). A unitary model for involutional osteoporosis: estrogen deficiency causes both type I and type II osteoporosis in postmenopausal women and contributes to bone loss in aging men. Journal of bone and mineral research : the official journal of the American Society for Bone and Mineral Research *13*, 763-773.

Roberts, J.A., and Evans, R.J. (2004). ATP binding at human P2X1 receptors. Contribution of aromatic and basic amino acids revealed using mutagenesis and partial agonists. The Journal of biological chemistry *279*, 9043-9055.

Robinson, L.J., Yaroslavskiy, B.B., Griswold, R.D., Zadorozny, E.V., Guo, L., Tourkova, I.L., and Blair, H.C. (2009). Estrogen inhibits RANKL-stimulated osteoclastic differentiation of human monocytes through estrogen and RANKL-regulated interaction of estrogen receptor-alpha with BCAR1 and Traf6. Exp Cell Res *315*, 1287-1301.

Roger, S., Mei, Z.Z., Baldwin, J.M., Dong, L., Bradley, H., Baldwin, S.A., Surprenant, A., and Jiang, L.H. (2009). Single nucleotide polymorphisms that were identified in affective mood disorders affect ATP-activated P2X7 receptor functions. Journal of psychiatric research *44*, 347-355.

Roger, S., and Pelegrin, P. (2011). P2X7 receptor antagonism in the treatment of cancers. Expert opinion on investigational drugs *20*, 875-880.

Roodman, G.D., and Windle, J.J. (2005). Paget disease of bone. The Journal of clinical investigation *115*, 200-208.

Rothe, L., Collin-Osdoby, P., Chen, Y., Sunyer, T., Chaudhary, L., Tsay, A., Goldring, S., Avioli, L., and Osdoby, P. (1998). Human osteoclasts and osteoclast-like cells synthesize and release high basal and inflammatory stimulated levels of the potent chemokine interleukin-8. Endocrinology *139*, 4353-4363.

Rumney, R.M.H., Wang, N., Agrawal, A., and Gartland, A. (2012). Purinergic signalling in bone. Frontiers in Endocrinology *3*.

Saftig, P., Hunziker, E., Wehmeyer, O., Jones, S., Boyde, A., Rommerskirch, W., Moritz, J.D., Schu, P., and von Figura, K. (1998). Impaired osteoclastic bone resorption leads to osteopetrosis in cathepsin-K-deficient mice. Proceedings of the National Academy of Sciences of the United States of America *95*, 13453-13458.

Sanz, J.M., and Di Virgilio, F. (2000). Kinetics and mechanism of ATP-dependent IL-1 beta release from microglial cells. Journal of immunology *164*, 4893-4898.

Saunders, B.M., Fernando, S.L., Sluyter, R., Britton, W.J., and Wiley, J.S. (2003). A loss-of-function polymorphism in the human P2X7 receptor abolishes ATP-mediated killing of mycobacteria. Journal of immunology *171*, 5442-5446.

Schlesinger, P.H., Blair, H.C., Teitelbaum, S.L., and Edwards, J.C. (1997). Characterization of the osteoclast ruffled border chloride channel and its role in bone resorption. The Journal of biological chemistry *272*, 18636-18643.

Schofl, C., Cuthbertson, K.S., Walsh, C.A., Mayne, C., Cobbold, P., von zur Muhlen, A., Hesch, R.D., and Gallagher, J.A. (1992). Evidence for P2-purinoceptors on human osteoblast-like cells. Journal of bone and mineral research : the official journal of the American Society for Bone and Mineral Research *7*, 485-491.

Schulze-Lohoff, E., Hugo, C., Rost, S., Arnold, S., Gruber, A., Brune, B., and Sterzel, R.B. (1998). Extracellular ATP causes apoptosis and necrosis of cultured mesangial cells via P2Z/P2X7 receptors. The American journal of physiology *275*, F962-971.

Schwartzberg, P.L., Xing, L., Hoffmann, O., Lowell, C.A., Garrett, L., Boyce, B.F., and Varmus, H.E. (1997). Rescue of osteoclast function by transgenic expression of kinase-deficient Src in src-/- mutant mice. Genes & development *11*, 2835-2844.

Shabbir, M., Ryten, M., Thompson, C., Mikhailidis, D., and Burnstock, G. (2008). Characterization of calcium-independent purinergic receptor-mediated apoptosis in hormone-refractory prostate cancer. BJU international *101*, 352-359.

Sharma, S., Kumar, V., Khosla, R., Kajal, N., Sarin, B., and Sehajpal, P. (2010). Association of P2X7 receptor +1513 (A-->C) polymorphism with tuberculosis in a Punjabi population. The international journal of tuberculosis and lung disease : the official journal of the International Union against Tuberculosis and Lung Disease *14*, 1159-1163.

Shemon, A.N., Sluyter, R., Fernando, S.L., Clarke, A.L., Dao-Ung, L.-P., Skarratt, K.K., Saunders, B.M., See Tan, K., Gu, B.J., Fuller, S.J*., et al.* (2006). A Thr^{357} to Ser polymorphism in homozygous and compound heterozygous subjects causes absent or reduced $P2X_7$ function and impairs ATP-induced mycobacterial killing by macrophages. The Journal of biological chemistry *281*, 2079-2086.

Simonet, W.S., Lacey, D.L., Dunstan, C.R., Kelley, M., Chang, M.S., Luthy, R., Nguyen, H.Q., Wooden, S., Bennett, L., Boone, T*., et al.* (1997). Osteoprotegerin: a novel secreted protein involved in the regulation of bone density. Cell *89*, 309-319.

Skarratt, K.K., Fuller, S.J., Sluyter, R., Dao-Ung, L.P., Gu, B.J., and Wiley, J.S. (2005). A 5' intronic splice site polymorphism leads to a null allele of the P2X7 gene in 1-2% of the Caucasian population. FEBS Lett *579*, 2675-2678.

Sluyter, R., Barden, J.A., and Wiley, J.S. (2001). Detection of P2X purinergic receptors on human B lymphocytes. Cell Tissue Res *304*, 231-236.

Sluyter, R., Shemon, A.N., Barden, J.A., and Wiley, J.S. (2004). Extracellular ATP increases cation fluxes in human erythrocytes by activation of the P2X7 receptor. The Journal of biological chemistry *279*, 44749-44755.

Sluyter, R., and Stokes, L. (2011). Significance of P2X7 receptor variants to human health and disease. Recent patents on DNA & gene sequences *5*, 41-54.

Smolen, J.S., Landewe, R., Breedveld, F.C., Dougados, M., Emery, P., Gaujoux-Viala, C., Gorter, S., Knevel, R., Nam, J., Schoels, M.*, et al.* (2010). EULAR recommendations for the management of rheumatoid arthritis with synthetic and biological disease-modifying antirheumatic drugs. Annals of the rheumatic diseases *69*, 964-975.

Sneddon, P., and Burnstock, G. (1984). Inhibition of excitatory junction potentials in guinea-pig vas deferens by alpha, beta-methylene-ATP: further evidence for ATP and noradrenaline as cotransmitters. European journal of pharmacology *100*, 85-90.

Solini, A., Chiozzi, P., Morelli, A., Fellin, R., and Di Virgilio, F. (1999). Human primary fibroblasts in vitro express a purinergic P2X7 receptor coupled to ion fluxes, microvesicle formation and IL-6 release. Journal of cell science *112 (Pt 3)*, 297-305.

Solini, A., Iacobini, C., Ricci, C., Chiozzi, P., Amadio, L., Pricci, F., Di Mario, U., Di Virgilio, F., and Pugliese, G. (2005). Purinergic modulation of mesangial extracellular matrix production: role in diabetic and other glomerular diseases. Kidney international *67*, 875-885.

Solle, M., Labasi, J., Perregaux, D.G., Stam, E., Petrushova, N., Koller, B.H., Griffiths, R.J., and Gabel, C.A. (2001). Altered cytokine production in mice lacking P2X(7) receptors. The Journal of biological chemistry *276*, 125-132.

Soriano, P., Montgomery, C., Geske, R., and Bradley, A. (1991). Targeted disruption of the c-src proto-oncogene leads to osteopetrosis in mice. Cell *64*, 693-702.

Spector, J.A., Luchs, J.S., Mehrara, B.J., Greenwald, J.A., Smith, L.P., and Longaker, M.T. (2001). Expression of bone morphogenetic proteins during membranous bone healing. Plastic and reconstructive surgery *107*, 124-134.

Sperlagh, B., Csolle, C., Ando, R.D., Goloncser, F., Kittel, A., and Baranyi, M. (2012). The role of purinergic signaling in depressive disorders. Neuropsychopharmacologia Hungarica : a Magyar Pszichofarmakologiai Egyesulet lapja = official journal of the Hungarian Association of Psychopharmacology *14*, 231-238.

Sperlagh, B., Kofalvi, A., Deuchars, J., Atkinson, L., Milligan, C.J., Buckley, N.J., and Vizi, E.S. (2002). Involvement of P2X7 receptors in the regulation of neurotransmitter release in the rat hippocampus. J Neurochem *81*, 1196-1211.

Srivastava, S., Toraldo, G., Weitzmann, M.N., Cenci, S., Ross, F.P., and Pacifici, R. (2001). Estrogen decreases osteoclast formation by down-regulating receptor activator of NF-kappa B ligand (RANKL)-induced JNK activation. The Journal of biological chemistry *276*, 8836-8840.

Srivastava, S., Weitzmann, M.N., Cenci, S., Ross, F.P., Adler, S., and Pacifici, R. (1999). Estrogen decreases TNF gene expression by blocking JNK activity and the resulting production of c-Jun and JunD. The Journal of clinical investigation *104*, 503-513.

Srivastava, S., Weitzmann, M.N., Kimble, R.B., Rizzo, M., Zahner, M., Milbrandt, J., Ross, F.P., and Pacifici, R. (1998). Estrogen blocks M-CSF gene

expression and osteoclast formation by regulating phosphorylation of Egr-1 and its interaction with Sp-1. The Journal of clinical investigation *102*, 1850-1859.

Stenbeck, G. (2002). Formation and function of the ruffled border in osteoclasts. Seminars in cell & developmental biology *13*, 285-292.

Stenbeck, G., Lawrence, K.M., and Albert, A.P. (2012). Hormone-stimulated modulation of endocytic trafficking in osteoclasts. Front Endocrinol (Lausanne) *3*, 103.

Stokes, L., Fuller, S.J., Sluyter, R., Skarratt, K.K., Gu, B.J., and Wiley, J.S. (2010). Two haplotypes of the P2X(7) receptor containing the Ala-348 to Thr polymorphism exhibit a gain-of-function effect and enhanced interleukin-1beta secretion. FASEB journal : official publication of the Federation of American Societies for Experimental Biology *24*, 2916-2927.

Stokes, L., Jiang, L.H., Alcaraz, L., Bent, J., Bowers, K., Fagura, M., Furber, M., Mortimore, M., Lawson, M., Theaker, J.*, et al.* (2006). Characterization of a selective and potent antagonist of human P2X(7) receptors, AZ11645373. British journal of pharmacology *149*, 880-887.

Su, C., Bevan, J.A., and Burnstock, G. (1971). [3H]adenosine triphosphate: release during stimulation of enteric nerves. Science *173*, 336-338.

Su, X., Floyd, D.H., Hughes, A., Xiang, J., Schneider, J.G., Uluckan, O., Heller, E., Deng, H., Zou, W., Craft, C.S.*, et al.* (2012). The ADP receptor P2RY12 regulates osteoclast function and pathologic bone remodeling. The Journal of clinical investigation *122*, 3579-3592.

Suh, B.C., Kim, J.S., Namgung, U., Ha, H., and Kim, K.T. (2001). P2X7 nucleotide receptor mediation of membrane pore formation and superoxide generation in human promyelocytes and neutrophils. Journal of immunology *166*, 6754-6763.

Sun, C., Chu, J., Singh, S., and Salter, R.D. (2009). Identification and characterization of a novel variant of the human P2X(7) receptor resulting in gain of function. Purinergic signalling *6*, 31-45.

Surprenant, A., and North, R.A. (2009). Signaling at purinergic P2X receptors. Annual review of physiology *71*, 333-359.

Surprenant, A., Rassendren, F., Kawashima, E., North, R.A., and Buell, G. (1996). The cytolytic P2Z receptor for extracellular ATP identified as a P2X receptor (P2X7). Science *272*, 735-738.

Swennen, E.L., Bast, A., and Dagnelie, P.C. (2005). Immunoregulatory effects of adenosine 5'-triphosphate on cytokine release from stimulated whole blood. Eur J Immunol *35*, 852-858.

Swirski, F.K., Nahrendorf, M., Etzrodt, M., Wildgruber, M., Cortez-Retamozo, V., Panizzi, P., Figueiredo, J.L., Kohler, R.H., Chudnovskiy, A., Waterman, P.*, et al.* (2009). Identification of splenic reservoir monocytes and their deployment to inflammatory sites. Science *325*, 612-616.

Syberg, S., Petersen, S., Beck Jensen, J.E., Gartland, A., Teilmann, J., Chessell, I., Steinberg, T.H., Schwarz, P., and Jorgensen, N.R. (2012a). Genetic Background Strongly Influences the Bone Phenotype of P2X7 Receptor Knockout Mice. Journal of osteoporosis *2012*, 391097.

Syberg, S., Schwarz, P., Petersen, S., Steinberg, T.H., Jensen, J.E., Teilmann, J., and Jorgensen, N.R. (2012b). Association between P2X7 Receptor Polymorphisms and Bone Status in Mice. Journal of osteoporosis *2012*, 637986.

Takahashi, N., Ejiri, S., Yanagisawa, S., and Ozawa, H. (2007). Regulation of osteoclast polarization. Odontology / the Society of the Nippon Dental University *95*, 1-9.

Takayanagi, H. (2009). [Molecular determinants in osteoclast differentiation and osteoimmunology]. [Rinsho ketsueki] The Japanese journal of clinical hematology *50*, 447-452.

Takayanagi, H., Kim, S., Koga, T., Nishina, H., Isshiki, M., Yoshida, H., Saiura, A., Isobe, M., Yokochi, T., Inoue, J.*, et al.* (2002). Induction and activation of the transcription factor NFATc1 (NFAT2) integrate RANKL signaling in terminal differentiation of osteoclasts. Developmental cell *3*, 889-901.

Teitelbaum, S.L., and Ross, F.P. (2003). Genetic regulation of osteoclast development and function. Nature reviews Genetics *4*, 638-649.

Tekin, D., Kayaalti, Z., Dalgic, N., Cakir, E., Soylemezoglu, T., Isin Kutlubay, B., and Aydin Kilic, B. (2010). Polymorphism in the p2x7 gene increases susceptibility to extrapulmonary tuberculosis in Turkish children. The Pediatric infectious disease journal *29*, 779-782.

Tokumitsu, H., Chijiwa, T., Hagiwara, M., Mizutani, A., Terasawa, M., and Hidaka, H. (1990). KN-62, 1-[N,O-bis(5-isoquinolinesulfonyl)-N-methyl-L-tyrosyl]-4-phenylpiperazi ne, a specific inhibitor of Ca2+/calmodulin-dependent protein kinase II. The Journal of biological chemistry *265*, 4315-4320.

Tondravi, M.M., McKercher, S.R., Anderson, K., Erdmann, J.M., Quiroz, M., Maki, R., and Teitelbaum, S.L. (1997). Osteopetrosis in mice lacking haematopoietic transcription factor PU.1. Nature *386*, 81-84.

Turner, R.T., Maran, A., Lotinun, S., Hefferan, T., Evans, G.L., Zhang, M., and Sibonga, J.D. (2001). Animal models for osteoporosis. Rev Endocr Metab Disord *2*, 117-127.

Vaira, S., Johnson, T., Hirbe, A.C., Alhawagri, M., Anwisye, I., Sammut, B., O'Neal, J., Zou, W., Weilbaecher, K.N., Faccio, R.*, et al.* (2008). RelB is the NF-kappaB subunit downstream of NIK responsible for osteoclast differentiation. Proceedings of the National Academy of Sciences of the United States of America *105*, 3897-3902.

van Furth, R., and Cohn, Z.A. (1968). The origin and kinetics of mononuclear phagocytes. The Journal of experimental medicine *128*, 415-435.

Viecilli, R.F., Katona, T.R., Chen, J., Hartsfield, J.K., Jr., and Roberts, W.E. (2009). Orthodontic mechanotransduction and the role of the P2X7 receptor. American journal of orthodontics and dentofacial orthopedics : official publication of the American Association of Orthodontists, its constituent societies, and the American Board of Orthodontics *135*, 694 e691-616; discussion 694-695.

Virginio, C., MacKenzie, A., North, R.A., and Surprenant, A. (1999a). Kinetics of cell lysis, dye uptake and permeability changes in cells expressing the rat P2X7 receptor. The Journal of physiology *519 Pt 2*, 335-346.

Virginio, C., MacKenzie, A., Rassendren, F.A., North, R.A., and Surprenant, A. (1999b). Pore dilation of neuronal P2X receptor channels. Nat Neurosci *2*, 315-321.

Walker, D.G. (1975). Control of bone resorption by hematopoietic tissue. The induction and reversal of congenital osteopetrosis in mice through use of bone marrow and splenic transplants. The Journal of experimental medicine *142*, 651-663.

Wang, N., Robaye, B., Agrawal, A., Skerry, T.M., Boeynaems, J.M., and Gartland, A. (2012). Reduced bone turnover in mice lacking the P2Y(13) receptor of ADP. Mol Endocrinol *26*, 142-152.

Wang, N., Rumney, R.M., Yang, L., Robaye, B., Boeynaems, J.M., Skerry, T.M., and Gartland, A. (2013). The P2Y13 receptor regulates extracellular ATP metabolism and the osteogenic response to mechanical loading. Journal of bone and mineral research : the official journal of the American Society for Bone and Mineral Research *28*, 1446-1456.

Wang, Q., Li, X., Wang, L., Feng, Y.H., Zeng, R., and Gorodeski, G. (2004a). Antiapoptotic effects of estrogen in normal and cancer human cervical epithelial cells. Endocrinology *145*, 5568-5579.

Wang, Q., Wang, L., Feng, Y.H., Li, X., Zeng, R., and Gorodeski, G.I. (2004b). P2X7 receptor-mediated apoptosis of human cervical epithelial cells. Am J Physiol Cell Physiol *287*, C1349-1358.

Wang, X., Arcuino, G., Takano, T., Lin, J., Peng, W.G., Wan, P., Li, P., Xu, Q., Liu, Q.S., Goldman, S.A*., et al.* (2004c). P2X7 receptor inhibition improves recovery after spinal cord injury. Nat Med *10*, 821-827.

Ward, J.R., West, P.W., Ariaans, M.P., Parker, L.C., Francis, S.E., Crossman, D.C., Sabroe, I., and Wilson, H.L. (2010). Temporal interleukin-1beta secretion from primary human peripheral blood monocytes by P2X7-independent and P2X7-dependent mechanisms. The Journal of biological chemistry *285*, 23147-23158.

Weitzmann, M.N., Roggia, C., Toraldo, G., Weitzmann, L., and Pacifici, R. (2002). Increased production of IL-7 uncouples bone formation from bone resorption during estrogen deficiency. The Journal of clinical investigation *110*, 1643-1650.

Wenham, R.M., Landt, M., Walters, S.M., Hidaka, H., and Easom, R.A. (1992). Inhibition of insulin secretion by KN-62, a specific inhibitor of the multifunctional Ca2+/calmodulin-dependent protein kinase II. Biochemical and biophysical research communications *189*, 128-133.

Wesselius, A., Bours, M.J., Agrawal, A., Gartland, A., Dagnelie, P.C., Schwarz, P., and Jorgensen, N.R. (2011). Role of purinergic receptor polymorphisms in human bone. Frontiers in bioscience : a journal and virtual library *16*, 2572-2585.

Wesselius, A., Bours, M.J., Arts, I.C., Theunisz, E.H., Geusens, P., and Dagnelie, P.C. (2012). The P2X(7) loss-of-function Glu496Ala polymorphism affects ex vivo cytokine release and protects against the cytotoxic effects of high ATP-levels. BMC Immunol *13*, 64.

Wesselius, A., Bours, M.J., Henriksen, Z., Syberg, S., Petersen, S., Schwarz, P., Jorgensen, N.R., van Helden, S., and Dagnelie, P.C. (2013). Association of P2X7 receptor polymorphisms with bone mineral density and osteoporosis risk in a cohort of Dutch fracture patients. Osteoporos Int *24*, 1235-1246.

Westra, J., Brouwer, E., Bouwman, E., Doornbos-van der Meer, B., Posthumus, M.D., van Leeuwen, M.A., Limburg, P.C., Ueda, Y., and Kallenberg, C.G. (2009). Role for CaMKII inhibition in rheumatoid arthritis: effects on HIF-1-induced VEGF production by rheumatoid synovial fibroblasts. Annals of the New York Academy of Sciences *1173*, 706-711.

Westra, J., Brouwer, E., van Roosmalen, I.A., Doornbos-van der Meer, B., van Leeuwen, M.A., Posthumus, M.D., and Kallenberg, C.G. (2010). Expression and regulation of HIF-1alpha in macrophages under inflammatory conditions; significant reduction of VEGF by CaMKII inhibitor. BMC musculoskeletal disorders *11*, 61.

White, N., and Burnstock, G. (2006). P2 receptors and cancer. Trends in pharmacological sciences *27*, 211-217.

White, N., Butler, P.E., and Burnstock, G. (2005). Human melanomas express functional P2 X(7) receptors. Cell Tissue Res *321*, 411-418.

Wiktor-Jedrzejczak, W.W., Ahmed, A., Szczylik, C., and Skelly, R.R. (1982). Hematological characterization of congenital osteopetrosis in op/op mouse. Possible mechanism for abnormal macrophage differentiation. The Journal of experimental medicine *156*, 1516-1527.

Wiley, J.S., Dao-Ung, L.-P., Li, C., Shemon, A.N., Gu, B.J., Smart, M.L., Fuller, S.J., Barden, J.A., Petrou, S., and Sluyter, R. (2003). An Ile-568 to Asn polymorphism prevents normal trafficking and function of the human $P2X_7$ receptor. The Journal of biological chemistry *278*, 17108-17113.

Wiley, J.S., Dao-Ung, L.P., Gu, B.J., Sluyter, R., Shemon, A.N., Li, C., Taper, J., Gallo, J., and Manoharan, A. (2002). A loss-of-function polymorphic mutation in the cytolytic P2X7 receptor gene and chronic lymphocytic leukaemia: a molecular study. Lancet *359*, 1114-1119.

Wiley, J.S., Gargett, C.E., Zhang, W., Snook, M.B., and Jamieson, G.P. (1998). Partial agonists and antagonists reveal a second permeability state of human lymphocyte P2Z/P2X7 channel. The American journal of physiology *275*, C1224-1231.

Wiley, J.S., Sluyter, R., Gu, B.J., Stokes, L., and Fuller, S.J. (2011). The human P2X7 receptor and its role in innate immunity. Tissue antigens *78*, 321-332.

Wilson, H.L., Varcoe, R.W., Stokes, L., Holland, K.L., Francis, S.E., Dower, S.K., Surprenant, A., and Crossman, D.C. (2007). P2X receptor characterization and IL-1/IL-1Ra release from human endothelial cells. British journal of pharmacology *151*, 115-127.

Wilson, H.L., Wilson, S.A., Surprenant, A., and North, R.A. (2002). Epithelial membrane proteins induce membrane blebbing and interact with the P2X7 receptor C terminus. The Journal of biological chemistry *277*, 34017-34023.

Winslow, M.M., Pan, M., Starbuck, M., Gallo, E.M., Deng, L., Karsenty, G., and Crabtree, G.R. (2006). Calcineurin/NFAT signaling in osteoblasts regulates bone mass. Developmental cell *10*, 771-782.

Wolber, F.M., Leonard, E., Michael, S., Orschell-Traycoff, C.M., Yoder, M.C., and Srour, E.F. (2002). Roles of spleen and liver in development of the murine hematopoietic system. Experimental hematology *30*, 1010-1019.

Xu, X.J., Boumechache, M., Robinson, L.E., Marschall, V., Gorecki, D.C., Masin, M., and Murrell-Lagnado, R.D. (2012). Splice variants of the P2X7 receptor reveal differential agonist dependence and functional coupling with pannexin-1. Journal of cell science *125*, 3776-3789.

Yamaki, M., Nakamura, H., Takahashi, N., Udagawa, N., and Ozawa, H. (2005). Transcytosis of calcium from bone by osteoclast-like cells evidenced by direct visualization of calcium in cells. Archives of biochemistry and biophysics *440*, 10-17.

Yao, G.Q., Sun, B.H., Weir, E.C., and Insogna, K.L. (2002). A role for cell-surface CSF-1 in osteoblast-mediated osteoclastogenesis. Calcified tissue international *70*, 339-346.

Yasuda, H., Shima, N., Nakagawa, N., Yamaguchi, K., Kinosaki, M., Mochizuki, S., Tomoyasu, A., Yano, K., Goto, M., Murakami, A*., et al.* (1998). Osteoclast differentiation factor is a ligand for osteoprotegerin/osteoclastogenesis-inhibitory factor and is identical to TRANCE/RANKL. Proceedings of the National Academy of Sciences of the United States of America *95*, 3597-3602.

Yoshida, H., Hayashi, S., Kunisada, T., Ogawa, M., Nishikawa, S., Okamura, H., Sudo, T., Shultz, L.D., and Nishikawa, S. (1990). The murine mutation

osteopetrosis is in the coding region of the macrophage colony stimulating factor gene. Nature *345*, 442-444.

Yu, Y., Ugawa, S., Ueda, T., Ishida, Y., Inoue, K., Kyaw Nyunt, A., Umemura, A., Mase, M., Yamada, K., and Shimada, S. (2008). Cellular localization of P2X7 receptor mRNA in the rat brain. Brain research *1194*, 45-55.

Zhang, X.J., Zheng, G.G., Ma, X.T., Lin, Y.M., Song, Y.H., and Wu, K.F. (2005). Effects of various inducers on the expression of P2X7 receptor in human peripheral blood mononuclear cells. Sheng Li Xue Bao *57*, 193-198.

Zheng, L.M., Zychlinsky, A., Liu, C.C., Ojcius, D.M., and Young, J.D.E. (1991). Extracellular Atp as a Trigger for Apoptosis or Programmed Cell-Death. J Cell Biol *112*, 279-288.

Zoricic, S., Maric, I., Bobinac, D., and Vukicevic, S. (2003). Expression of bone morphogenetic proteins and cartilage-derived morphogenetic proteins during osteophyte formation in humans. Journal of anatomy *202*, 269-277.